N72-18007

[redacted]

NASA TECHNICAL MEMORANDUM

NASA TM X-2060

NASA TM X-2060

CLASSIFICATION CHANGED
TO [redacted]
By Authority of TO-22-112 Date 2 MAR 1972

CASE FILE COPY

Declassified by authority of NASA
Classification Change Notices No. [redacted]
Dated [redacted]

AERODYNAMIC CHARACTERISTICS OF A SIX-JET V/STOL CONFIGURATION WITH FOUR SWING-OUT LIFT JETS IN THE TRANSITION SPEED RANGE

by Arthur W. Carter

Langley Research Center
Hampton, Va. 23365

NATIONAL AERONAUTICS AND SPACE ADMINISTRATION • WASHINGTON, D. C. • NOVEMBER 1970

[redacted]

[redacted]

1. Report No.	2. Government Accession No.	3. Recipient's Catalog No.
NASA TM X-2060		

4. Title and Subtitle	5. Report Date
AERODYNAMIC CHARACTERISTICS OF A SIX-JET V/STOL CONFIGURATION WITH FOUR SWING-OUT LIFT JETS IN THE TRANSITION SPEED RANGE (U)	November 1970
	6. Performing Organization Code
7 Author(s)	8. Performing Organization Report No.
Arthur W. Carter	L-7246
	10. Work Unit No.
9. Performing Organization Name and Address	721-01-11-01
NASA Langley Research Center Hampton, Va. 23365	11 Contract or Grant No.
	13. Type of Report and Period Covered
12. Sponsoring Agency Name and Address	Technical Memorandum
National Aeronautics and Space Administration Washington, D.C. 20546	14. Sponsoring Agency Code

15. Supplementary Notes

16. Abstract

A wind-tunnel investigation has been made of the longitudinal aerodynamic characteristics and jet-interference effects of a model of a jet V/STOL variable-sweep fighter airplane that employs four direct-lift engines which swing out from the fuselage and two lift-cruise engines located in the rear part of the fuselage. Data were obtained with two wing areas for various forward speeds and power conditions in the transition speed range. The data are presented without analysis or discussion.

17. Key Words (Suggested by Author(s))	18. Distribution Statement
Jet V/STOL Jet interference Aerodynamic characteristics	[redacted]

19. Security Classif. (of this report)	20. Security Classif. (of this page)	21 No. of Pages	22. Price
[redacted]	Unclassified	191	

[redacted]

AERODYNAMIC CHARACTERISTICS OF A SIX-JET V/STOL CONFIGURATION WITH FOUR SWING-OUT LIFT JETS IN THE TRANSITION SPEED RANGE*

By Arthur W. Carter
Langley Research Center

SUMMARY

A wind-tunnel investigation has been made of the longitudinal aerodynamic characteristics and jet-interference effects of a model of a jet V/STOL variable-sweep fighter airplane that employs four direct-lift engines which swing out from the fuselage and two lift-cruise engines located in the rear part of the fuselage. Data were obtained with two wing areas for various forward speeds and power conditions in the transition speed range. The data are presented without analysis or discussion.

INTRODUCTION

The National Aeronautics and Space Administration and the aircraft industry have conducted research on aircraft which have the capability for vertical or short take-off and landing (V/STOL). These aircraft combine the utility of the helicopter with the higher speed and longer range capability of conventional airplanes. Jet V/STOL configurations have the capability of performing high-subsonic and supersonic cruise missions. Results of the investigations of the aerodynamic characteristics of several typical jet VTOL and V/STOL aircraft in the transition speed range have been presented in references 1 to 6.

The present investigation was undertaken to provide data on the longitudinal aerodynamic characteristics of a model of a jet V/STOL variable-sweep fighter airplane which employs two lift-cruise engines located in the rear part of the fuselage and four direct-lift engines which swing out from the fuselage ahead of the wing. The aerodynamic characteristics and jet-interference effects were investigated for various power conditions at airspeeds simulating transition flight. The power-on tests were performed in the 17-foot (5.18-meter) test section of the Langley 300-MPH 7- by 10-foot tunnel. The data from the investigation are presented without analysis.

---

*Title, Unclassified.

SYMBOLS

The longitudinal aerodynamic data (lift, drag, and pitching-moment coefficients) in this paper are referred to the stability-axis system. All of the data are referred to a moment center located on the fuselage reference line at the 15-percent point of the mean aerodynamic chord of the reference wing as shown in figure 1. The forces and moments were nondimensionalized by using the geometry of the reference wing.

The physical quantities in this paper are given both in the U.S. Customary Units and in the International System of Units (SI). Factors relating these two systems of units are presented in reference 7.

A_j total area of operating jet exit nozzles, square feet (square meters)

$\bar{c}$ reference wing mean aerodynamic chord, feet (meters)

c wing chord, feet (meters)

C_D drag coefficient, $D/q_\infty S$

C_L lift coefficient, $L/q_\infty S$

C_m pitching-moment coefficient, $M/q_\infty S\bar{c}$

C_T thrust coefficient, $T/q_\infty S$

D drag, pounds force (newtons)

D_e effective diameter of thrust nozzles (diameter of circle having same area as sum of operating nozzles), feet (meters)

i_t tail incidence, degrees

L measured lift, pounds force (newtons)

M pitching moment, foot-pounds (meter-newtons)

q_∞ free-stream dynamic pressure, pounds force/foot^2 (newtons/meter^2)

[redacted]

S	wing reference area (area of theoretical wing excluding wing stub), feet^2 (meters^2)
T	thrust, pounds force (newtons)
V_j	velocity at jet exhaust, feet/second (meters/second)
V_∞	free-stream velocity, feet/second (meters/second)
α	angle of attack of wing, degrees
δ_j	deflection of jet exhaust with respect to fuselage reference plane, degrees
$\delta_{LE,IB}$	deflection of wing inboard leading-edge slat (positive when leading edge is deflected down), degrees
$\delta_{LE,OB}$	deflection of wing outboard leading-edge slat (positive when leading edge is deflected down), degrees
$\delta_{LE,ST}$	deflection of leading-edge Krueger flap on wing stub (positive when leading edge is deflected down), degrees
$\delta_{TE,ST}$	deflection of trailing-edge flap on wing stub (positive when trailing edge is deflected down), degrees
$\delta_{TE,W}$	deflection of full-span trailing-edge wing flap (positive when trailing edge is deflected down), degrees
$\delta_{TE,W,P}$	deflection of partial-span trailing-edge wing flap (positive when trailing edge is deflected down), degrees (see fig. 1)
ρ_j	mass density of jet exhaust, slugs per cubic foot (kilograms per cubic meter)
ρ_∞	mass density of free-stream air, slugs per cubic foot (kilograms per cubic meter)

[redacted]

MODEL AND APPARATUS

The model used in this investigation was a 1/10-scale model of a jet V/STOL variable-sweep fighter airplane powered by two lift-cruise and four direct-lift engines. Geometric characteristics of the configuration are shown in figure 1. The fixed stub part of the wing has a leading-edge sweep of 65° and the movable part in the fully extended position has a leading-edge sweep of 25°. The movable part of the wing has a 10-percent chord extension at the leading edge over the outboard 23 percent of the span. Details of the wing high-lift devices are shown in figure 2. The fixed stub part of the wing has a constant-chord split trailing-edge flap and a leading-edge Krueger flap. The movable wing section has a 30-percent-chord single-slotted trailing-edge Fowler flap and a 17.5-percent-chord leading-edge slat.

The two lift-cruise engines, which make up the main propulsion system for normal flight, are mounted horizontally in the rear part of the fuselage with individual side and top inlets and with individual exhaust nozzles. The exhaust nozzles of these engines are capable of being rotated about the Y-axis to any position from horizontal to vertical. The four direct-lift engines are mounted forward of the wing, in pairs, on arms which swing out from the fuselage. The engines and arms are stowed completely within the fuselage for normal forward flight. The direct-lift engines may be rotated about the Y-axis to any desired deflection. This engine arrangement eliminates the need for a separate reaction-control system for hovering and low speeds inasmuch as adequate control can be provided by differential deflection of the direct-lift engines for yaw control and by selective throttling of all three pairs of engines for pitch and roll control.

In the transition speed range of the investigation, the airplane would operate with the wing fully extended; therefore, the model was constructed with the wing fixed in this position as shown in figure 1. The model was mounted on a sting-supported six-component strain-gage balance for direct measurement of the forces and moments on the model. The balance was located on the model reference line with the moment center of the balance located at the 20-percent mean-aerodynamic-chord station of the wing. The pitching-moment data have been transferred horizontally to a moment center located at the 15-percent mean-aerodynamic-chord station of the wing. An electronic clinometer was located in the fuselage for use in determining the geometric angle of attack of the wing during the investigation.

The principal model configurations investigated are identified in the following table:

Configuration	$\delta_{LE,OB}$	$\delta_{LE,IB}$	$\delta_{TE,W}$	$\delta_{TE,W}$	$\delta_{LE,ST}$	$\delta_{TE,ST}$
A	30°	30°	---	40°	Retracted	40°
B	Retracted	Retracted	---	Retr	tracted	Retracted
C	32°	32°	50°	---	tracted	40°

[redacted]

Photographs of the sting-supported model in the 17-foot test section of the Langley 300-MPH 7- by 10-foot tunnel are shown as figure 3. The photographs show configuration A with the engines deflected to 90° for vertical take-off and landing and deflected to 45° for short take-off and landing. A description of the tunnel is given in reference 8.

A modified wing of smaller area was also investigated. The plan view and details of the high-lift devices for the modified wing are shown in figure 4. Double-slotted trailing-edge flaps on the movable wing section replaced the single-slotted trailing-edge Fowler flap of the original wing. Otherwise, the high-lift systems of the two wings are similar. Photographs of the model with the modified wing are shown as figure 5. This model is shown with the direct-lift engines stowed in the fuselage to simulate the configuration for cruise speeds and with the direct-lift engines deflected at 90° for vertical take-off and landing.

THRUST SIMULATION

The thrust for the model was provided by six ejector-type jet-engine simulators. A description of the ejectors and their use for jet-engine simulation in wind-tunnel models is presented in reference 9. The pair of lift-cruise engines has an effective diameter of 3.82 inches (9.7028 centimeters). One set of inlets for these engines are located on top of the rear part of the fuselage. The other set of inlets are located on the sides of the fuselage and were simulated on the model but were blocked for the investigation inasmuch as these inlets are in the region of the direct-lift-engine exhaust and are normally closed during take-off and transition flight. The four direct-lift engines have an effective diameter of 4.00 inches (10.16 centimeters). These engines are positioned outside the model during operation and are equipped with simple individual bellmouth inlets. The six engines have an effective diameter of 5.53 inches (14.05 centimeters).

The six ejectors were powered by cold, dry compressed air which was brought onboard the model with thin-wall metal tubing bent to follow the sting support and to form a limber spring across the strain-gage balance so that the balance sensitivity was not changed. A sheet-metal fairing was used to shield these air lines from the airstream as shown in figures 3 and 5.

The three pairs of ejectors were calibrated statically and the thrust was determined as the resultant force of the normal and axial forces on the strain-gage balance. Turning vanes were used in the ducts ahead of the nozzles of the lift-cruise engines to deflect the jet exhaust. The deflection of the jet exhaust relative to the horizontal plane of the model fuselage was determined from the normal and axial forces on the balance. The variation of the jet-exhaust deflection with thrust for the lift-cruise engines is shown in figure 6. As shown in this figure, the deflection of the jet exhaust for the 0°

[redacted]

and 45° nozzles was approximately the same as the deflection of the exhaust nozzles; whereas, the jet exhaust from the 25° nozzles was deflected to only about 20° and the exhaust from the 90° nozzles was deflected approximately 93°. Turning vanes were not incorporated in the two pairs of direct-lift engines inasmuch as each pair of engines was rotated on the extended arm supports. The jet exhaust, therefore, was deflected at virtually the same angle as the rotated engines.

During the wind-tunnel investigation, the thrust from each of the three pairs of ejectors was determined from the difference between the total-pressure and static-pressure measurements in each of the jet exits in a manner similar to that used in reference 9. Thrust coefficients and effective velocity ratios were determined from the total thrust measurements by use of the following equations:

$$C_T = \frac{T}{q_\infty S} \tag{1}$$

$$\sqrt{\frac{\rho_\infty V_\infty^2}{\rho_j V_j^2}} = \sqrt{\frac{q_\infty}{T/2A_j}} \tag{2}$$

$$C_T = \frac{2A_j/S}{\left(\frac{\rho_\infty V_\infty^2}{\rho_j V_j^2}\right)} \tag{3}$$

TEST CONDITIONS

The power-off data presented in figures 7 to 17 for the basic wing and for various components of the wing high-lift system were obtained in the 7- by 10-foot (2.13- by 3.05-meter) test section of the tunnel at a free-stream dynamic pressure of 28.75 pounds force/foot^2 (1377 newtons/meter^2). The Reynolds number for these power-off tests based on this free-stream dynamic pressure and the wing mean aerodynamic chord was 0.9×10^6. Similar power-off data for the modified wing were obtained in the 17-foot test section of the tunnel at a free-stream dynamic pressure of 11 pounds force/foot^2 (527 newtons/meter^2), and the Reynolds number based on this free-stream dynamic pressure and the mean aerodynamic chord of the modified wing was 0.55×10^6. All power-on test data were obtained in the 17-foot test section of the tunnel, and the Reynolds number based on the free-stream dynamic pressure and the mean aerodynamic chord of the particular wing under investigation ranged up to 0.55×10^6.

The longitudinal aerodynamic characteristics of the model were obtained through a range of angles of attack from approximately -5° to 26° at four thrust coefficients which ranged from 0 to 8. Data were obtained through a range of effective velocity ratios at an angle of attack of 12°. The free-stream dynamic pressure and the engine thrust were varied in order to simulate effective velocity ratios from 0 to approximately 0.22 with the engines deflected at 45° and 90° and up to approximately 0.33 with the engines deflected 0° and 25°.

No corrections have been made to the data for model blockage or jet boundary effects inasmuch as these corrections are not considered to be significant.

PRESENTATION OF RESULTS

In order to hasten the availability of these data on this six-jet V/STOL configuration with four swing-out lift-jets, the longitudinal aerodynamic characteristics of the model are being presented without analysis or discussion. The data, as presented, will be useful in predicting the interference effects of direct-lift engines which are located forward of the leading edge of the wing and for comparing the longitudinal aerodynamic characteristics with those of other jet V/STOL configurations. Ratios of lift and drag to thrust and of pitching moment to the product of the thrust and the effective diameter of the operating jets are presented at an angle of attack of 12° for several wing configurations and several jet deflections through a range of effective velocity ratios. The lift, drag, and pitching-moment coefficients in the stability-axis system are presented through a range of angles of attack. However, in each case, the thrust data are also presented where applicable. Tail-on data are presented for all configurations and tail-off data are presented for several of the configurations.

Results of the investigation are presented in the following figures:

	Figure
Engines removed from model:	
Fuselage alone	7
Fuselage with stub wing	8
Fuselage with complete wing; high-lift devices retracted	9
Various components of high-lift devices on wing	10 to 17
Engines installed on model:	
Configuration A with direct-lift engines and lift-cruise engines deflected 90°:	
Power off	18
Power on	19 to 22

Figure

Configuration A with direct-lift engines deflected 90° and lift-cruise engines off:
Power off 23
Power on . . . . . 24 to 27
Configuration B with direct-lift engines and lift-cruise engines deflected 90°:
Power off 28
Power on . . . . . 29 to 32
Configuration A with direct-lift engines and lift-cruise engines deflected 45°:
Power off 33
Power on . . . . . 34 to 37
Configuration A with direct-lift engines and lift-cruise engines deflected 0°:
Power off 38
Power on . . . . . 39 to 42
Engines removed from model with modified wing:
Fuselage with stub wing 43
Fuselage with complete wing; high-lift devices retracted 44
Various components of high-lift devices on wing . . . . . 45 to 50
Engines installed on model with modified wing:
Configuration C with direct-lift engines and lift-cruise engines deflected 90°:
Power off 51
Power on . . . . . 52 to 55
Configuration C with direct-lift engines and lift-cruise engines deflected 25°:
Power off 56
Power on . . . . . 57 to 60

Langley Research Center,
National Aeronautics and Space Administration,
Hampton, Va., July 10, 1970.

[redacted]

REFERENCES

1. Williams, John; and Wood, Maurice N.: Aerodynamic Interference Effects With Jet-Lift V/STOL Aircraft Under Static and Forward-Speed Conditions. Tech. Rep. No. 66403, Brit. R.A.E., Dec. 1966.

2. Otis, James H., Jr.: Induced Interference Effects on a Four-Jet VTOL Configuration With Various Wing Planforms in the Transition Speed Range. NASA TN D-1400, 1962.

3. Vogler, Raymond D.; and Kuhn, Richard E.: Longitudinal and Lateral Stability Characteristics of Two Four-Jet VTOL Models in the Transition Speed Range. NASA TM X-1092, 1965.

4. Winston, Matthew M.: Wind-Tunnel Data From a 0.16-Scale V/STOL Model With Direct-Lift and Lift-Cruise Jets. NASA TM X-1758, 1969.

5. Margason, Richard J.; and Gentry, Garl L., Jr.: Aerodynamic Characteristics of a Five-Jet VTOL Configuration in the Transition Speed Range. NASA TN D-4812, 1968.

6. Carter, Arthur W.: Effects of Jet-Exhaust Location on the Longitudinal Aerodynamic Characteristics of a Jet V/STOL Model. NASA TN D-5333, 1969.

7. Mechtly, E. A.: The International System of Units – Physical Constants and Conversion Factors. NASA SP-7012, 1964.

8. Kuhn, Richard E.; and Hayes, William C., Jr.: Wind-Tunnel Investigation of Longitudinal Aerodynamic Characteristics of Three Propeller-Driven VTOL Configurations in the Transition Speed Range, Including Effects of Ground Proximity. NASA TN D-55, 1960.

9. Margason, Richard J.; and Gentry, Garl L.: Static Calibration of an Ejector Unit for Simulation of Jet Engines in Small-Scale Wind-Tunnel Models. NASA TN D-3867, 1967.

[redacted]

Wing (reference wing)	
Aspect ratio	6.024
Span	61.2 (155.45)
Area	4.318 ft^2 (.4012 meter^2)
Root chord	15.05 (38.23)
Tip chord	5.27 (13.39)
Mean aerodynamic chord, $\bar{c}$	10.95 (27.813)
Sweep of leading edge	25°
Dihedral	-3°
Taper ratio	0.35
Horizontal tail (exposed)	
Span	29.0 (73.66)
Area	1.04 ft^2 (.0966 meter^2)

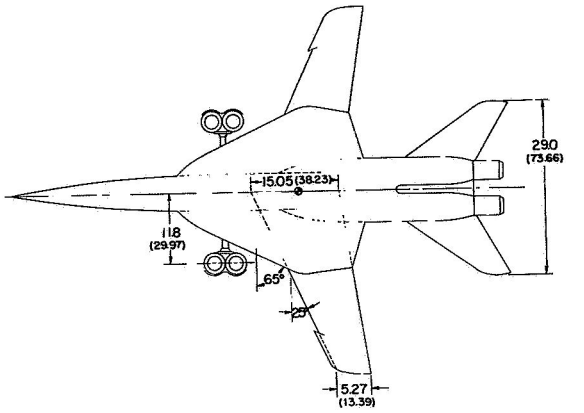

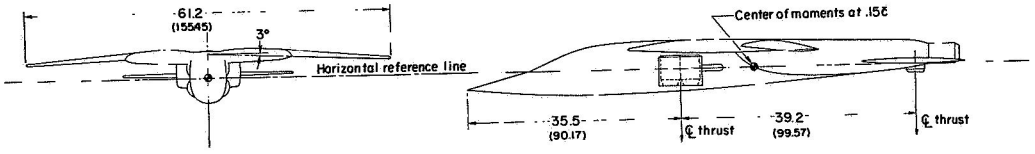

Figure 1.- Three-view drawing and geometric characteristics of model. Dimensions are given in inches and parenthetically in centimeters unless otherwise noted.

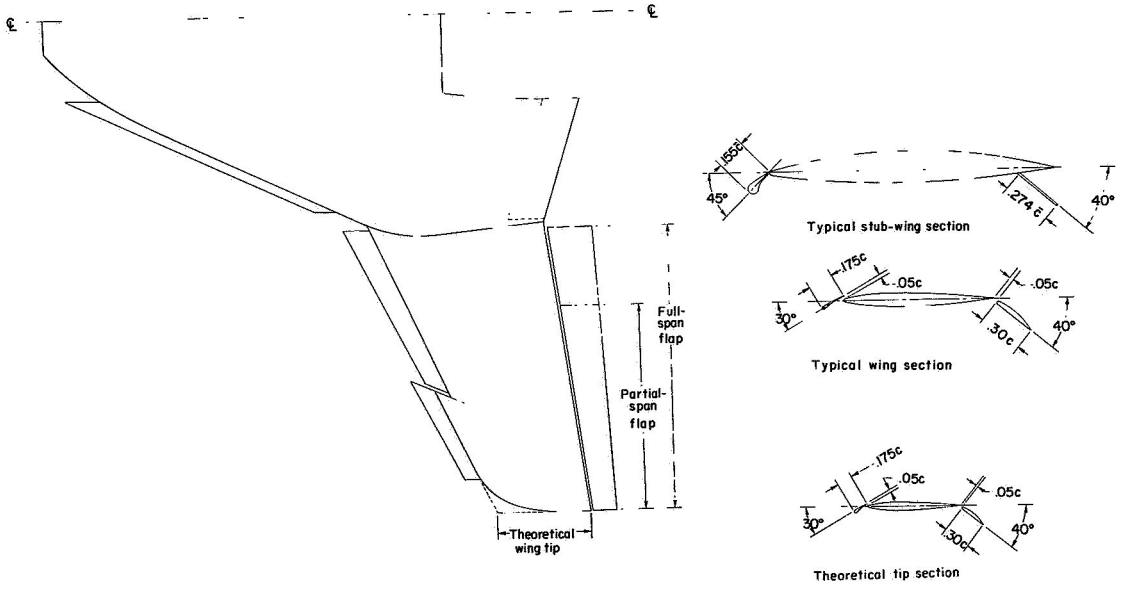

Figure 2.- Details of wing high-lift devices.

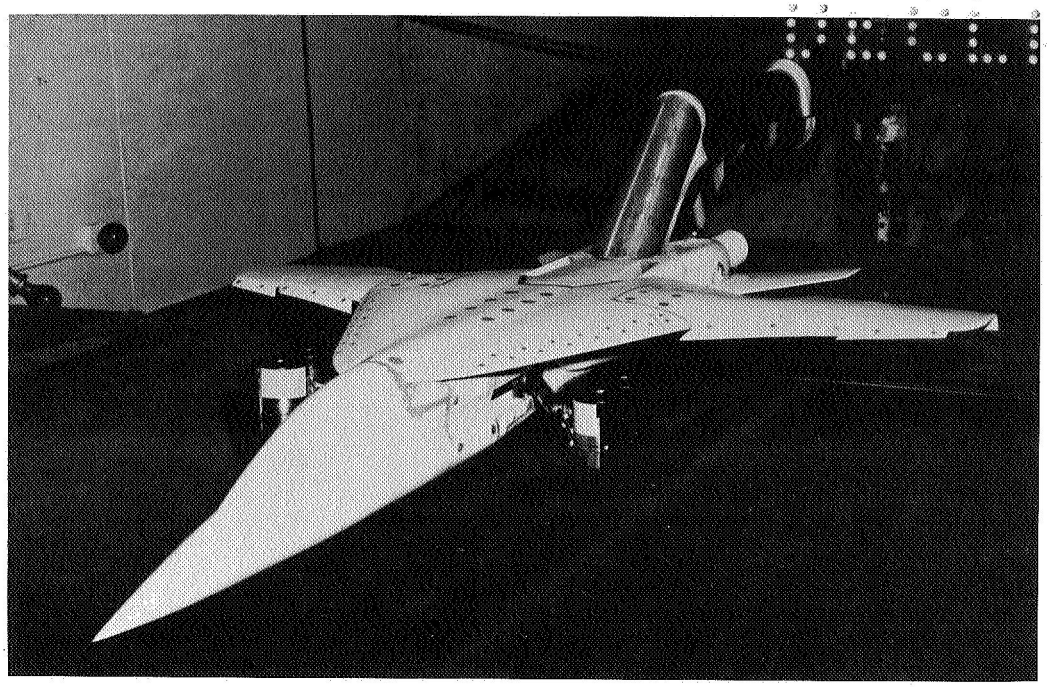

L-66-4928

(a) View showing direct-lift engines at 90° for VTOL.

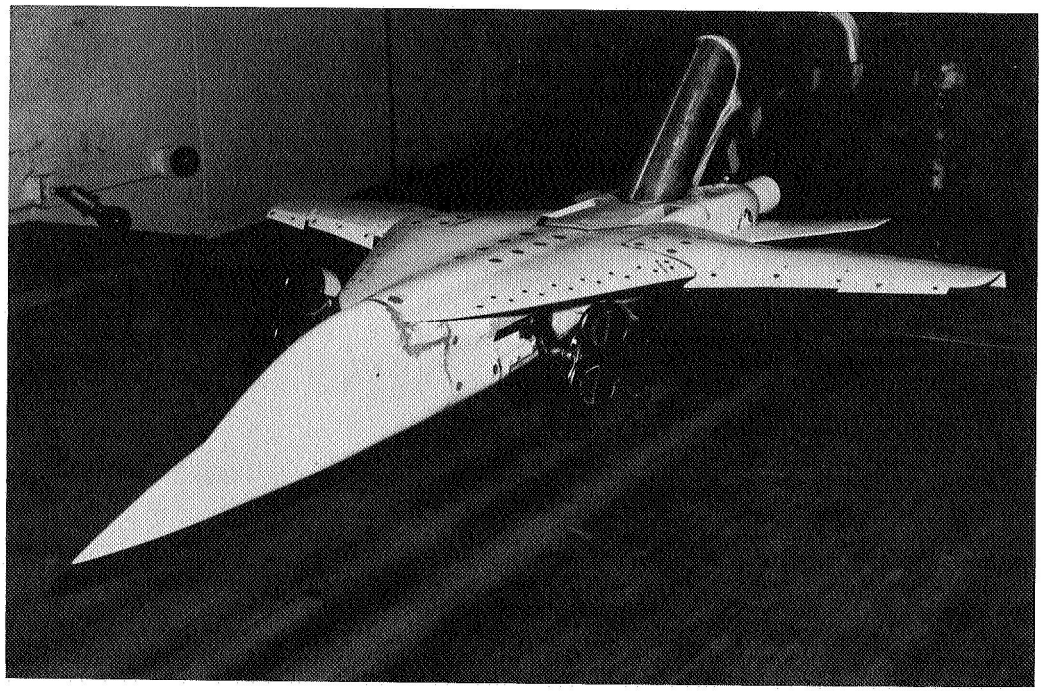

L-66-4927

(b) View showing direct-lift engines at 45° for STOL.

Figure 3.- Photographs of configuration A in the 17-foot (5.18-meter) test section of the Langley 300-MPH 7- by 10-foot tunnel. (Photographs show the model near the floor of the tunnel; however, all test data were obtained with the model at the center line of the tunnel.)

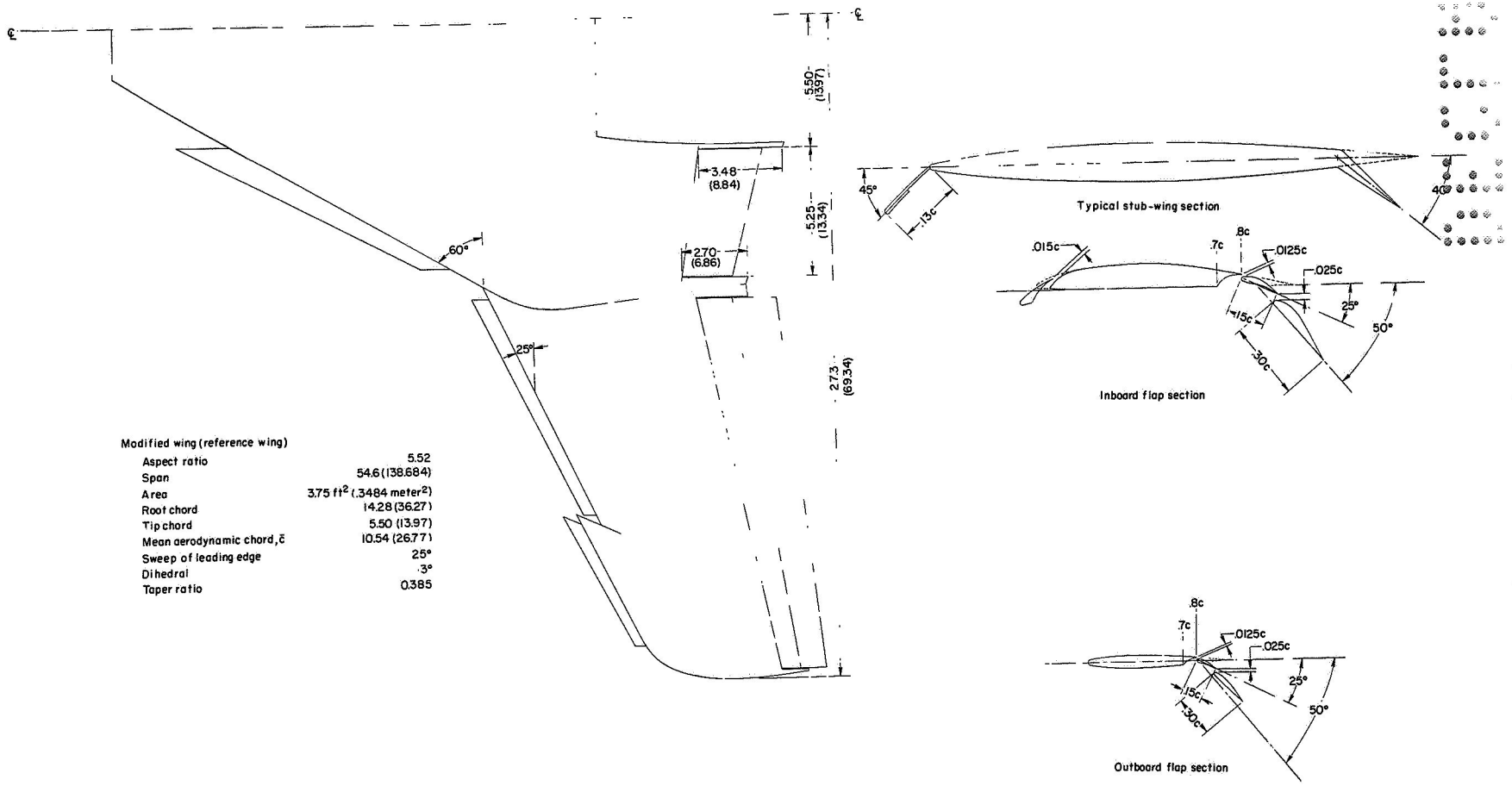

Figure 4.- Modified wing with details of high-lift devices. Dimensions are given in inches and parenthetically in centimeters unless otherwise noted.

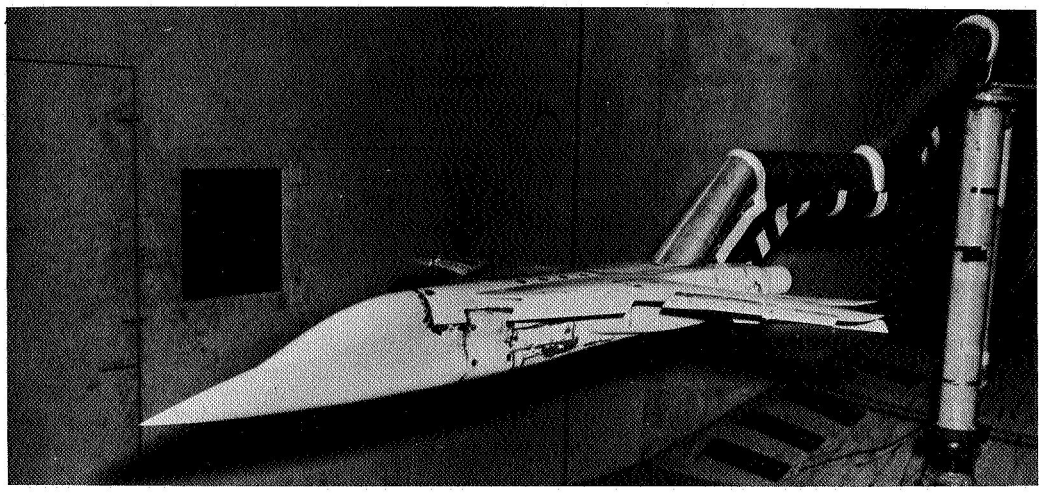

L-66-5096

(a) View showing direct-lift engines in stowed position for cruise.

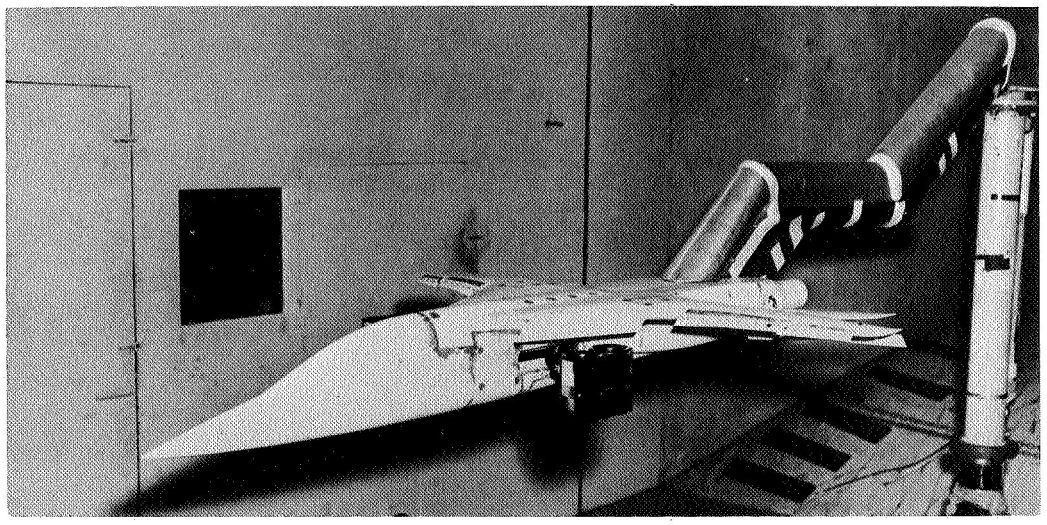

L-66-5095

(b) View showing direct-lift engines in position for vertical take-off.

Figure 5.- Photographs of the model with the modified wing in the 17-foot (5.18-meter) test section of the Langley 300-MPH 7- by 10-foot tunnel.

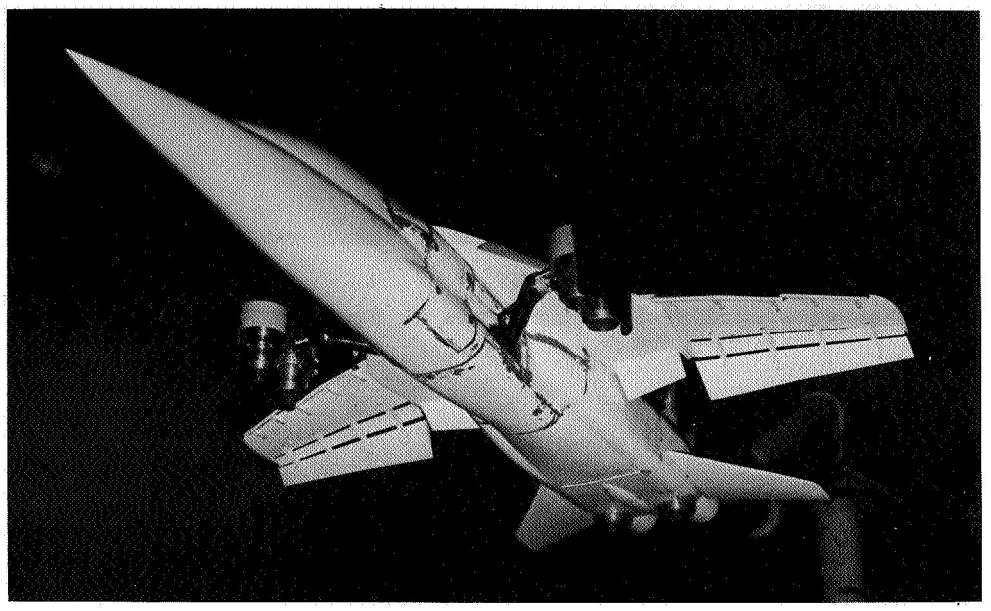

L-66-5097

(c) View showing direct-lift engines and lift-cruise engines in position for vertical take-off.

Figure 5.- Concluded.

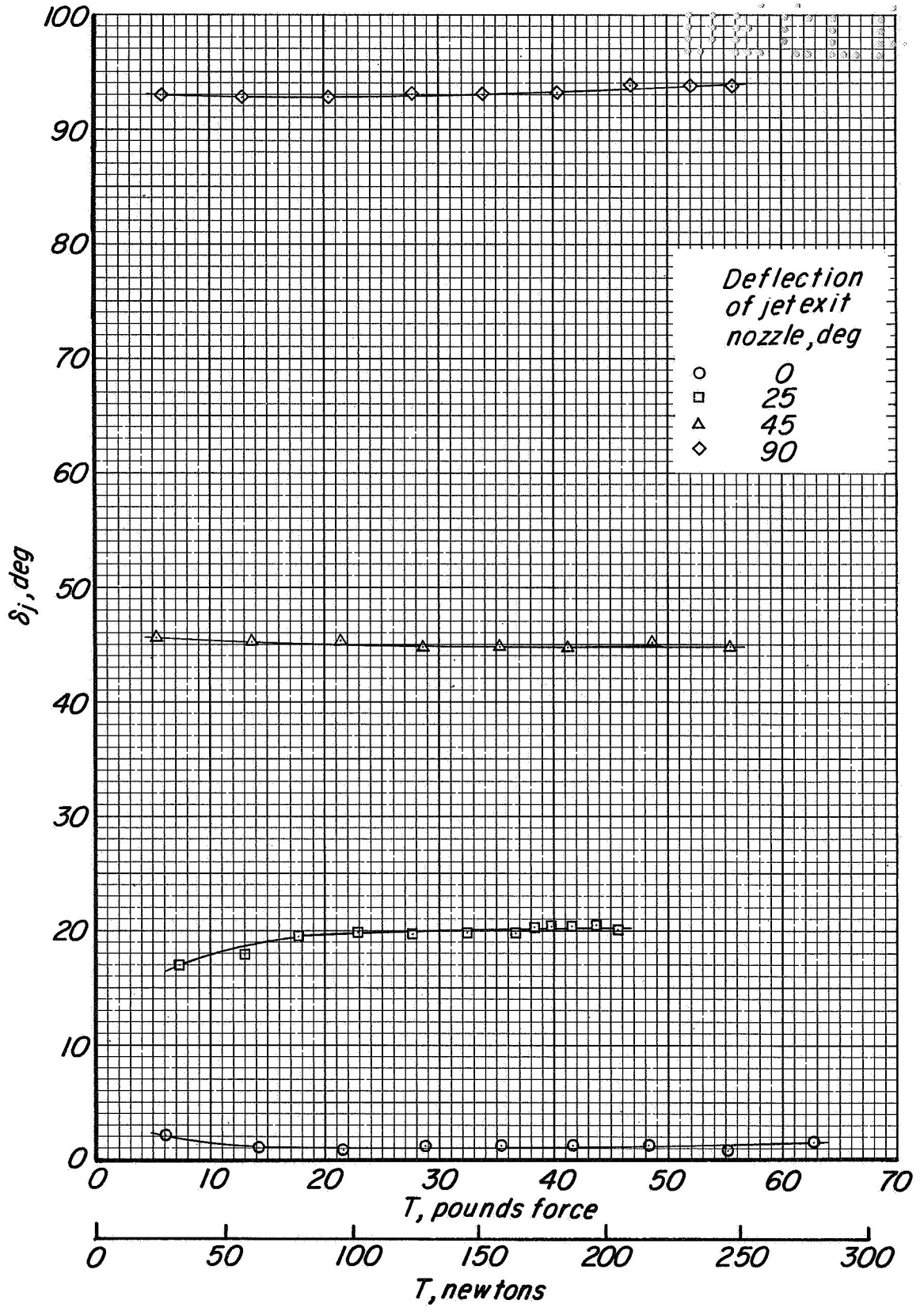

Figure 6.- Variation of jet-exhaust deflection with thrust for lift-cruise engines.

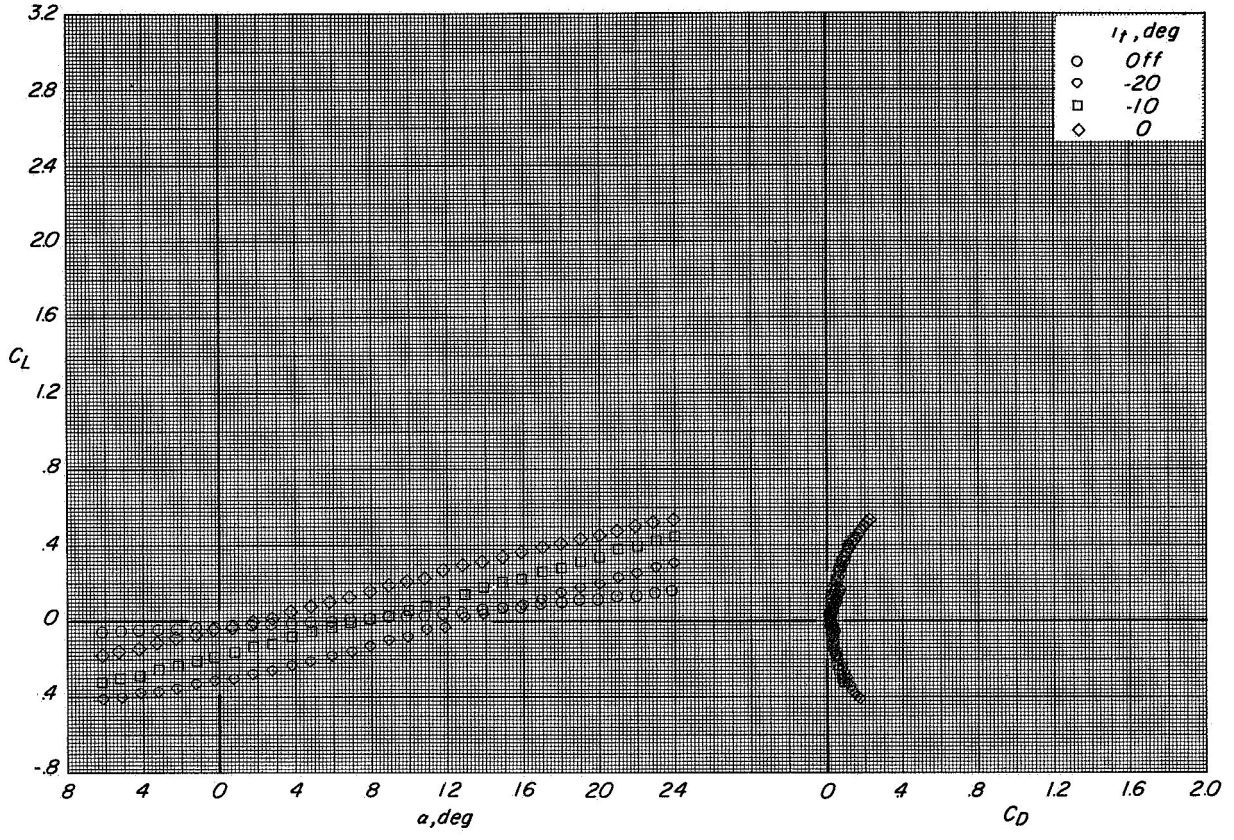

(a) Variation of C_L with α and C_D with C_L.

Figure 7.- Longitudinal aerodynamic characteristics of model fuselage alone $C_T = 0$.

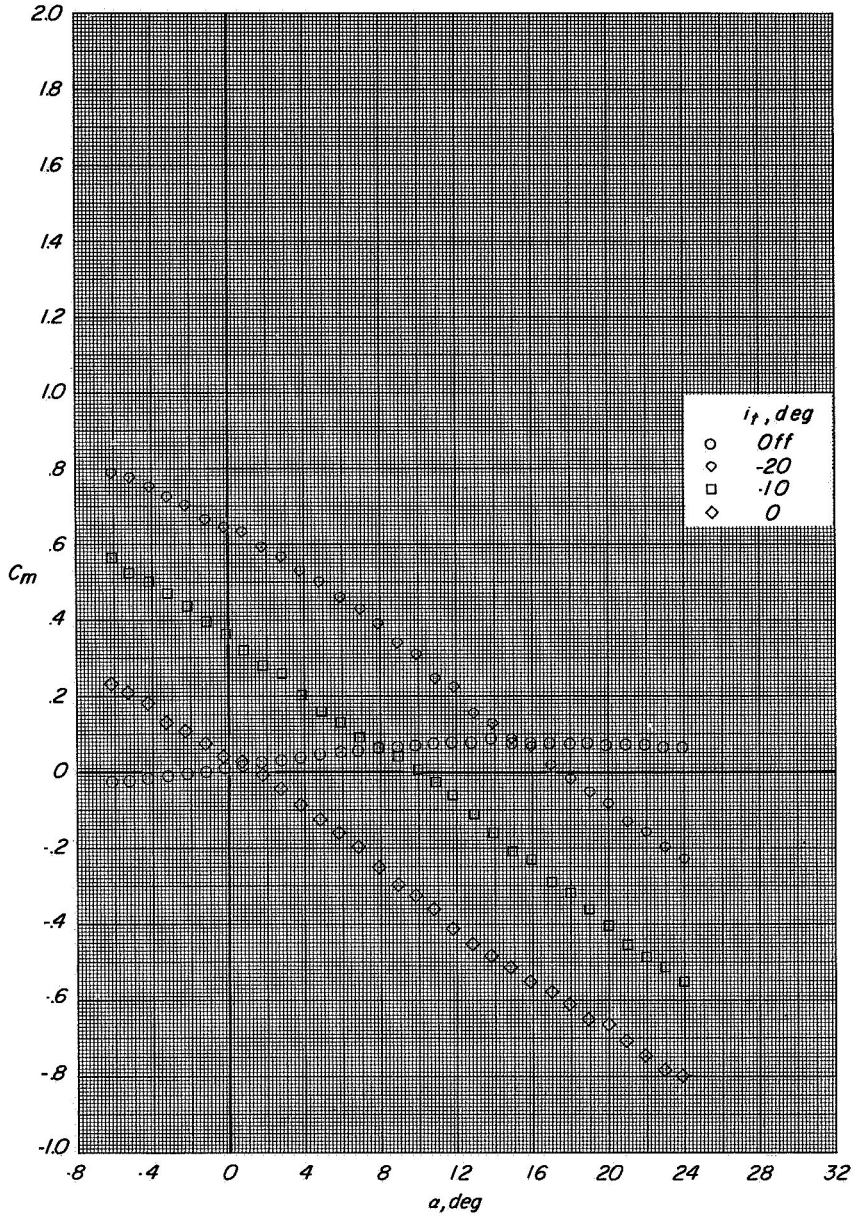

(b) Variation of C_m with α.

Figure 7.- Continued.

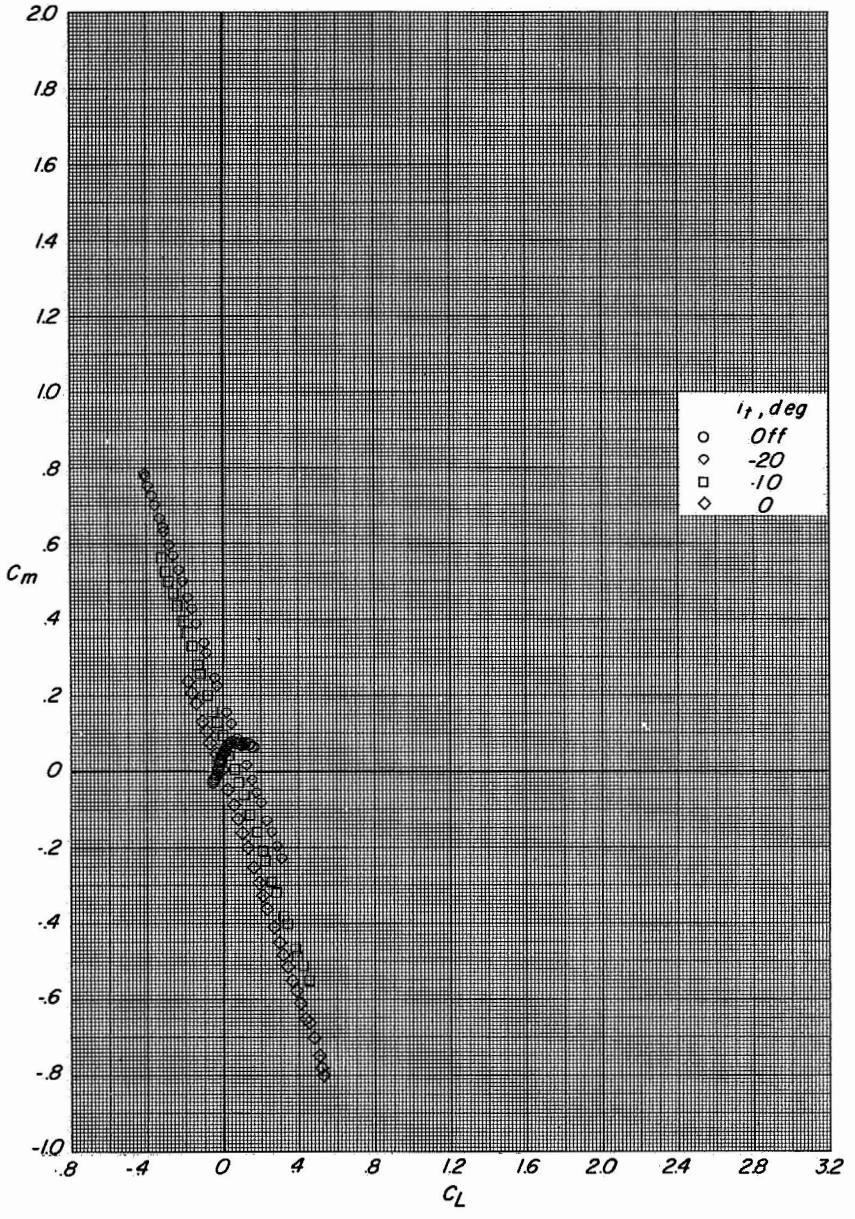

(c) Variation of C_m with C_L.

Figure 7.- Concluded.

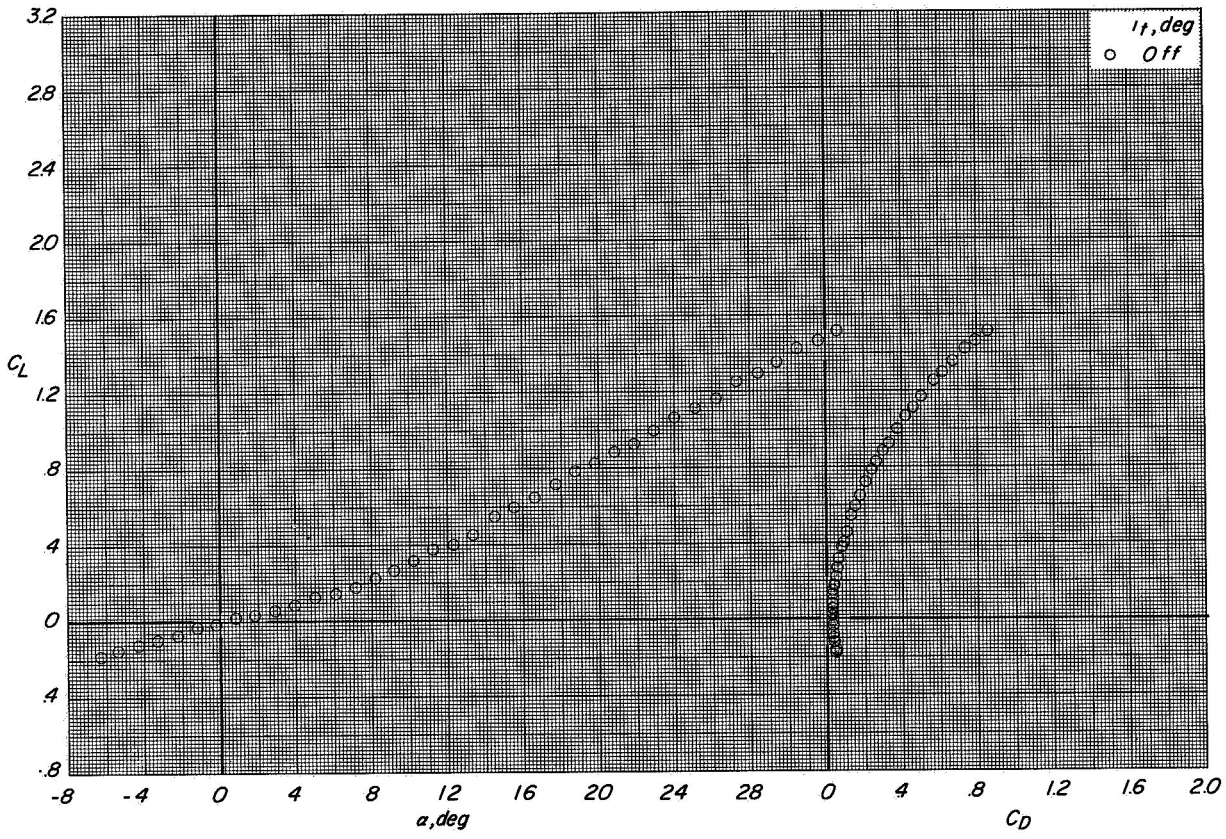

(a) Variation of C_L with α and C_D with C_L.

Figure 8.- Longitudinal aerodynamic characteristics of model fuselage with stub wing. $C_T = 0$.

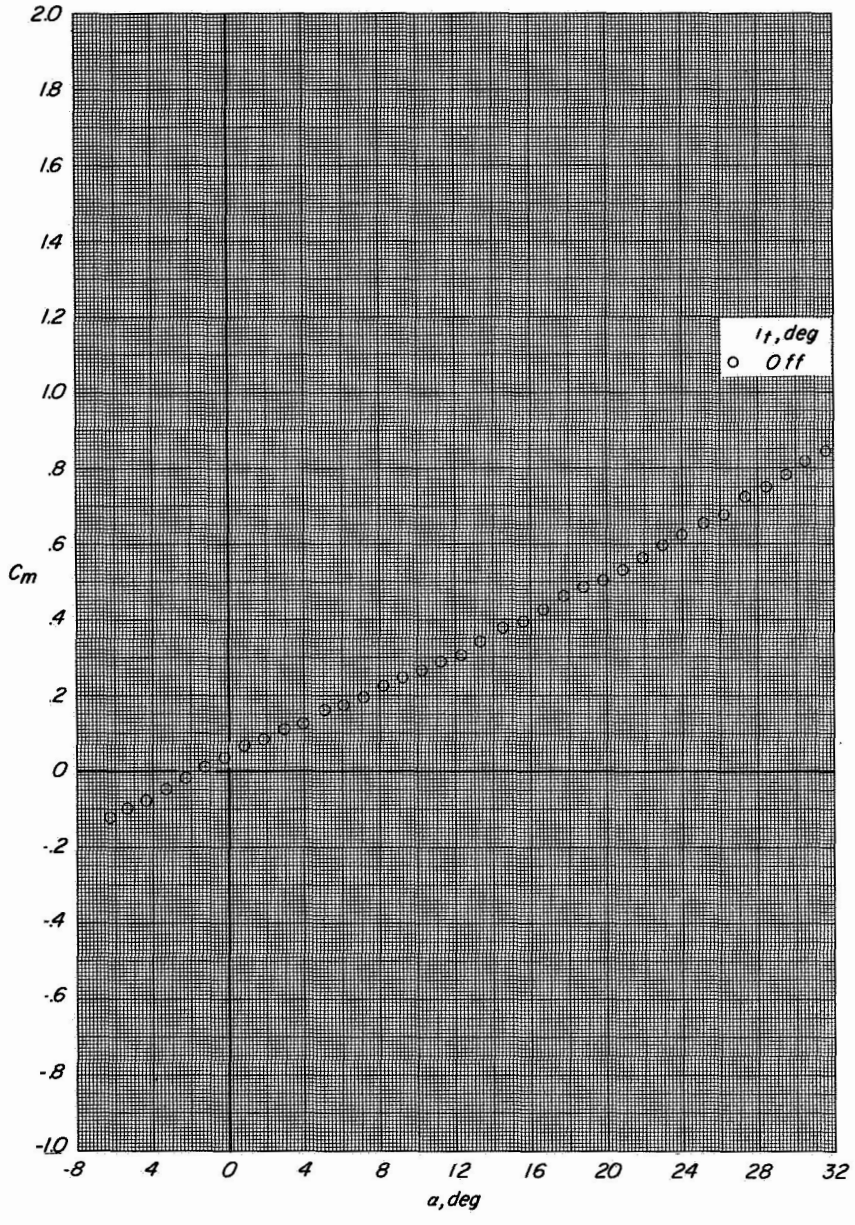

(b) Variation of C_m with α.

Figure 8.- Continued.

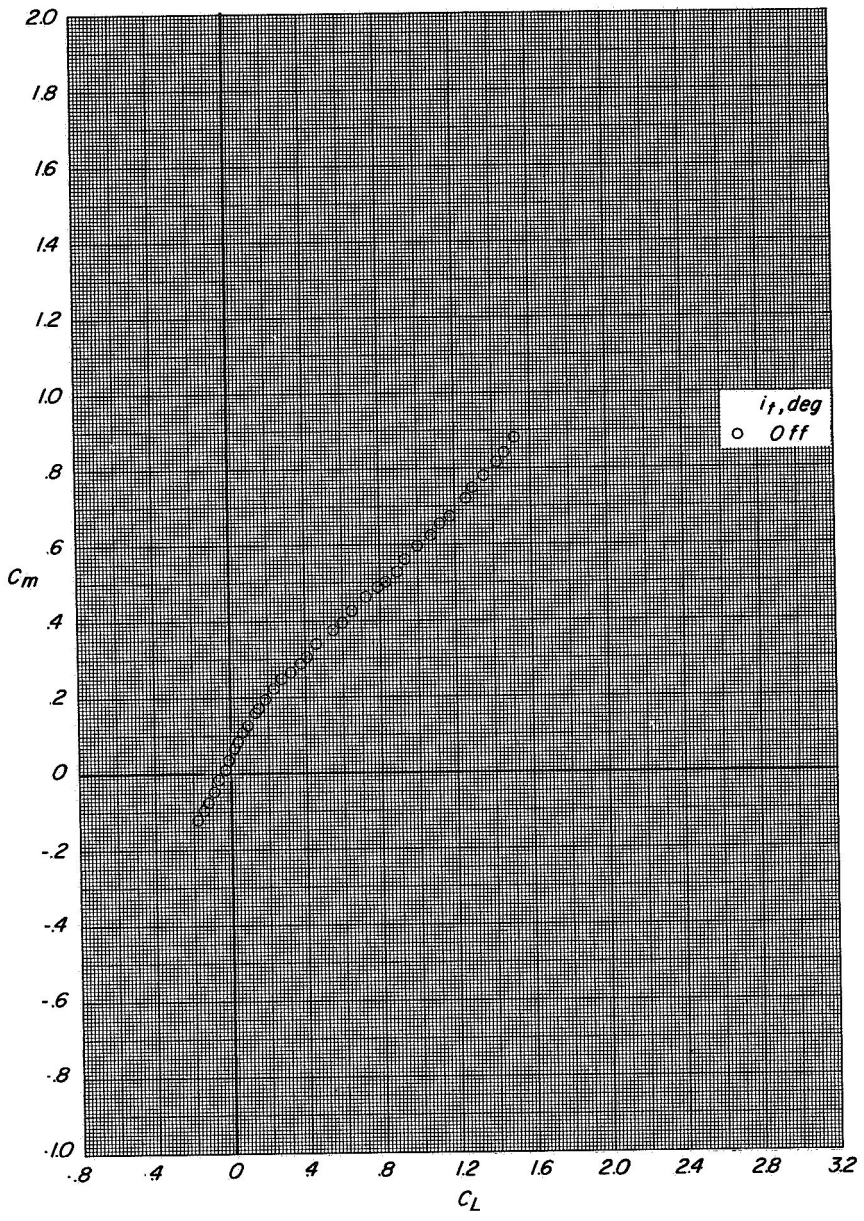

(c) Variation of C_m with C_L.

Figure 8.- Concluded.

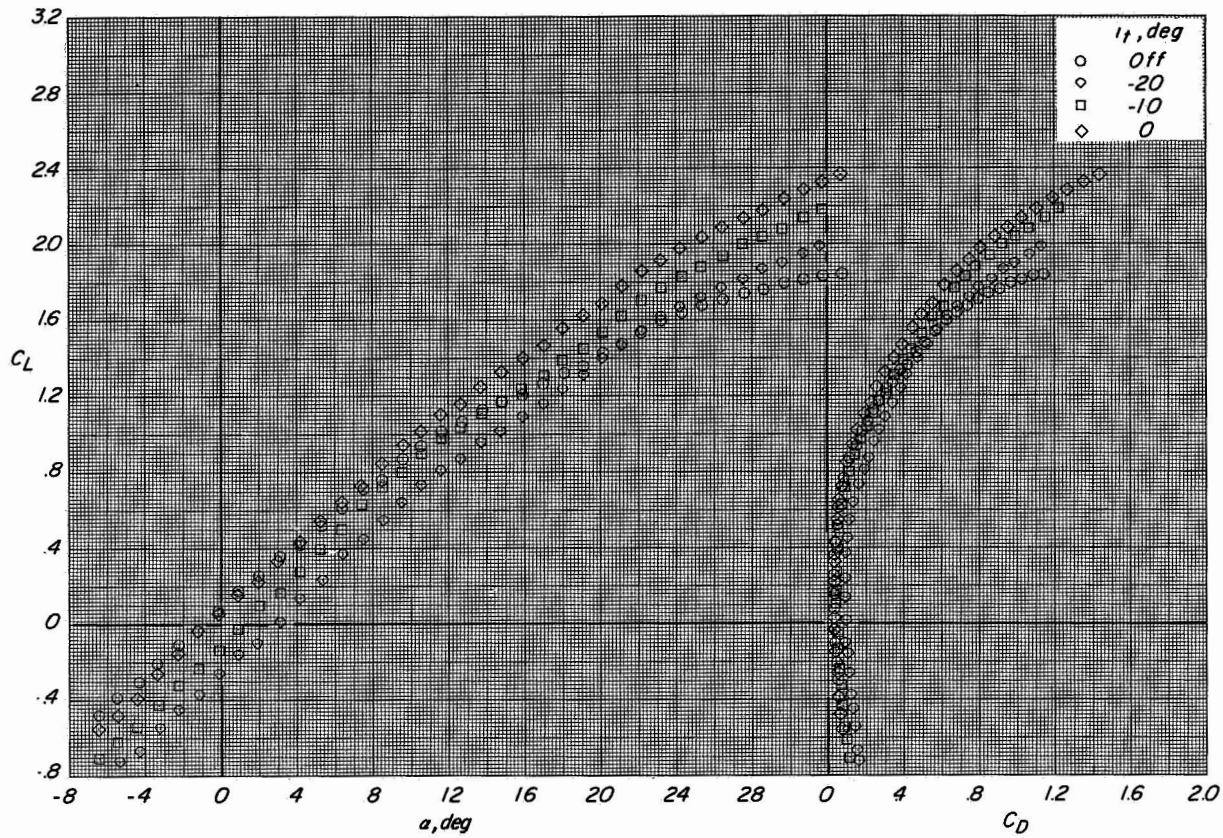

(a) Variation of C_L with α and C_D with C_L.

Figure 9.- Longitudinal aerodynamic characteristics of model fuselage with complete wing. High-lift devices retracted; configuration B; $C_T = 0$.

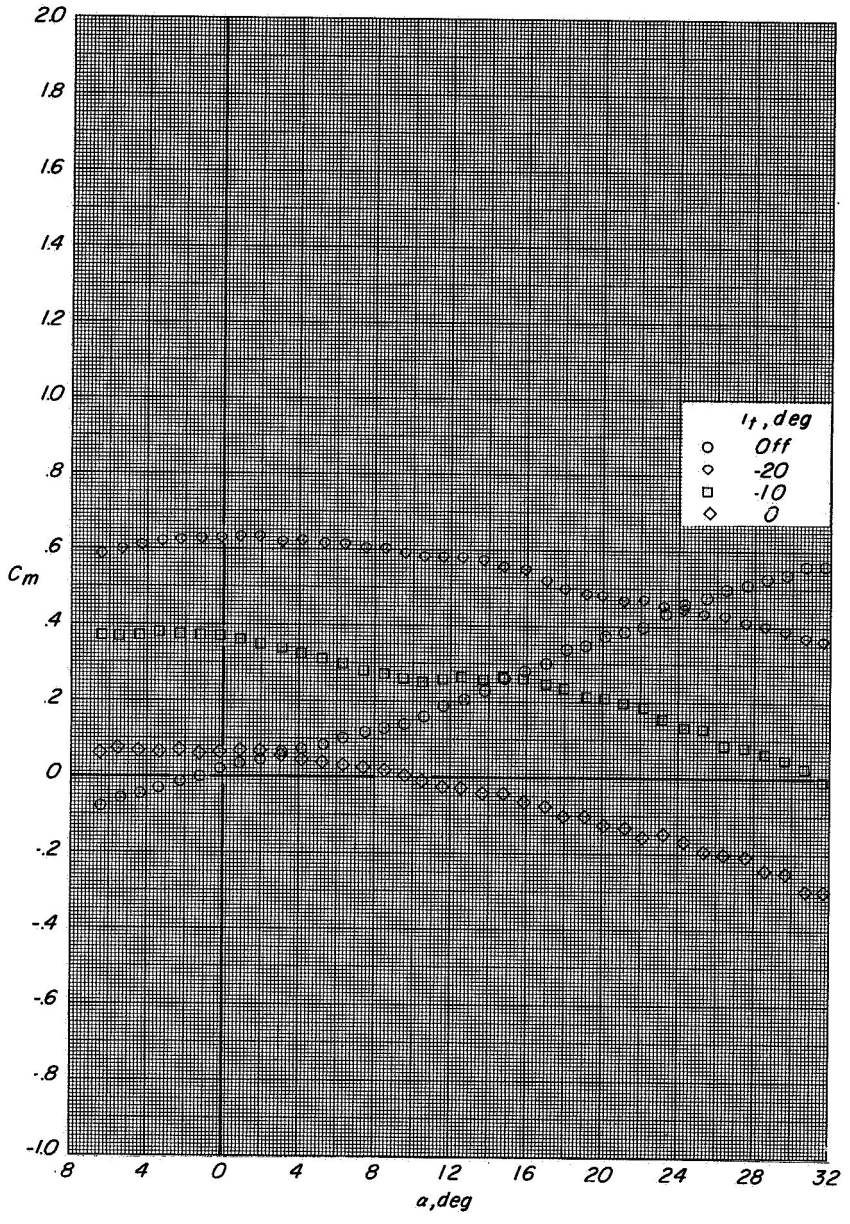

(b) Variation of C_m with α.

Figure 9.- Continued.

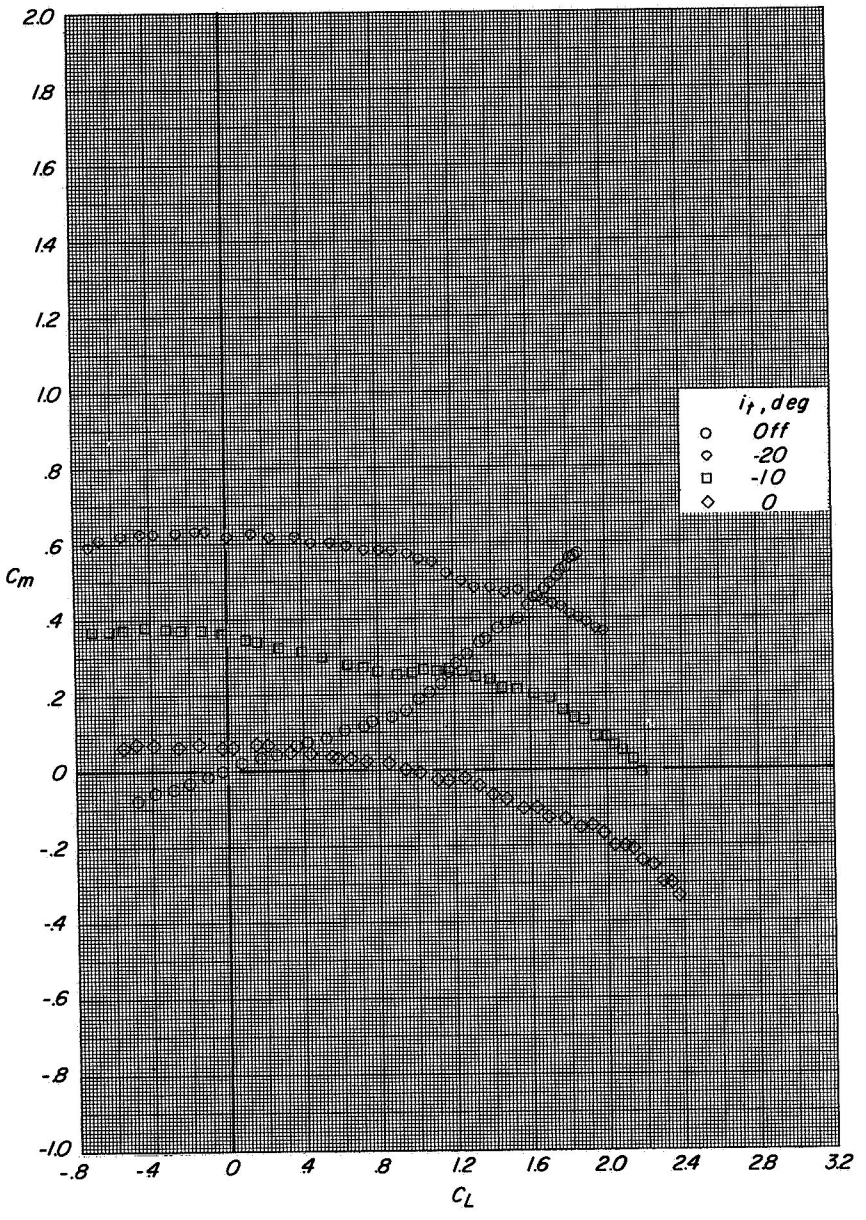

(c) Variation of C_m with C_L.

Figure 9.- Concluded.

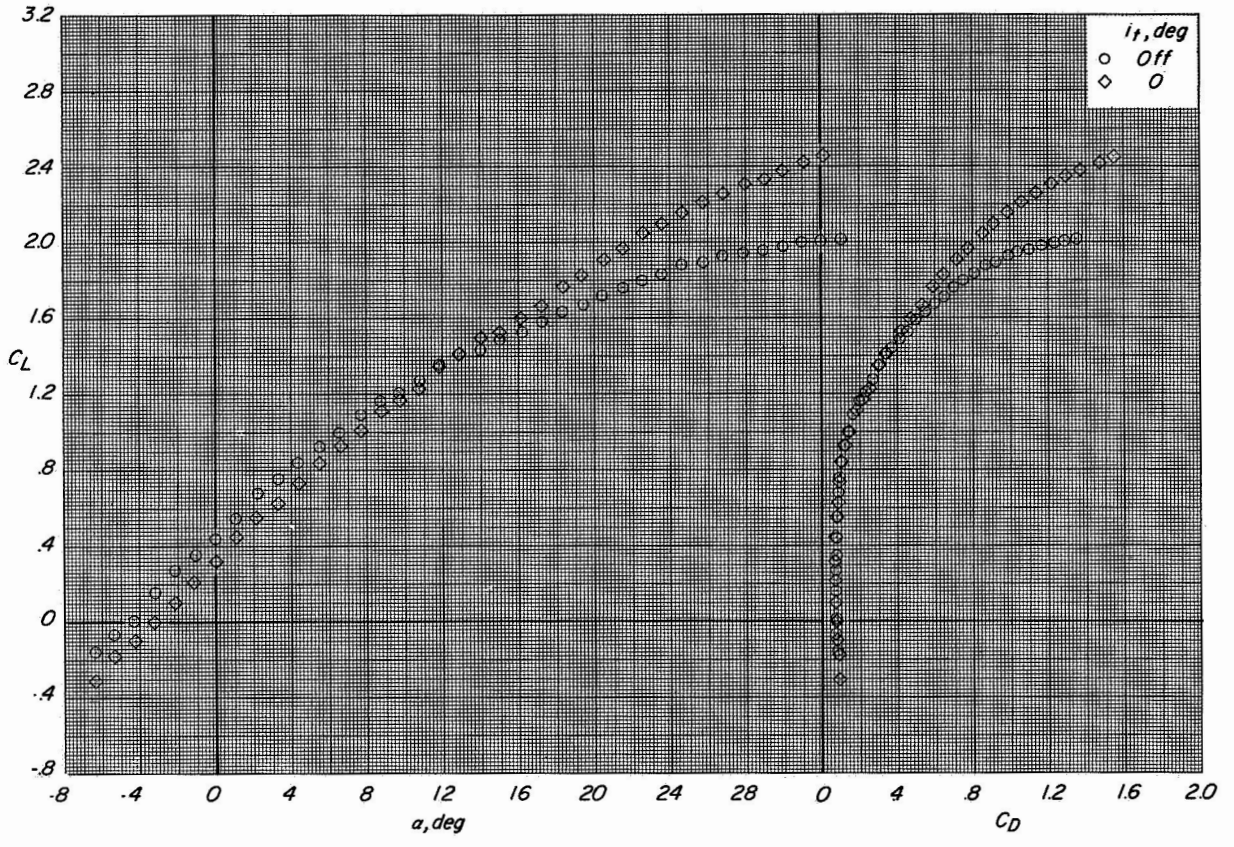

(a) Variation of C_L with α and C_D with C_L.

Figure 10.- Longitudinal aerodynamic characteristics of model. $\delta_{LE,OB} = 0^\circ$; $\delta_{LE,IB} = 0^\circ$; $\delta_{TE,W} = 0^\circ$; $\delta_{LE,ST} = 0^\circ$; $\delta_{TE,ST} = 40^\circ$; $C_T = 0$.

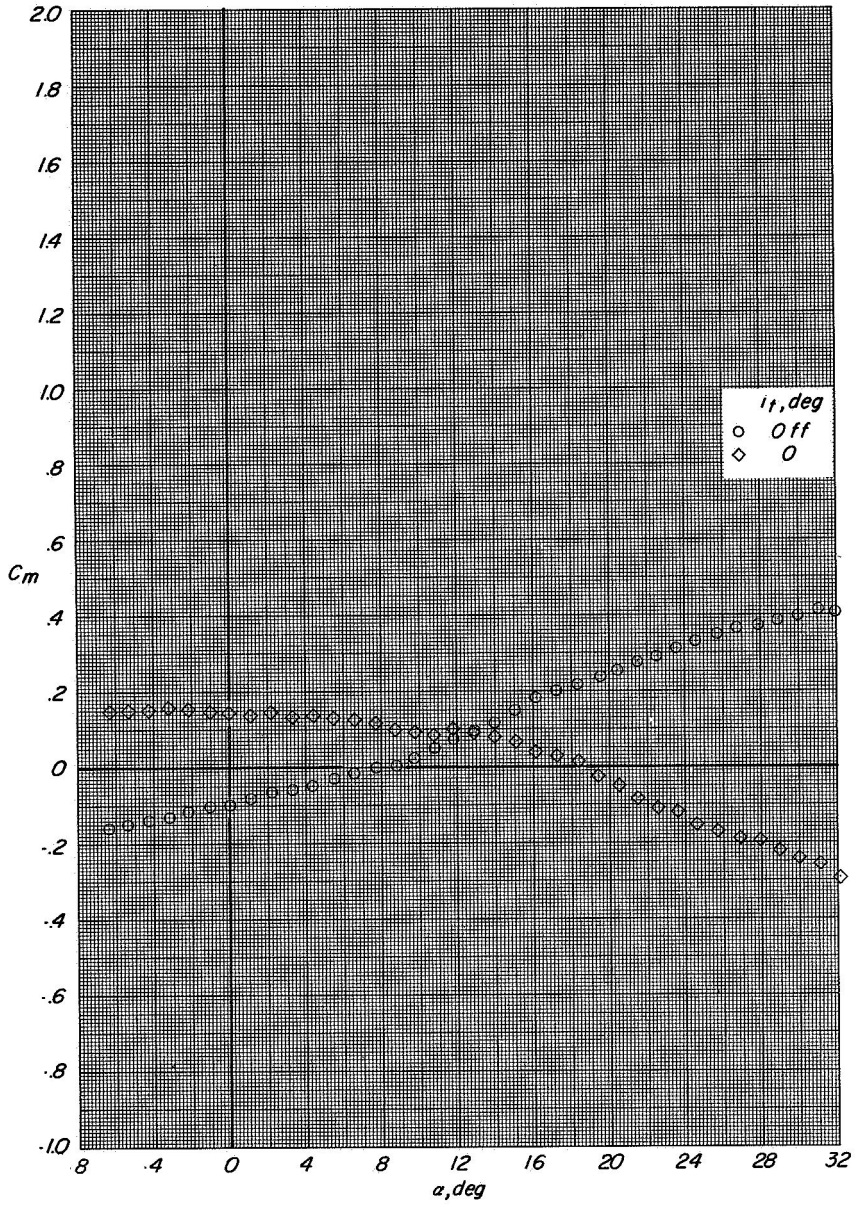

(b) Variation of C_m with α.

Figure 10.- Continued.

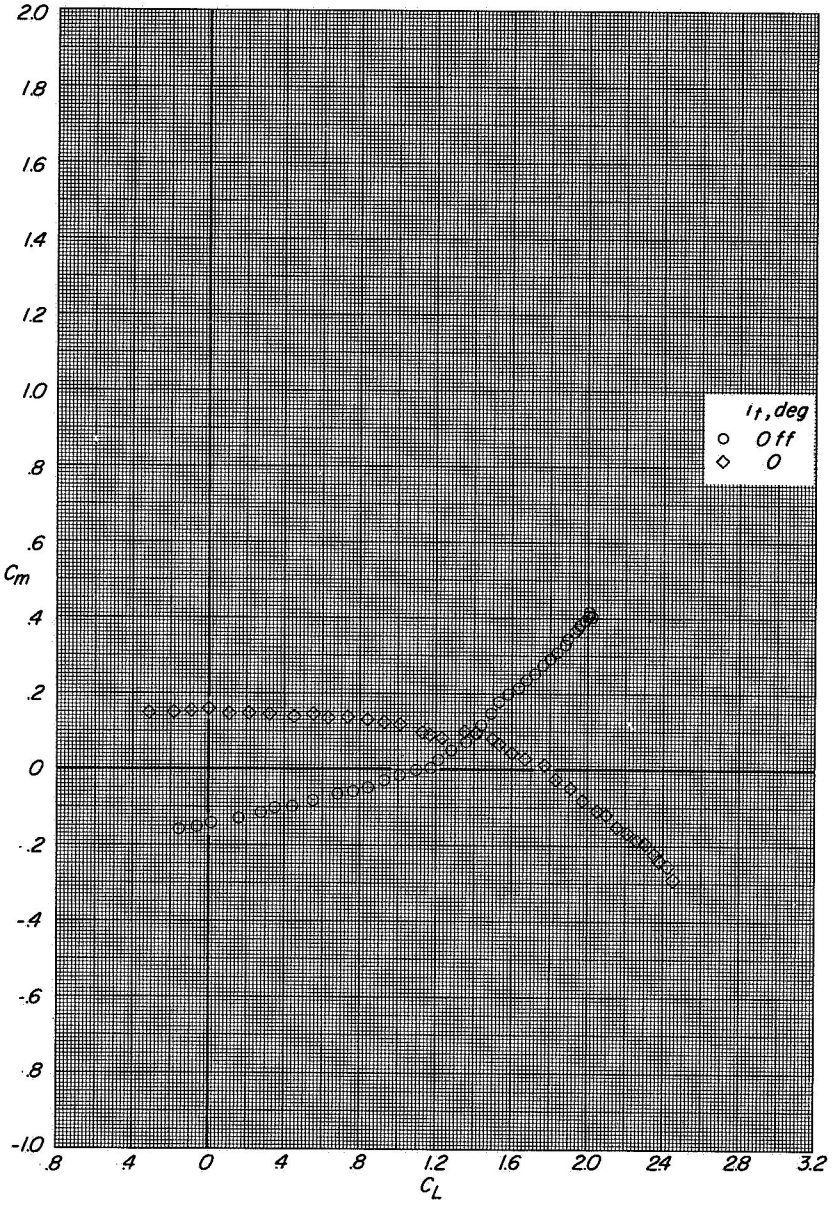

(c) Variation of C_m with C_L.

Figure 10.- Concluded.

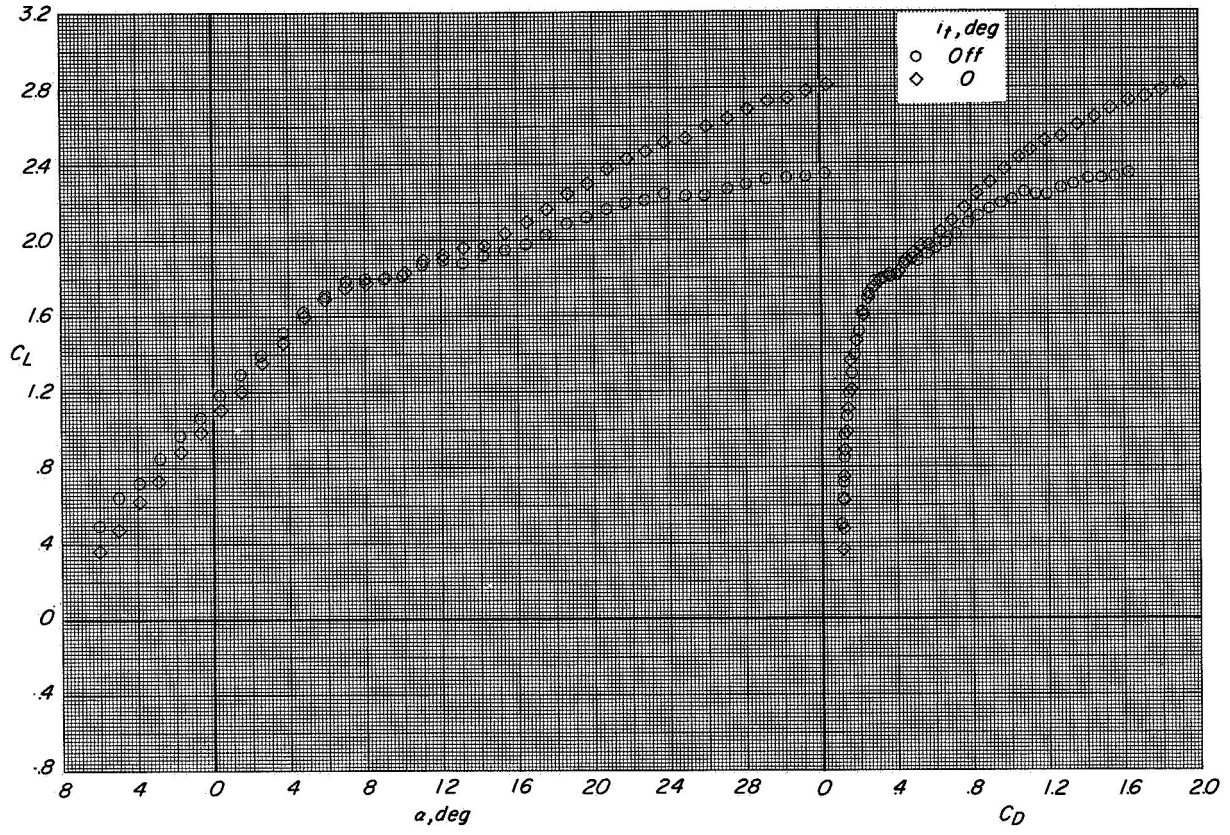

(a) Variation of C_L with α and C_D with C_L.

Figure 11.- Longitudinal aerodynamic characteristics of model. $\delta_{LE,OB} = 0^\circ$; $\delta_{LE,IB} = 0^\circ$; $\delta_{TE,W} = 32^\circ$; $\delta_{LE,ST} = 0^\circ$; $\delta_{TE,ST} = 40^\circ$; $C_T = 0$.

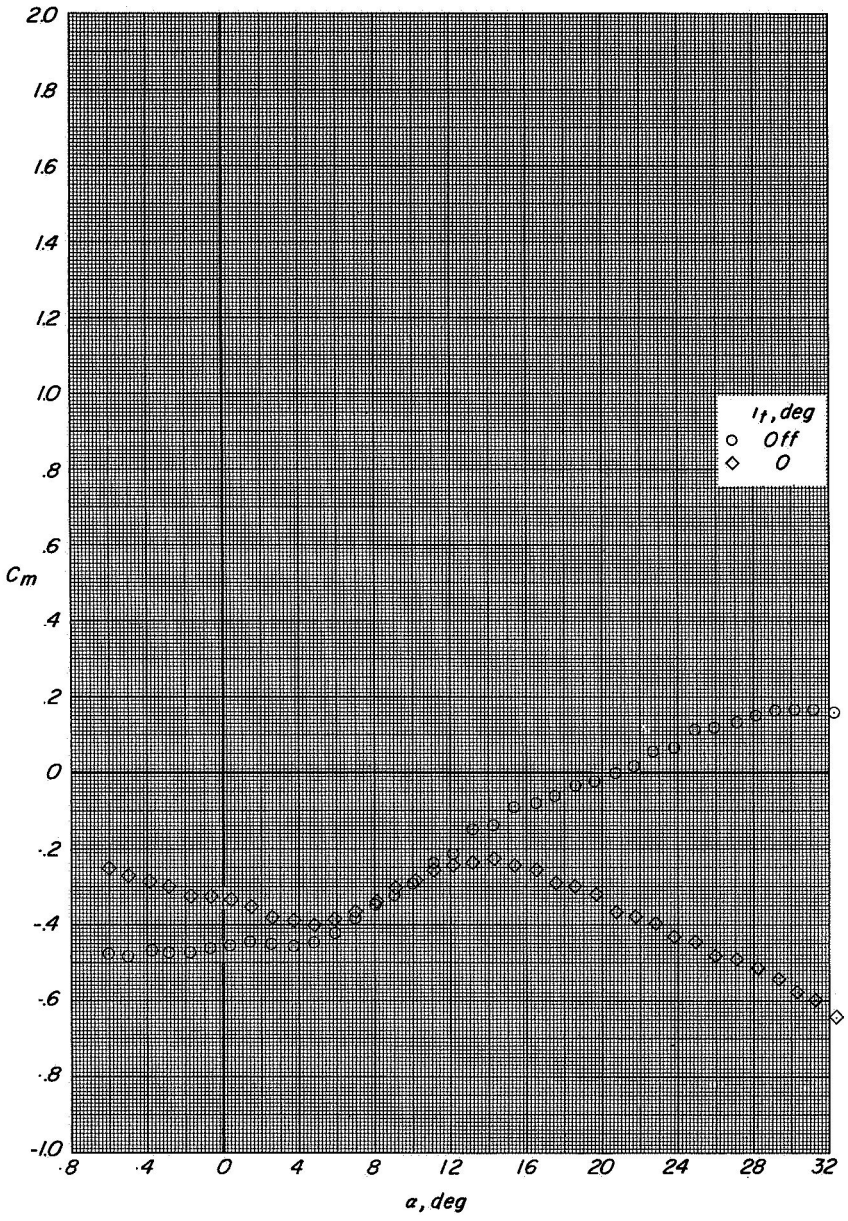

(b) Variation of C_m with α.

Figure 11.- Continued.

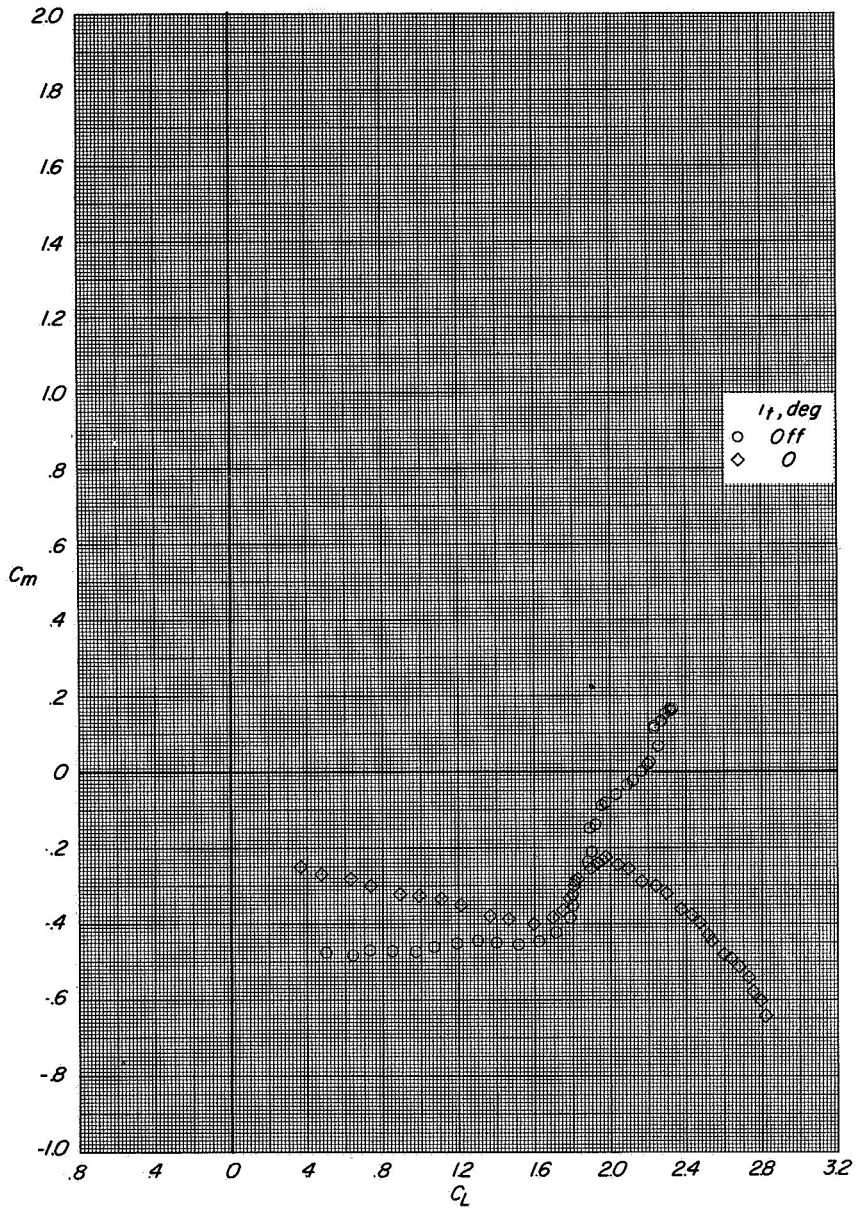

(c) Variation of C_m with C_L.

Figure 11.- Concluded.

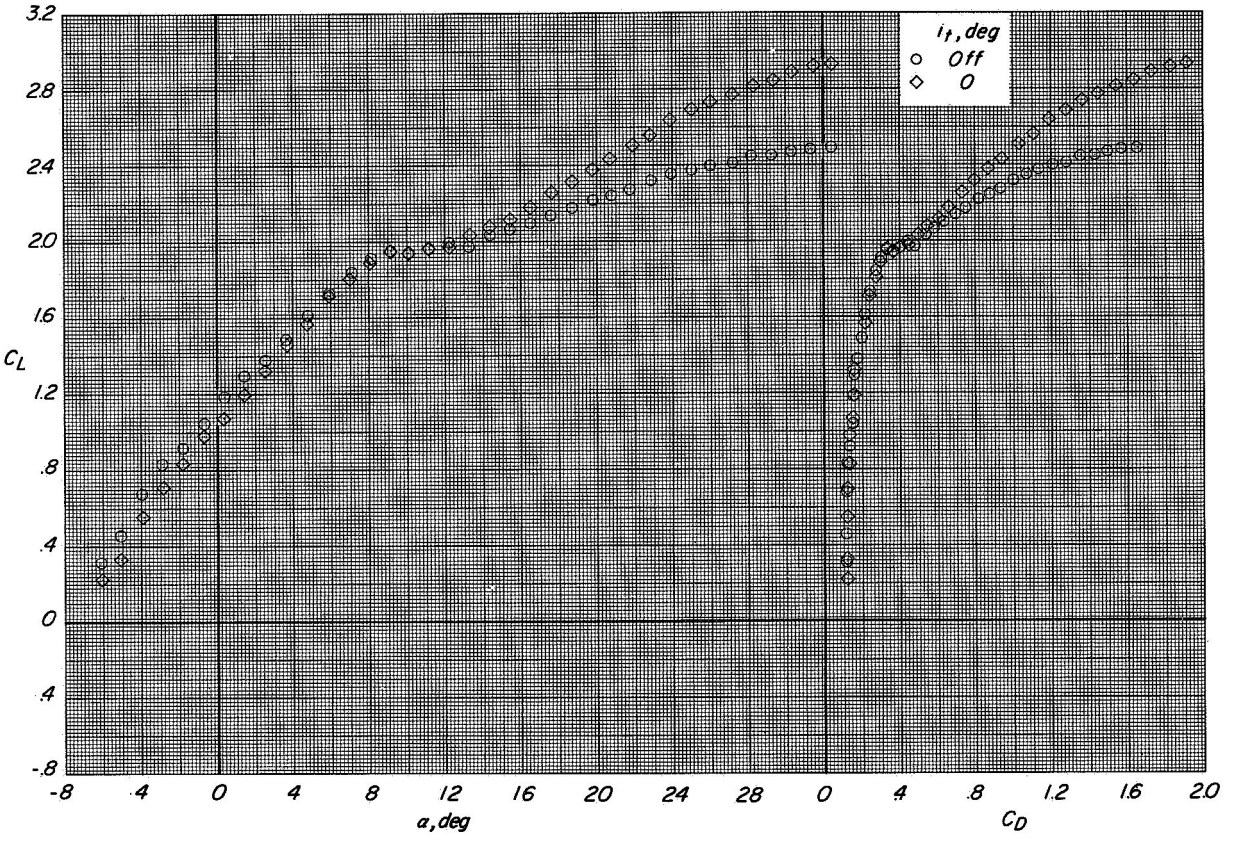

(a) Variation of C_L with α and C_D with C_L.

Figure 12.- Longitudinal aerodynamic characteristics of model. $\delta_{LE,OB} = 0^\circ$; $\delta_{LE,IB} = 30^\circ$; $\delta_{TE,W} = 32^\circ$; $\delta_{LE,ST} = 0^\circ$; $\delta_{TE,ST} = 40^\circ$; $C_T = 0$.

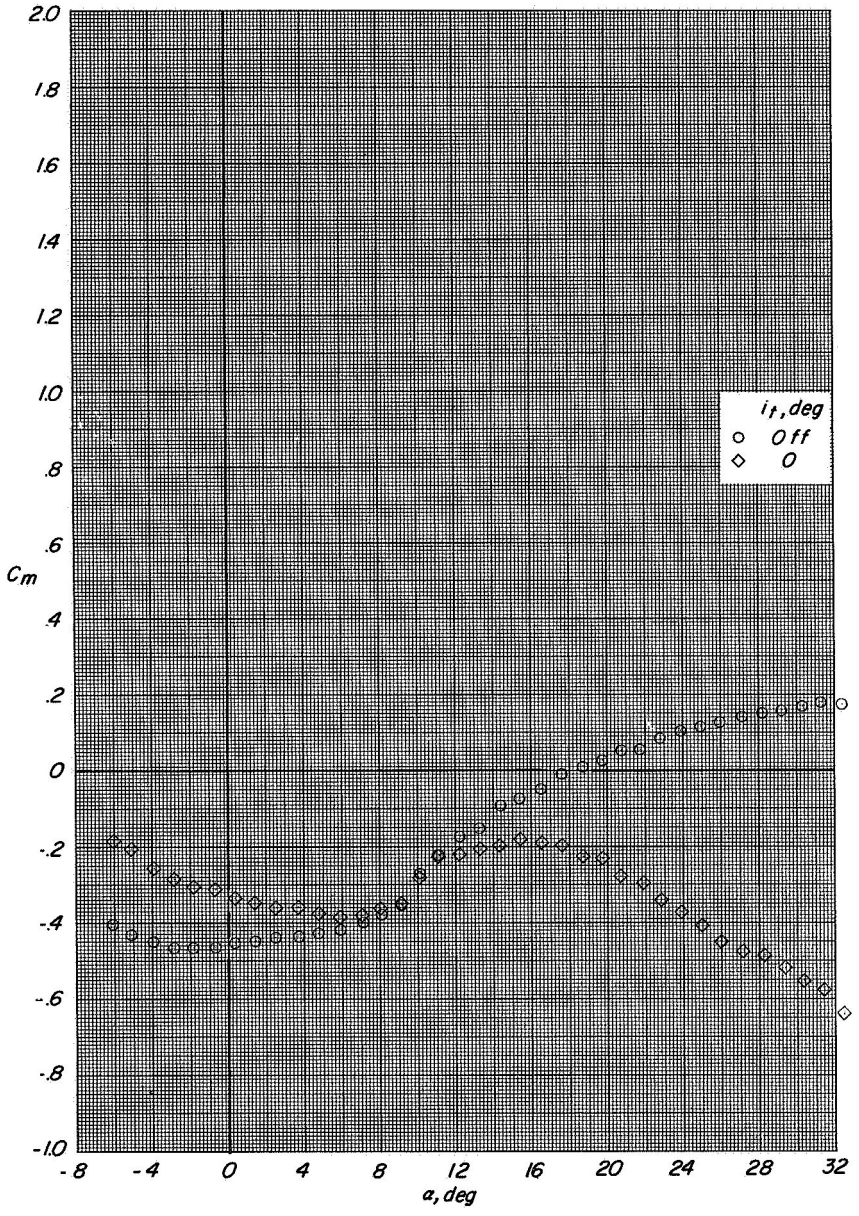

(b) Variation of C_m with α.

Figure 12.- Continued.

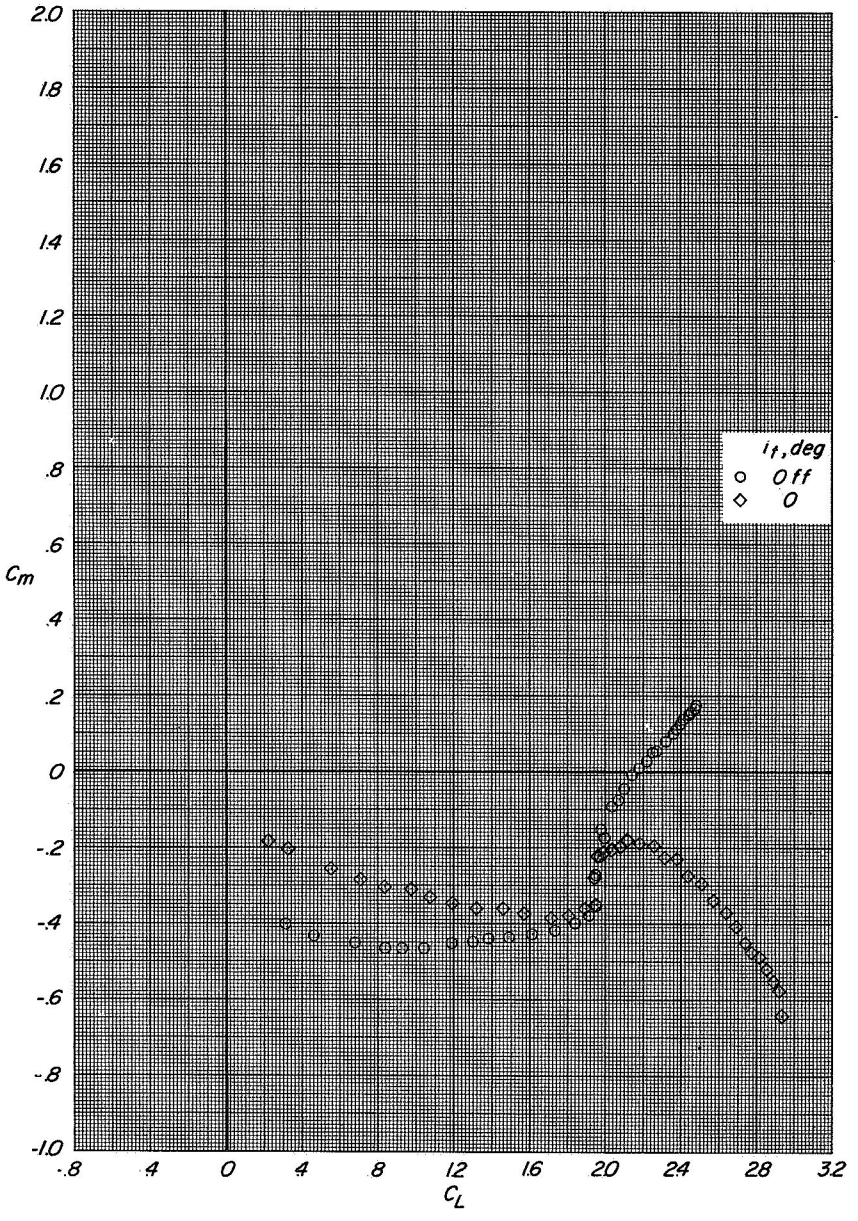

(c) Variation of C_m with C_L.

Figure 12.- Concluded.

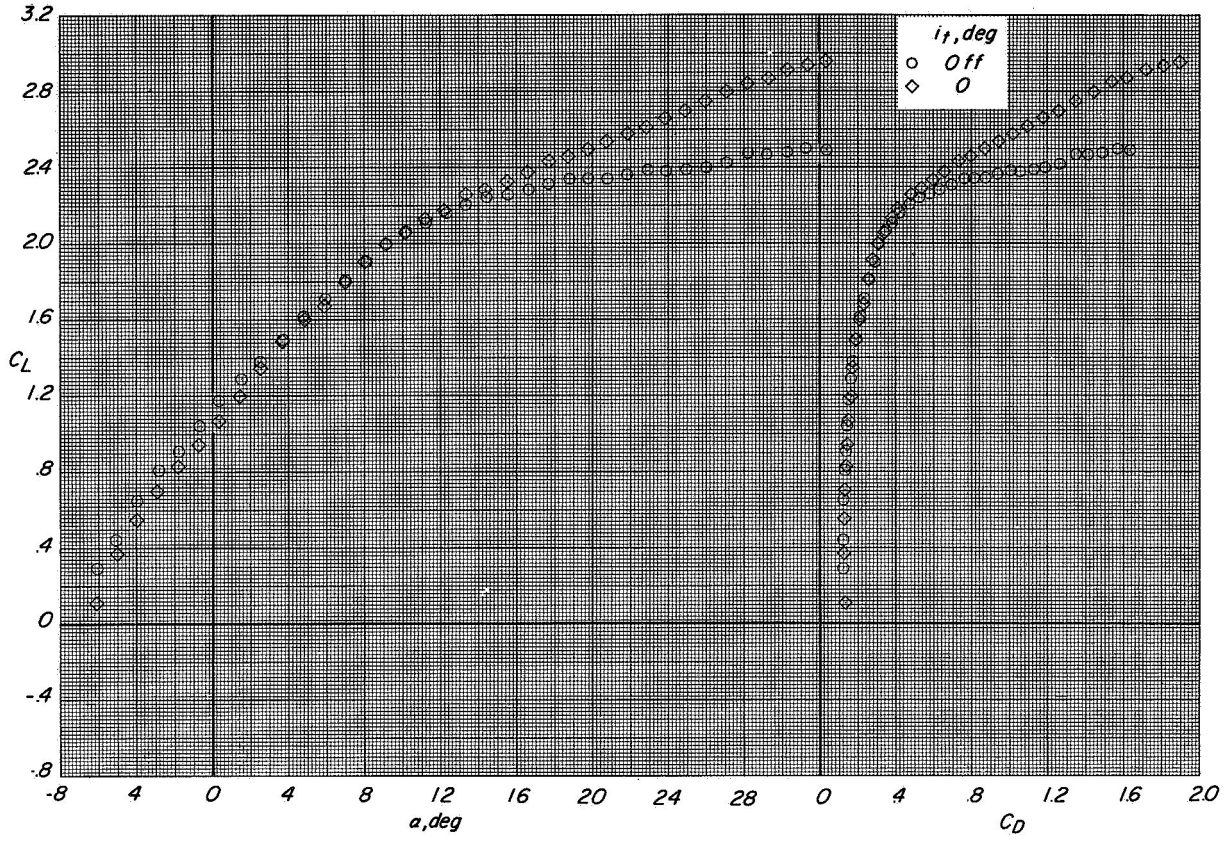

(a) Variation of C_L with α and C_D with C_L.

Figure 13.- Longitudinal aerodynamic characteristics of model. $\delta_{LE,OB} = 30^\circ$; $\delta_{LE,IB} = 30^\circ$; $\delta_{TE,W} = 32^\circ$; $\delta_{LE,ST} = 0^\circ$; $\delta_{TE,ST} = 40^\circ$; $C_T = 0$.

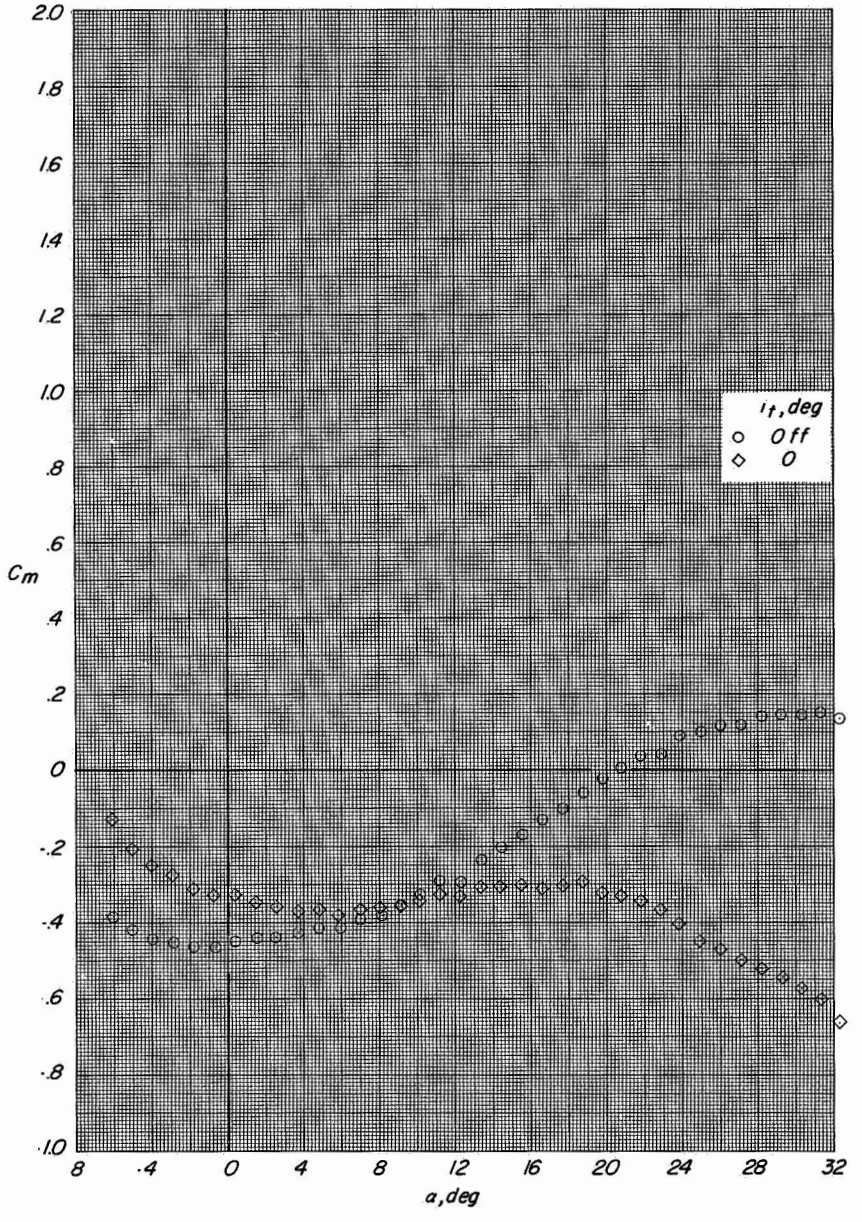

(b) Variation of C_m with α.

Figure 13.- Continued.

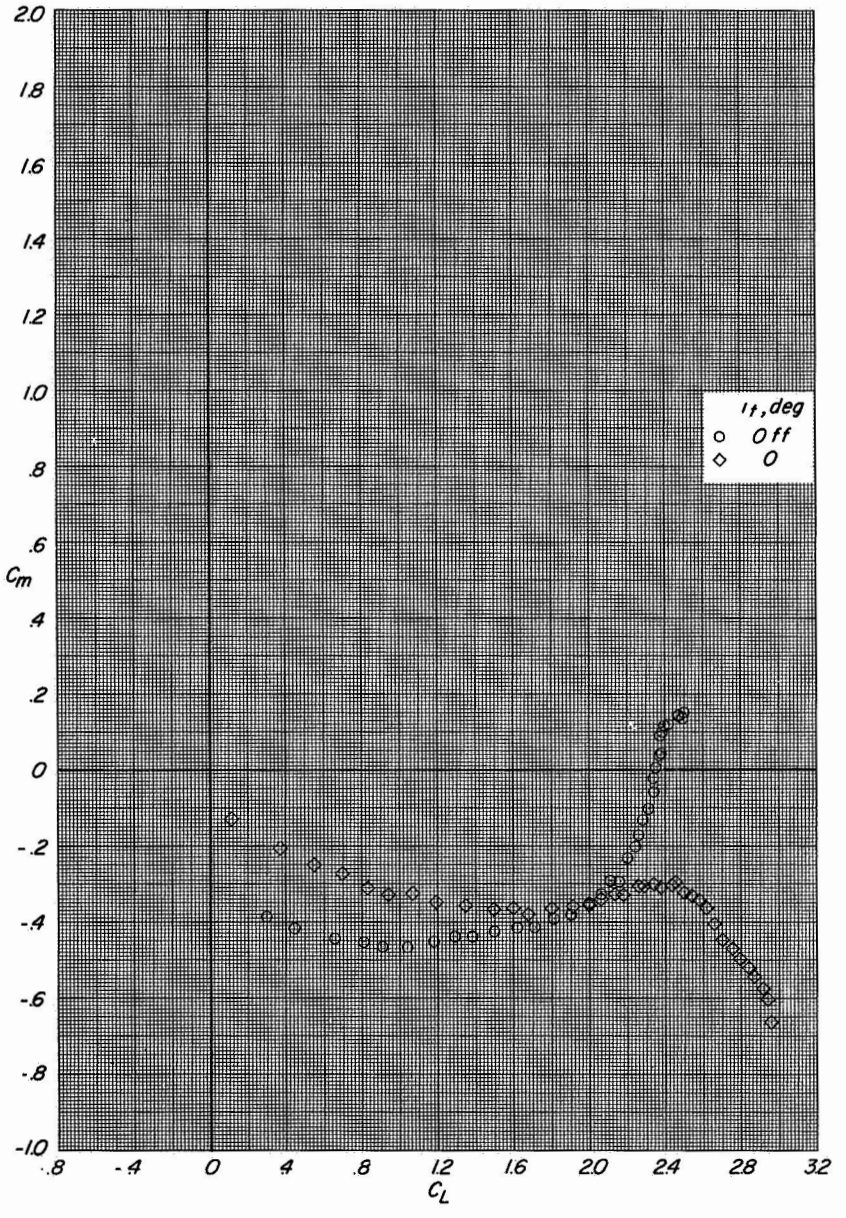

(c) Variation of C_m with C_L.

Figure 13.- Concluded.

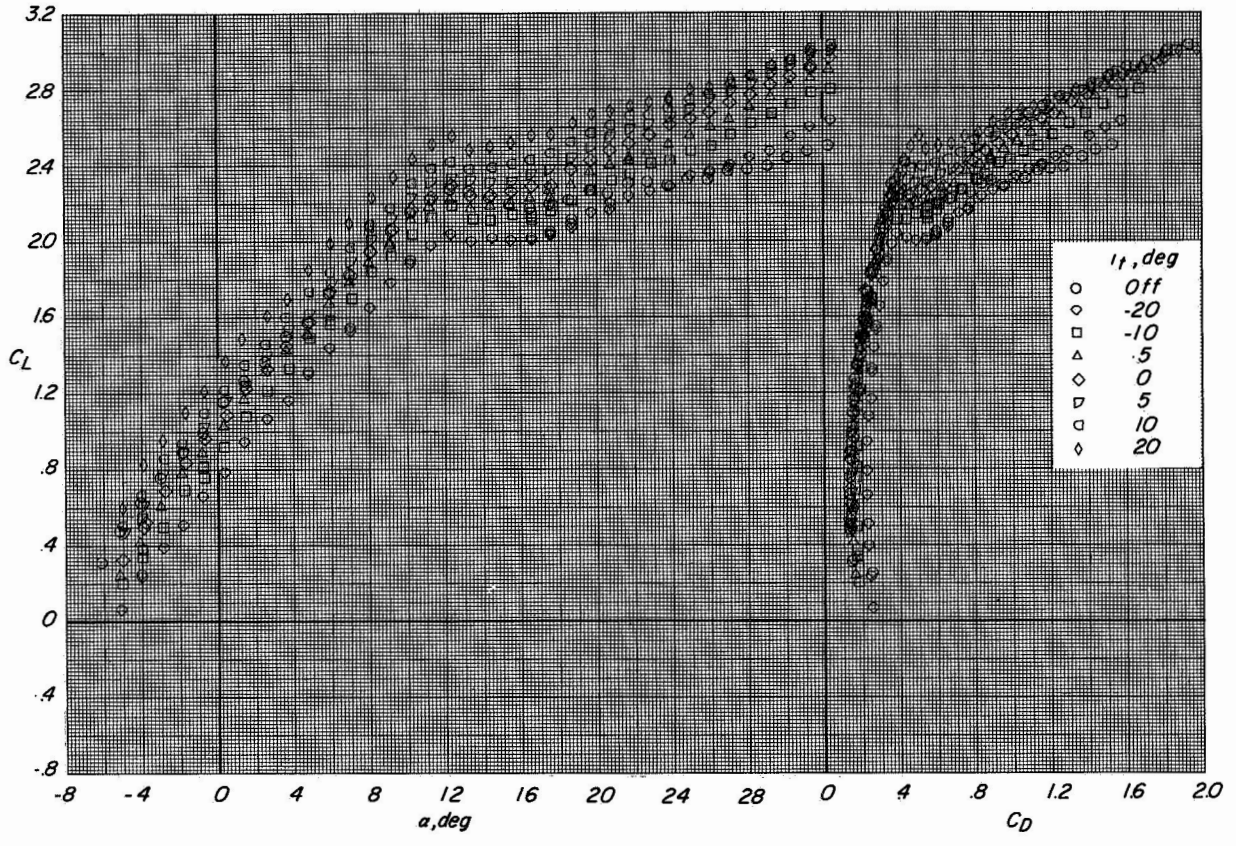

(a) Variation of C_L with α and C_D with C_L.

Figure 14 - Longitudinal aerodynamic characteristics of model. $\delta_{LE,OB} = 30^\circ$; $\delta_{LE,IB} = 30^\circ$; $\delta_{TE,W} = 32^\circ$; $\delta_{LE,ST} = 45^\circ$; $\delta_{TE,ST} = 40^\circ$; $C_T = 0$.

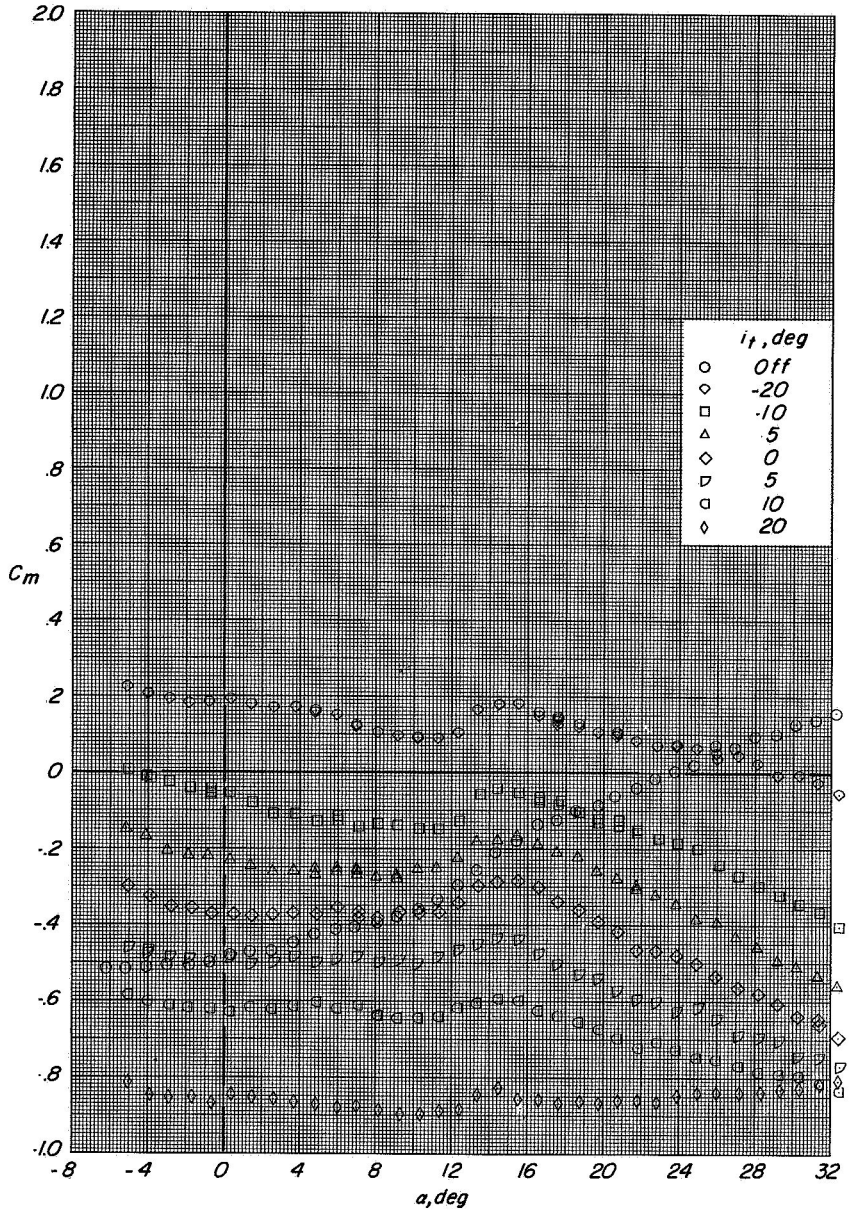

(b) Variation of C_m with α.

Figure 14.- Continued.

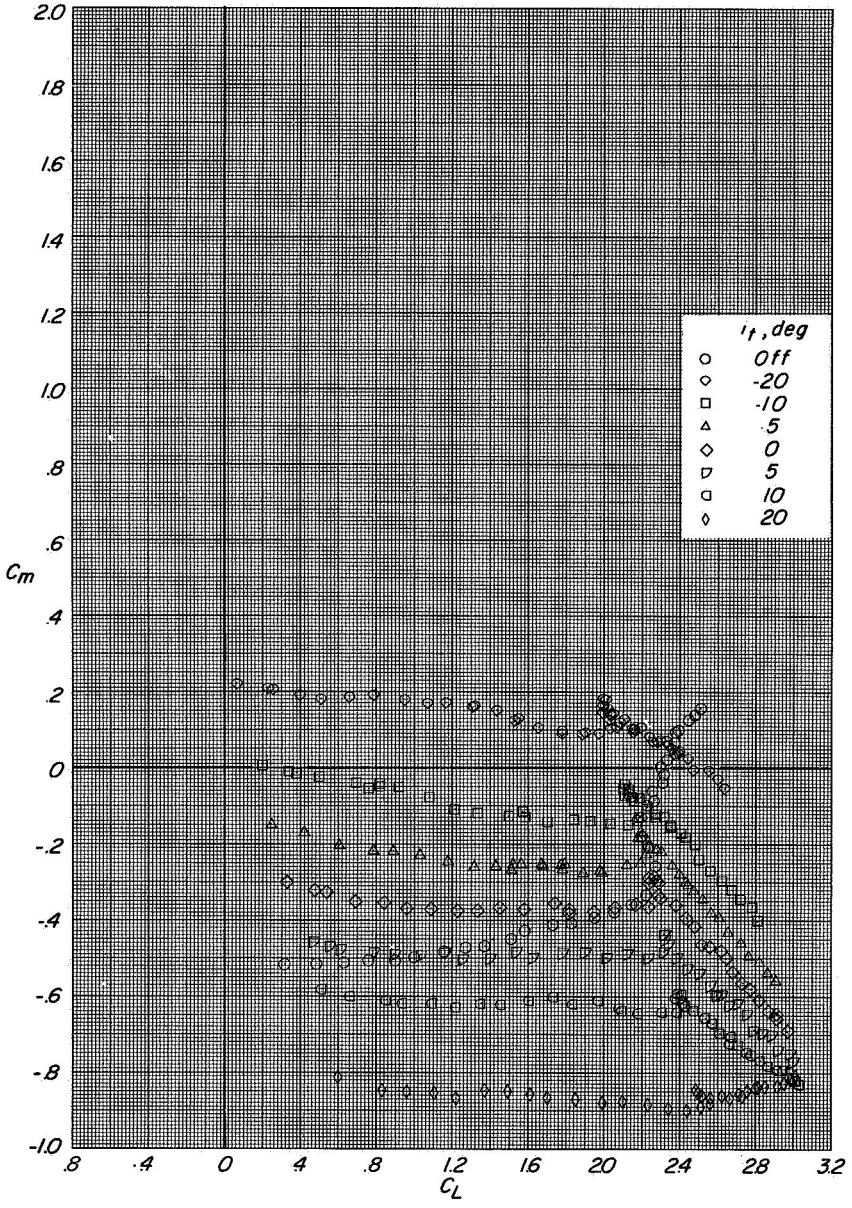

(c) Variation of C_m with C_L.

Figure 14.- Concluded.

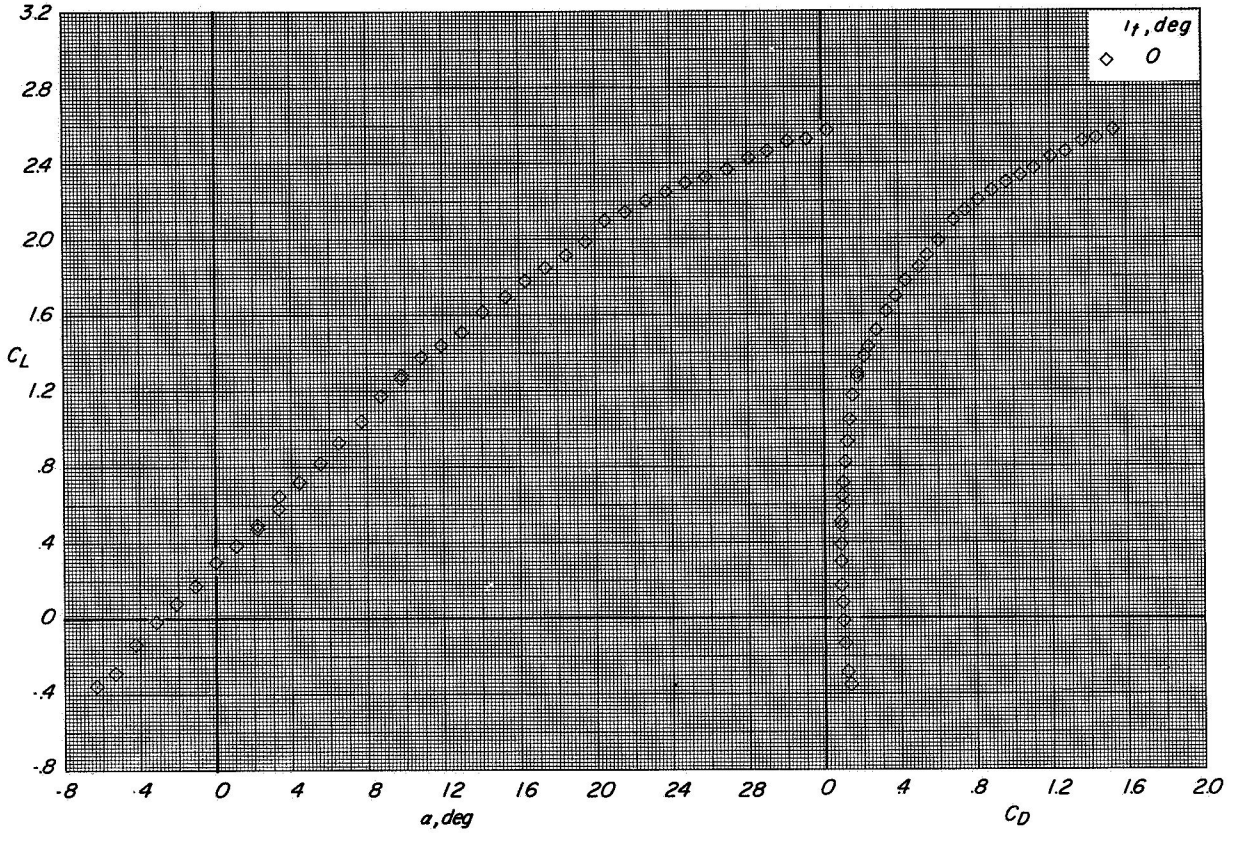

(a) Variation of C_L with α and C_D with C_L.

Figure 15.- Longitudinal aerodynamic characteristics of model. $\delta_{LE,OB} = 30^\circ$; $\delta_{LE,IB} = 30^\circ$; $\delta_{TE,W} = 0^\circ$; $\delta_{LE,ST} = 0^\circ$; $\delta_{TE,ST} = 40^\circ$; $C_T = 0$.

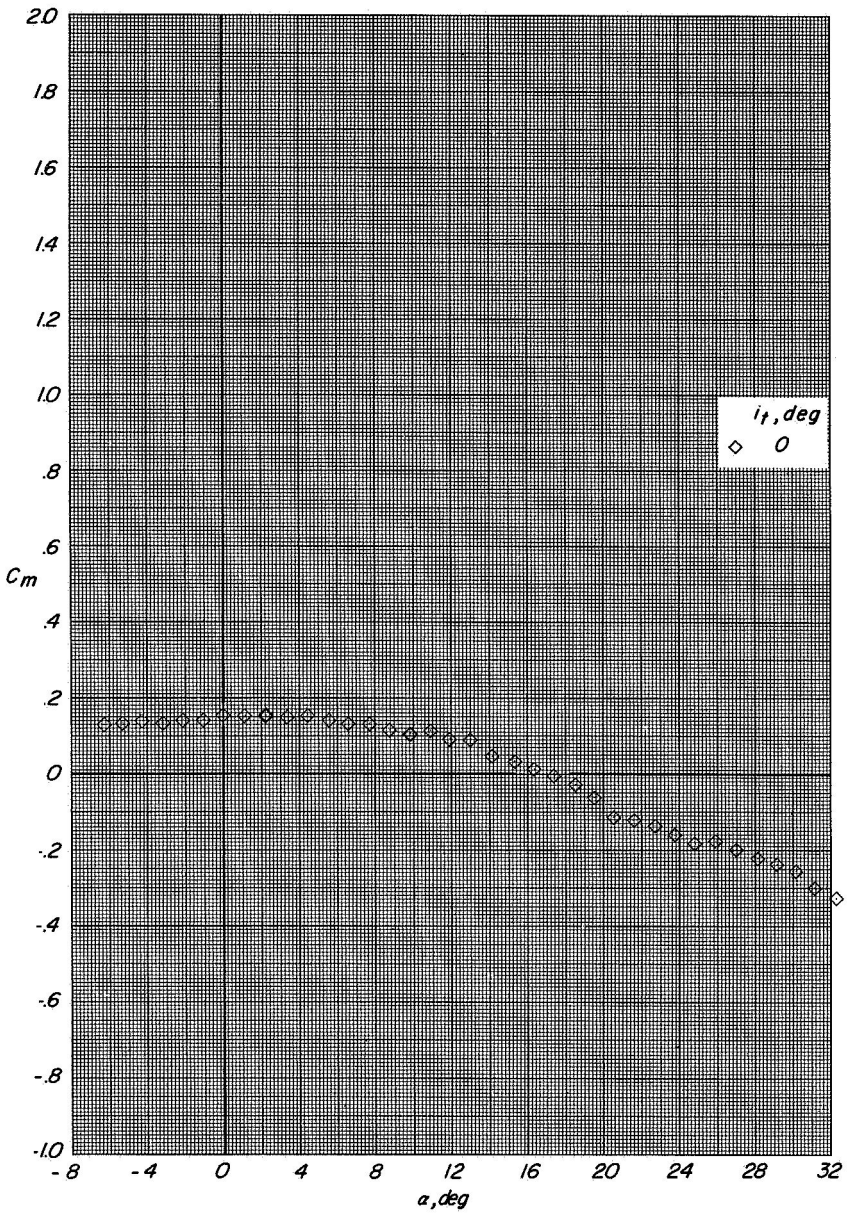

(b) Variation of C_m with α.

Figure 15.- Continued.

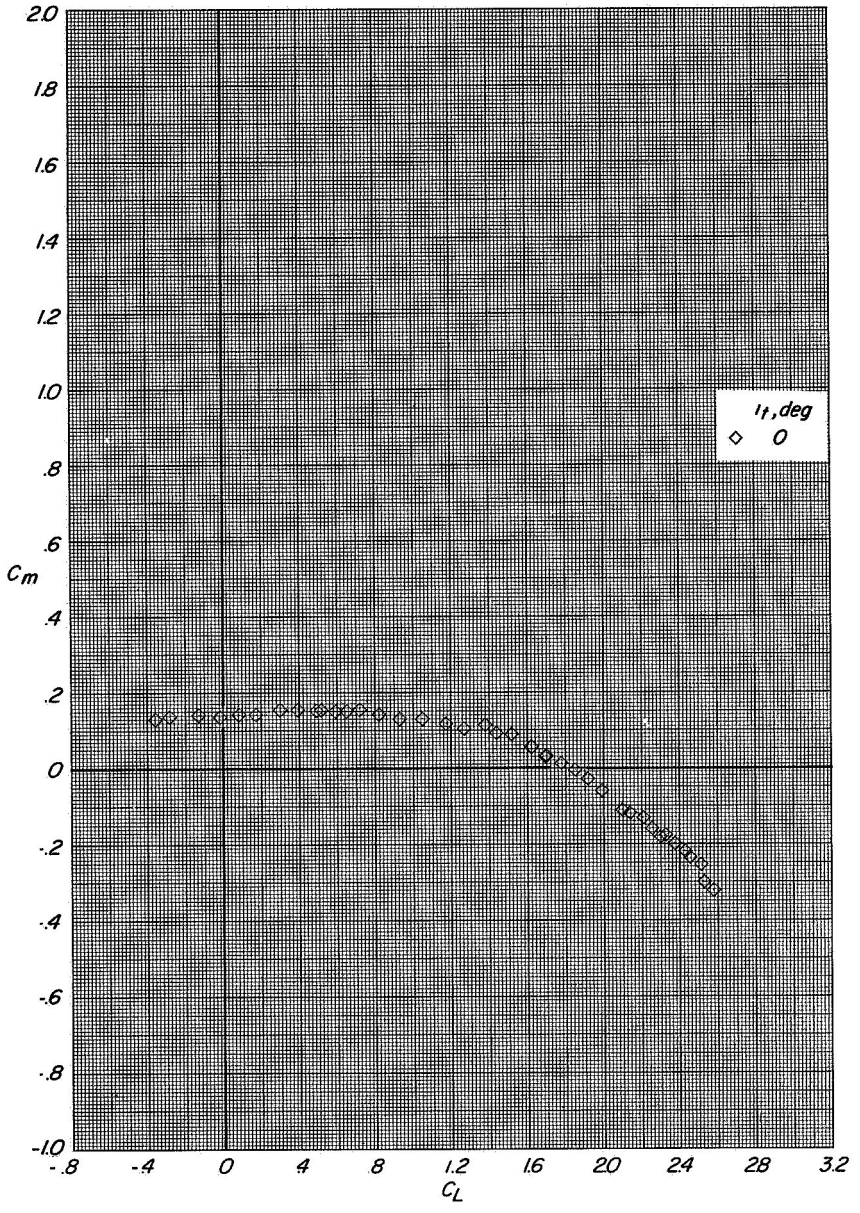

(c) Variation of C_m with C_L.

Figure 15.- Concluded.

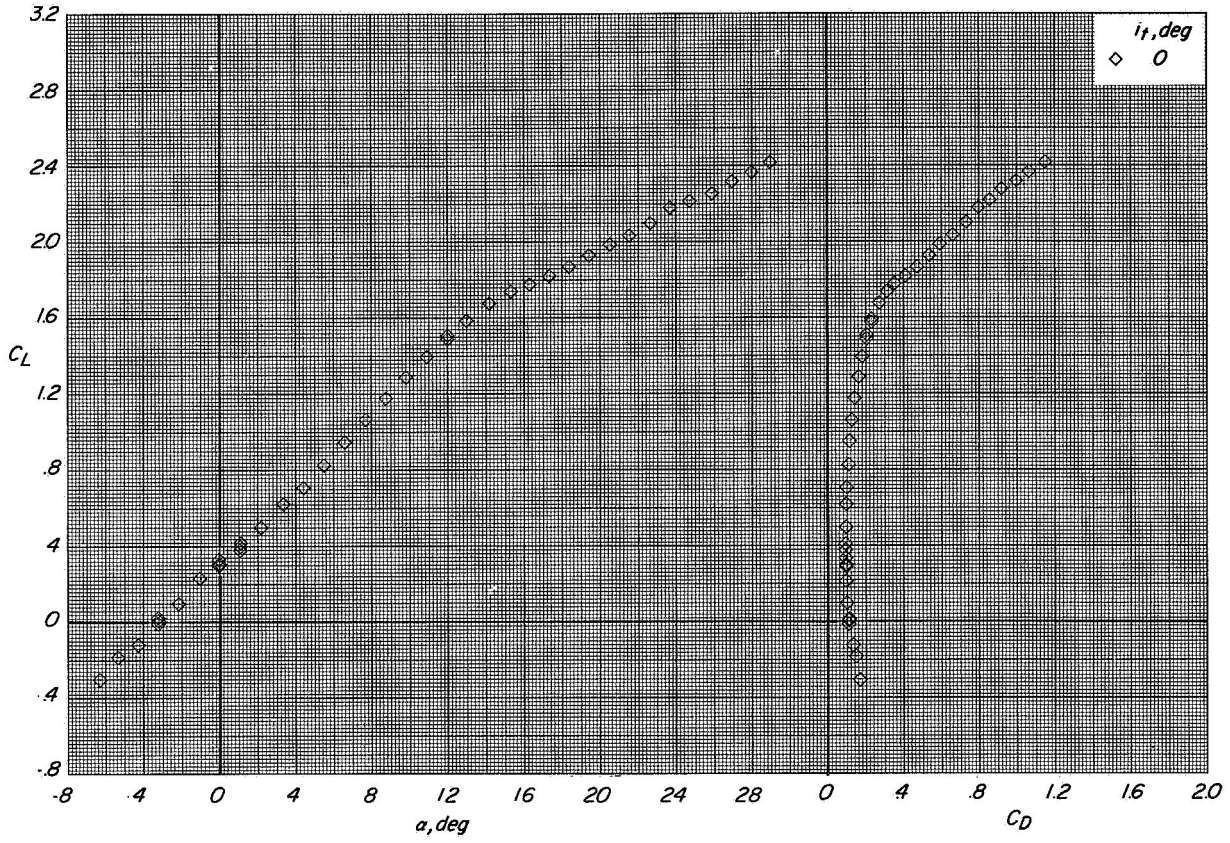

(a) Variation of C_L with α and C_D with C_L

Figure 16.- Longitudinal aerodynamic characteristics of model. $\delta_{LE,OB} = 30^\circ$; $\delta_{LE,IB} = 30^\circ$; $\delta_{TE,W} = 0^\circ$; $\delta_{LE,ST} = 45^\circ$; $\delta_{TE,ST} = 40^\circ$; $C_T = 0$.

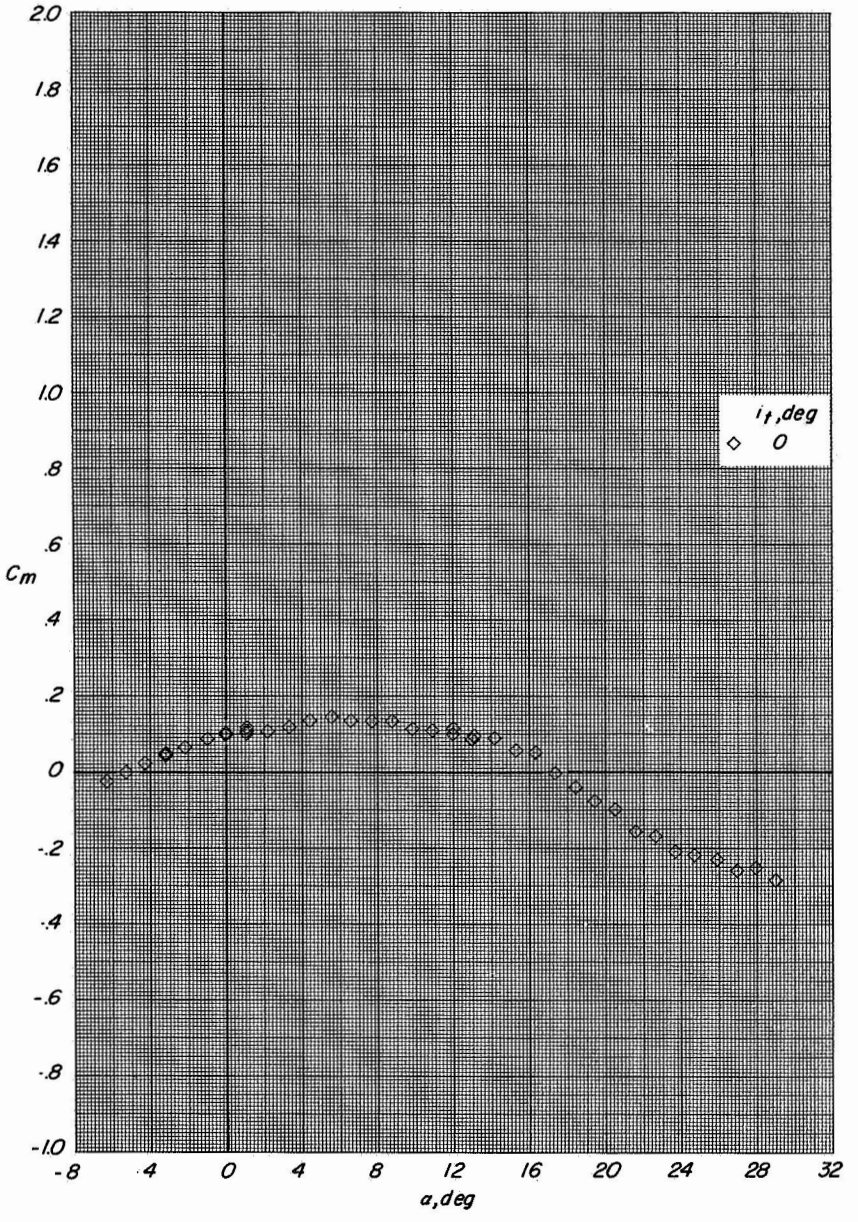

(b) Variation of C_m with α.

Figure 16.- Continued.

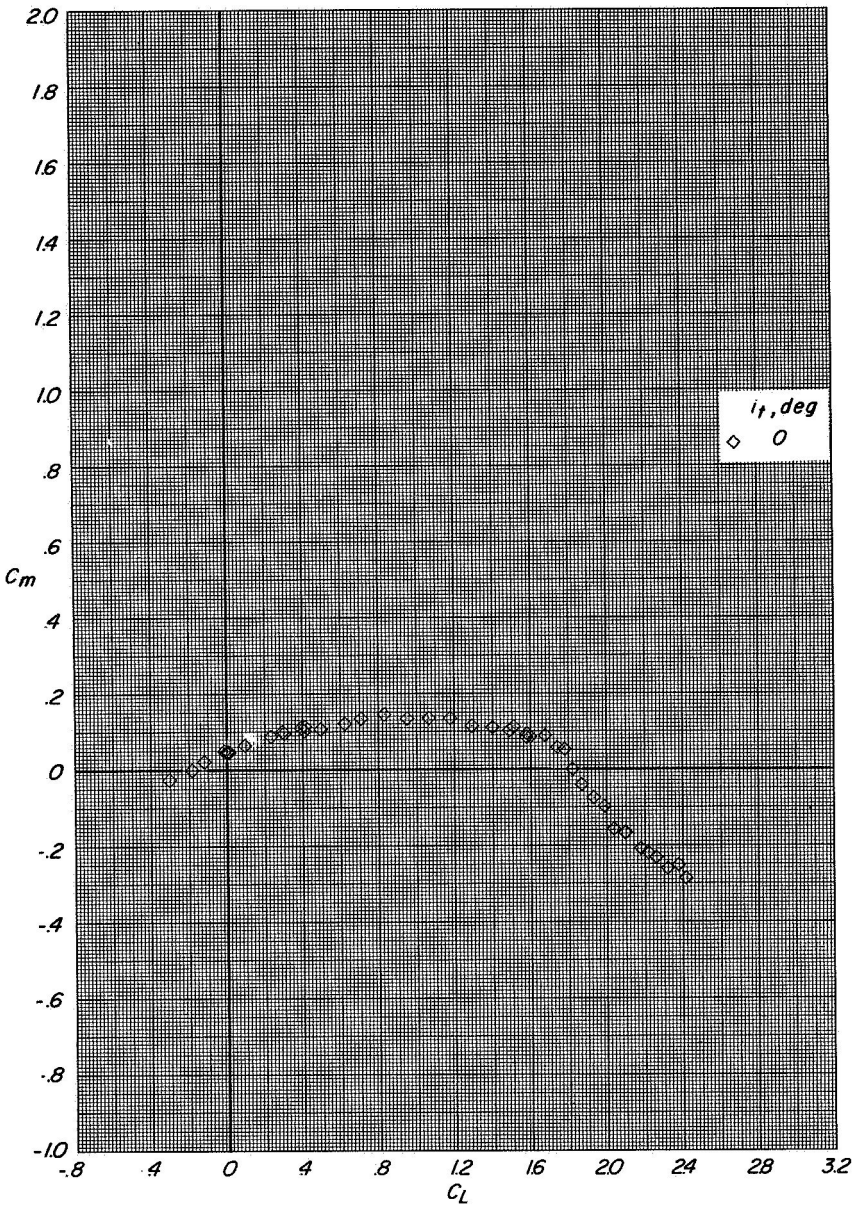

(c) Variation of C_m with C_L.

Figure 16.- Concluded.

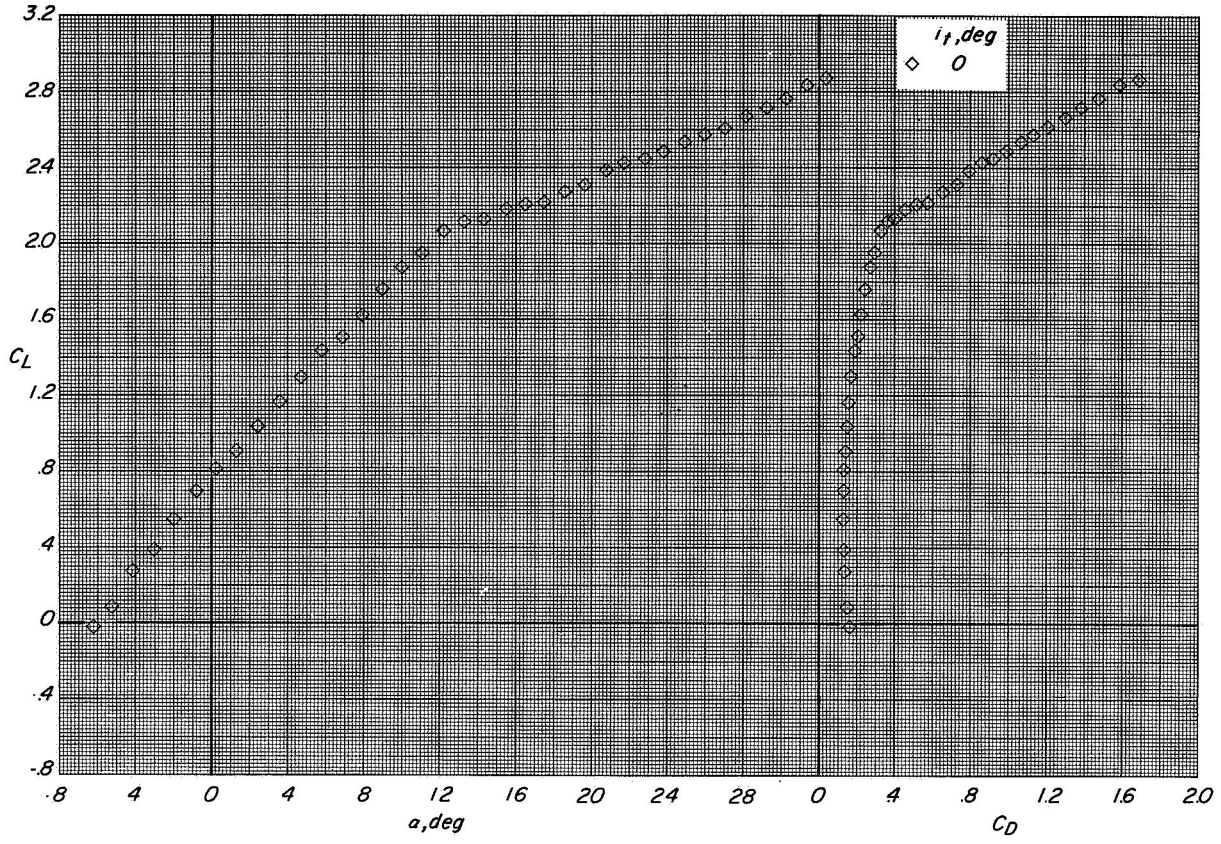

(a) Variation of C_L with α and C_D with C_L.

Figure 17.- Longitudinal aerodynamics characteristics of model. $\delta_{LE,OB} = 30^\circ$; $\delta_{LE,IB} = 30^\circ$; $\delta_{TE,W,P} = 32^\circ$; $\delta_{LE,ST} = 45^\circ$; $\delta_{TE,ST} = 40^\circ$; $C_T = 0$.

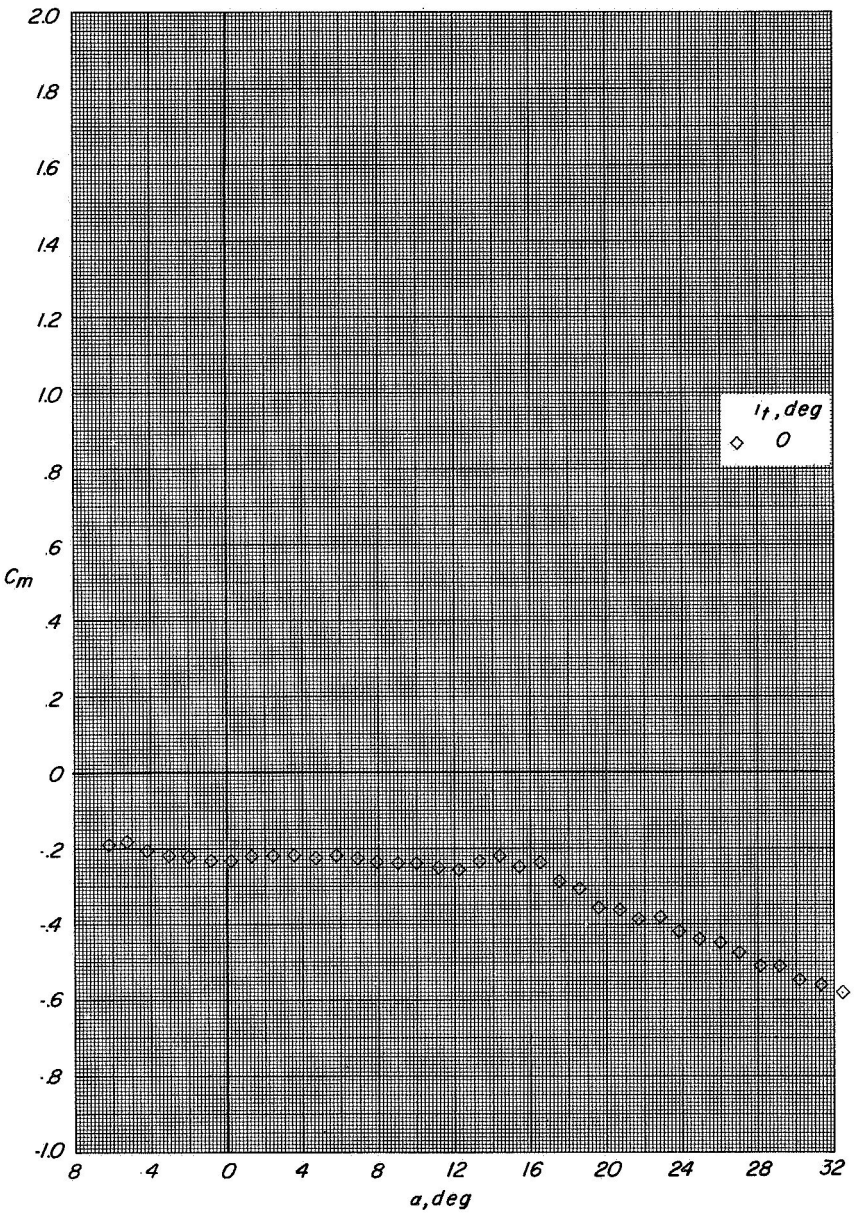

(b) Variation of C_m with α.

Figure 17 - Continued.

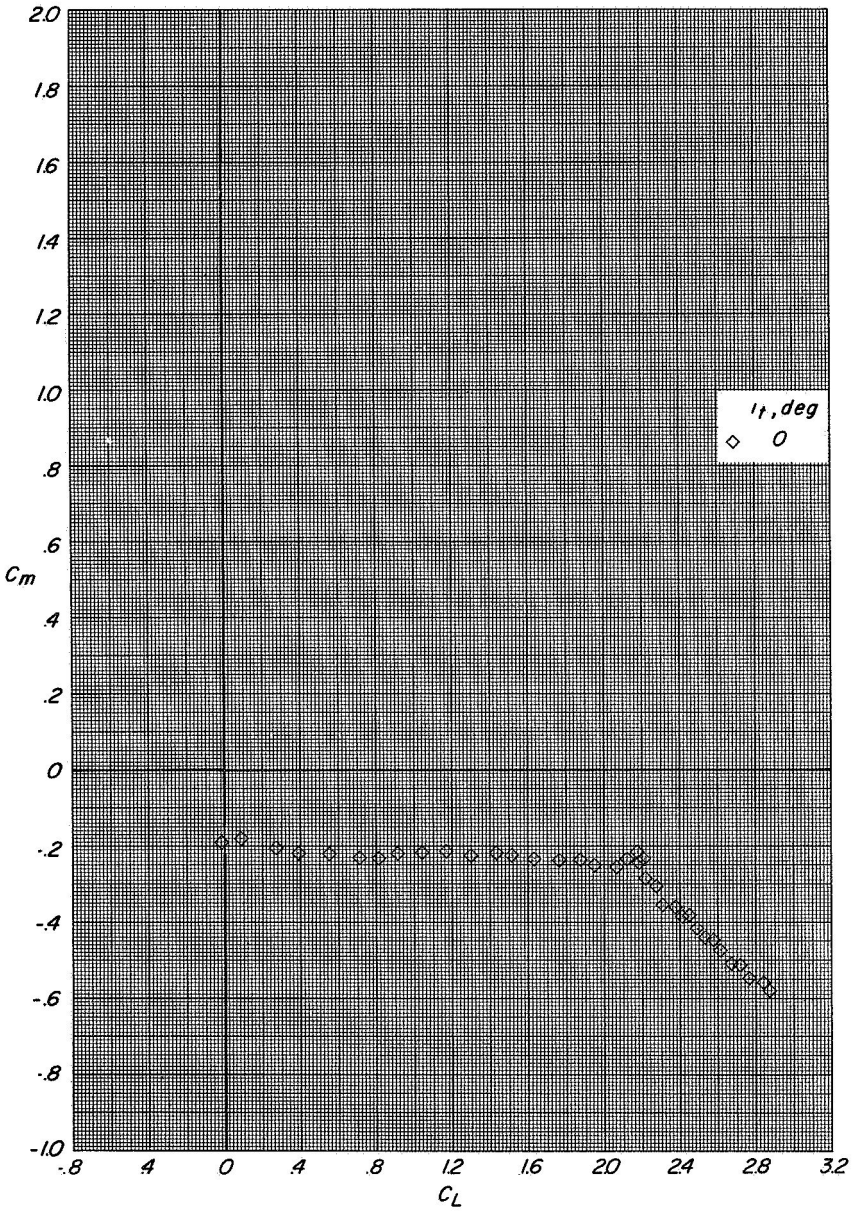

(c) Variation of C_m with C_L.

Figure 17.- Concluded.

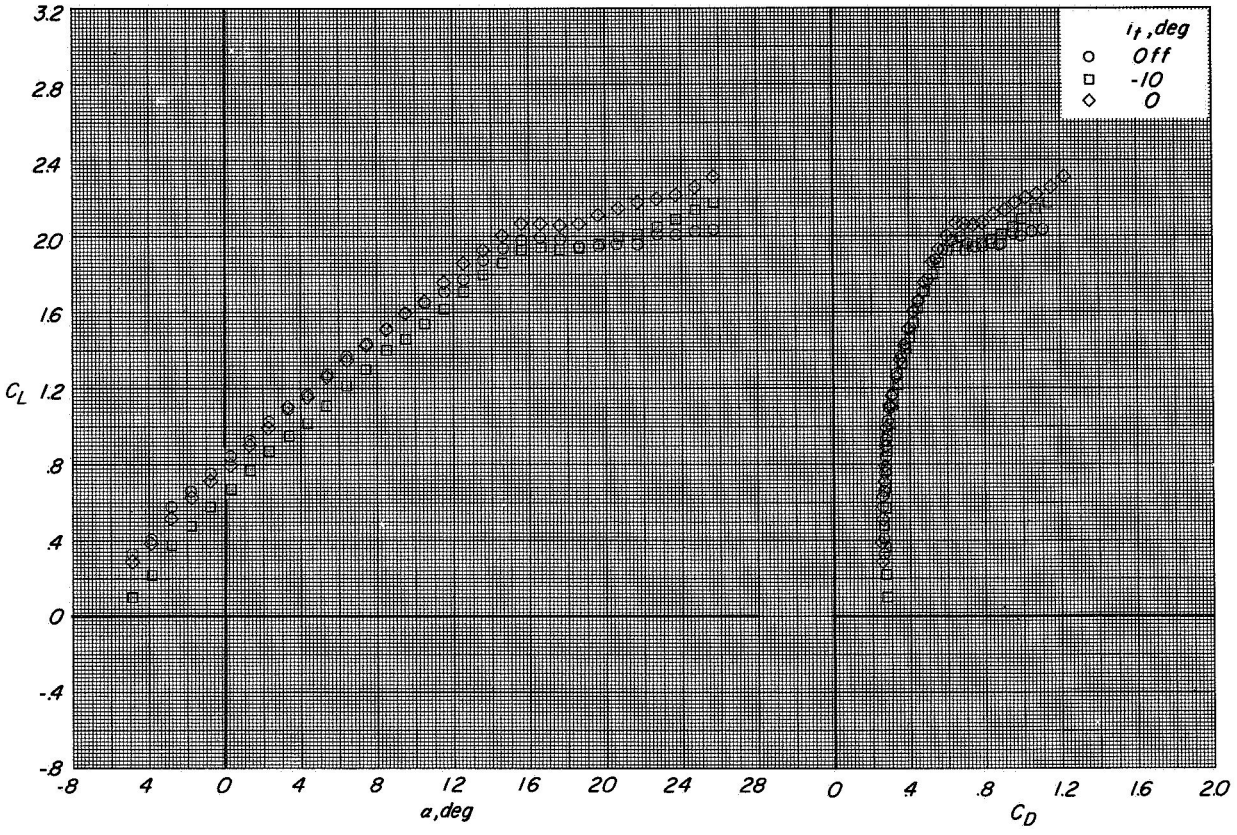

(a) Variation of C_L with α and C_D with C_L.

Figure 18.- Longitudinal aerodynamic characteristics of configuration A with direct-lift engines and lift-cruise engines deflected 90°. C_T = 0.

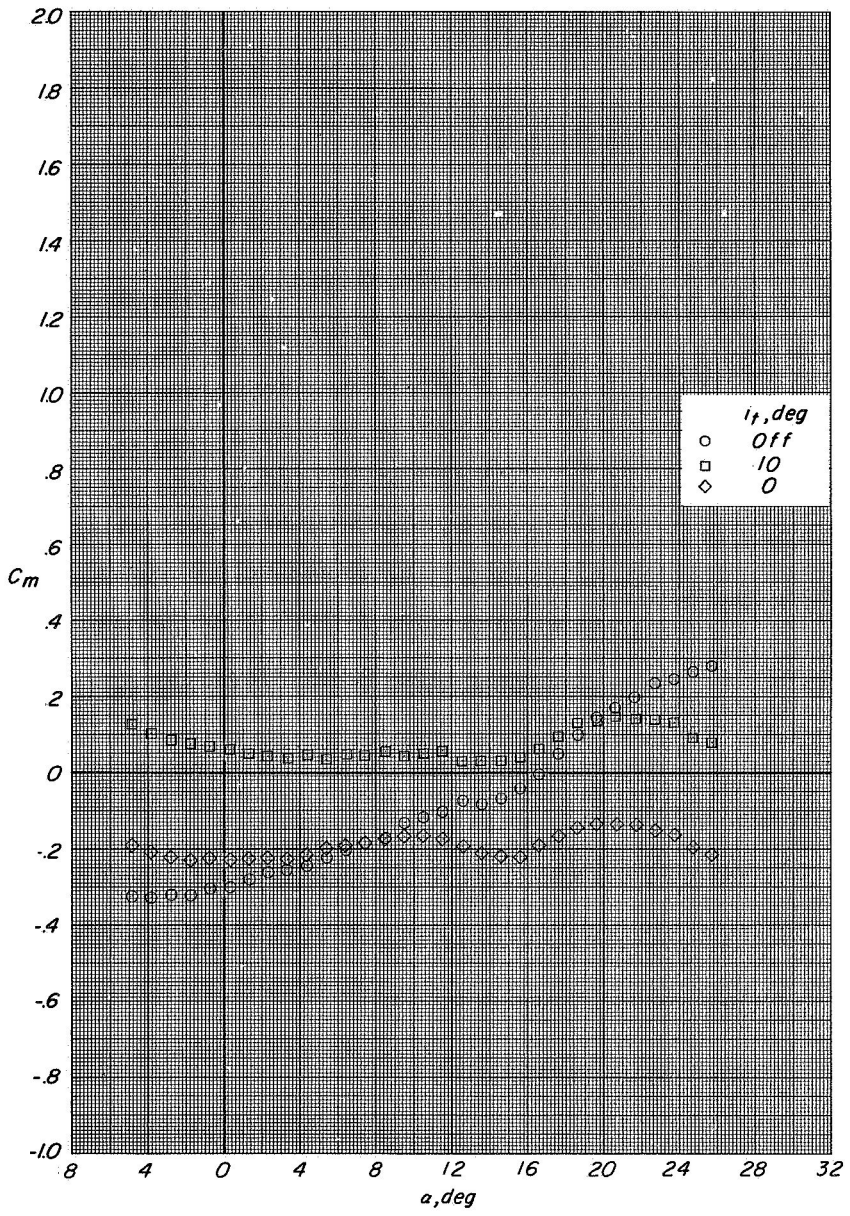

(b) Variation of C_m with α.

Figure 18.- Continued.

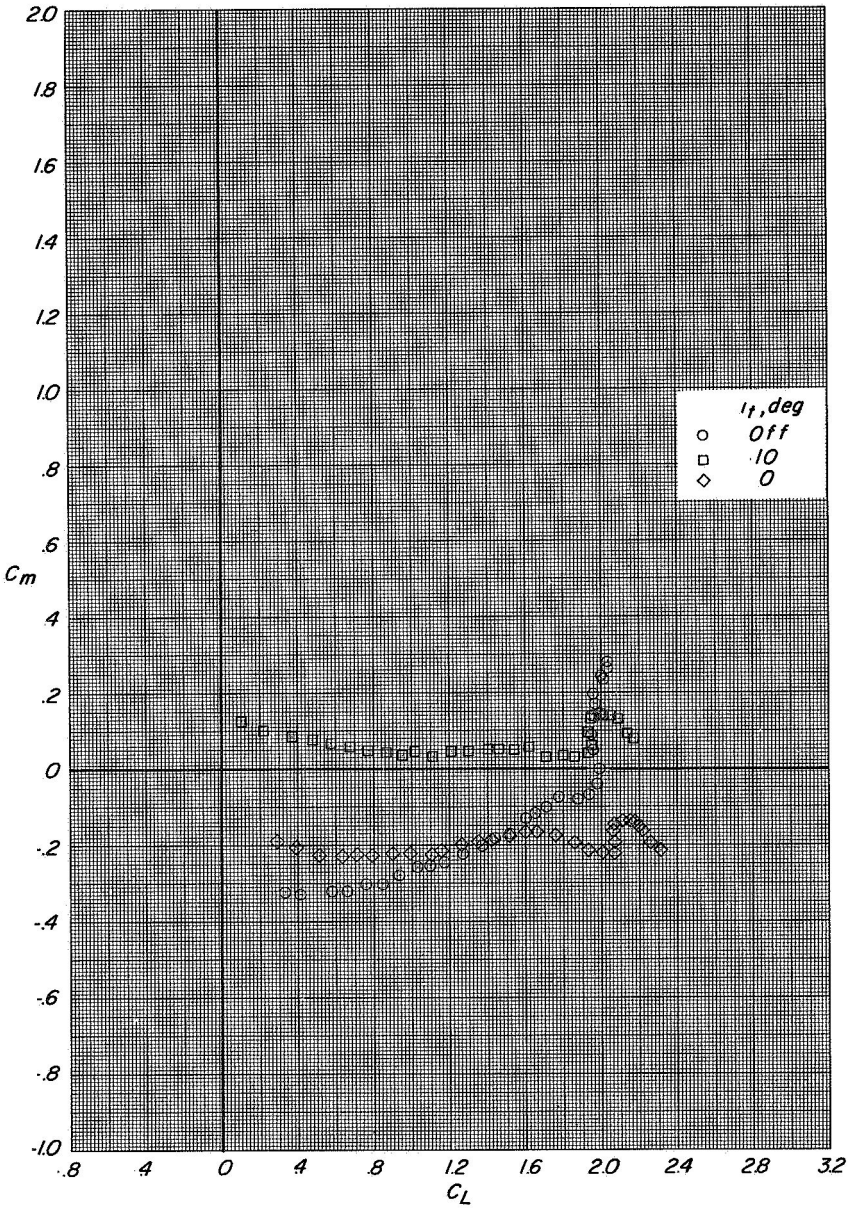

(c) Variation of C_m with C_L.

Figure 18.- Concluded.

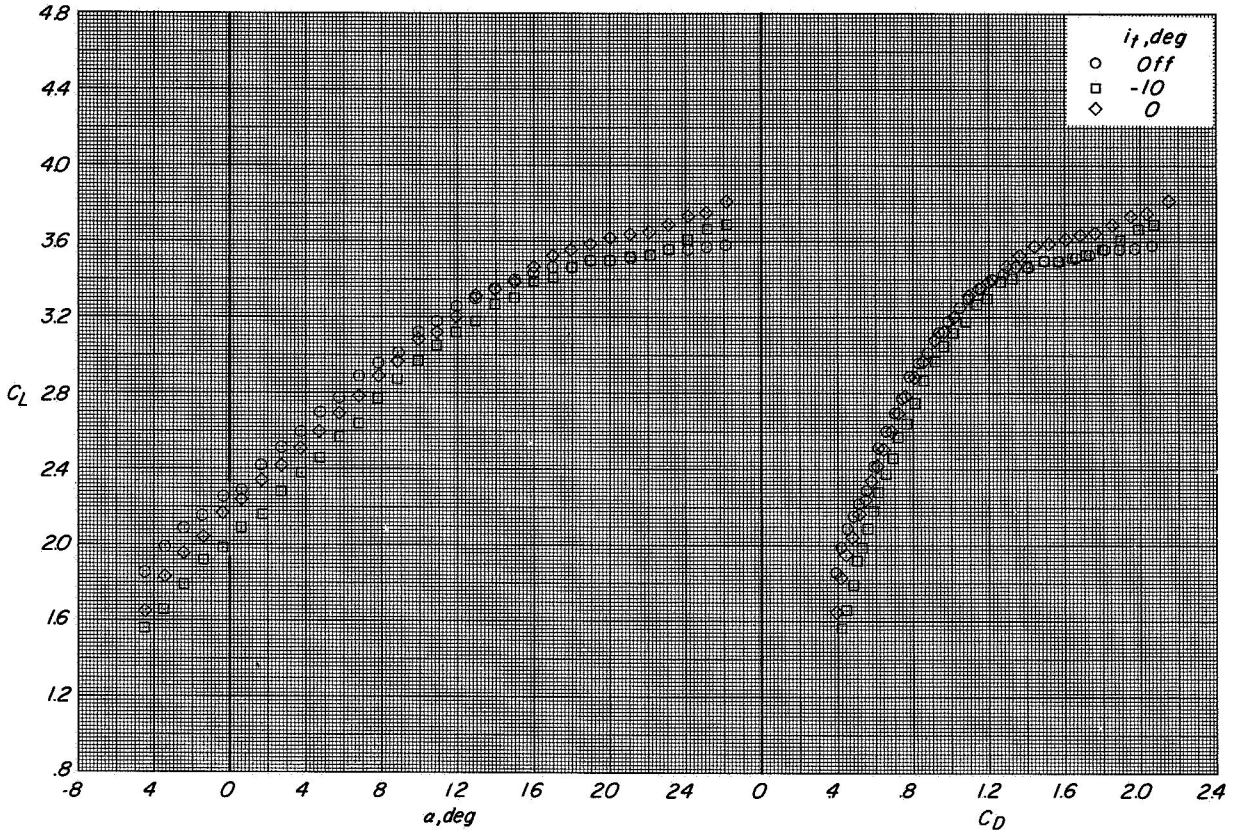

(a) Variation of C_L with α and C_D with C_L.

Figure 19.- Longitudinal aerodynamic characteristics of configuration A with direct-lift engines and lift-cruise engines deflected 90°. $C_T \approx 1.45$.

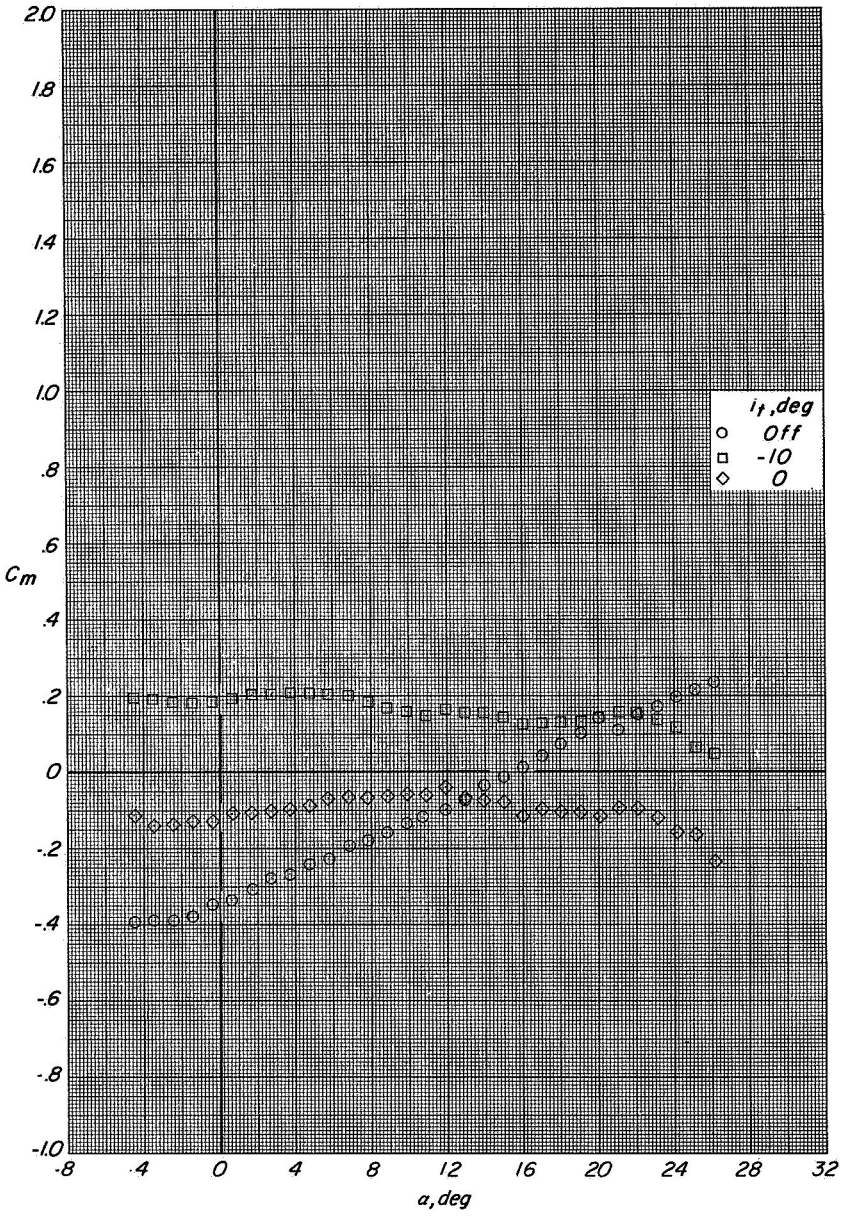

(b) Variation of C_m with α.

Figure 19.- Continued.

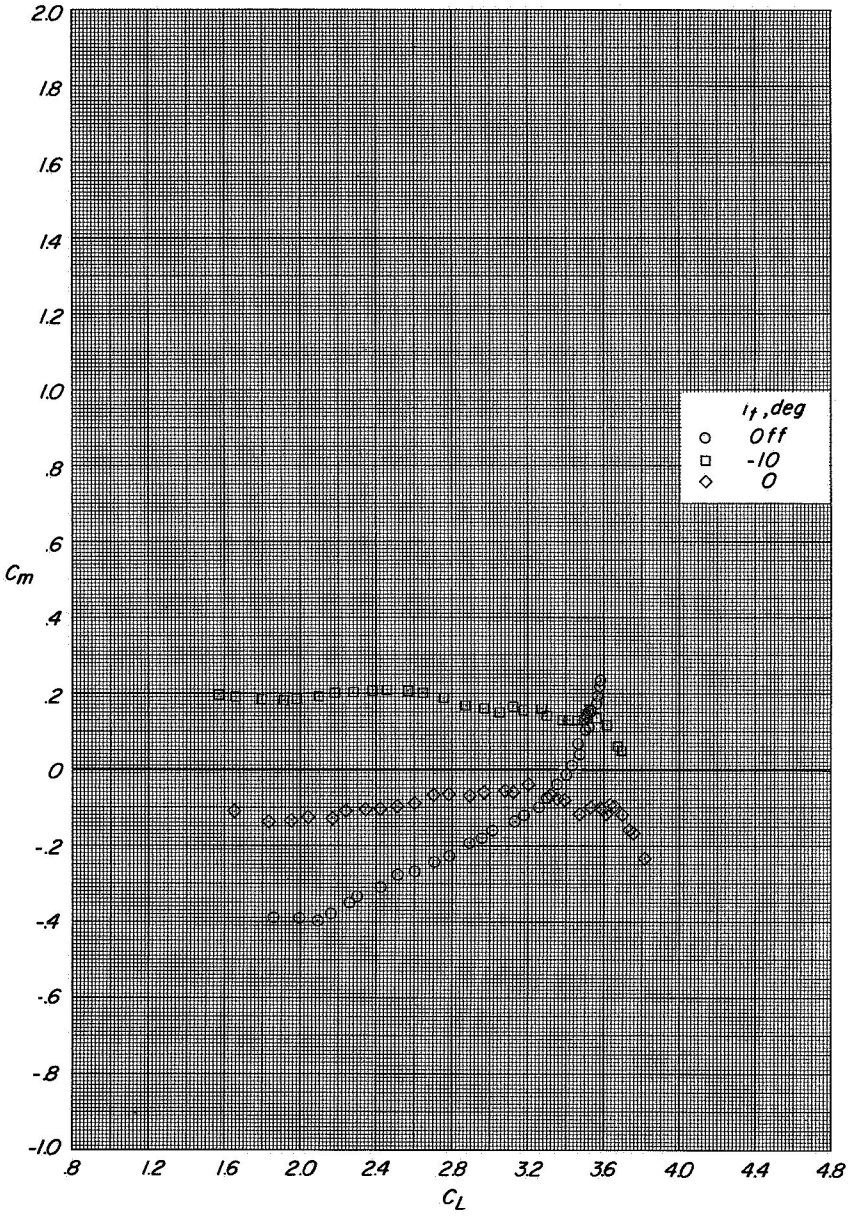

(c) Variation of C_m with C_L.

Figure 19.- Continued.

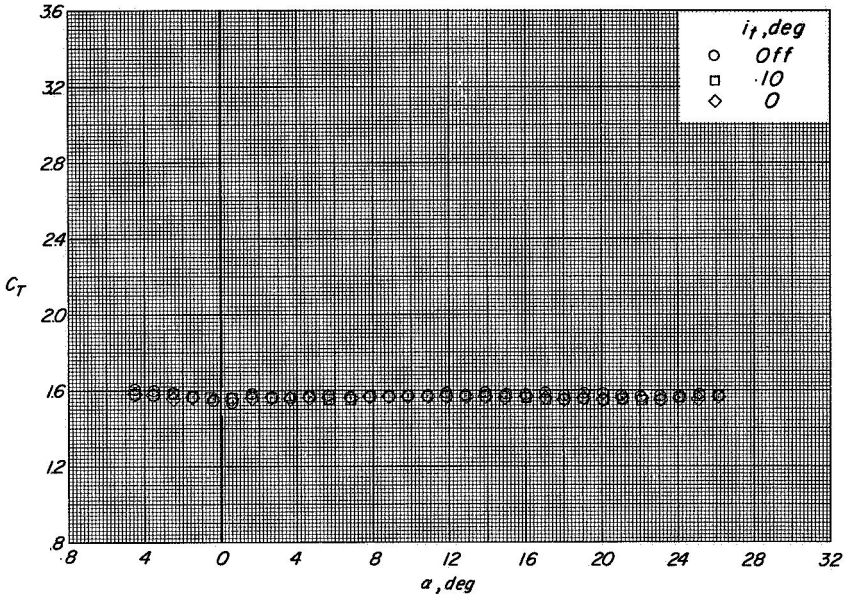

(d) Variation of C_T with α.

Figure 19.- Concluded.

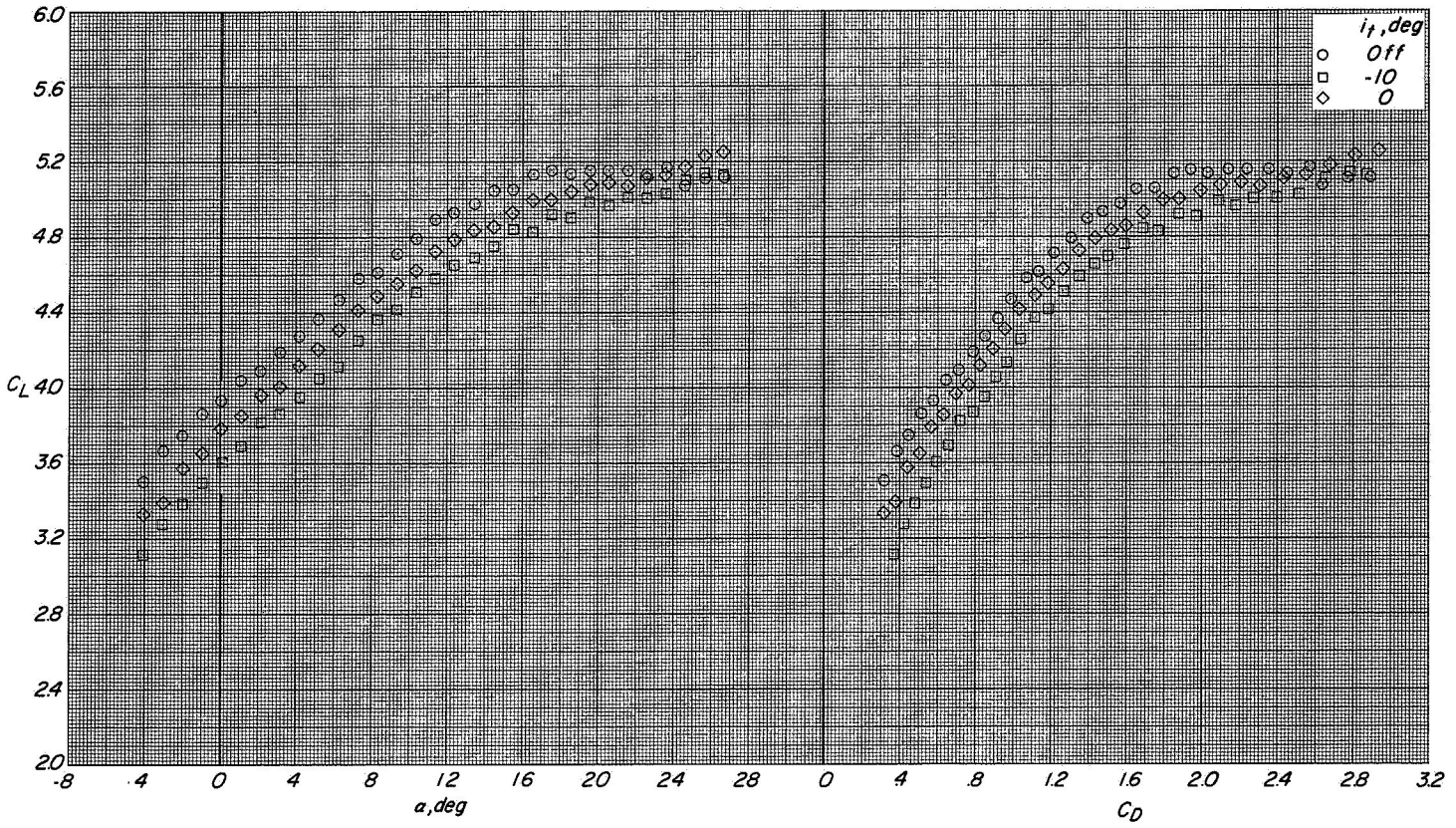

(a) Variation of C_L with α and C_D with C_L.

Figure 20.- Longitudinal aerodynamic characteristics of configuration A with direct-lift engines and lift-cruise engines deflected 90°. $C_T \approx 3.3$

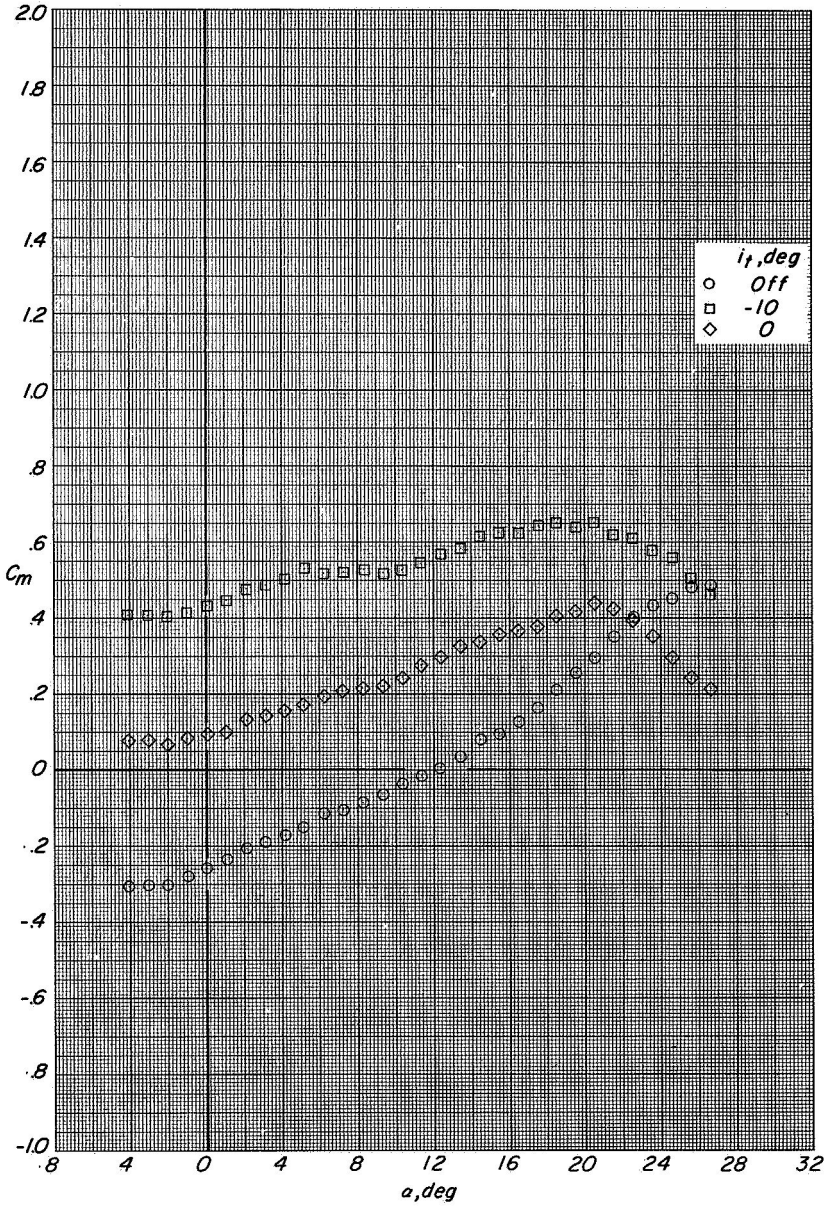

(b) Variation of C_m with α.

Figure 20.- Continued.

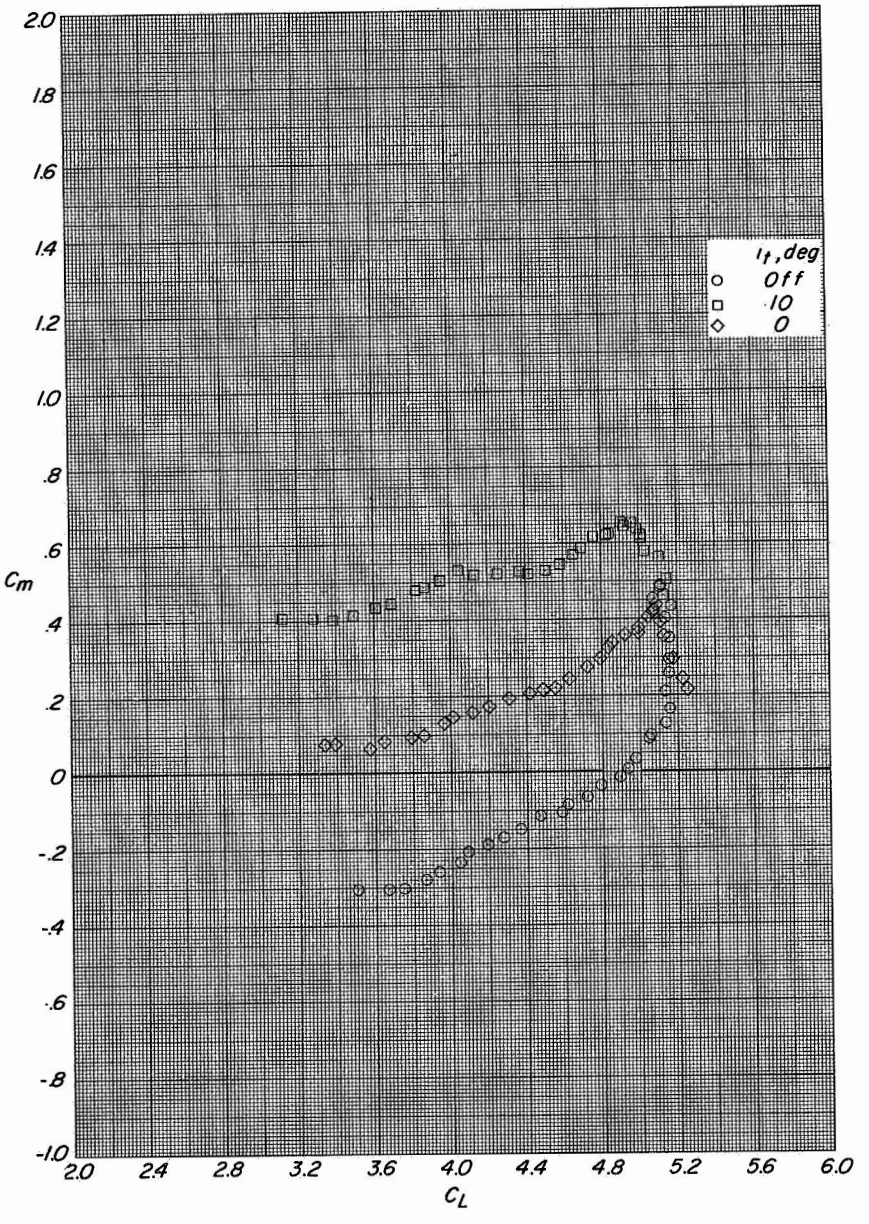

(c) Variation of C_m with C_L.

Figure 20.- Continued.

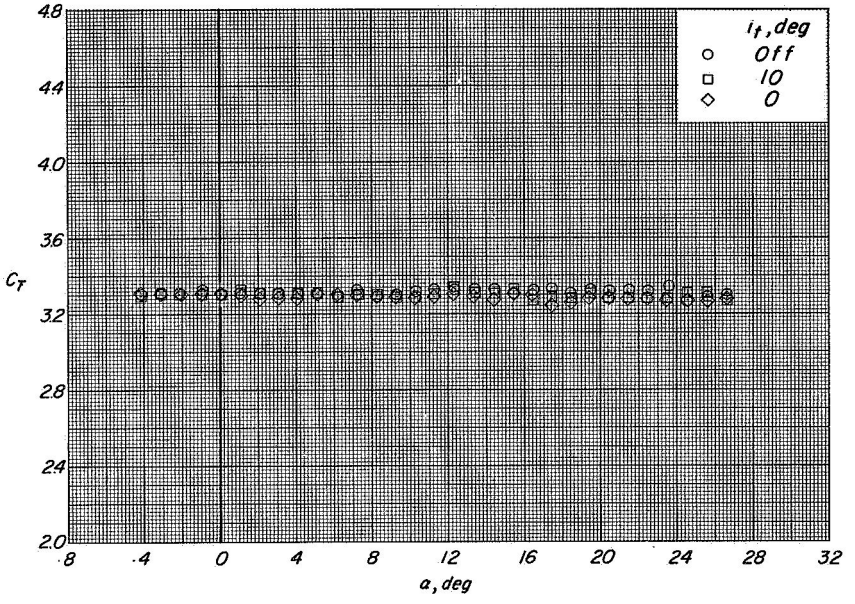

(d) Variation of C_T with α.

Figure 20. - Concluded.

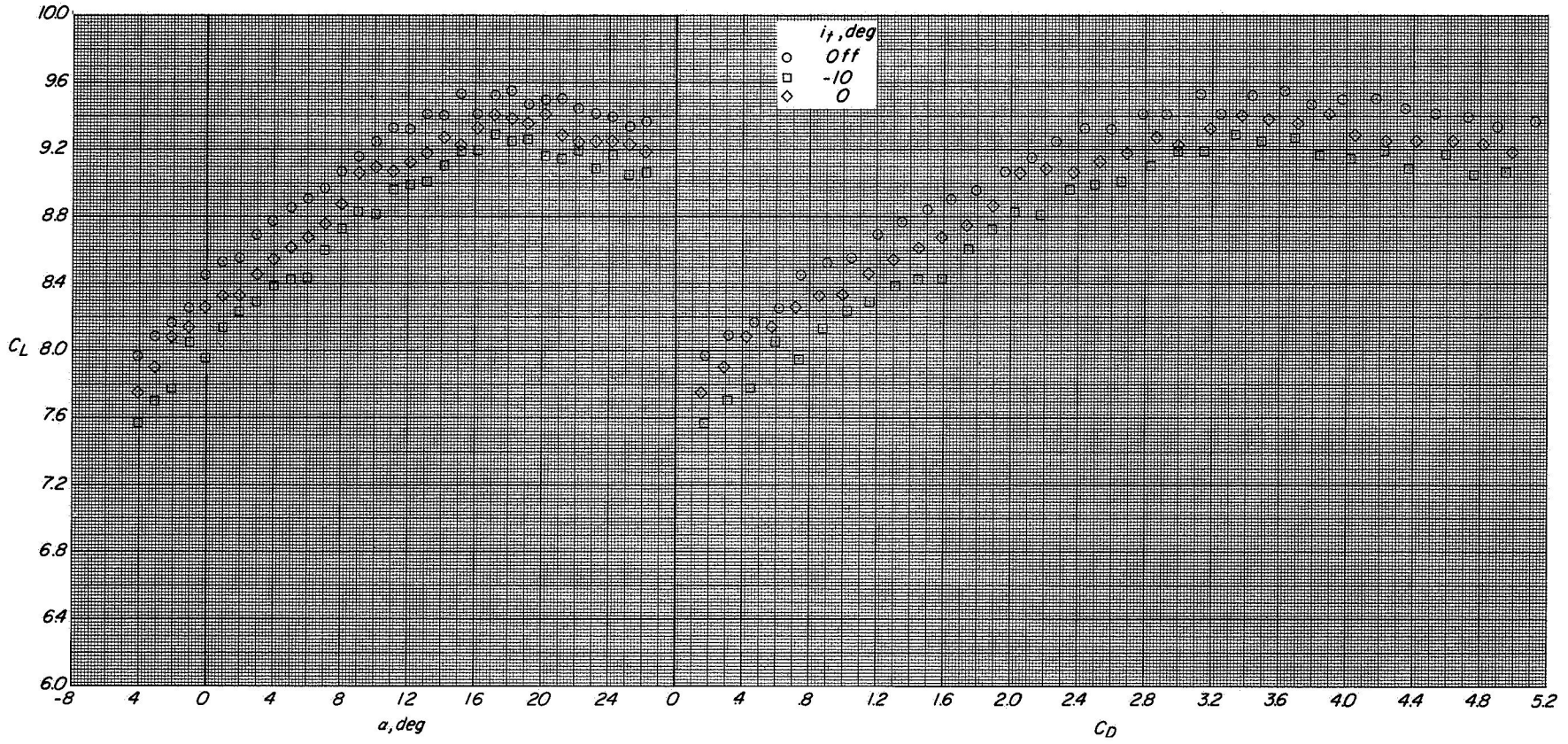

(a) Variation of C_L with α and C_D with C_L.

Figure 21.- Longitudinal aerodynamic characteristics of configuration A with direct-lift engines and lift-cruise engines deflected 90°. $C_T \approx 8$.

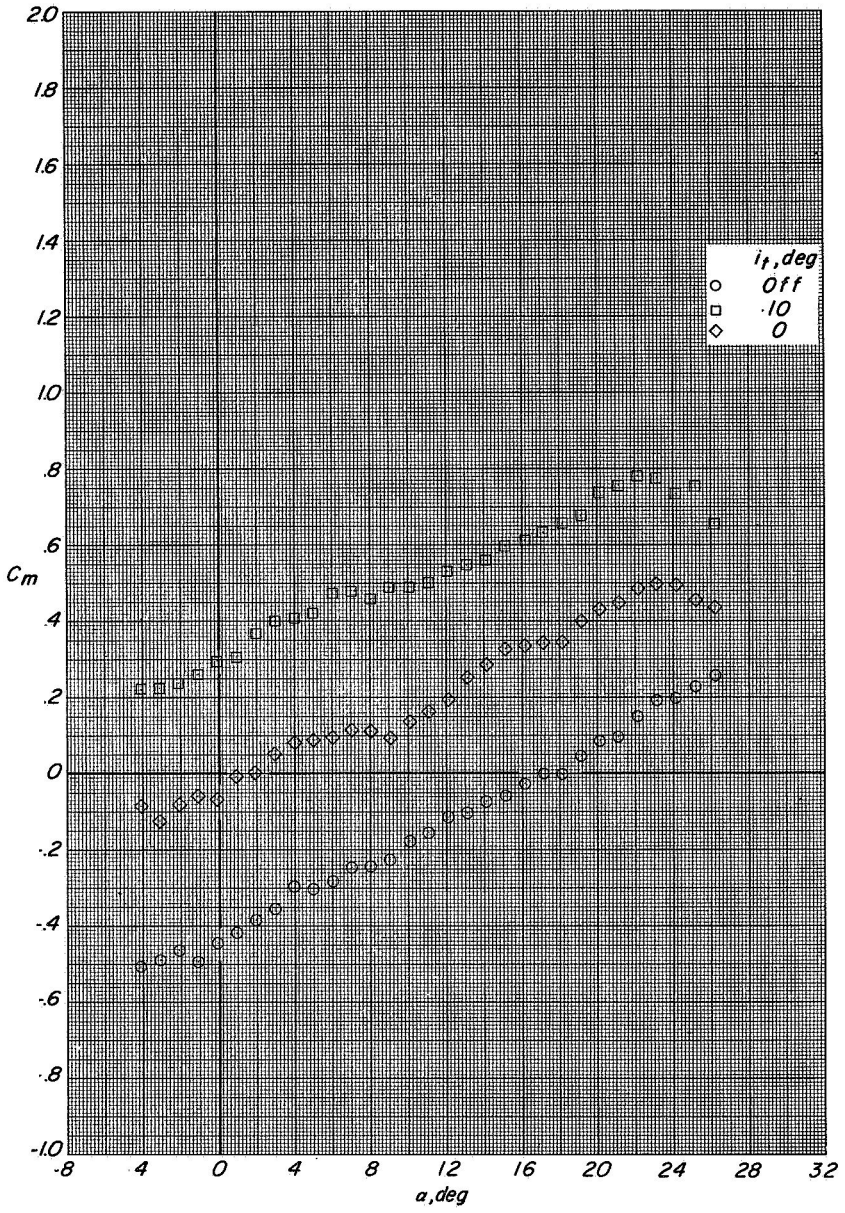

(b) Variation of C_m with α.

Figure 21.- Continued.

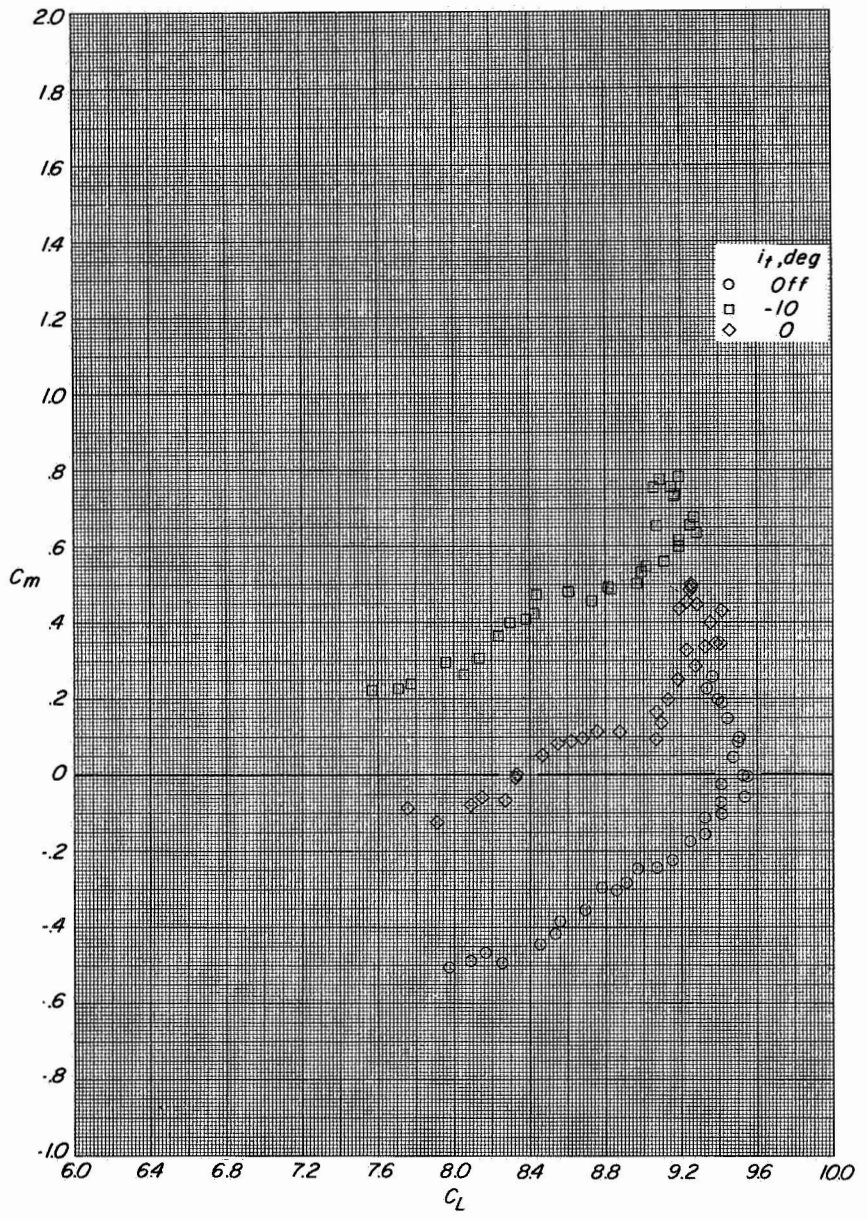

(c) Variation of C_m with C_L.

Figure 21.- Continued.

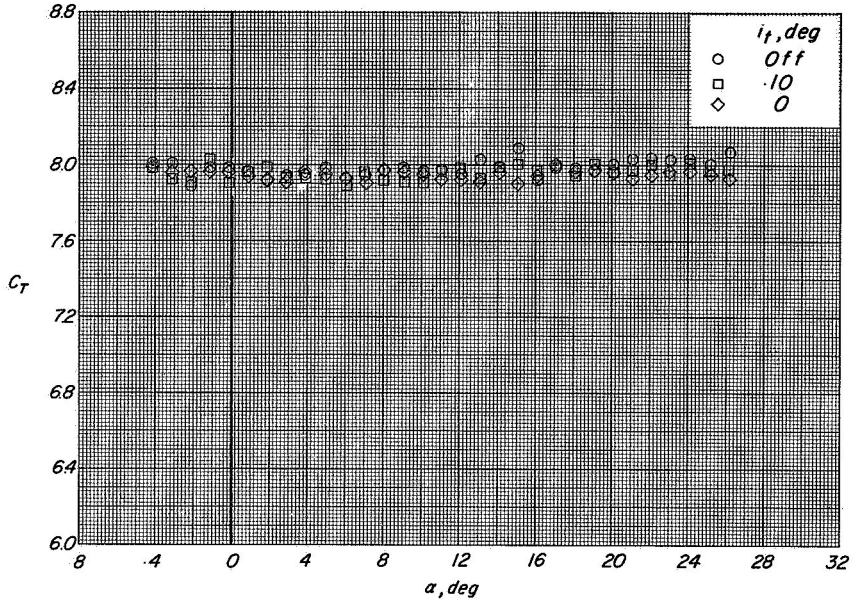

(d) Variation of C_T with α.

Figure 21.- Concluded.

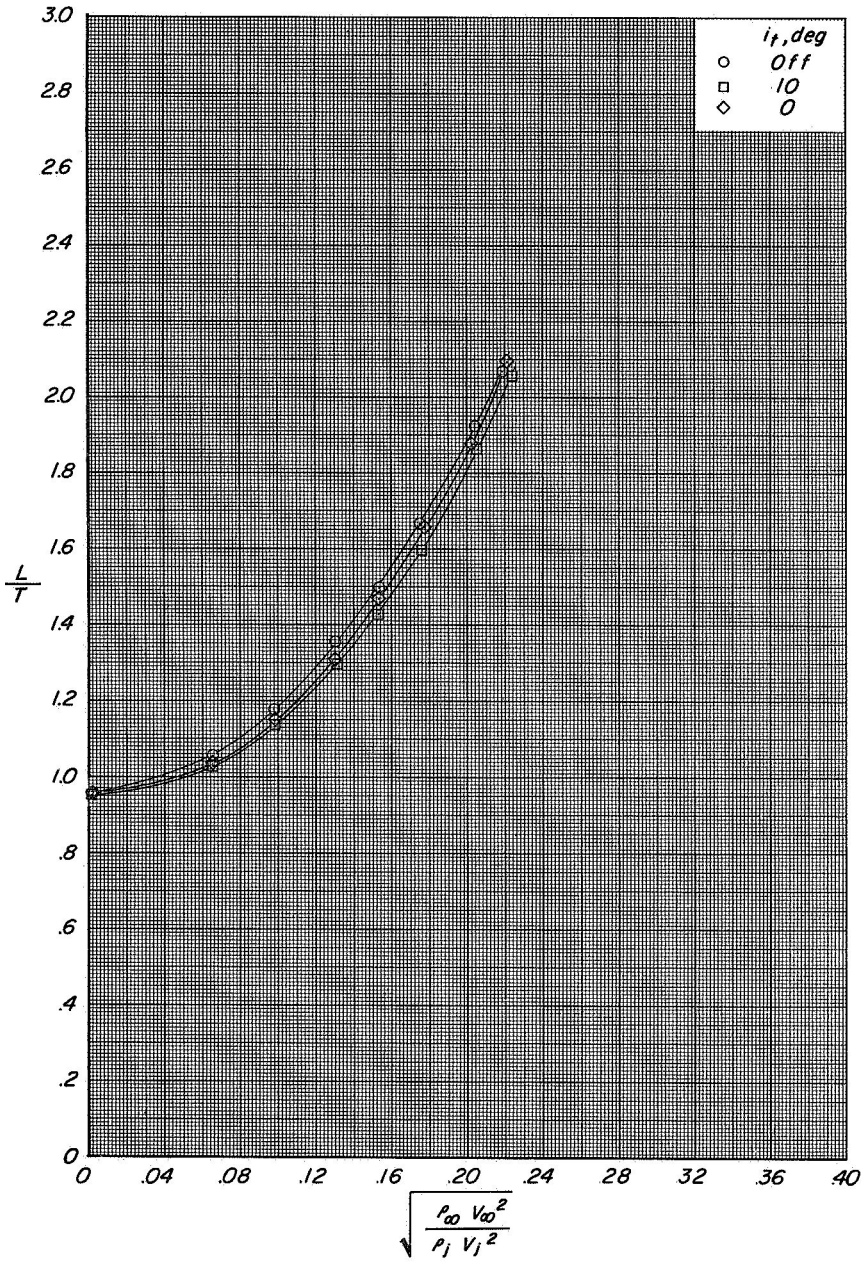

(a) Variation of L/T with effective velocity ratio.

Figure 22.- Longitudinal aerodynamic characteristics of configuration A with direct-lift engines and lift-cruise engines deflected 90° $\alpha = 12°$.

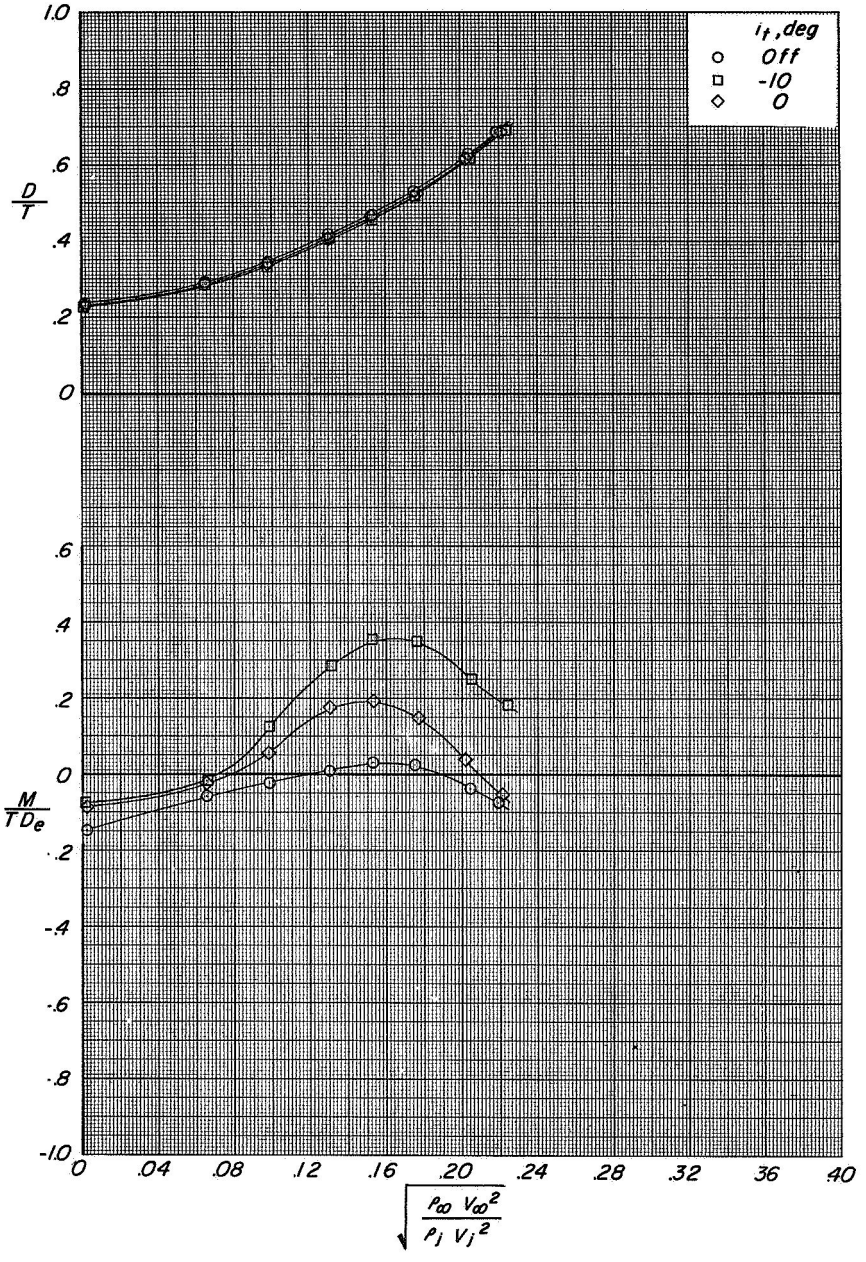

(b) Variation of D/T and M/TD_e with effective velocity ratio.

Figure 22.- Concluded.

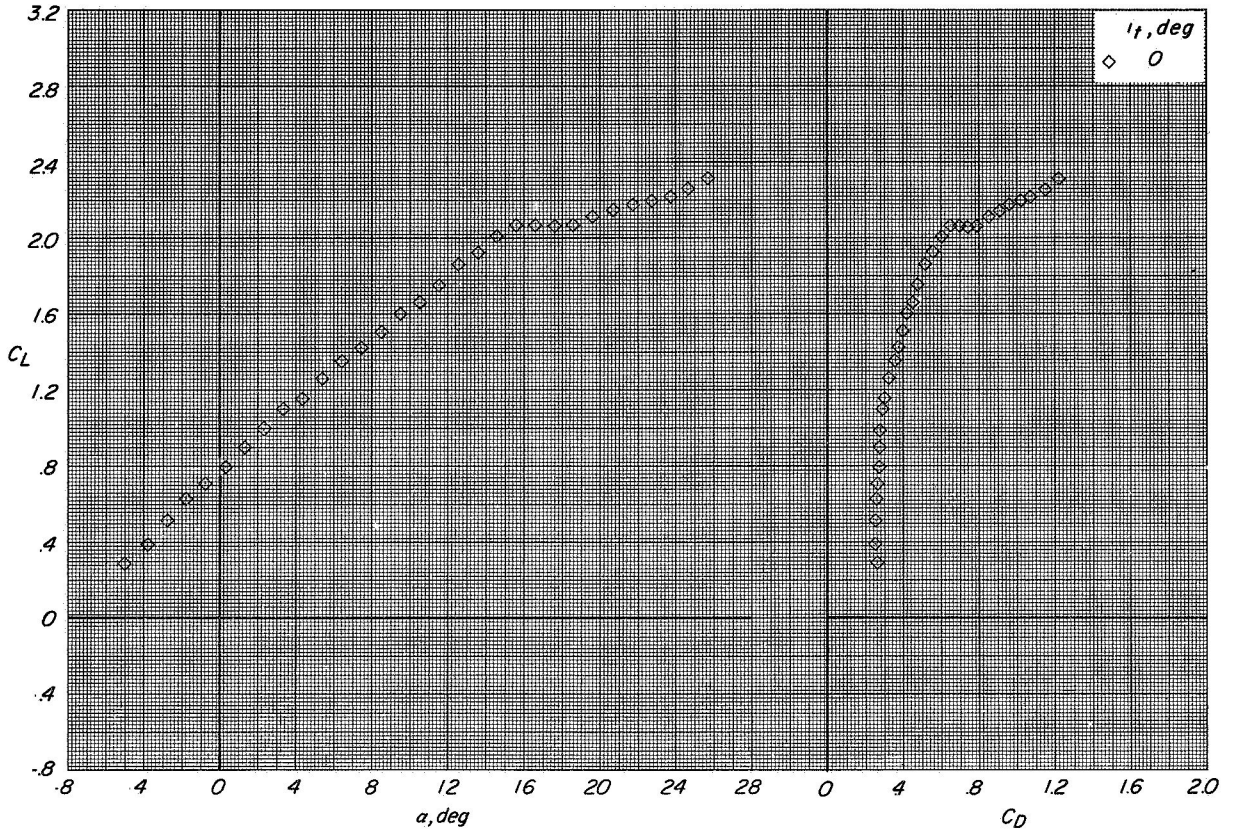

(a) Variation of C_L with α and C_D with C_L.

Figure 23.- Longitudinal aerodynamic characteristics of configuration A with direct-lift engines deflected 90° and lift-cruise engines off $C_T = 0$.

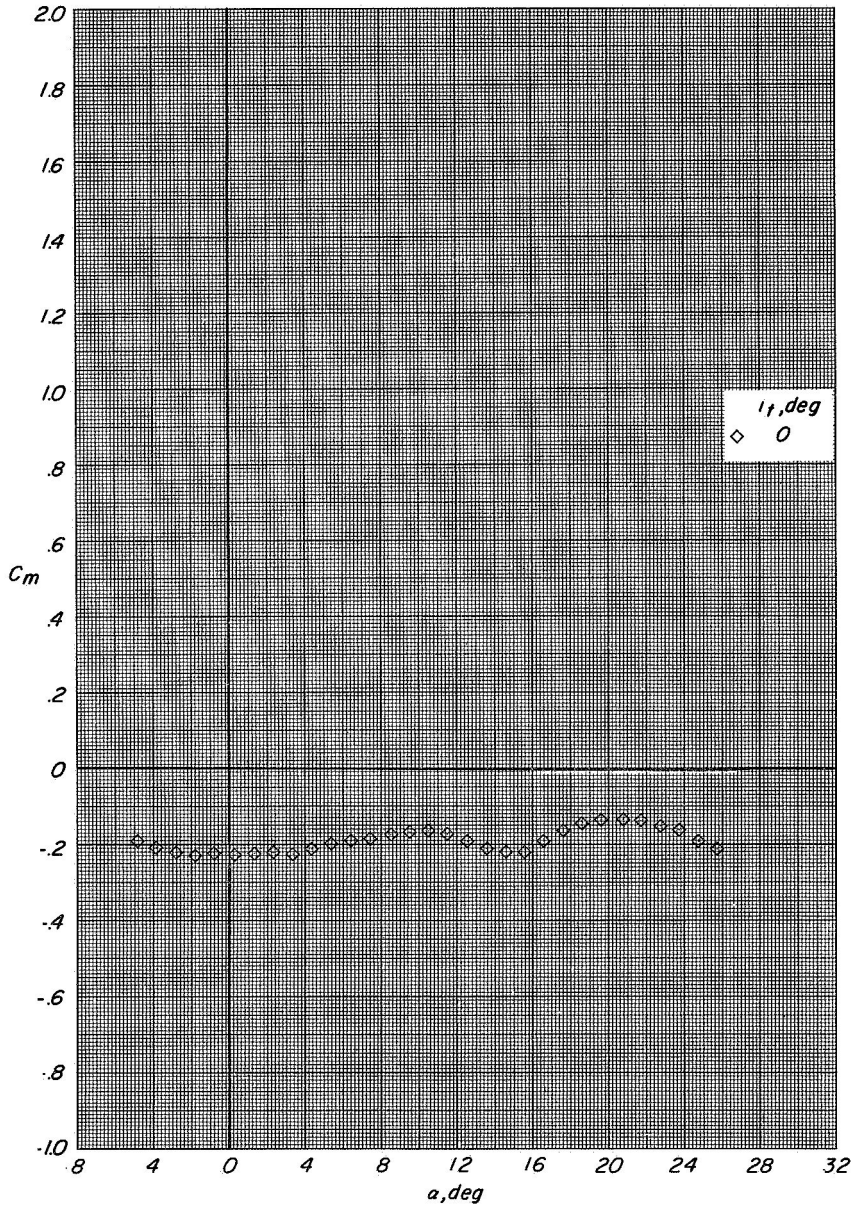

(b) Variation of C_m with α.

Figure 23.- Continued.

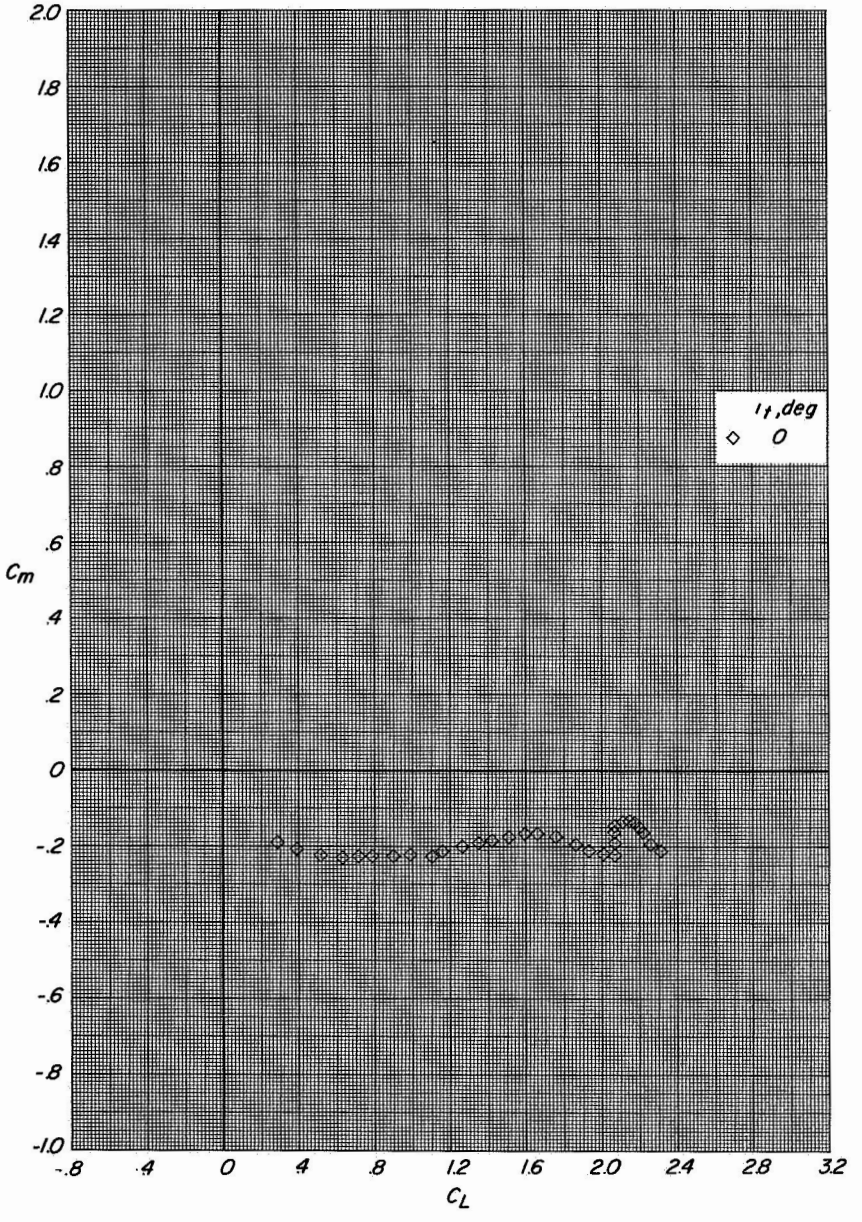

(c) Variation of C_m with C_L.

Figure 23.- Concluded.

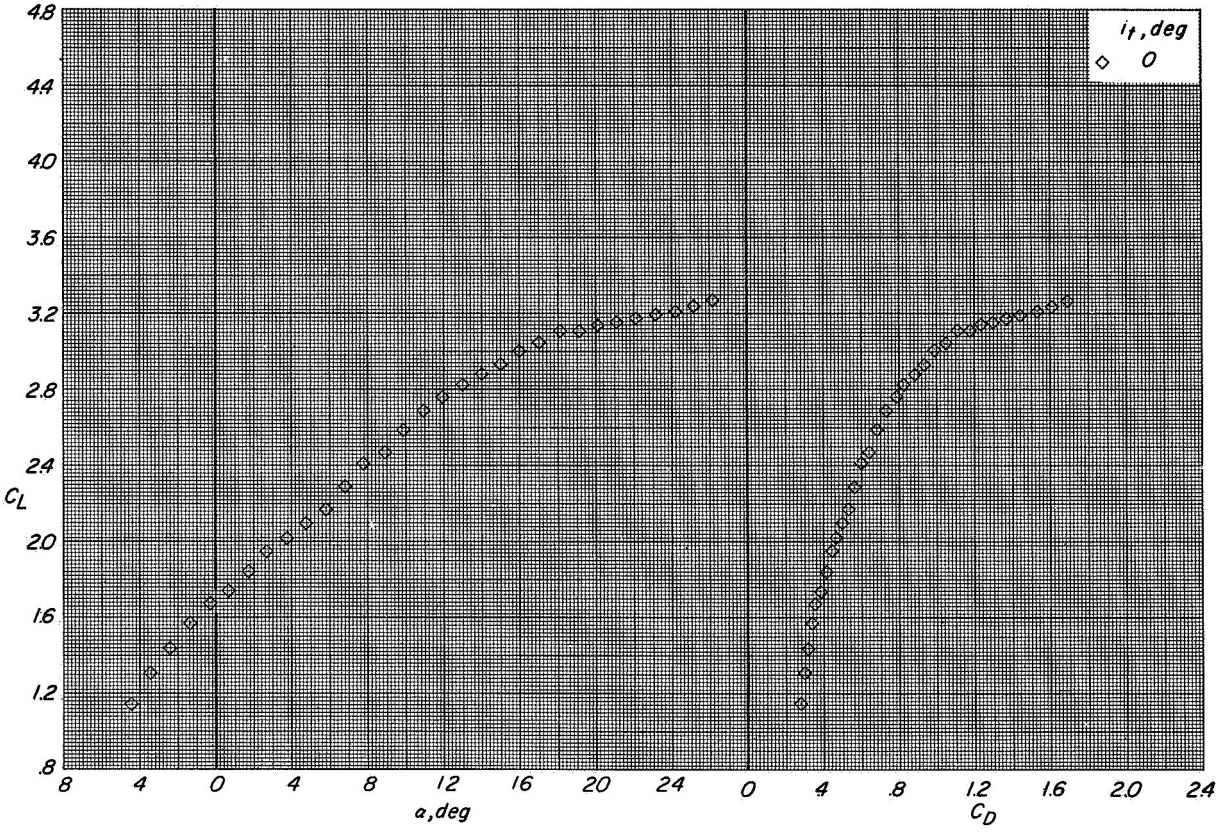

(a) Variation of C_L with α and C_D with C_L.

Figure 24.- Longitudinal aerodynamic characteristics of configuration A with direct-lift engines deflected 90° and lift-cruise engines off. $C_T \approx 1.2$.

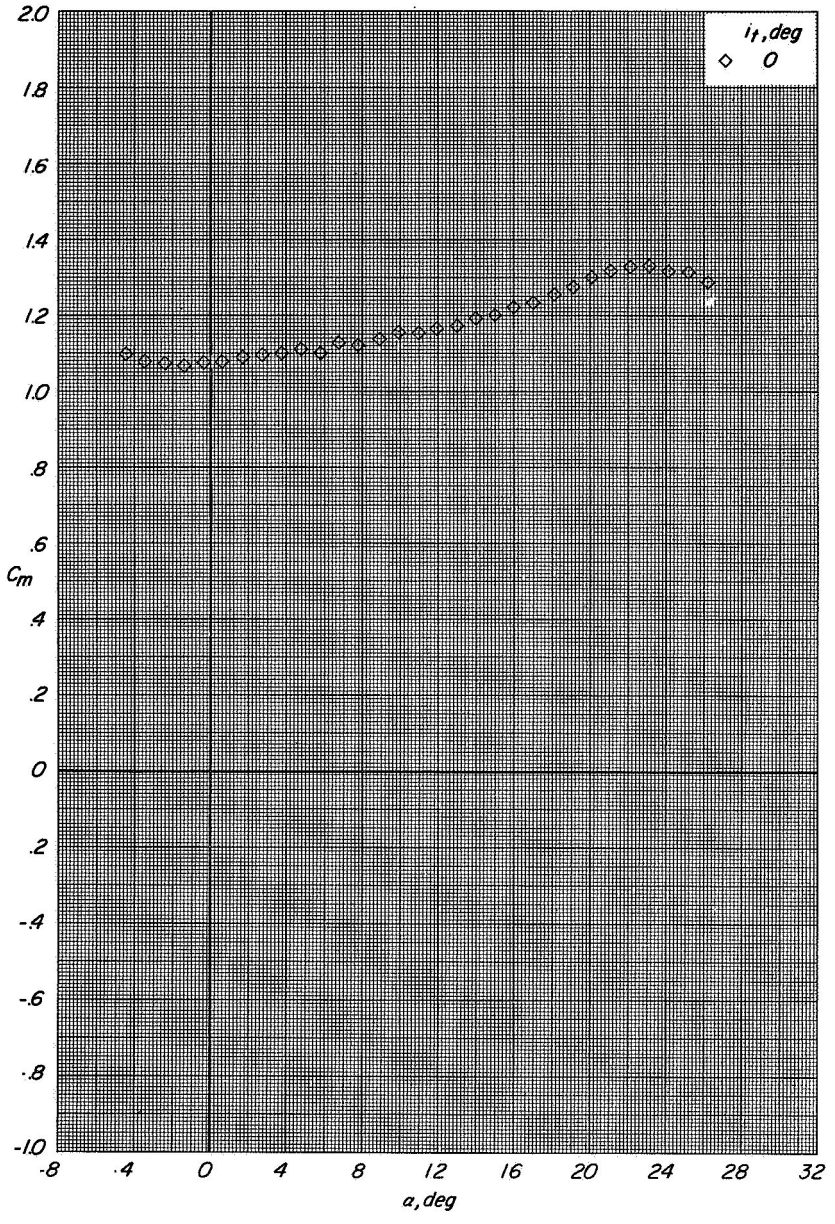

(b) Variation of C_m with α.

Figure 24.- Continued.

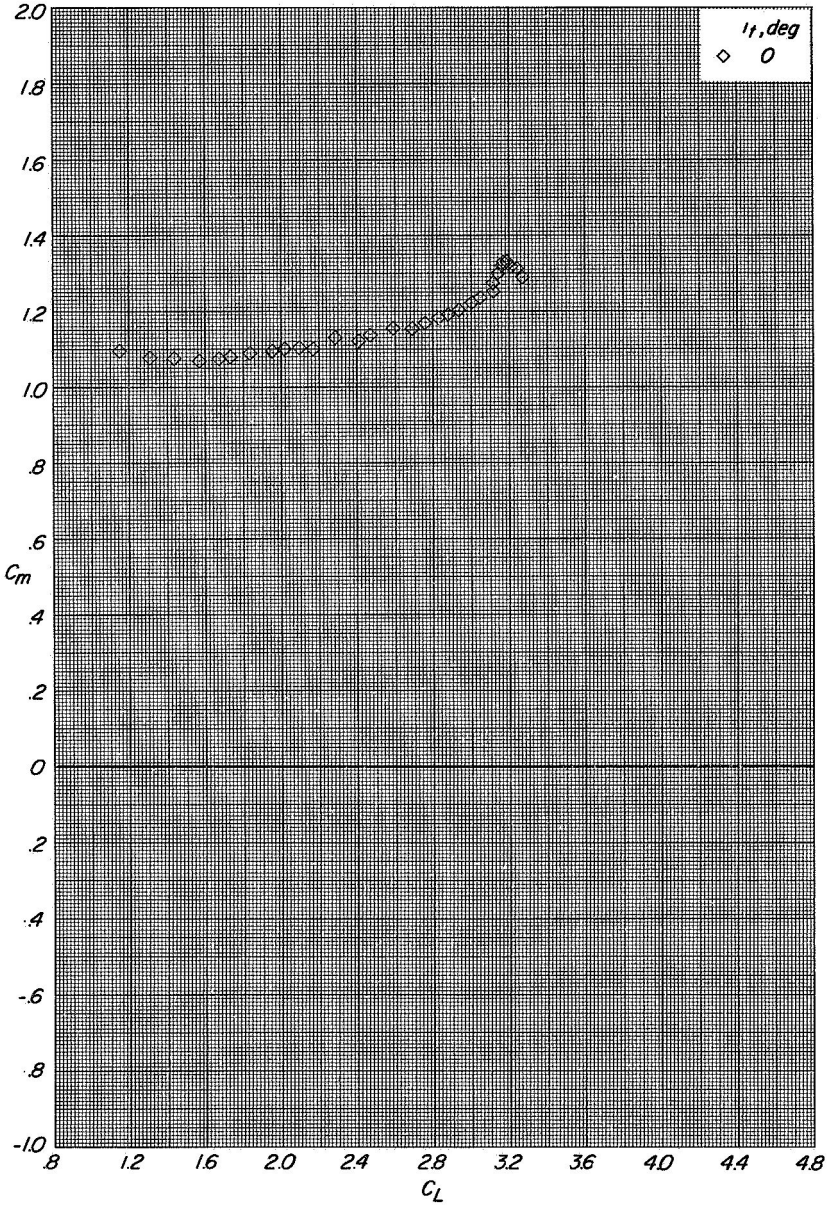

(c) Variation of C_m with C_L.

Figure 24.- Continued.

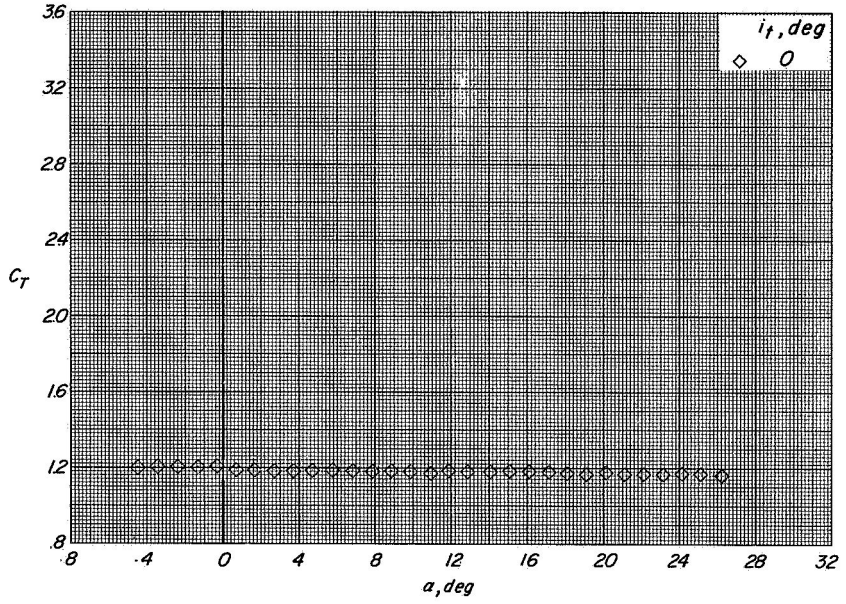

(d) Variation of C_T with α.

Figure 24.- Concluded.

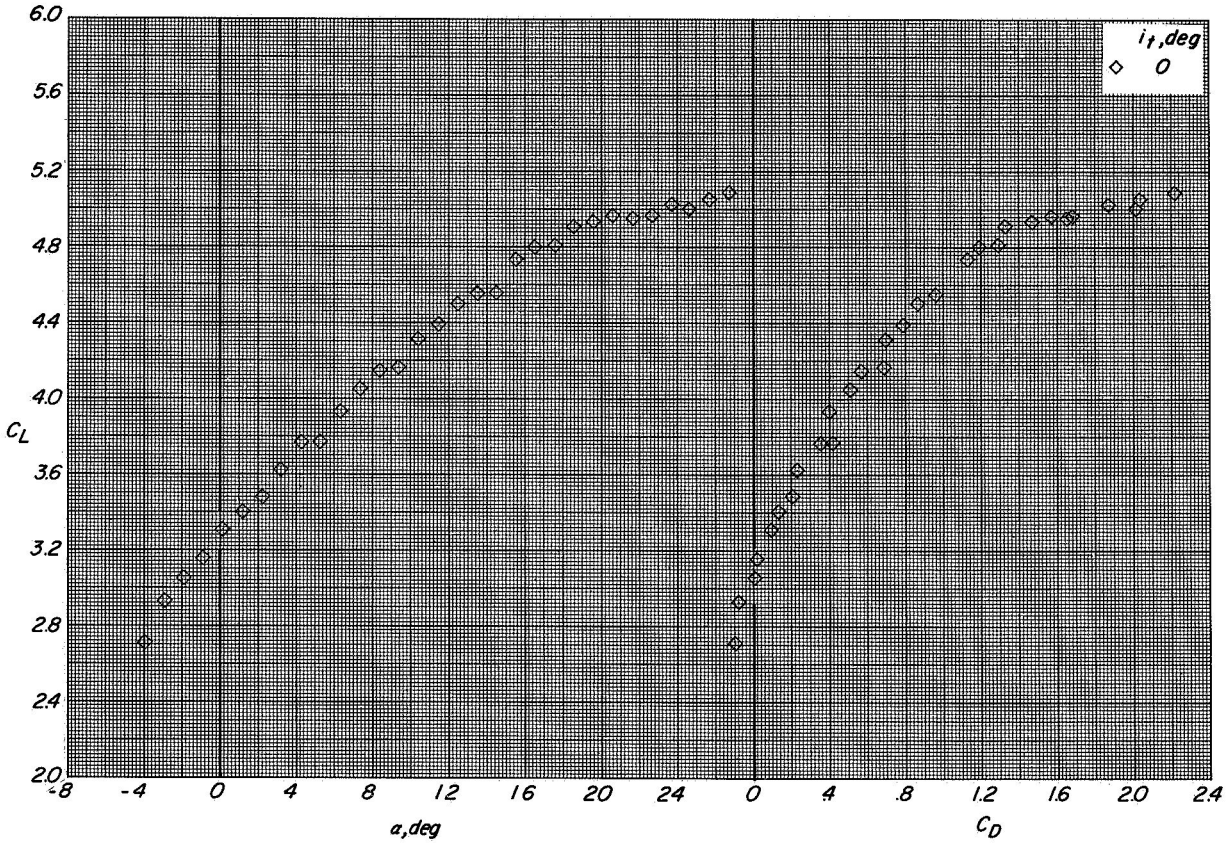

(a) Variation of C_L with α and C_D with C_L.

Figure 25.- Longitudinal aerodynamic characteristics of configuration A with direct-lift engines deflected 90° and lift-cruise engines off $C_T \approx 2.5$

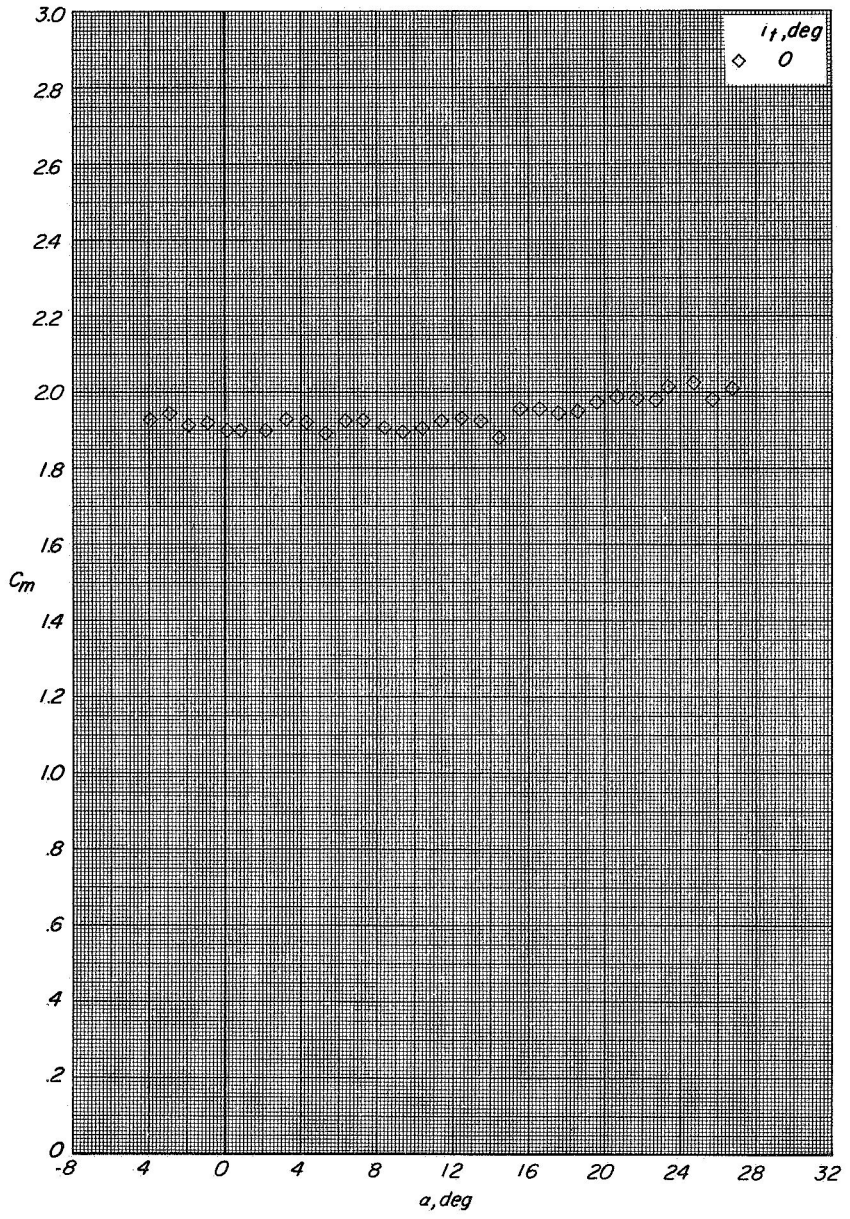

(b) Variation of C_m with α.

Figure 25.- Continued.

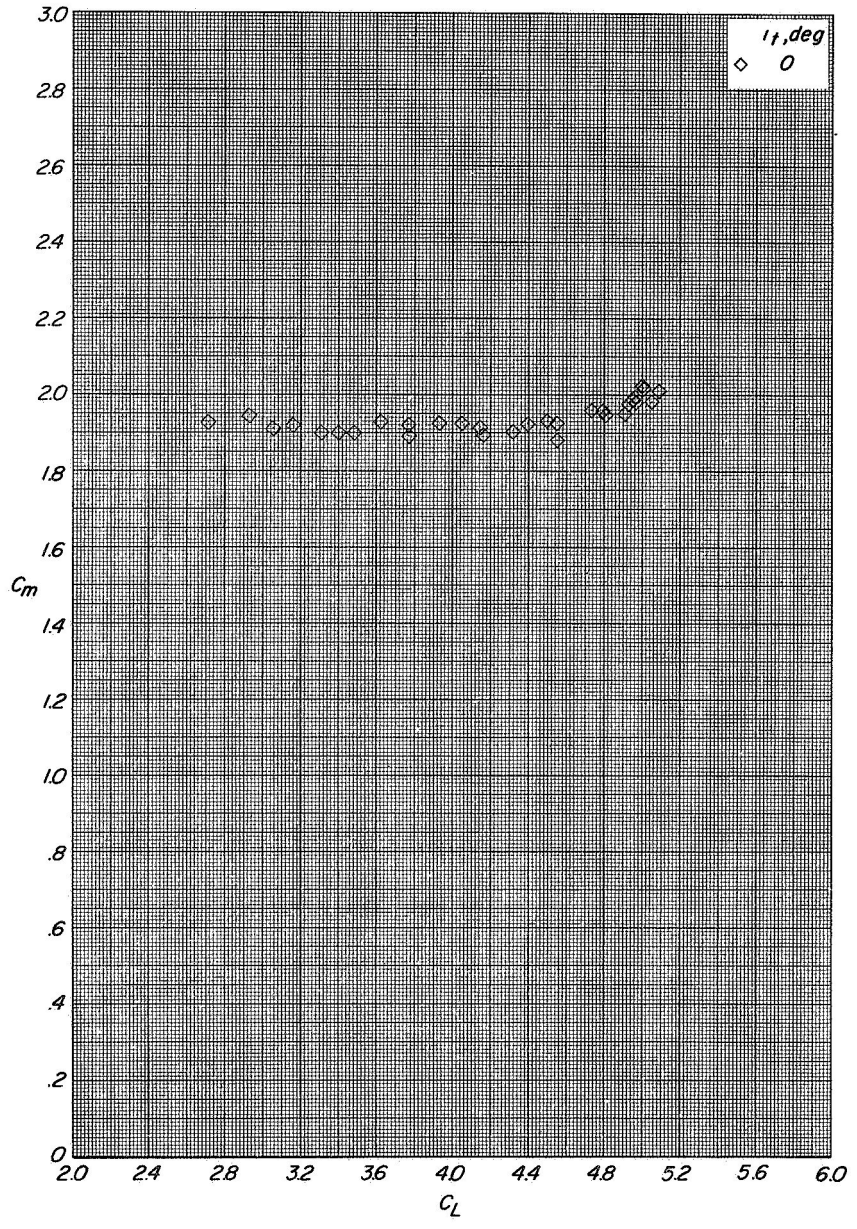

(c) Variation of C_m with C_L.

Figure 25.- Continued.

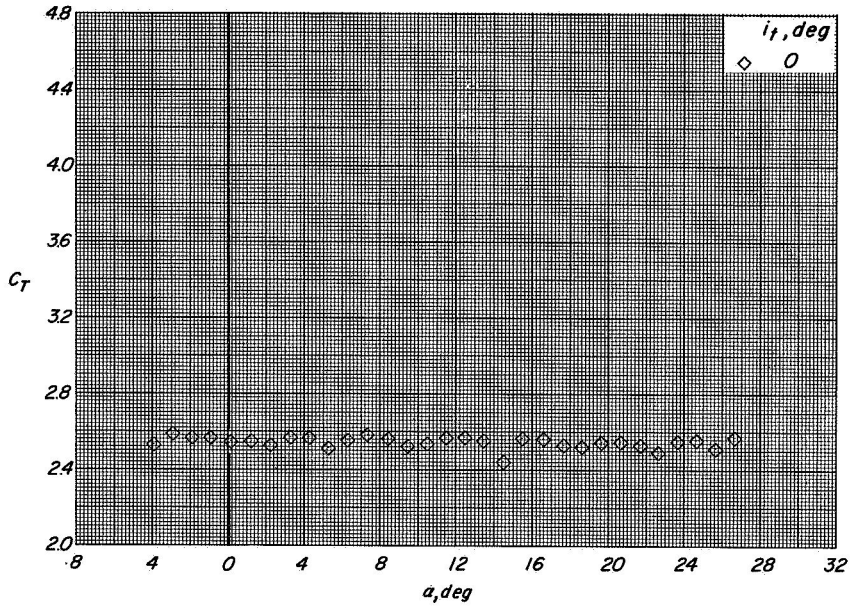

(d) Variation of C_T with α.

Figure 25.- Concluded.

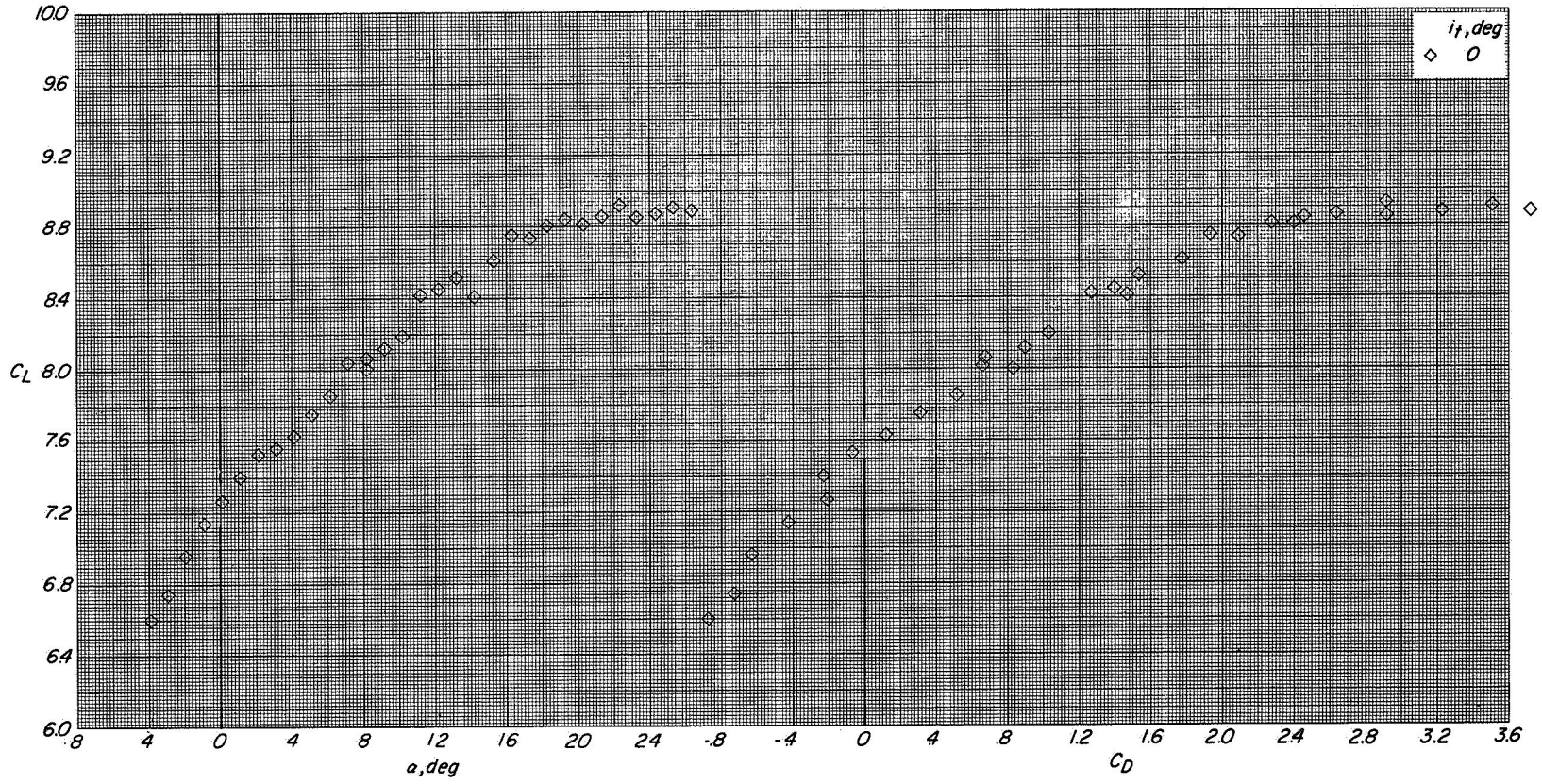

(a) Variation of C_L with α and C_D with C_L.

Figure 26.- Longitudinal aerodynamic characteristics of configuration A with direct-lift engines deflected 90° and lift-cruise engines off. $C_T \approx 6$ 2.

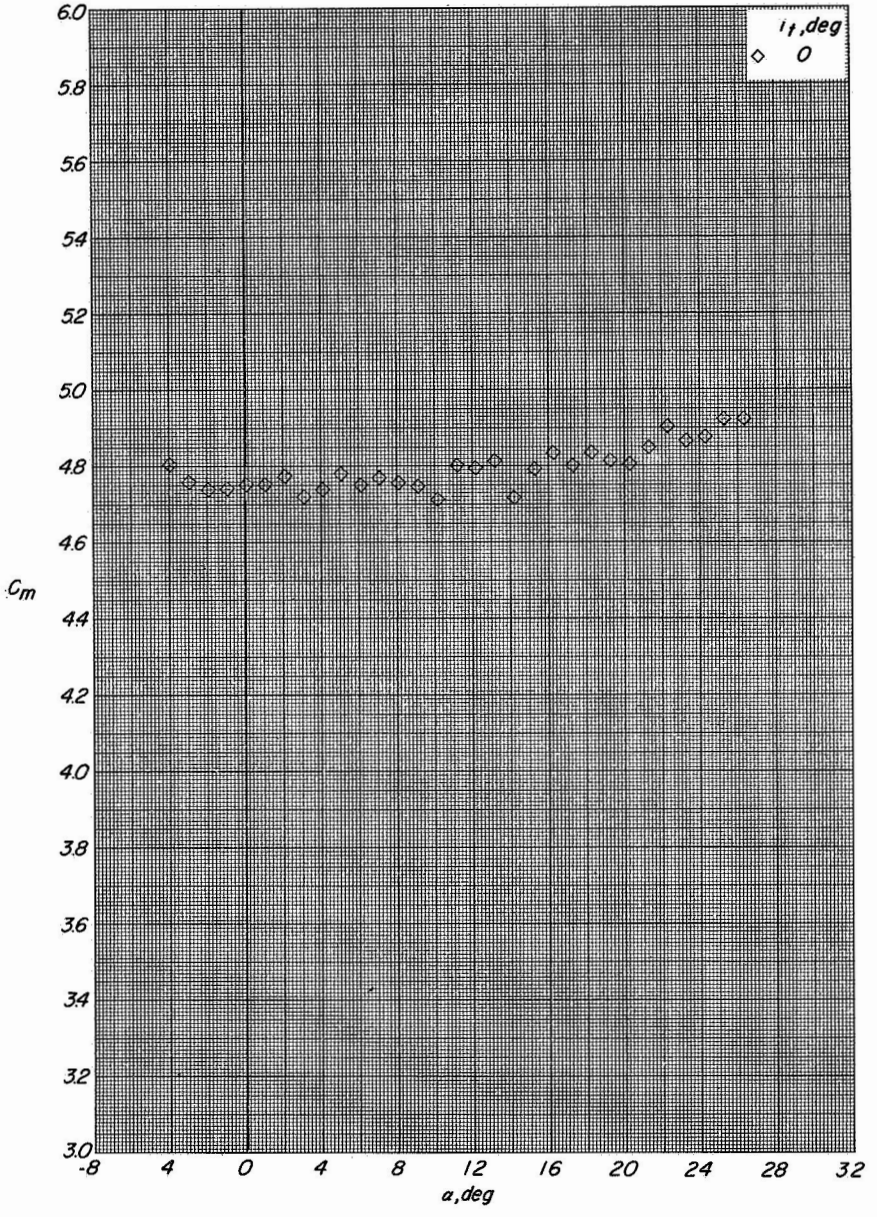

(b) Variation of C_m with α.

Figure 26.- Continued.

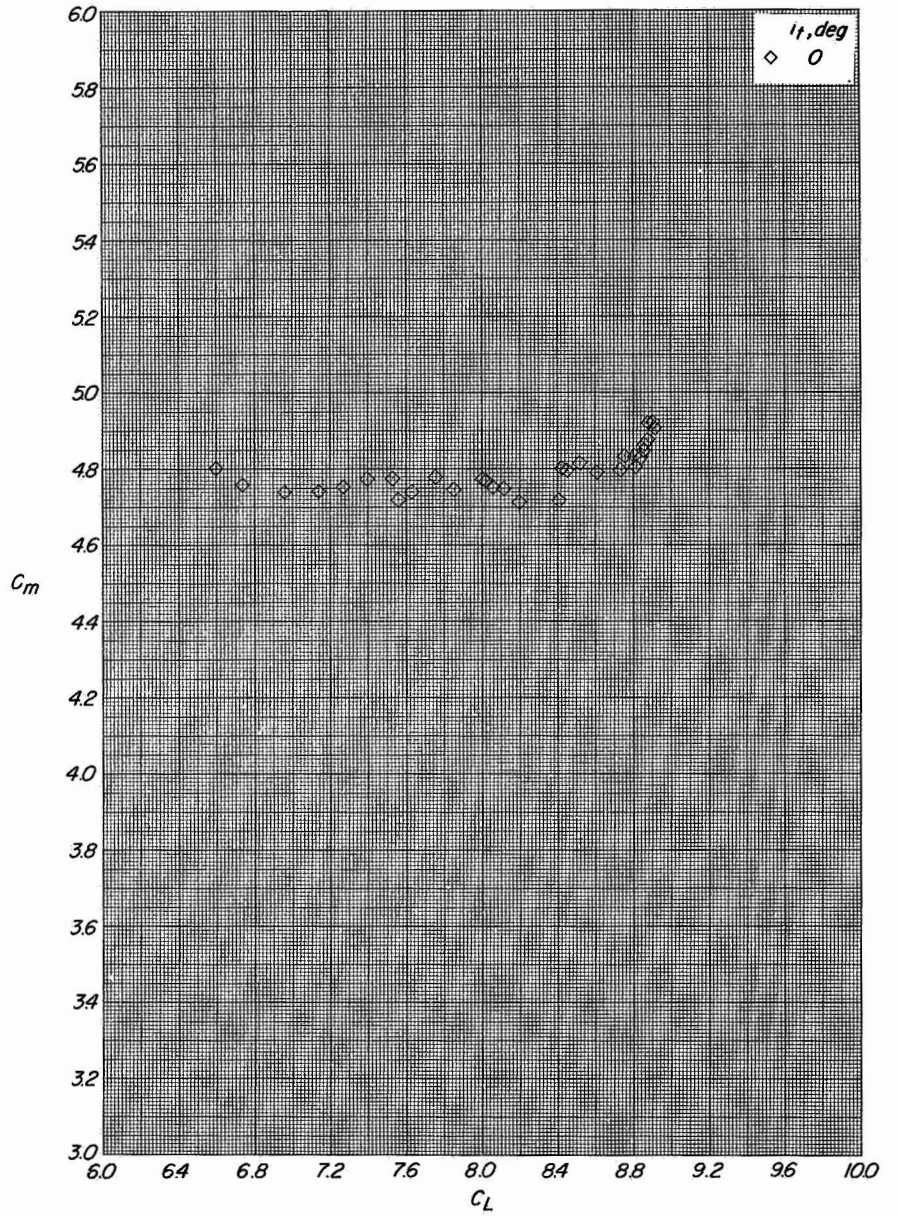

(c) Variation of C_m with C_L.

Figure 26.- Continued.

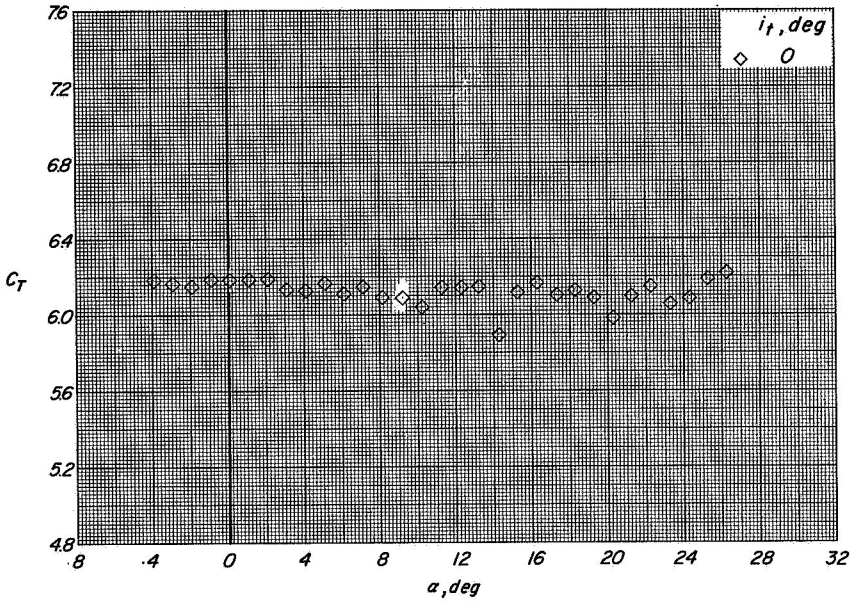

(d) Variation of C_T with α.

Figure 26.- Concluded.

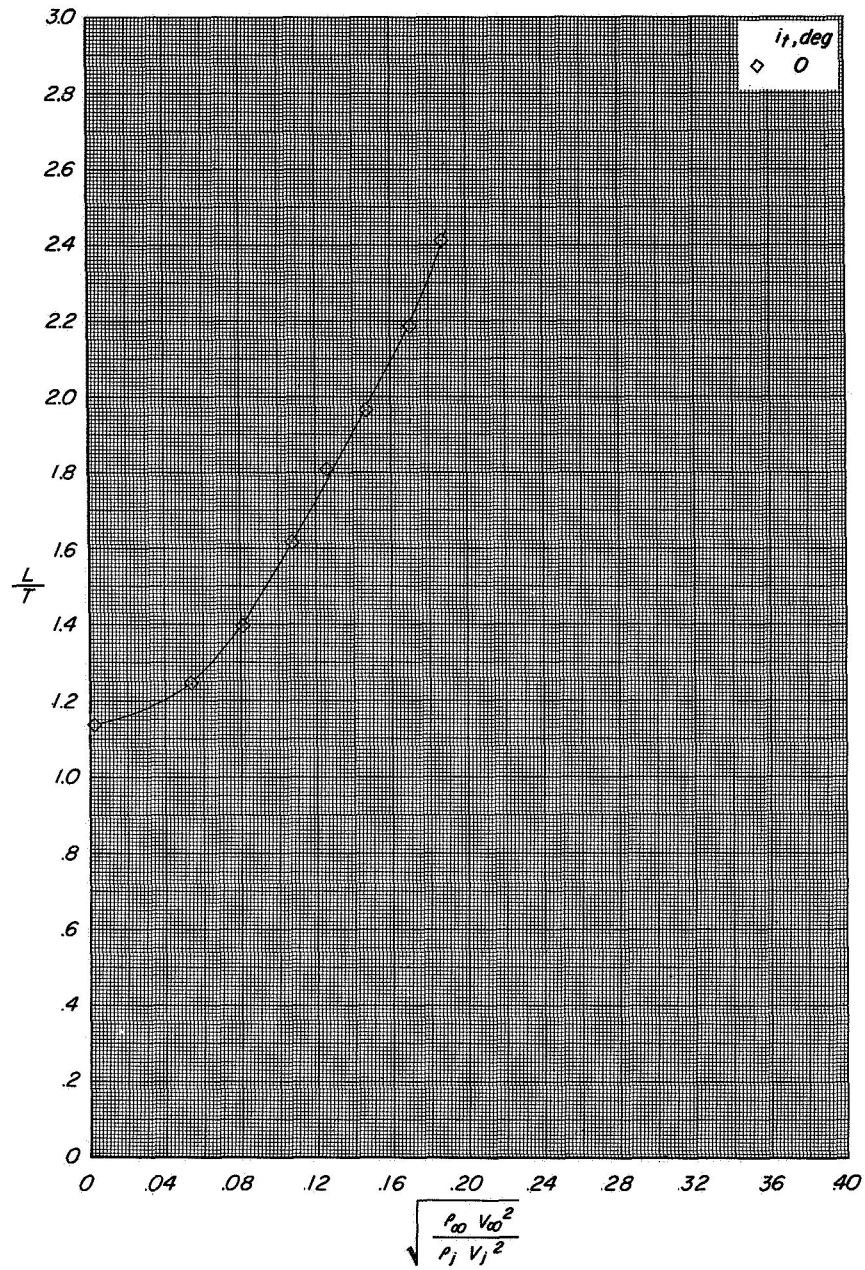

(a) Variation of L/T with effective velocity ratio.

Figure 27.- Longitudinal aerodynamic characteristics of configuration A with direct-lift engines deflected 90° and lift-cruise engines off. $\alpha = 12^\circ$.

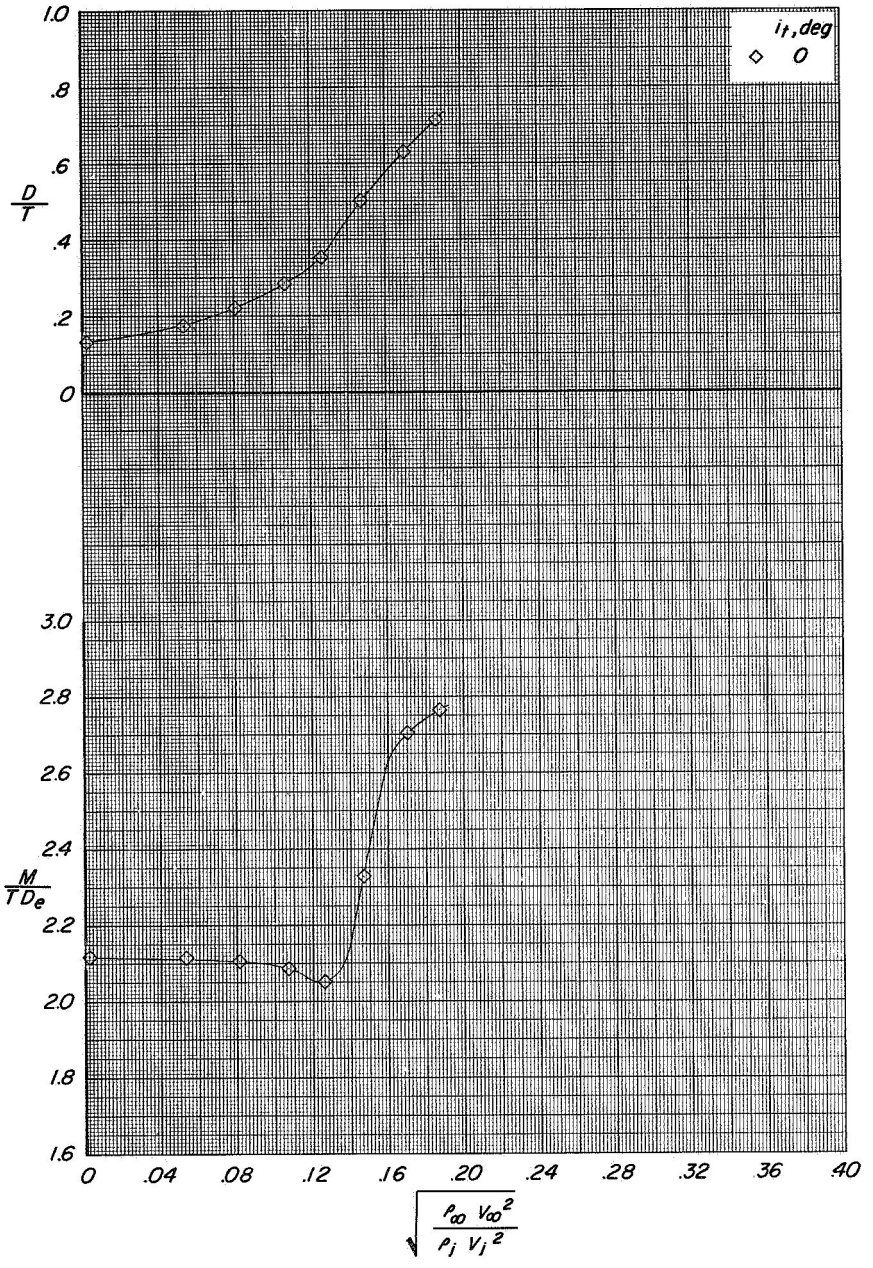

(b) Variation of D/T and M/TD_e with effective velocity ratio.

Figure 27.- Concluded

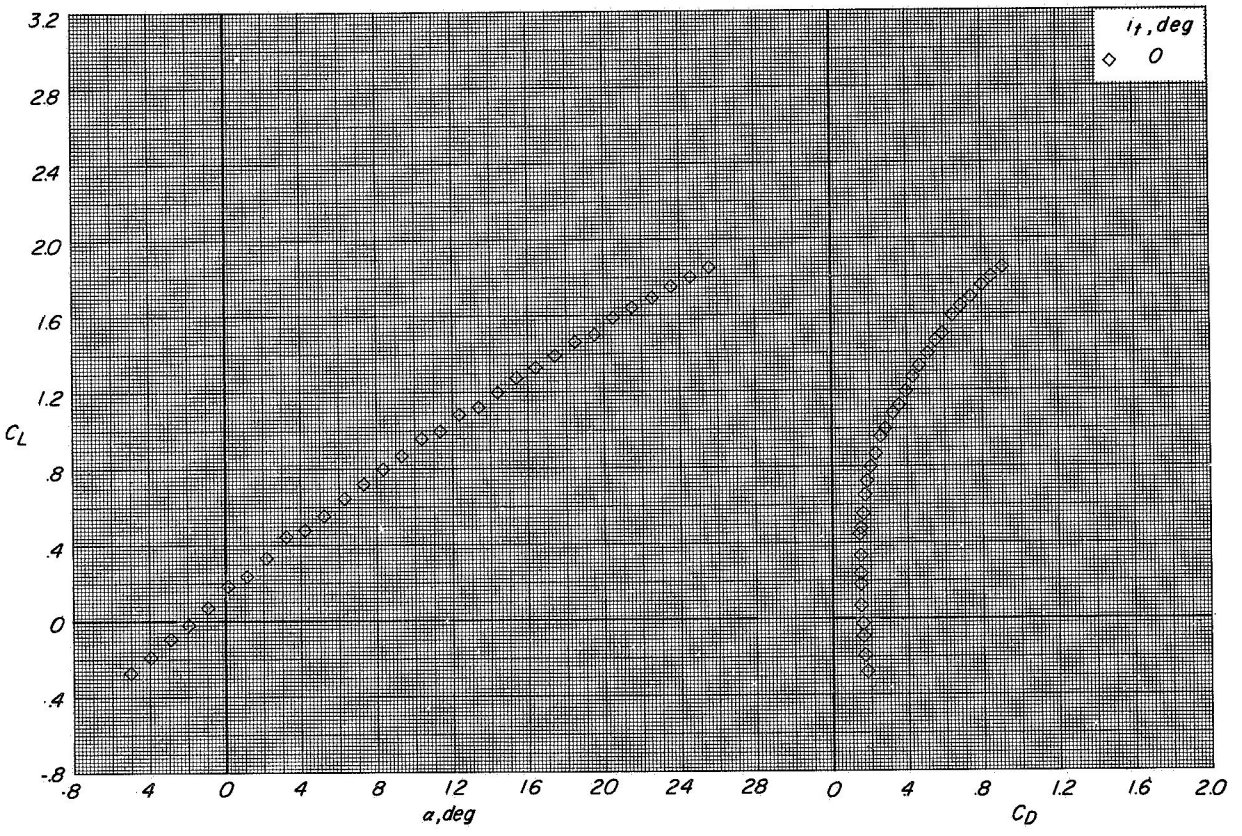

(a) Variation of C_L with α and C_D with C_L

Figure 28.- Longitudinal aerodynamic characteristics of configuration B with direct-lift engines and lift-cruise engines deflected 90°. $C_T = 0$.

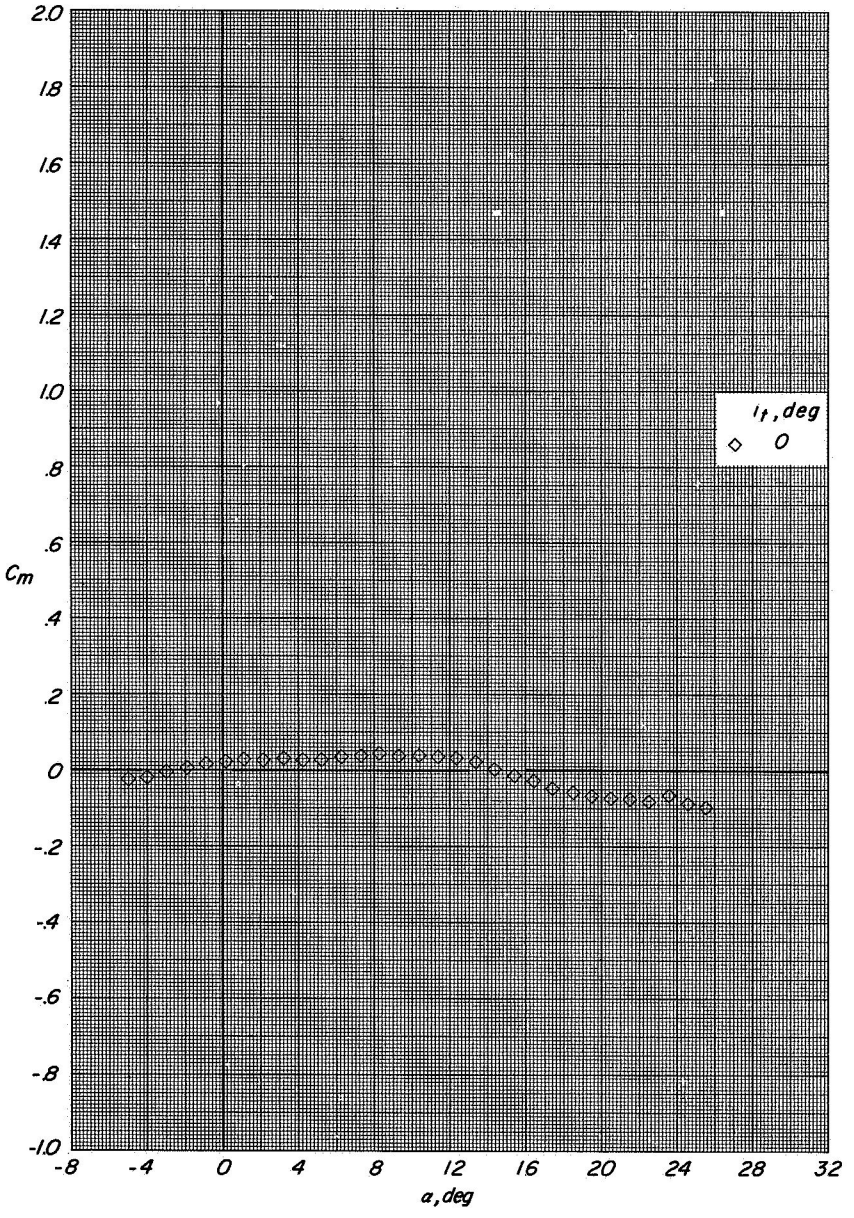

(b) Variation of C_m with α.

Figure 28.- Continued.

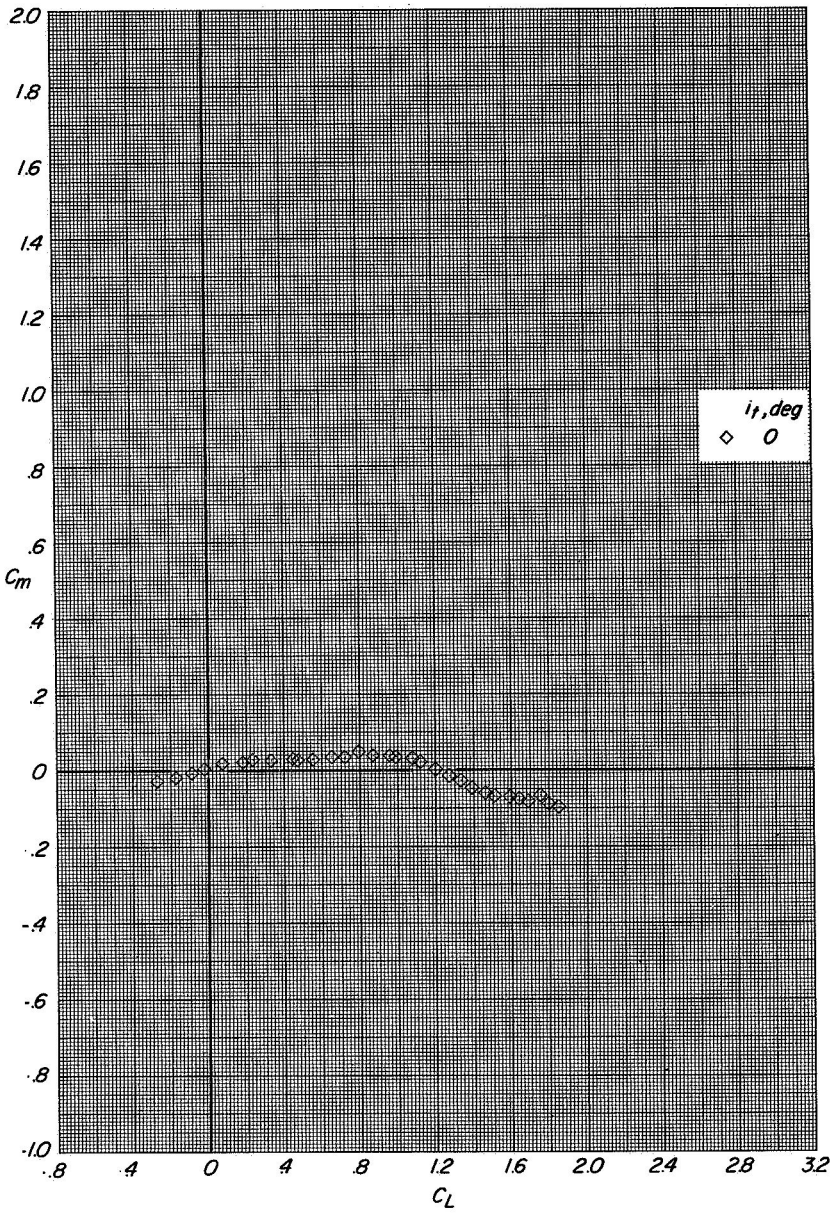

(c) Variation of C_m with C_L

Figure 28.- Concluded.

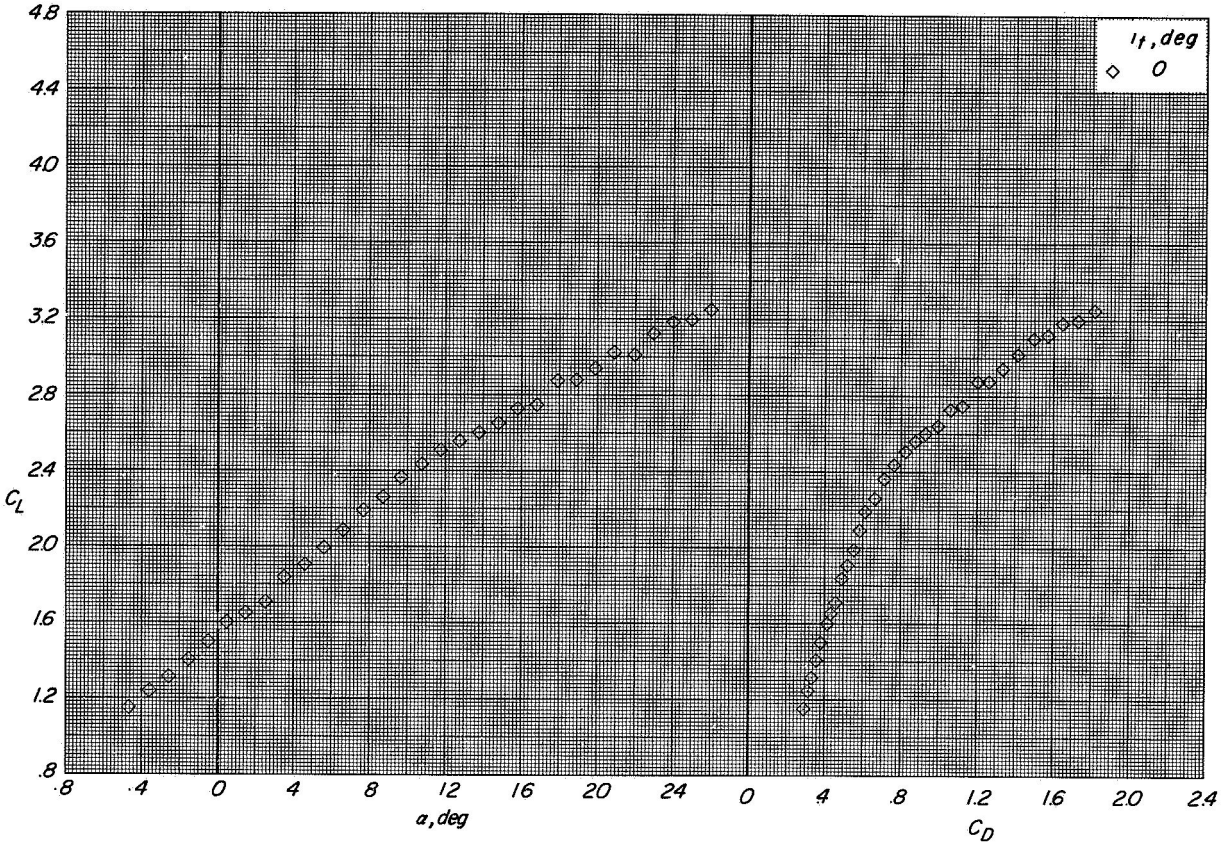

(a) Variation of C_L with α and C_D with C_L.

Figure 29 - Longitudinal aerodynamic characteristics of configuration B with direct-lift engines and lift-cruise engines deflected 90°. $C_T \approx 1.45$.

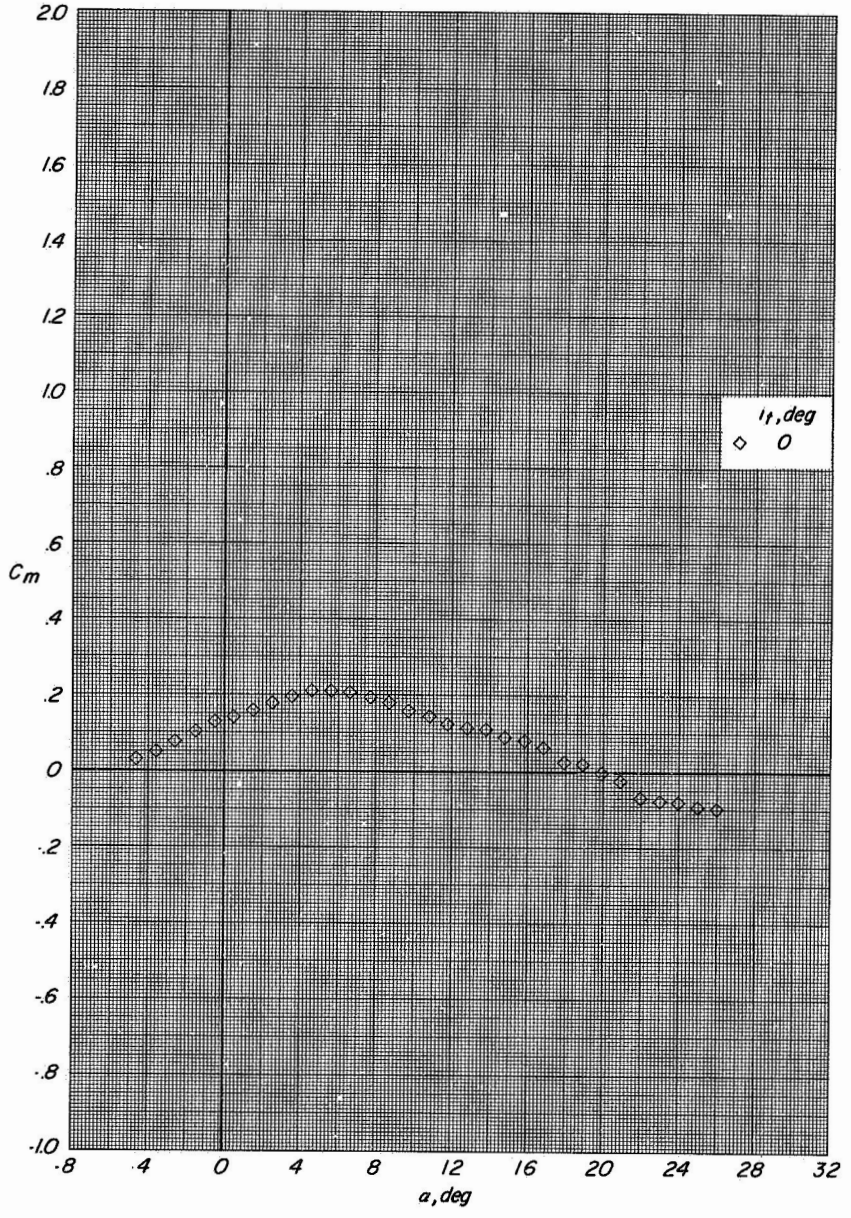

(b) Variation of C_m with α.

Figure 29.- Continued.

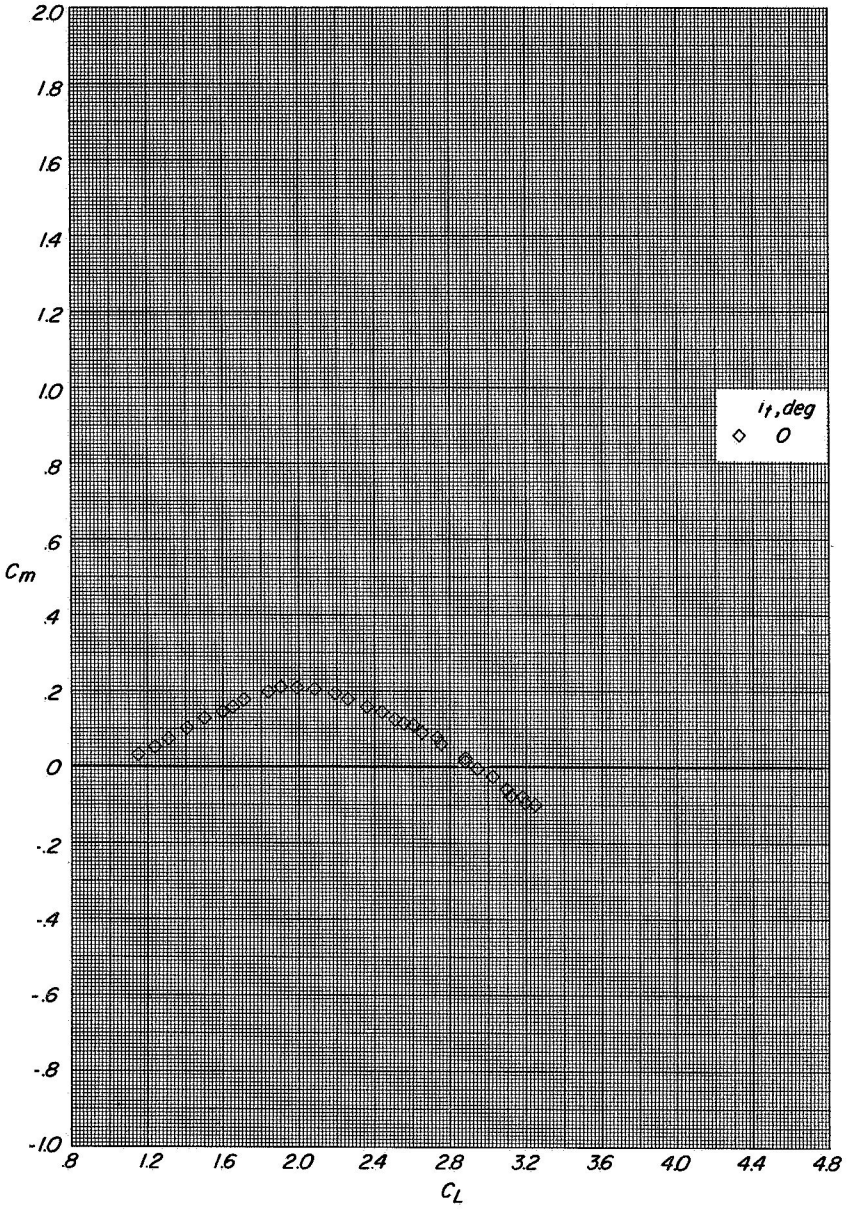

(c) Variation of C_m with C_L.

Figure 29.- Continued.

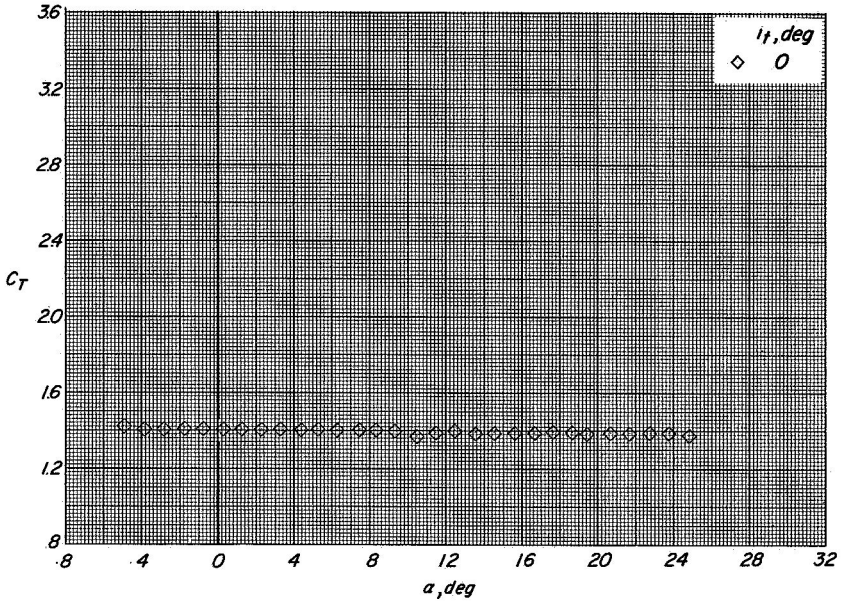

(d) Variation of C_T with α.

Figure 29.- Concluded.

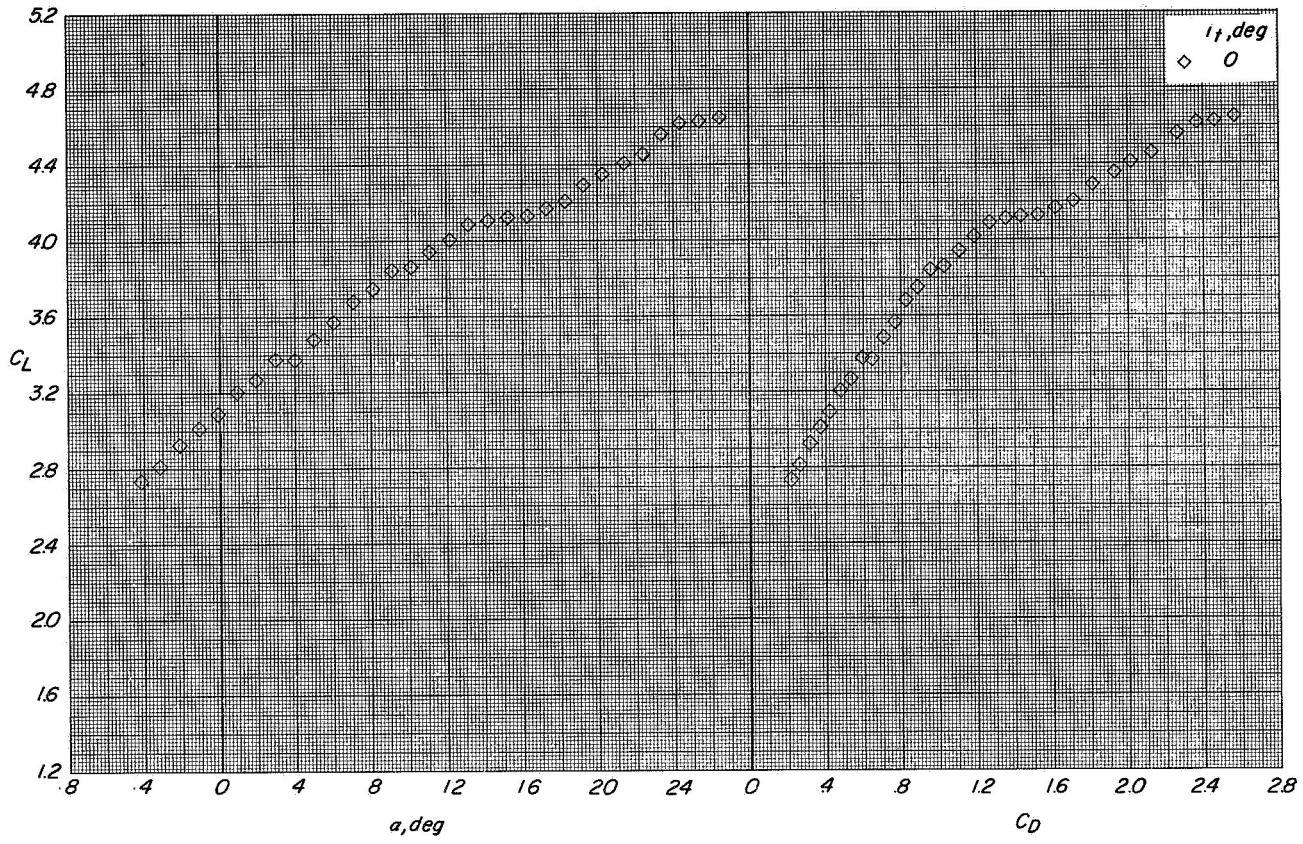

(a) Variation of C_L with α and C_D with C_L.

Figure 30.- Longitudinal aerodynamic characteristics of configuration B with direct-lift engines and lift-cruise engines deflected 90° $C_T \approx 3.3$

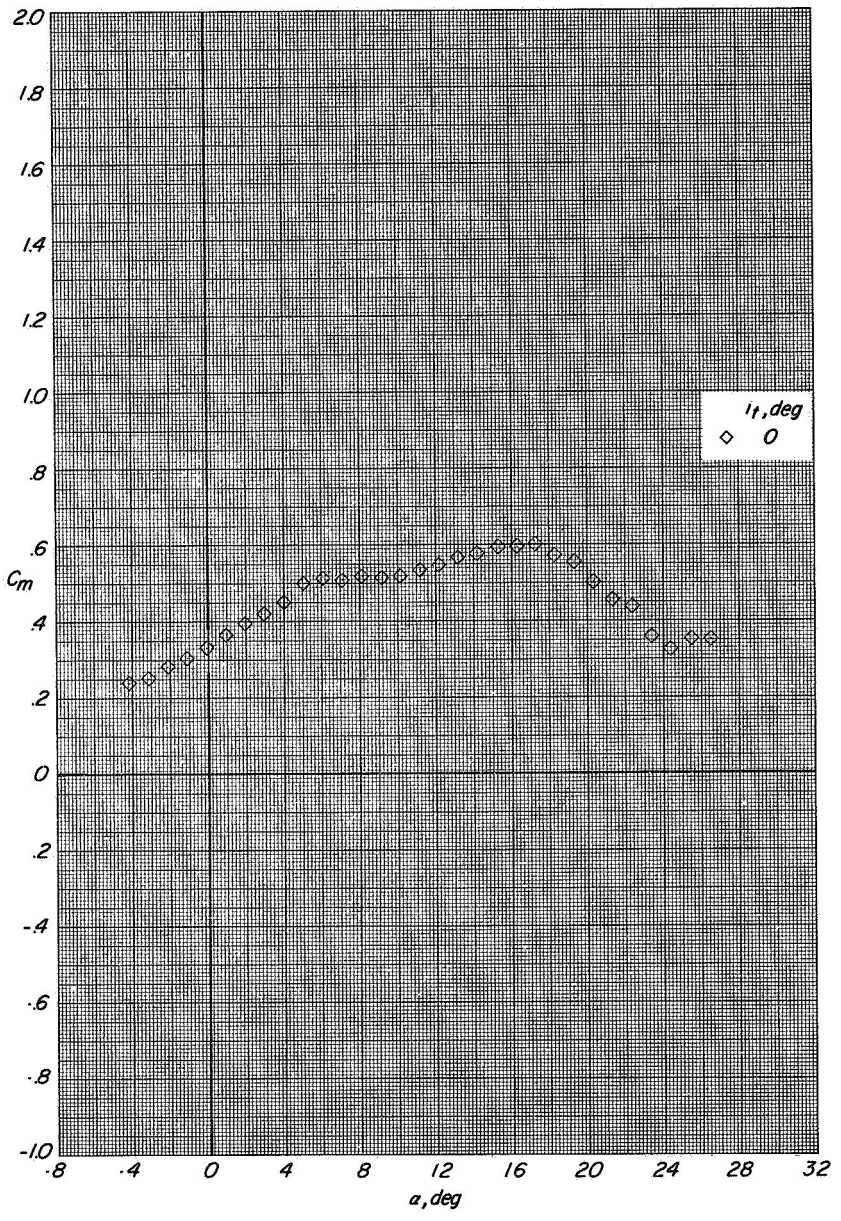

(b) Variation of C_m with α.

Figure 30.- Continued.

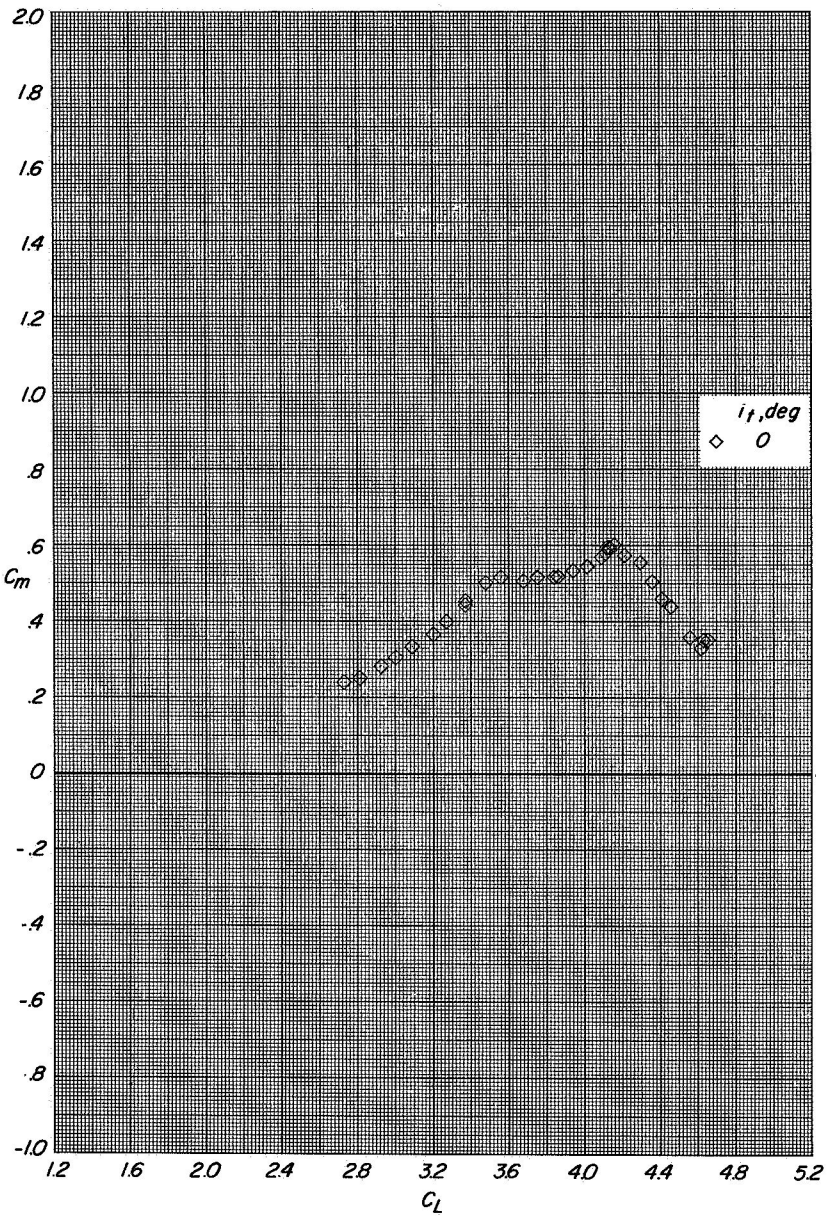

(c) Variation of C_m with C_L.

Figure 30.- Continued.

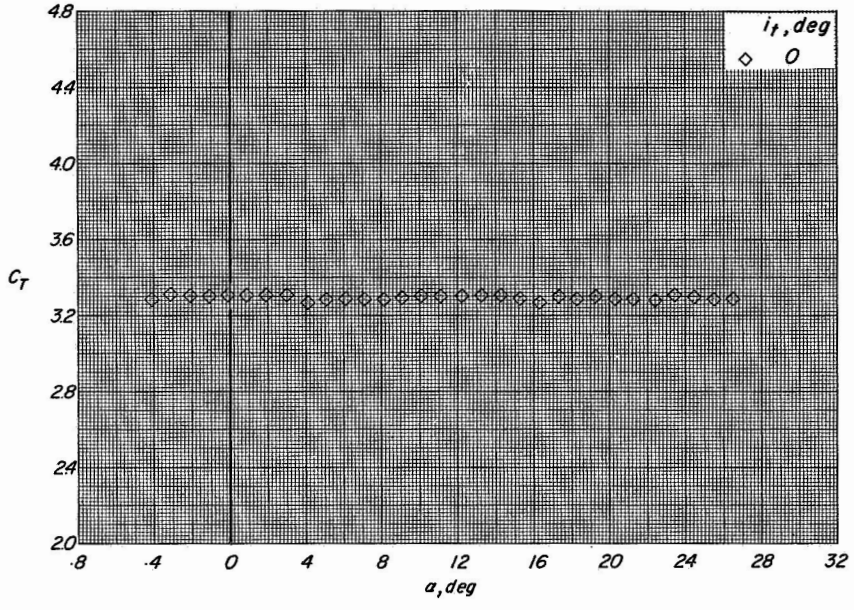

(d) Variation of C_T with α.

Figure 30.- Concluded.

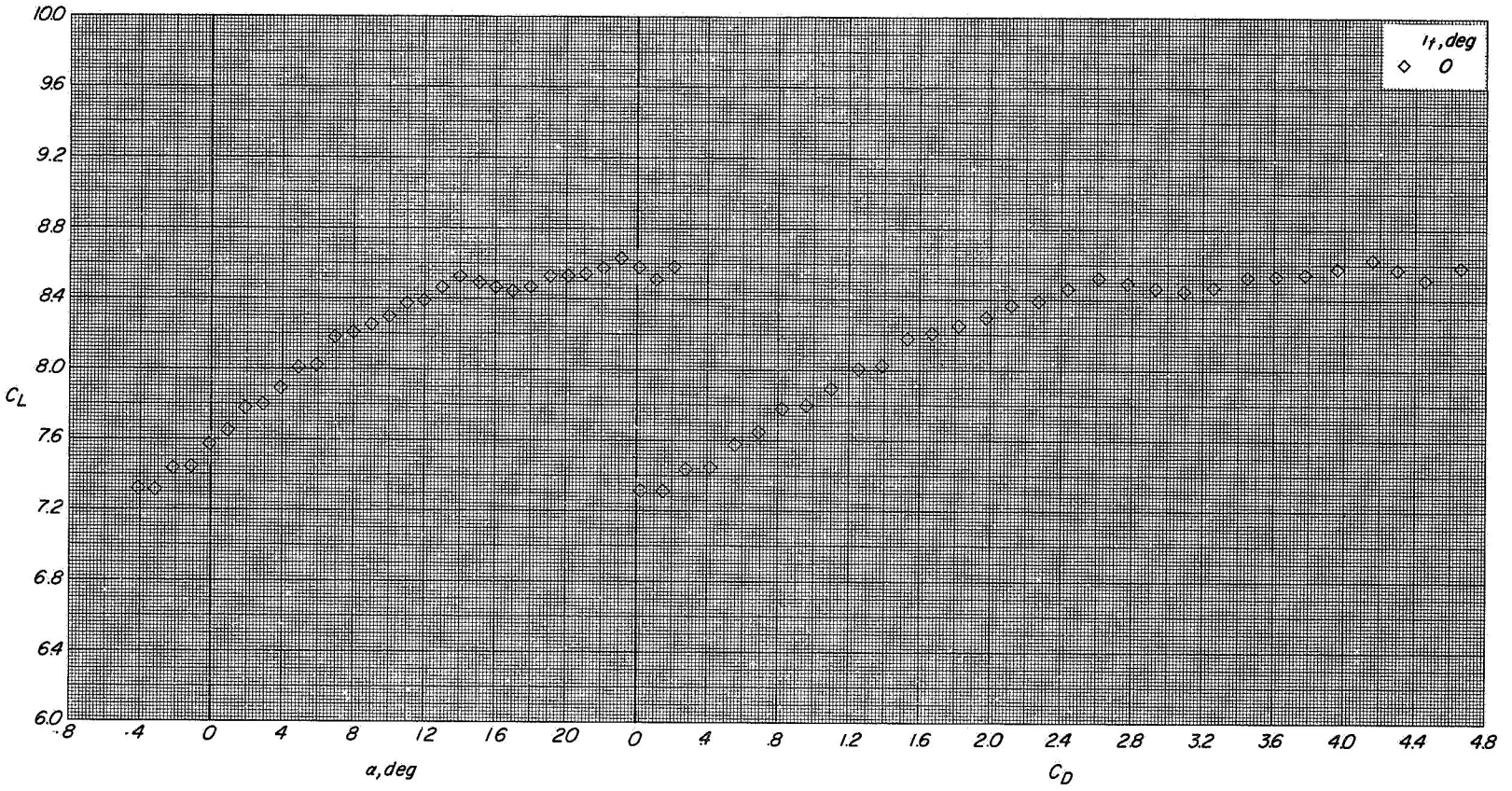

(a) Variation of C_L with α and C_D with C_L

Figure 31.- Longitudinal aerodynamic characteristics of configuration B with direct-lift engines and lift-cruise engines deflected 90°. $C_T \approx 8$.

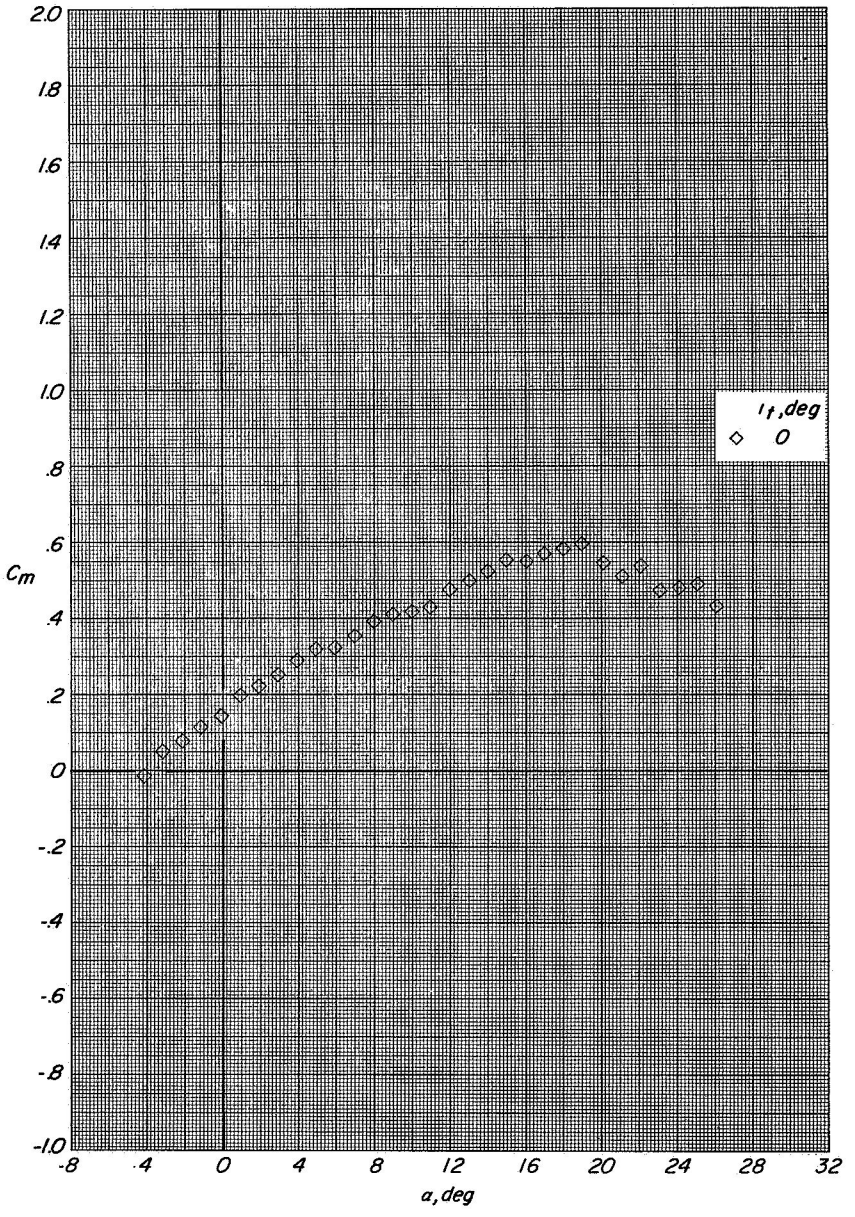

(b) Variation of C_m with α.

Figure 31.- Continued.

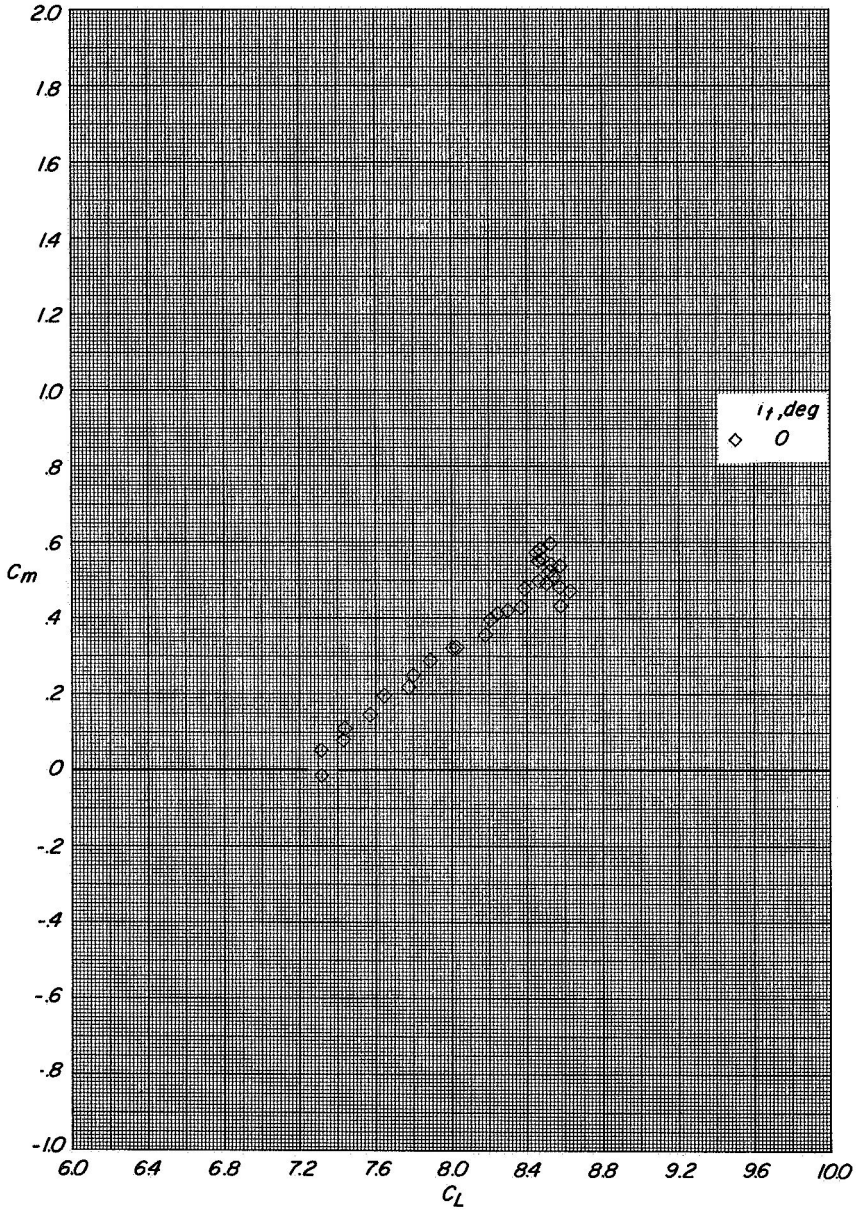

(c) Variation of C_m with C_L.

Figure 31.- Continued.

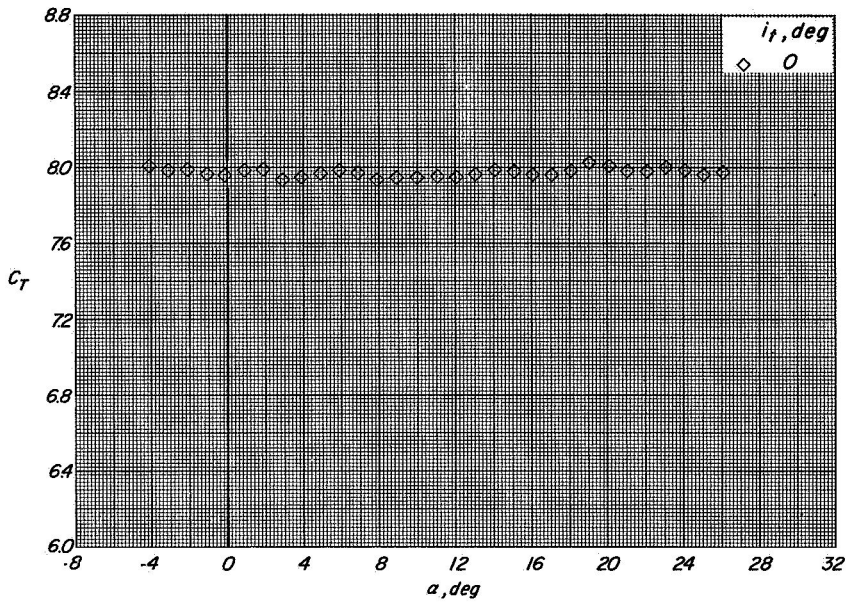

(d) Variation of C_T with α.

Figure 31.- Concluded.

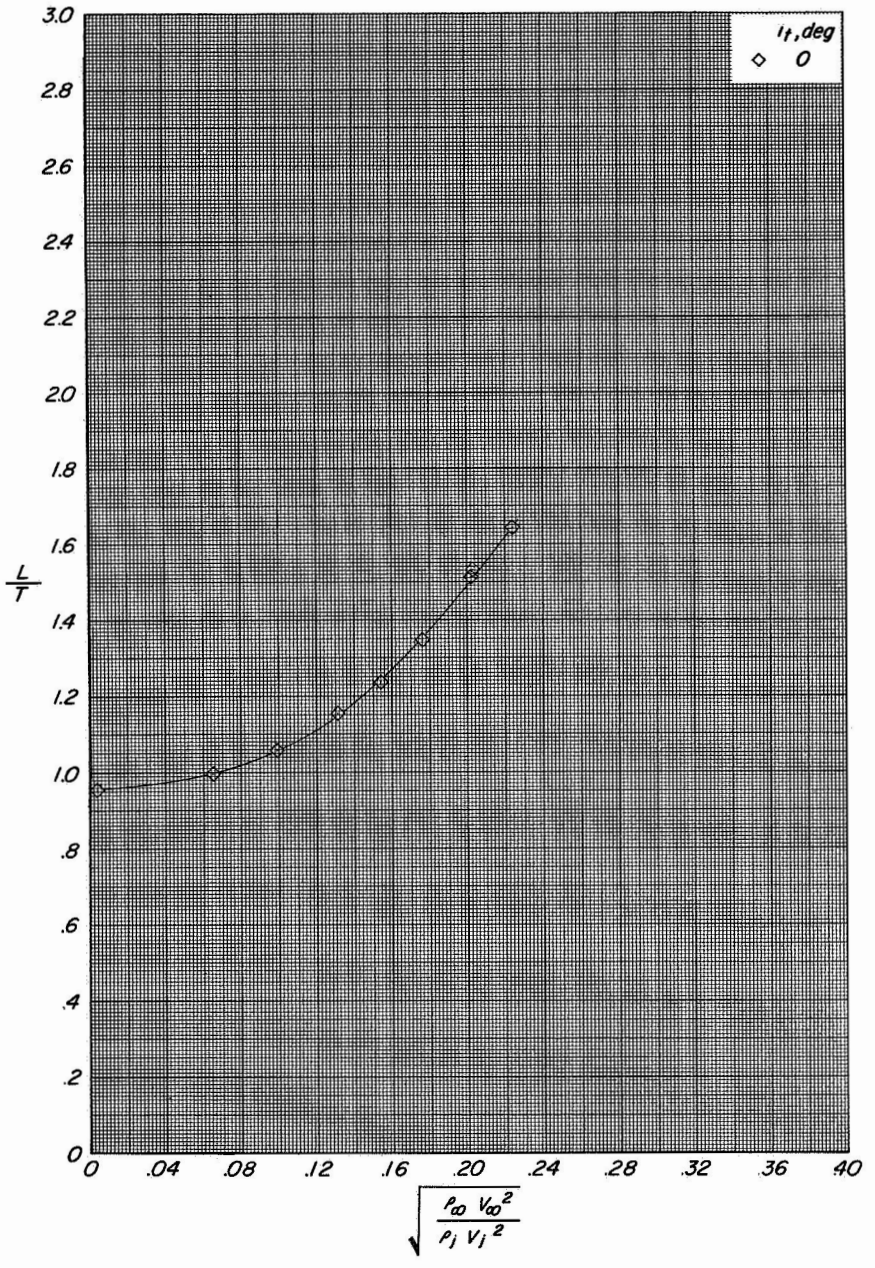

(a) Variation of L/T with effective velocity ratio.

Figure 32.- Longitudinal aerodynamic characteristics of configuration B with direct-lift engines and lift-cruise engines deflected 90°. $\alpha = 12°$.

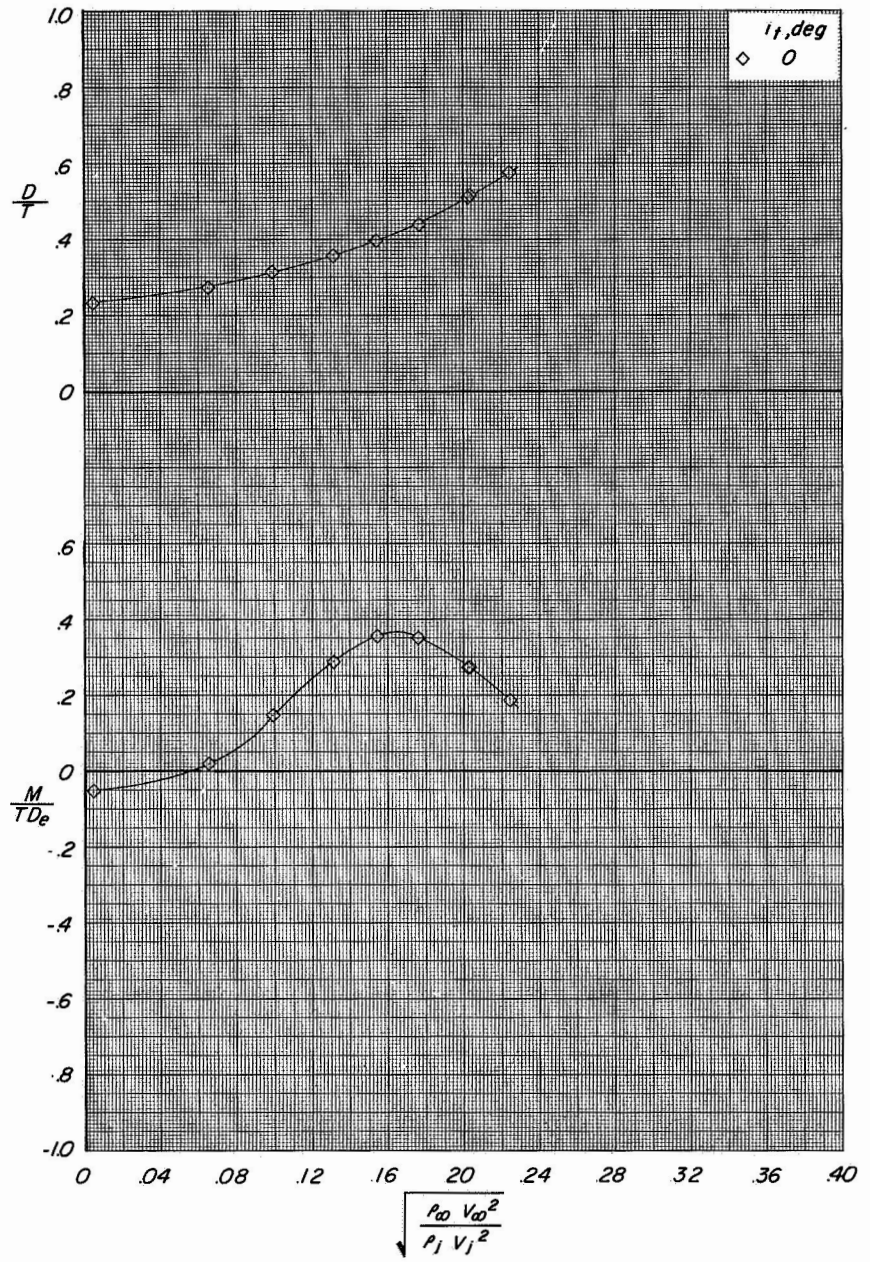

(b) Variation of D/T and M/TD_e with effective velocity ratio

Figure 32.- Concluded.

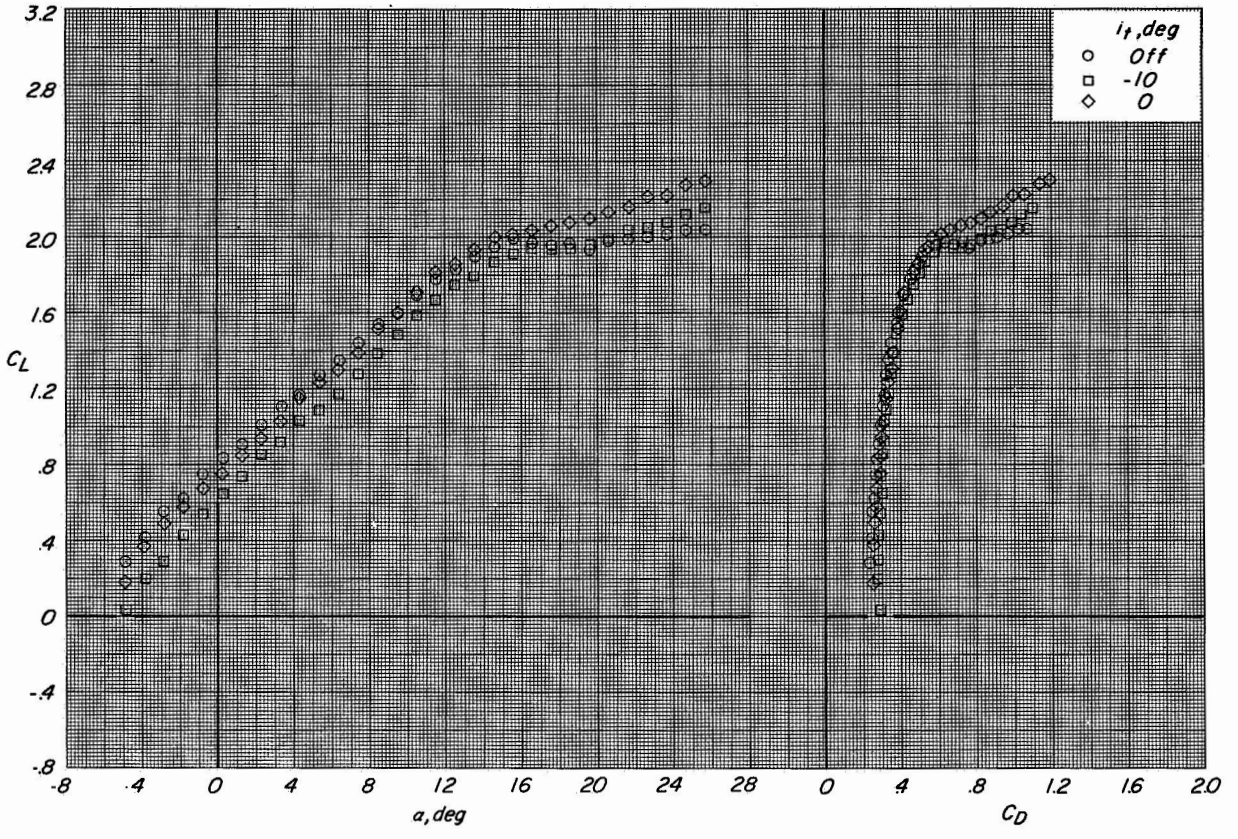

(a) Variation of C_L with α and C_D with C_L.

Figure 33.- Longitudinal aerodynamic characteristics of configuration A with direct-lift engines and lift-cruise engines deflected 45°. $C_T = 0$.

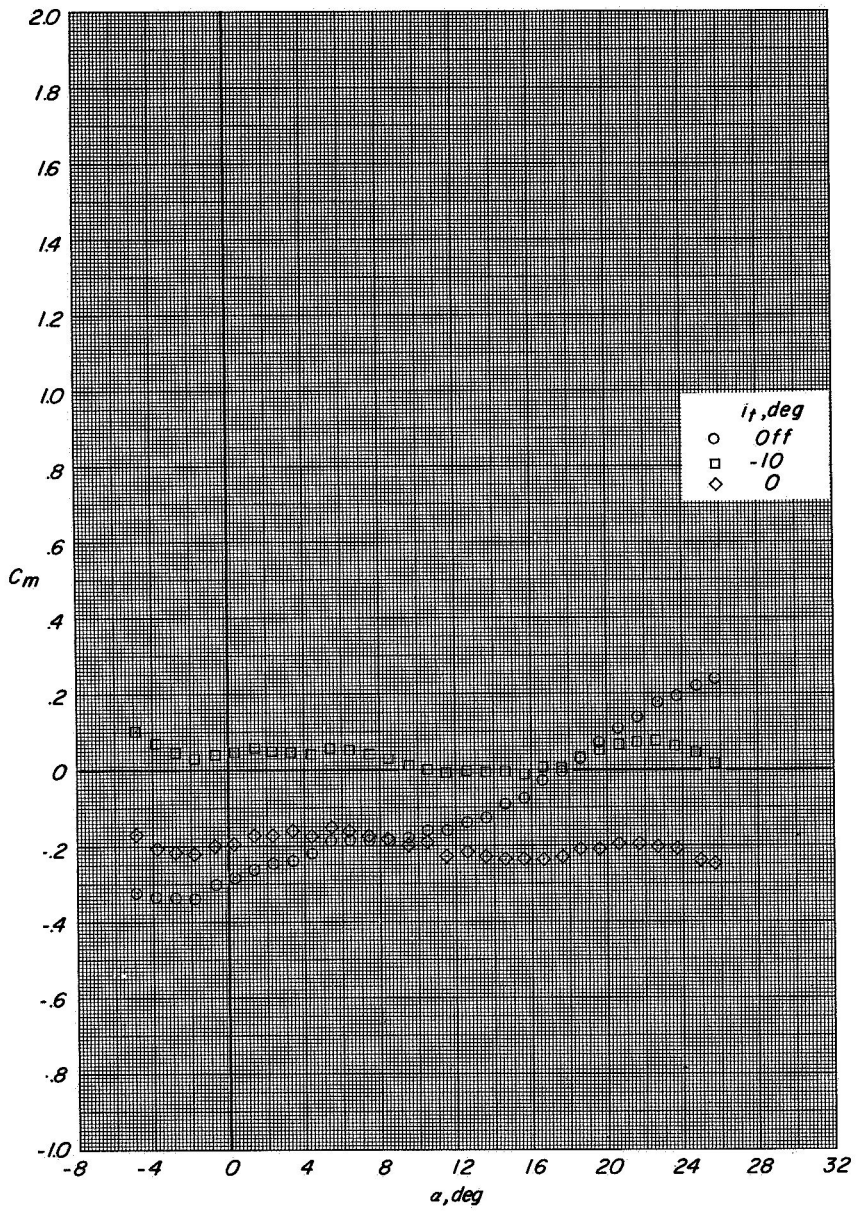

(b) Variation of C_m with α.

Figure 33.- Continued.

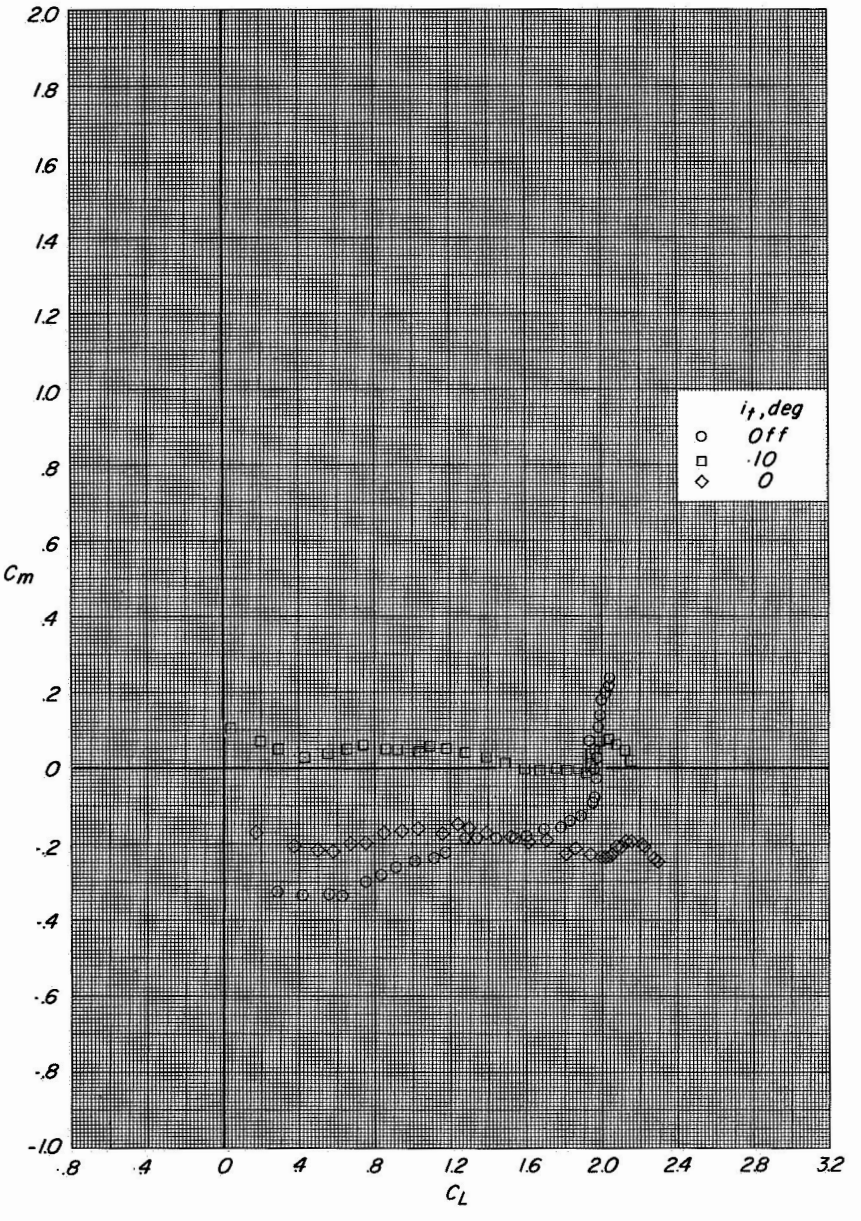

(c) Variation of C_m with C_L.

Figure 33.- Concluded.

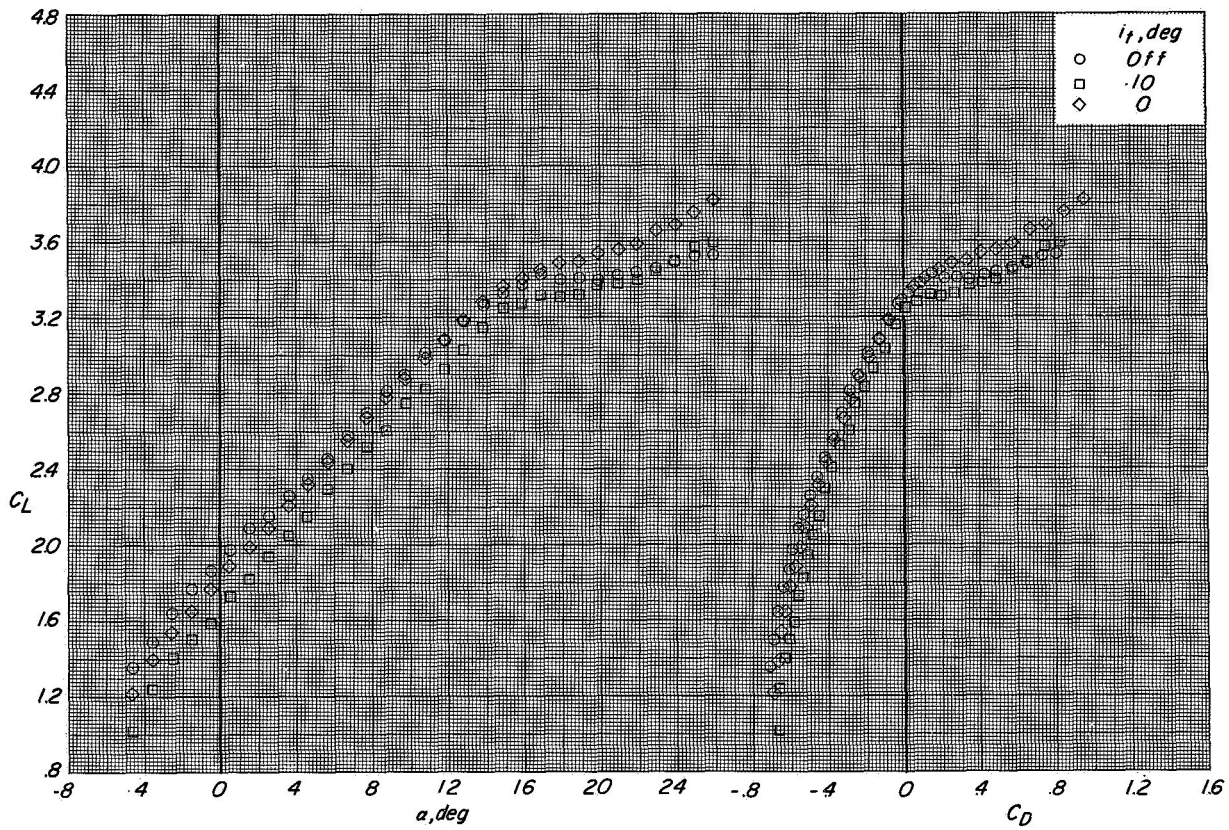

(a) Variation of C_L with α and C_D with C_L.

Figure 34.- Longitudinal aerodynamic characteristics of configuration A with direct-lift engines and lift-cruise engines deflected 45°. $C_T \approx 1$ 45

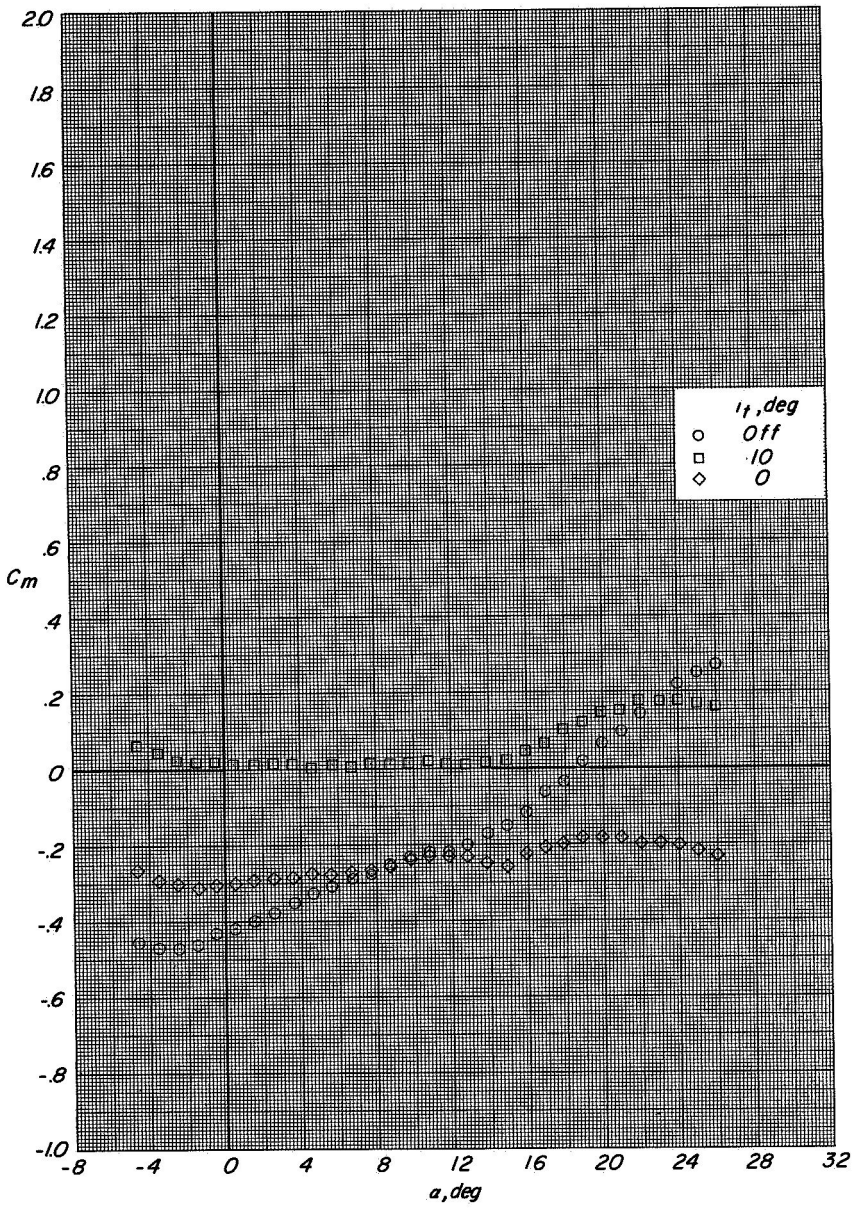

(b) Variation of C_m with α.

Figure 34 - Continued.

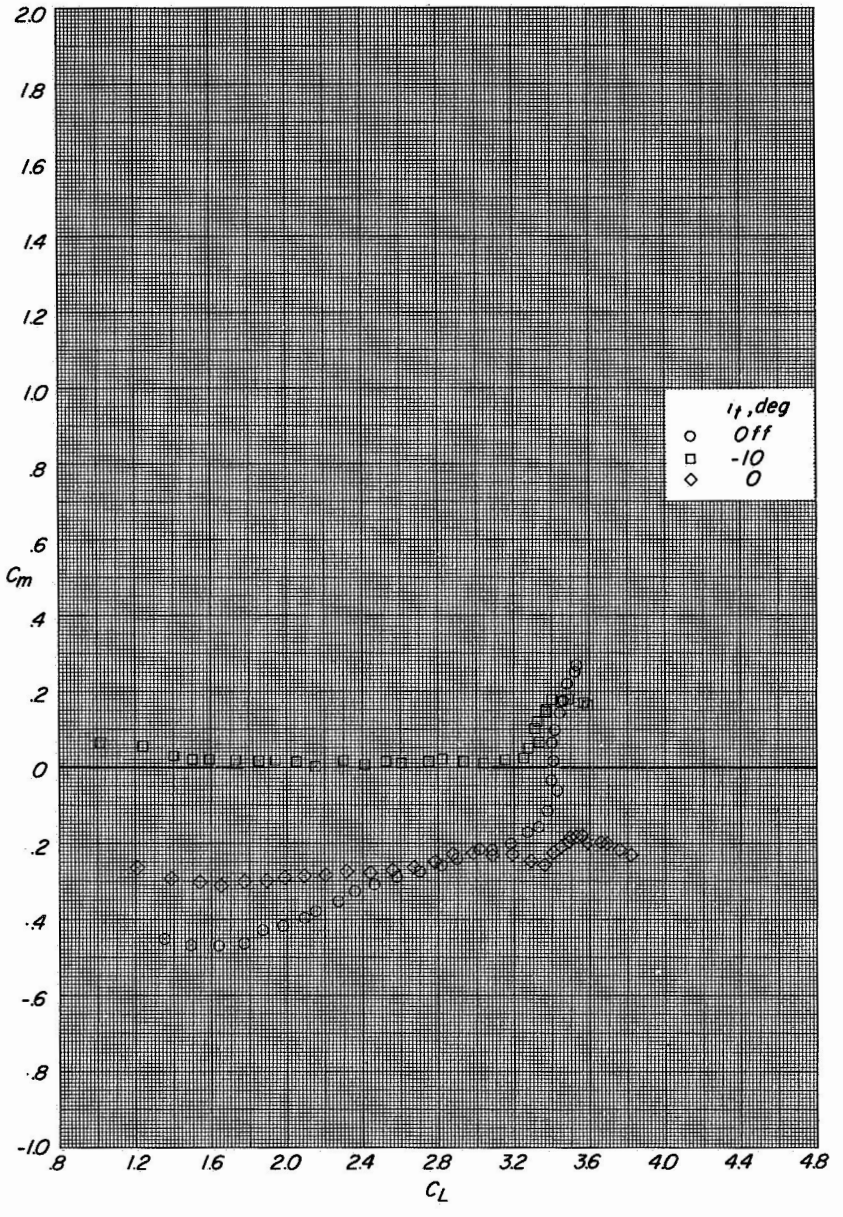

(c) Variation of C_m with C_L

Figure 34.- Continued.

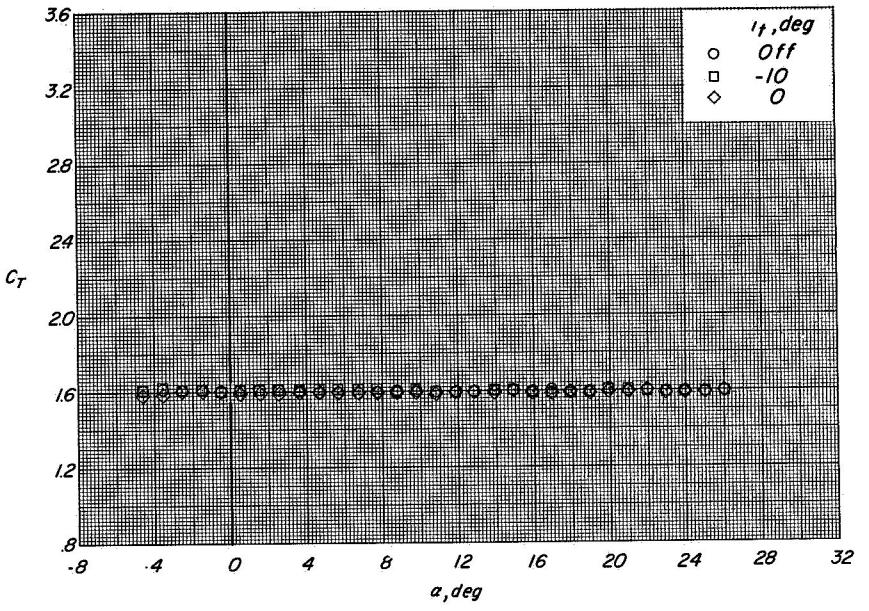

(d) Variation of C_T with α.

Figure 34.- Concluded.

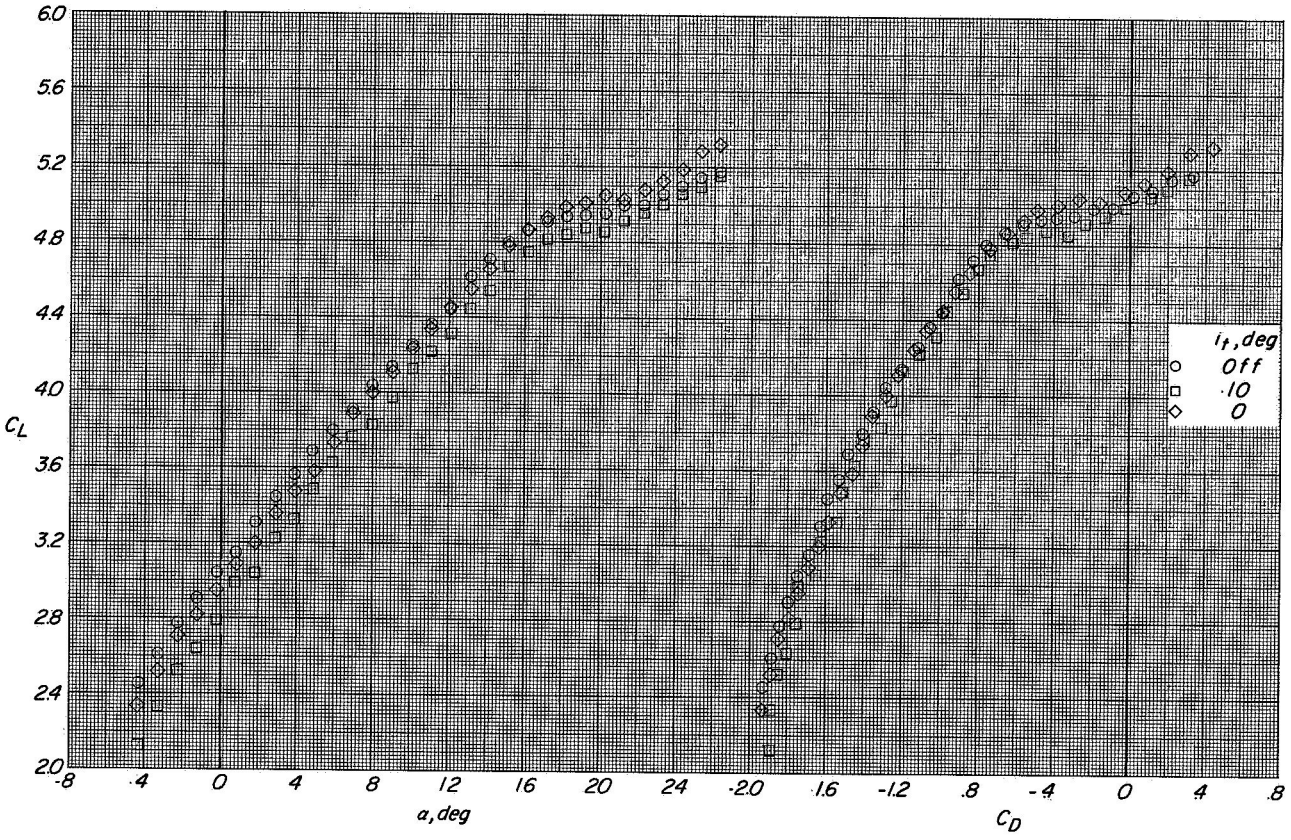

(a) Variation of C_L with α and C_D with C_L.

Figure 35.- Longitudinal aerodynamic characteristics of configuration A with direct-lift engines and lift-cruise engines deflected 45°. $C_T \approx 3.3$.

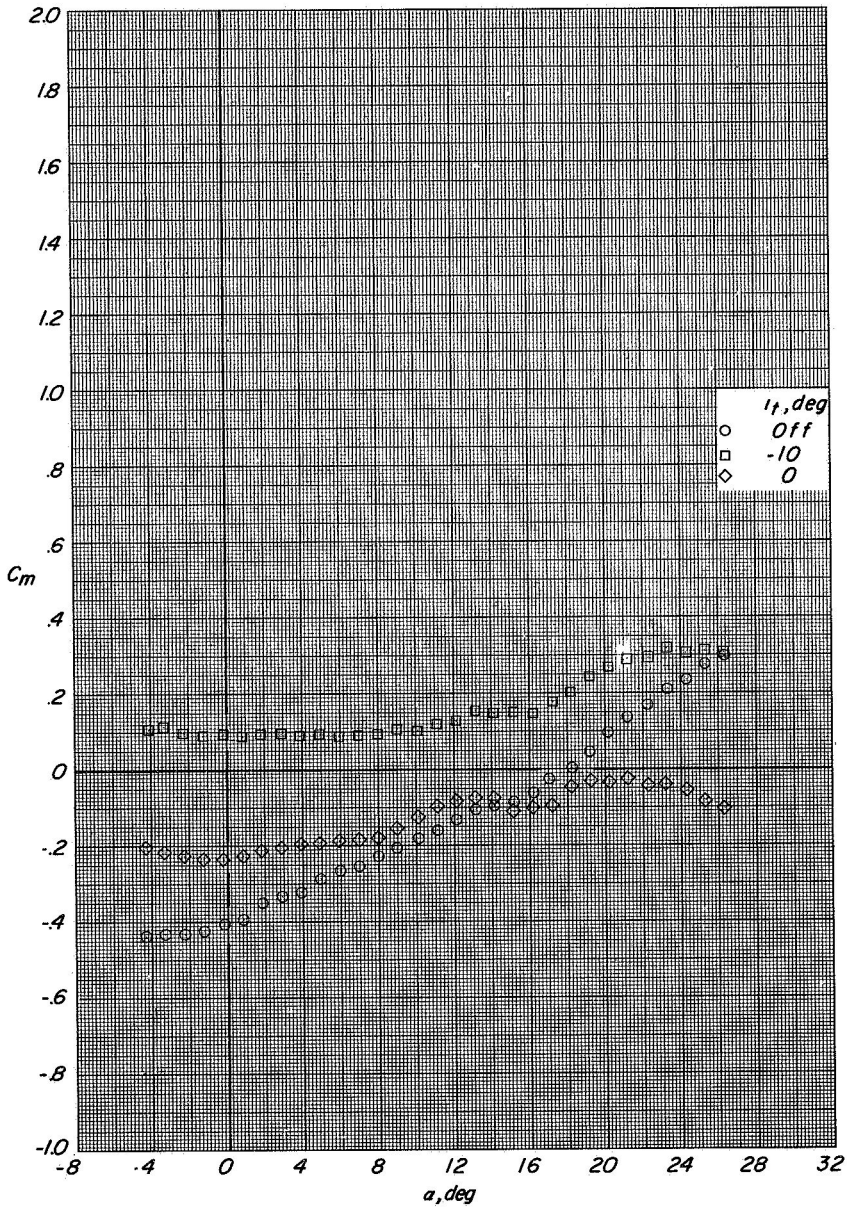

(b) Variation of C_m with α.

Figure 35.- Continued.

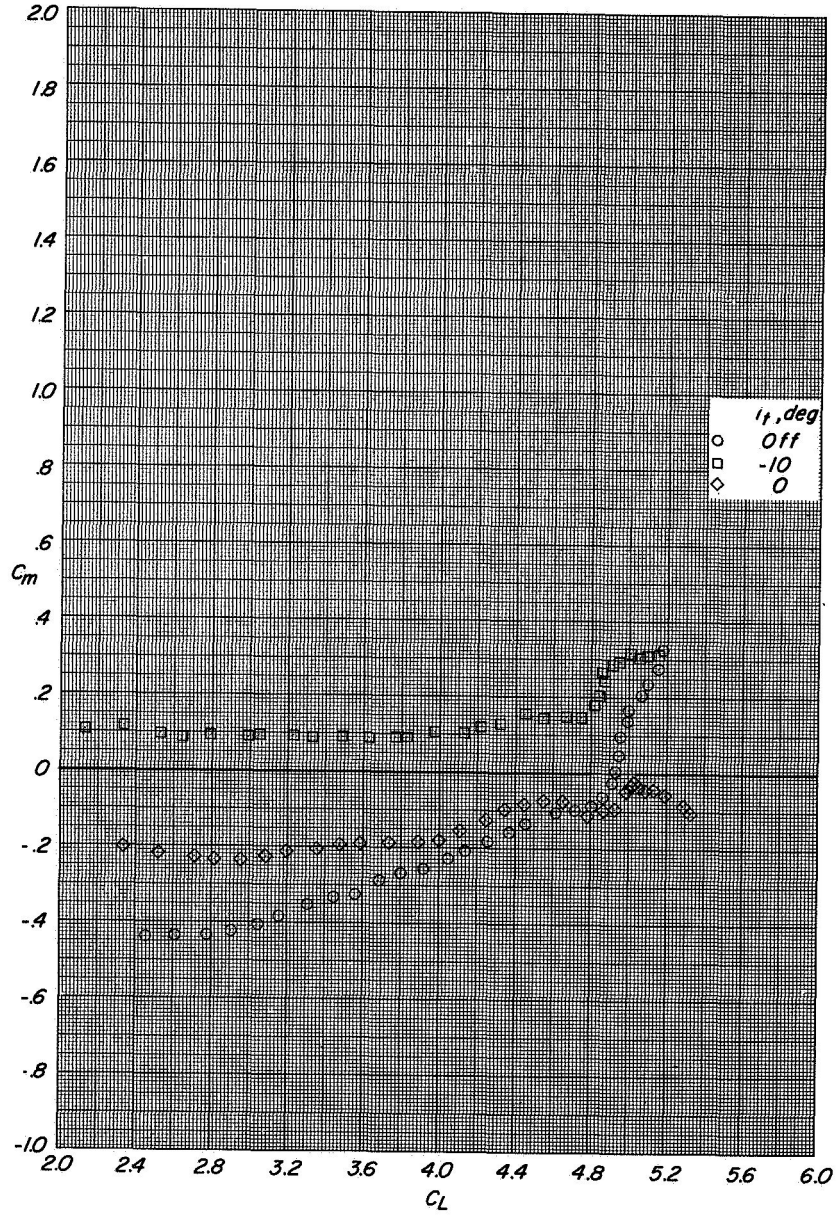

(c) Variation of C_m with C_L.

Figure 35.- Continued.

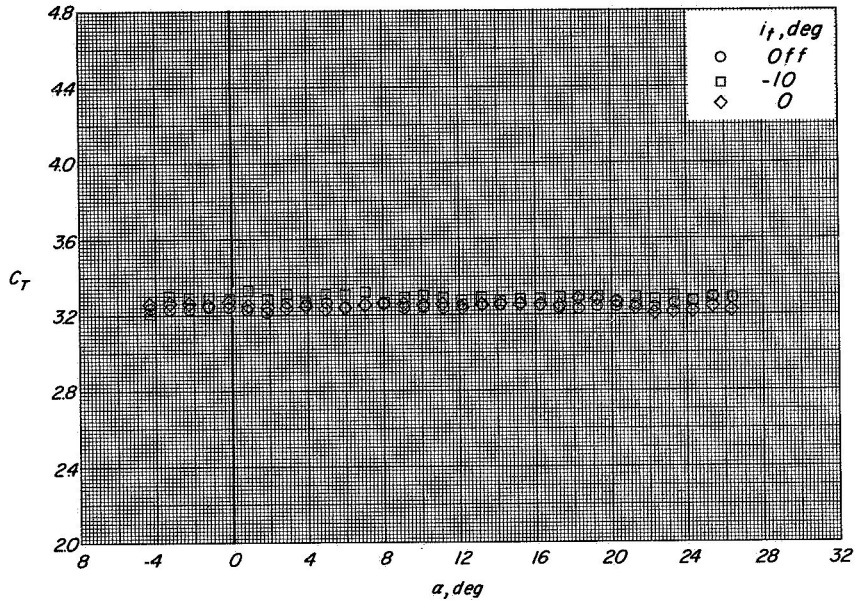

(d) Variation of C_T with α.

Figure 35.- Concluded.

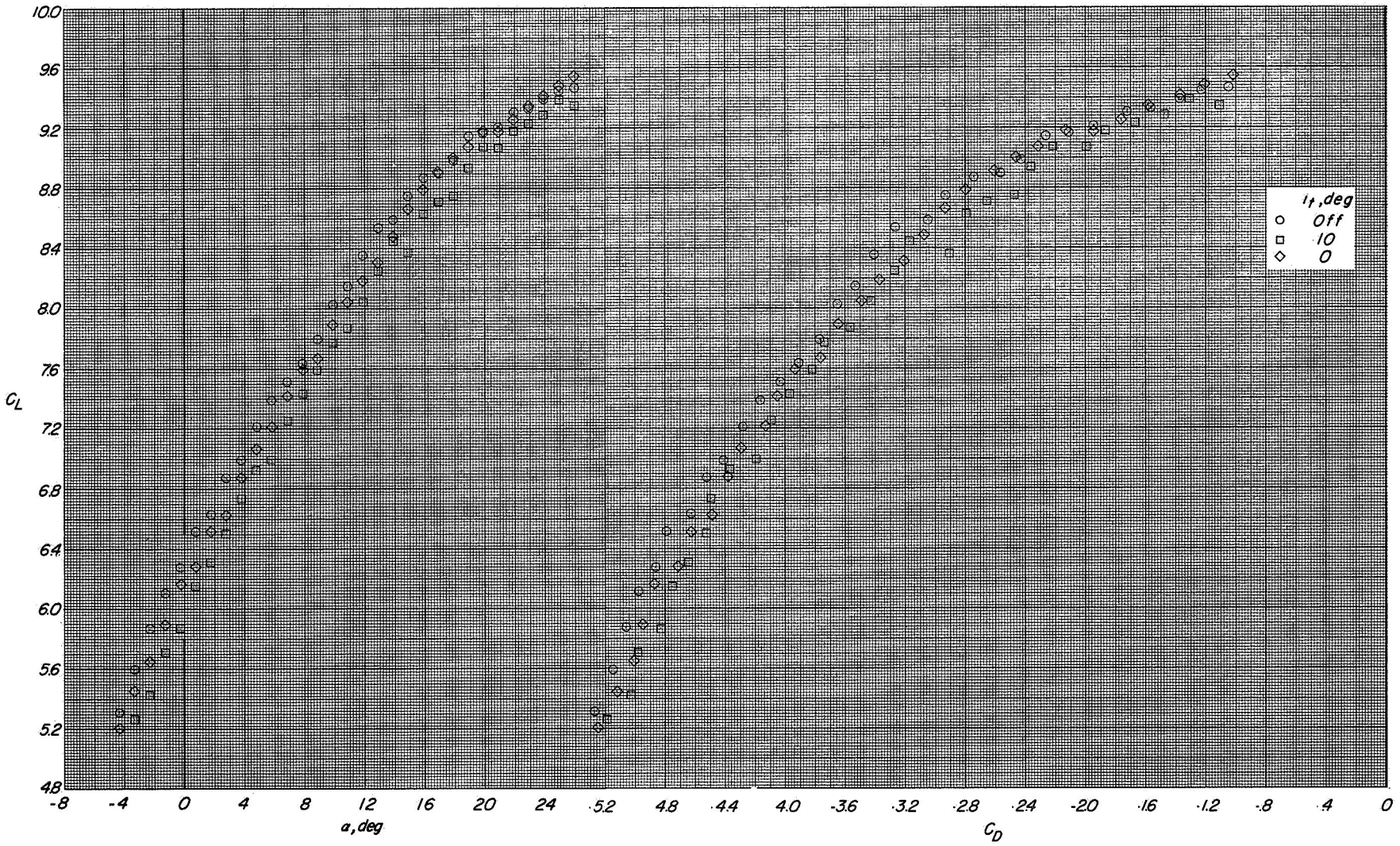

(a) Variation of C_L with α and C_D with C_L.

Figure 36.- Longitudinal aerodynamic characteristics of configuration A with direct-lift engines and lift-cruise engines deflected 45°. $C_T \approx 8$.

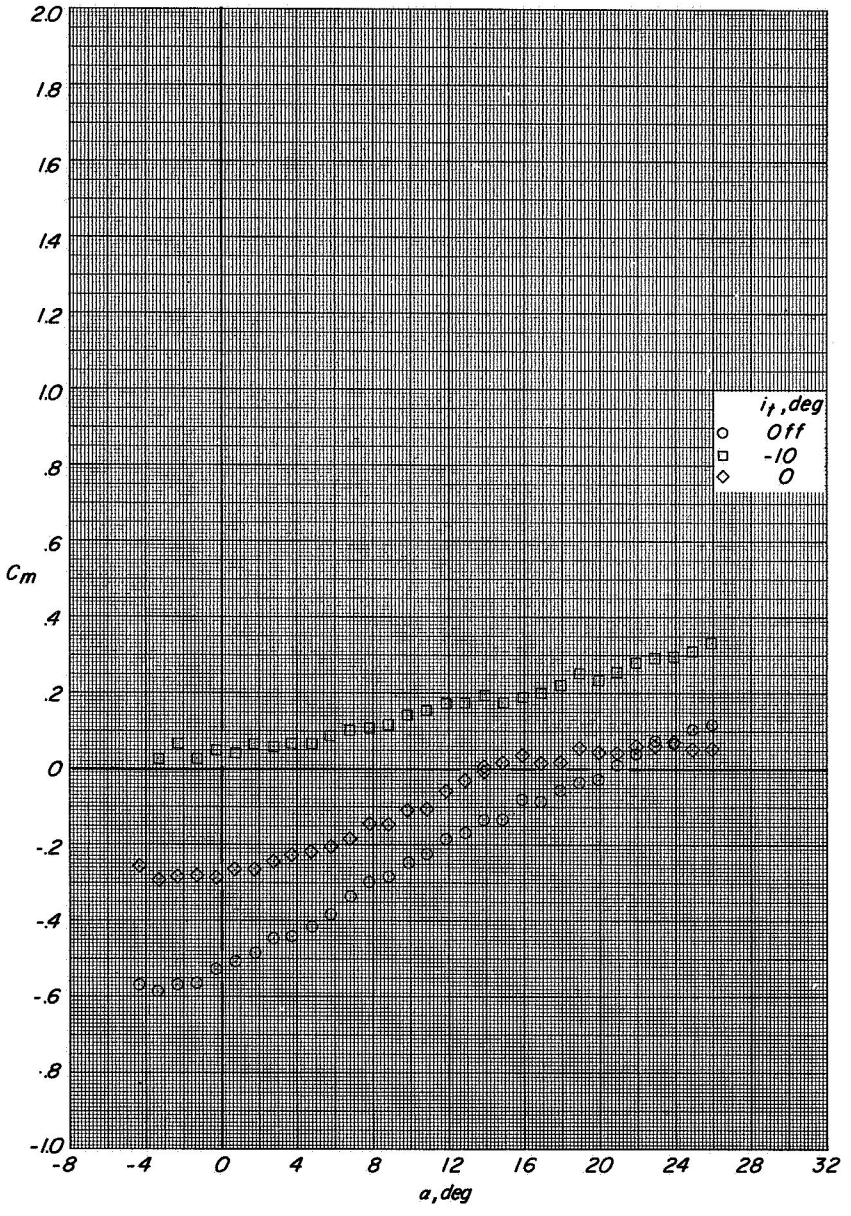

(b) Variation of C_m with α.

Figure 36.- Continued.

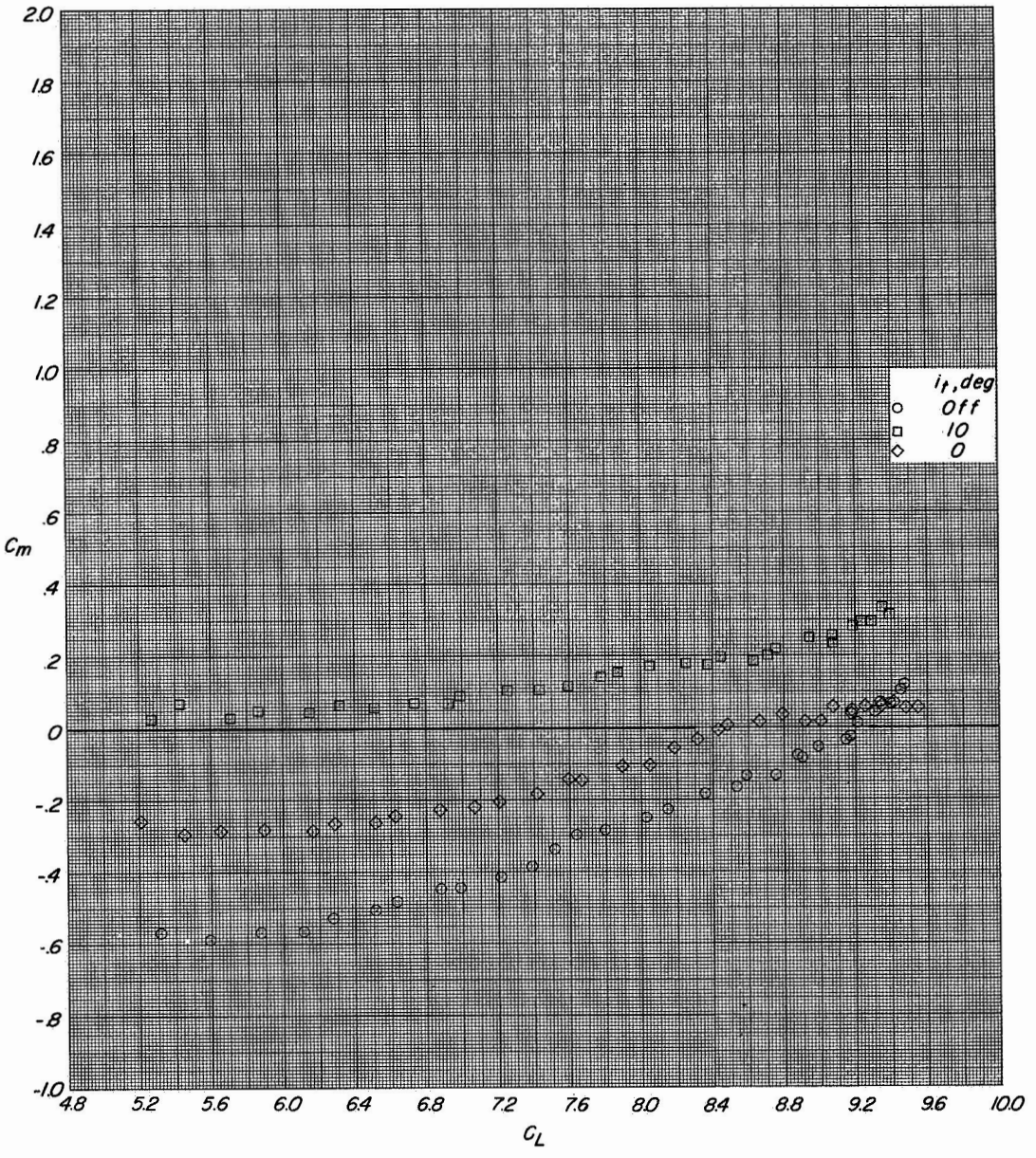

(c) Variation of C_m with C_L.

Figure 36.- Continued.

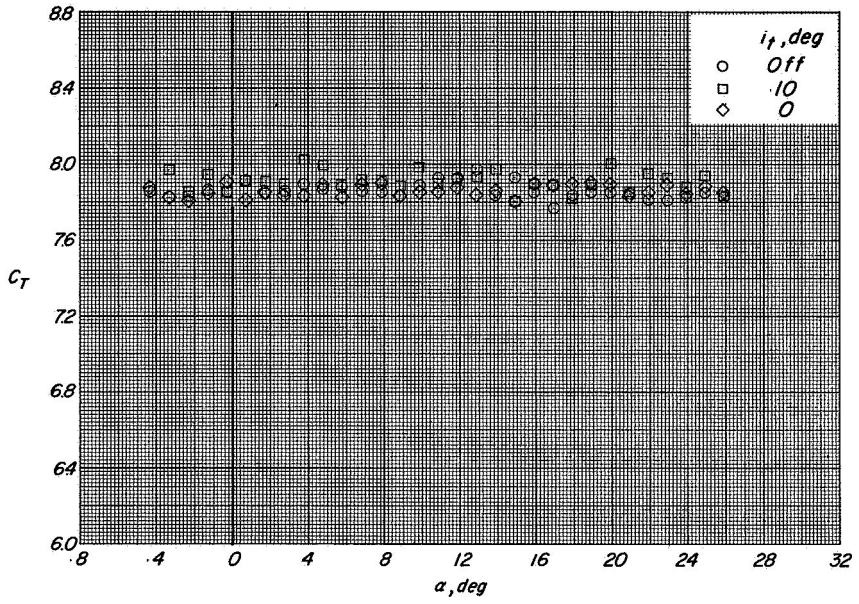

(d) Variation of C_T with α.

Figure 36.- Concluded.

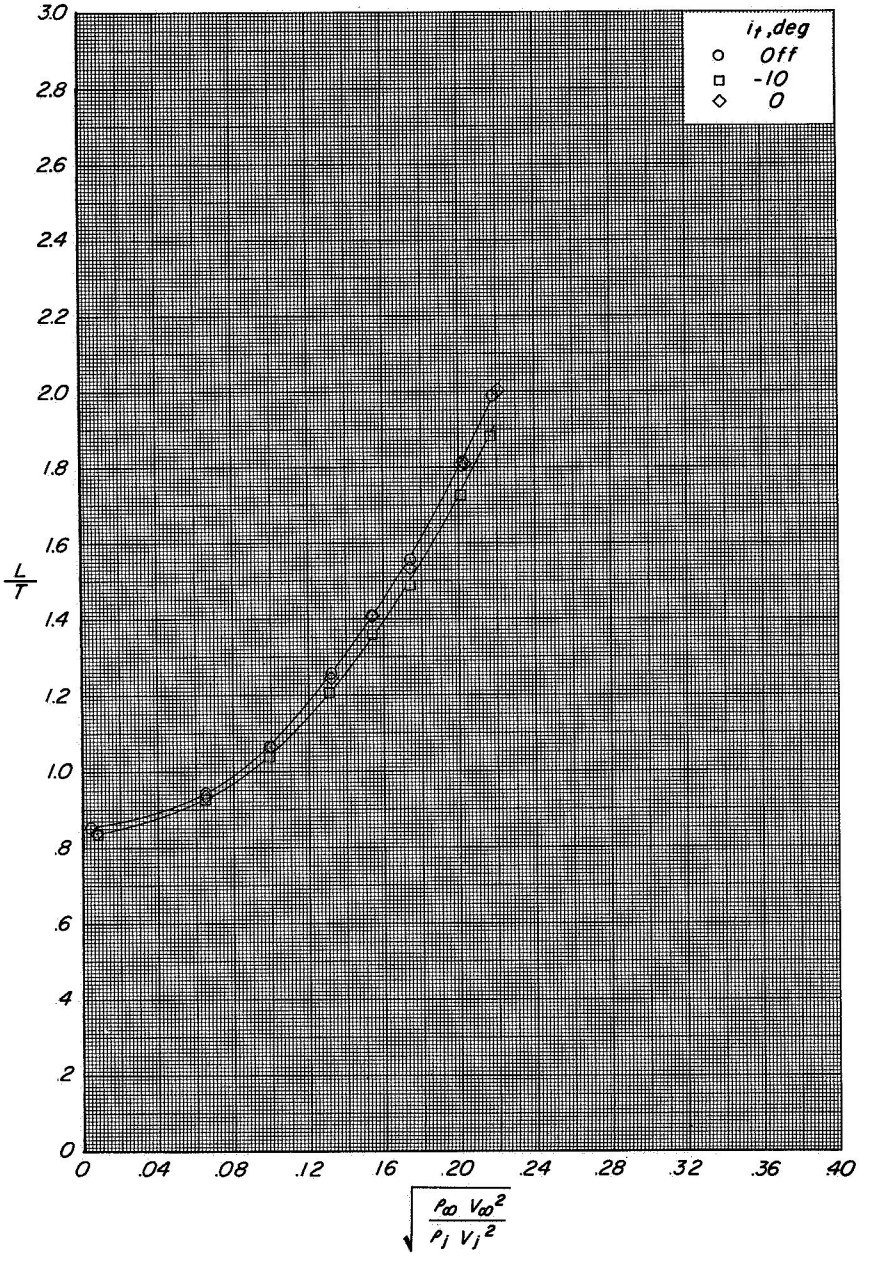

(a) Variation of L/T with effective velocity ratio.

Figure 37.- Longitudinal aerodynamic characteristics of configuration A with direct-lift engines and lift-cruise engines deflected 45°. $\alpha = 12°$.

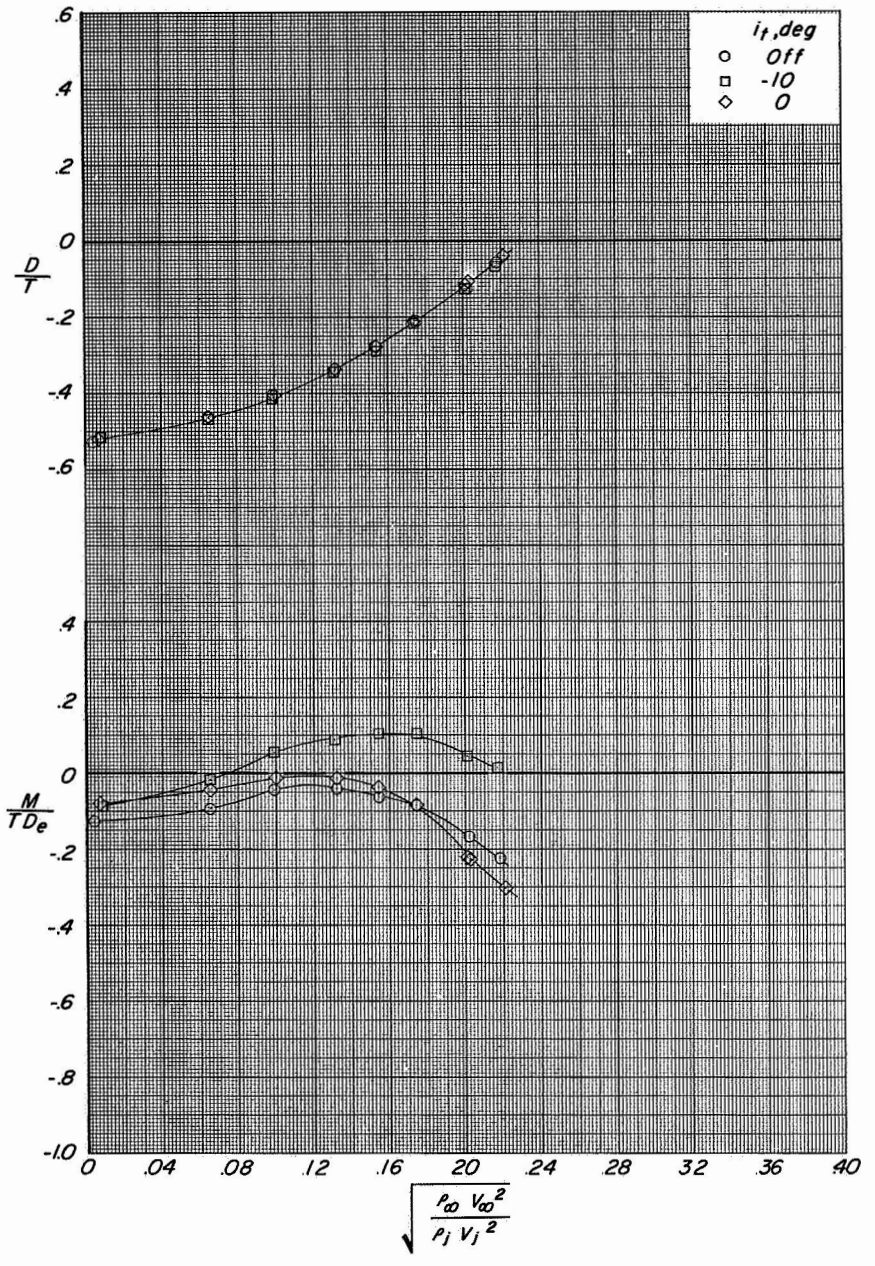

(b) Variation of D/T and M/TD_e with effective velocity ratio.

Figure 37.- Concluded.

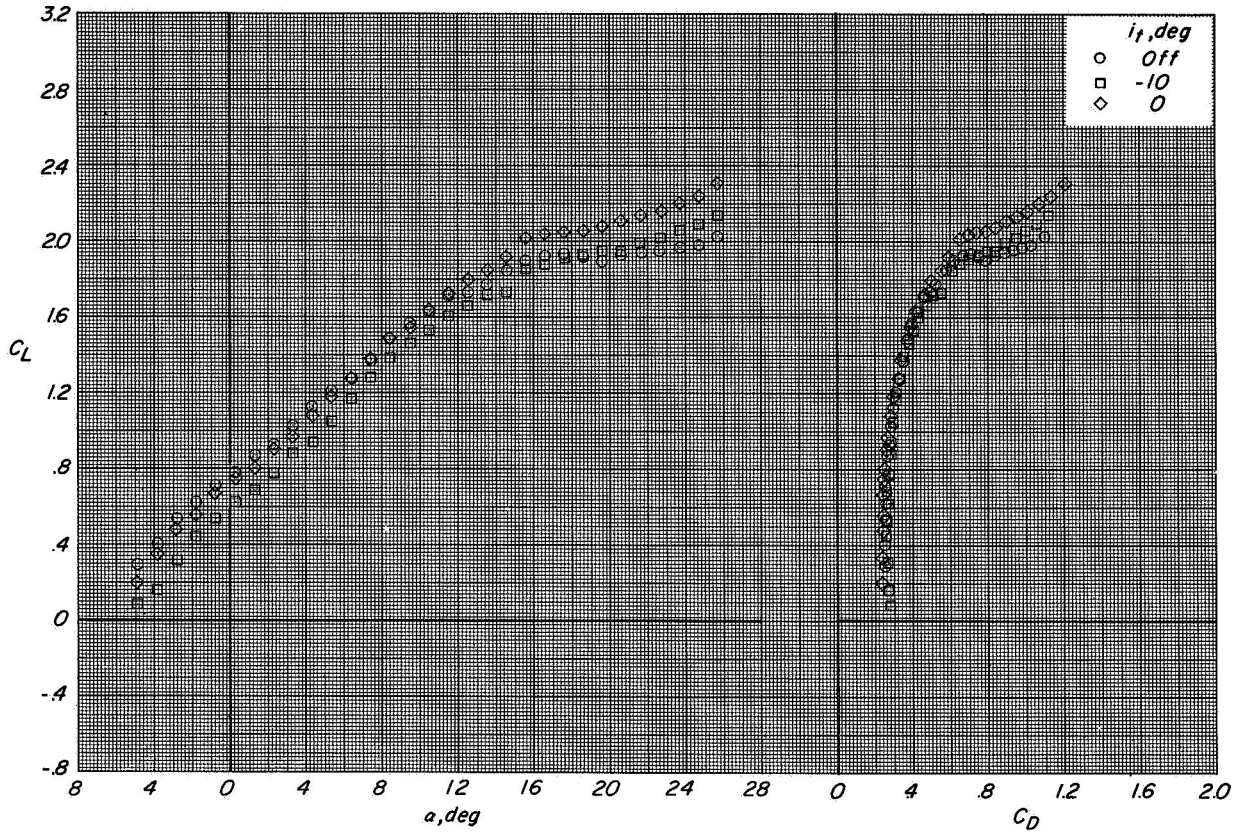

(a) Variation of C_L with α and C_D with C_L.

Figure 38.- Longitudinal aerodynamic characteristics of configuration A with direct-lift engines and lift-cruise engines deflected 0°. C_T = 0.

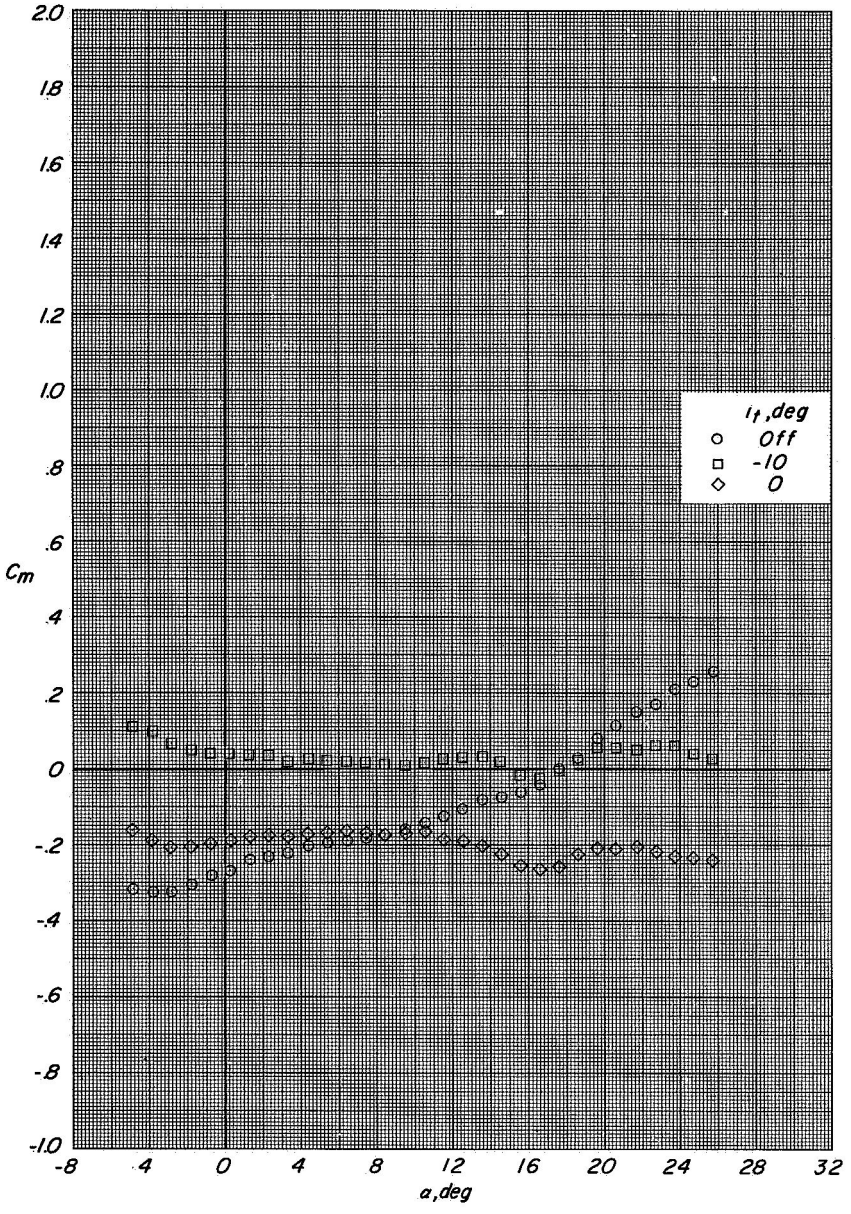

(b) Variation of C_m with α.

Figure 38.- Continued.

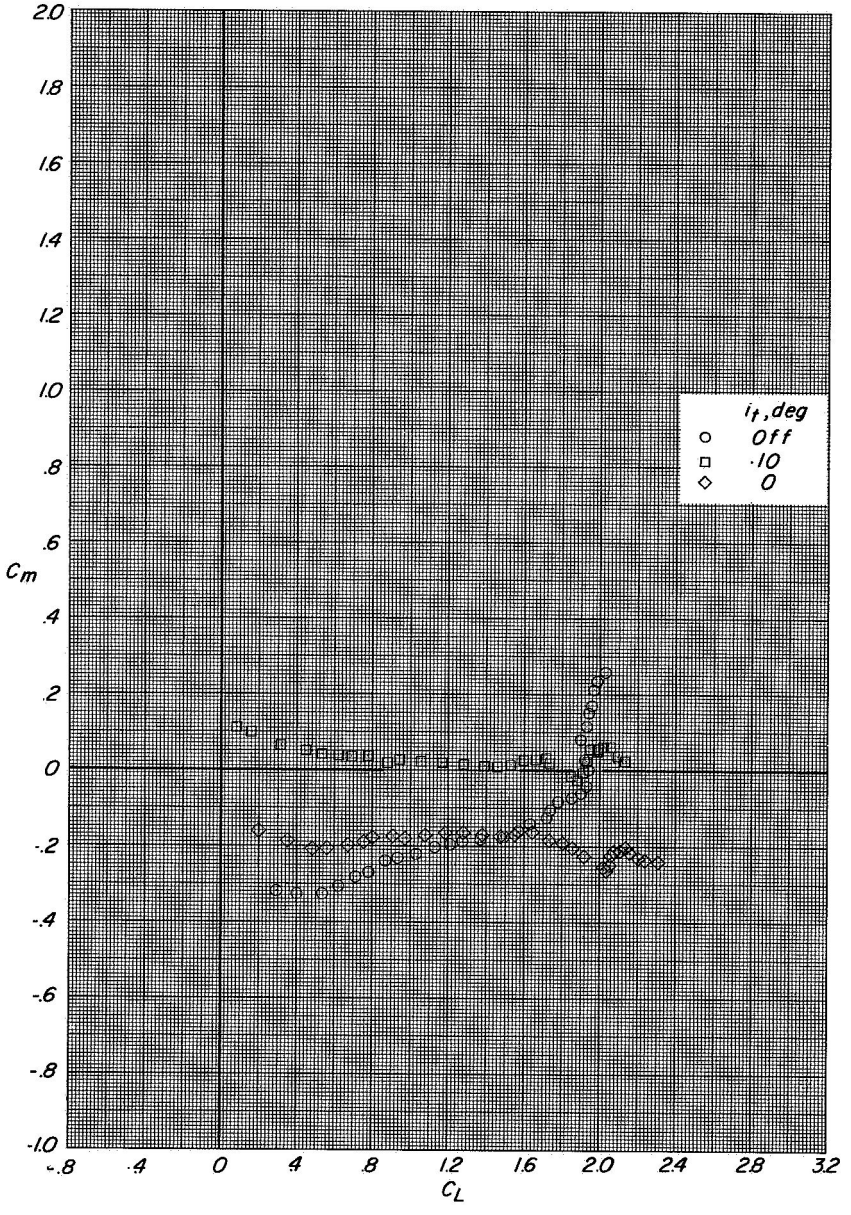

(c) Variation of C_m with C_L.

Figure 38.- Concluded.

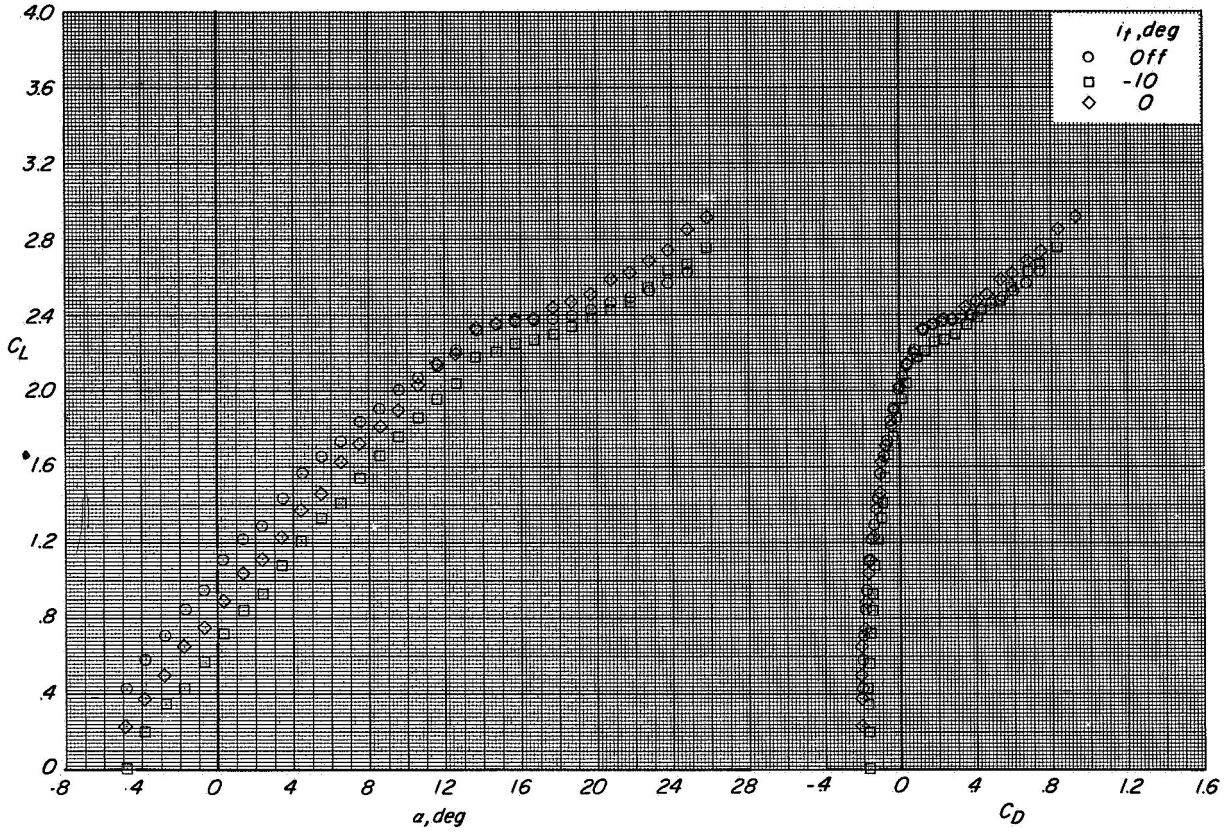

(a) Variation of C_L with α and C_D with C_L.

Figure 39.- Longitudinal aerodynamic characteristics of configuration A with direct-lift engines and lift-cruise engines deflected 0°. $C_T \approx 0.65$.

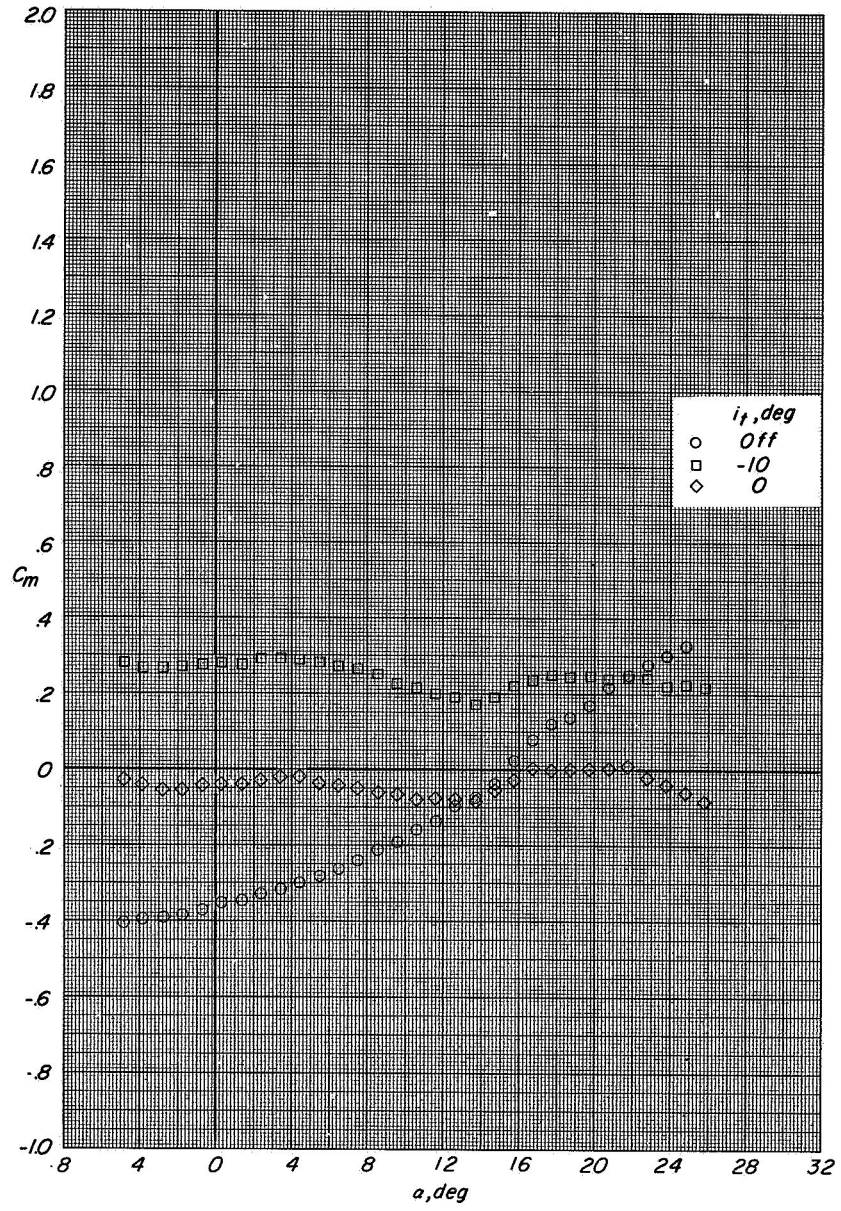

(b) Variation of C_m with α.

Figure 39.- Continued.

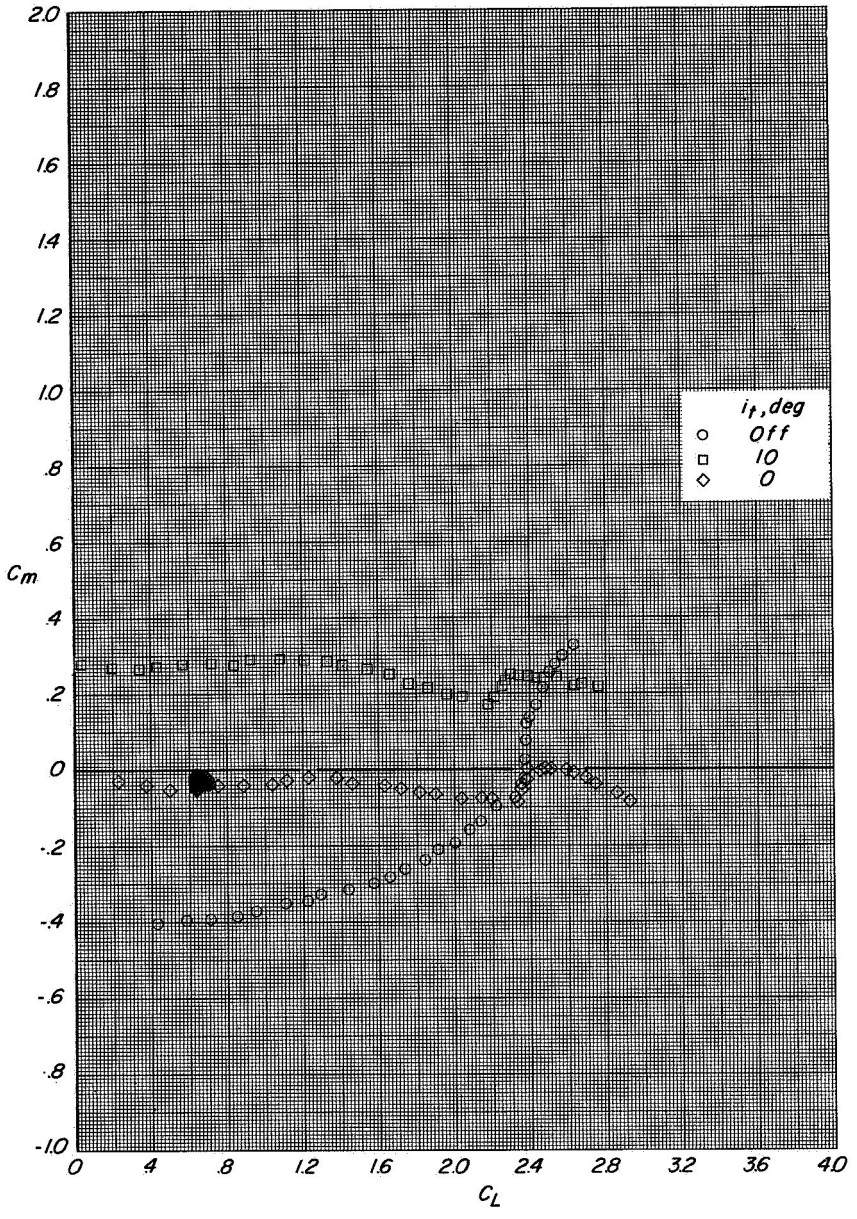

(c) Variation of C_m with C_L.

Figure 39.- Continued.

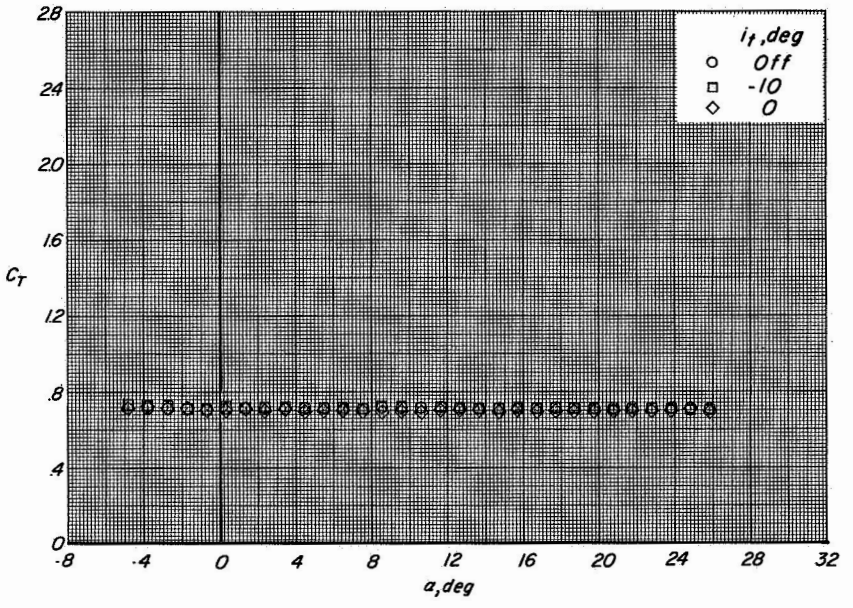

(d) Variation of C_T with α.

Figure 39.- Concluded.

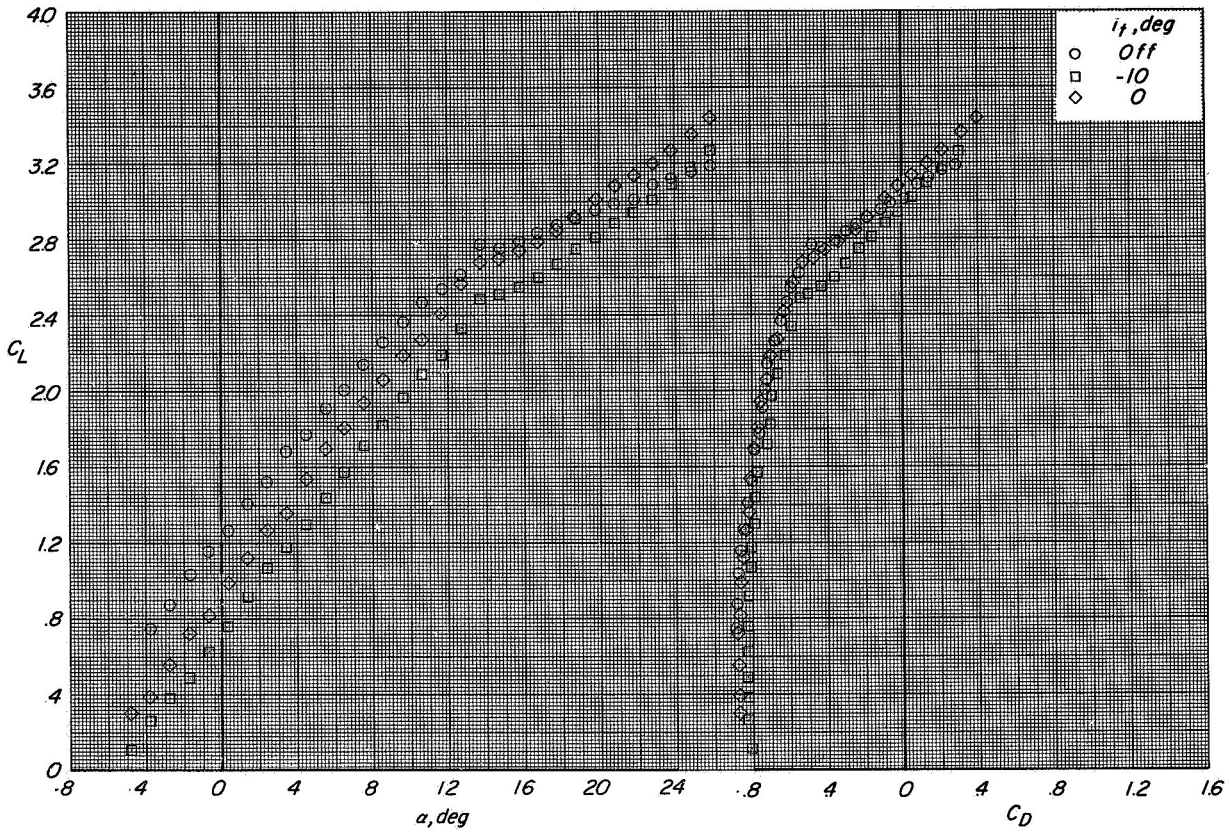

(a) Variation of C_L with α and C_D with C_L.

Figure 40.- Longitudinal aerodynamic characteristics of configuration A with direct-lift engines and lift-cruise engines deflected 0°. $C_T \approx 1.45$.

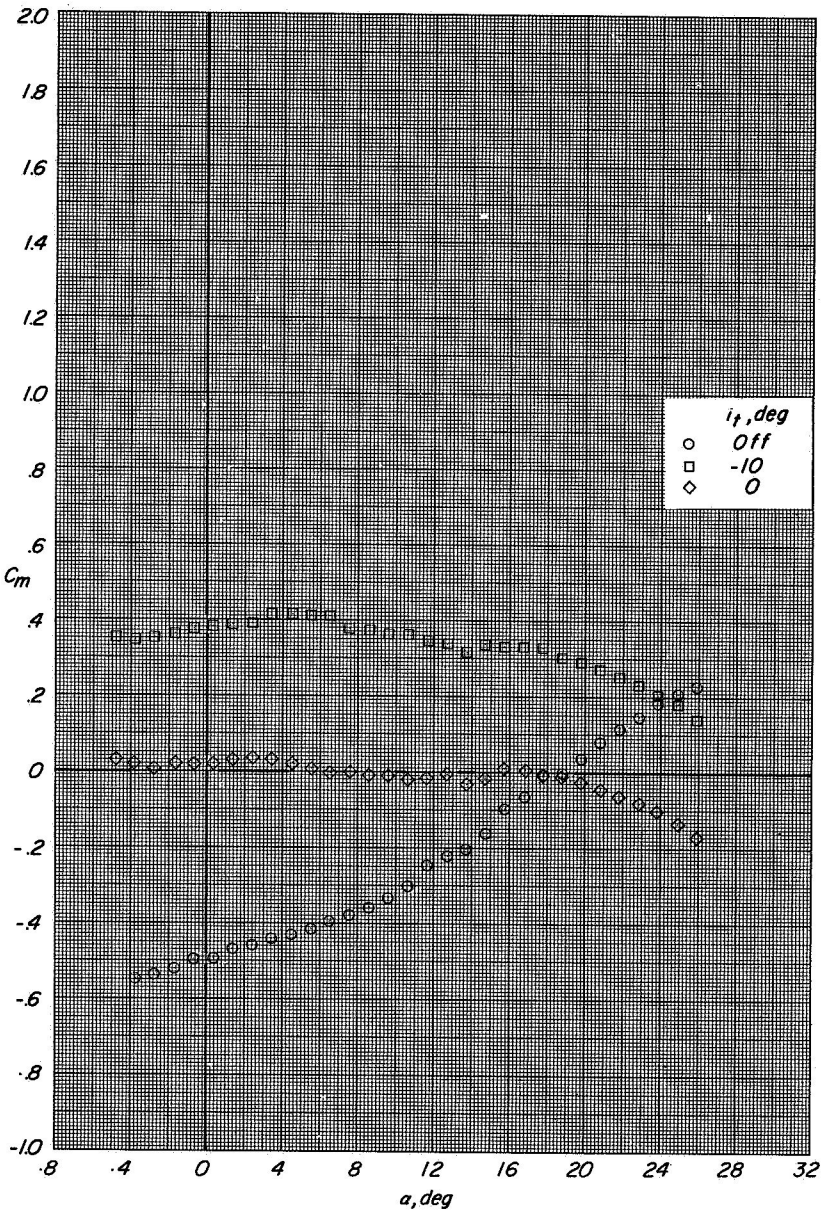

(b) Variation of C_m with α.

Figure 40.- Continued.

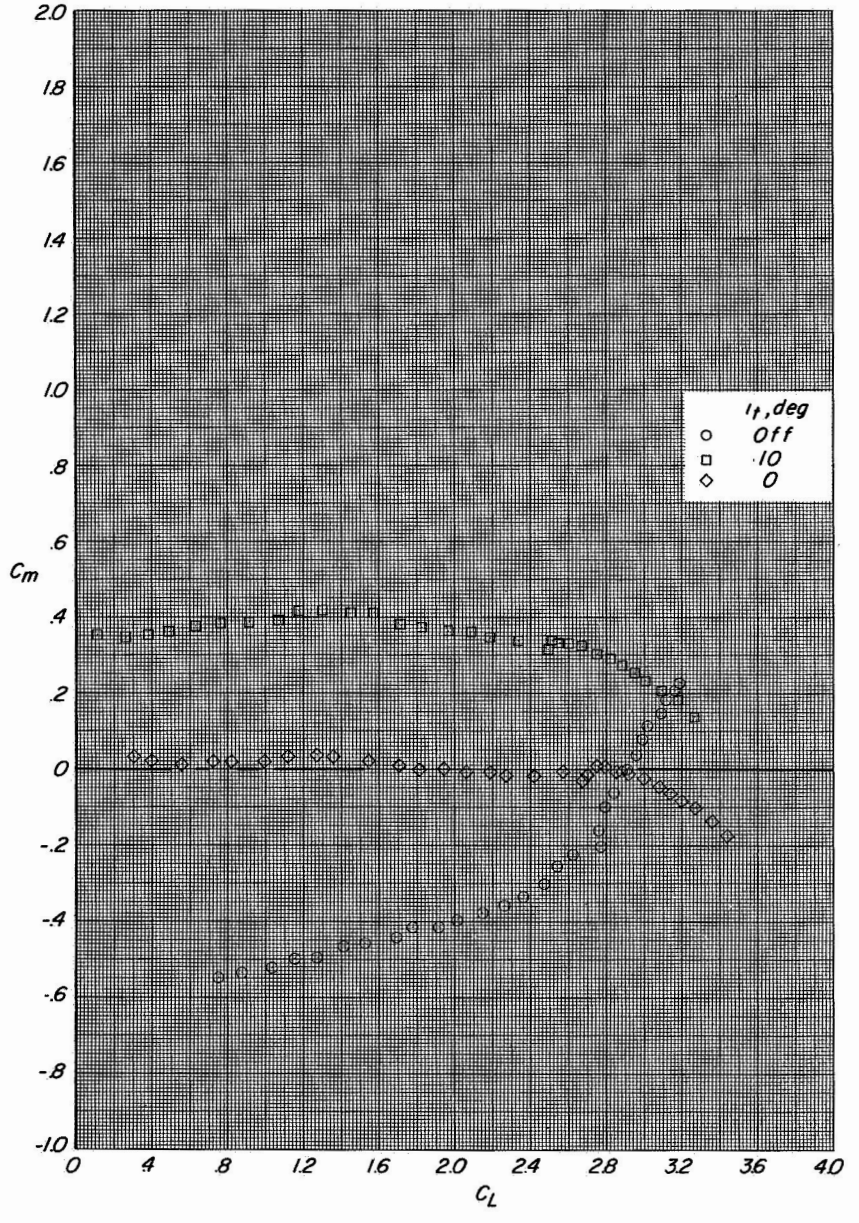

(c) Variation of C_m with C_L.

Figure 40.- Continued.

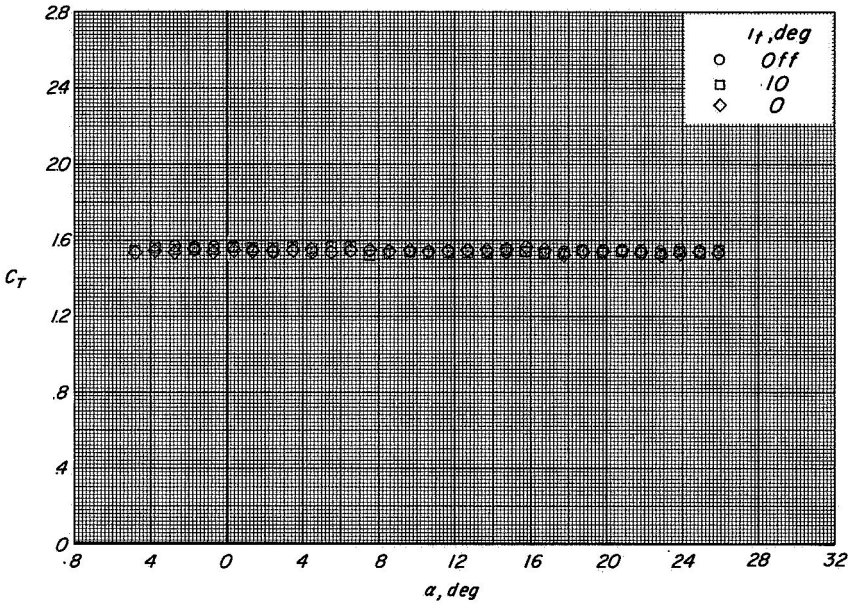

(d) Variation of C_T with α.

Figure 40.- Concluded.

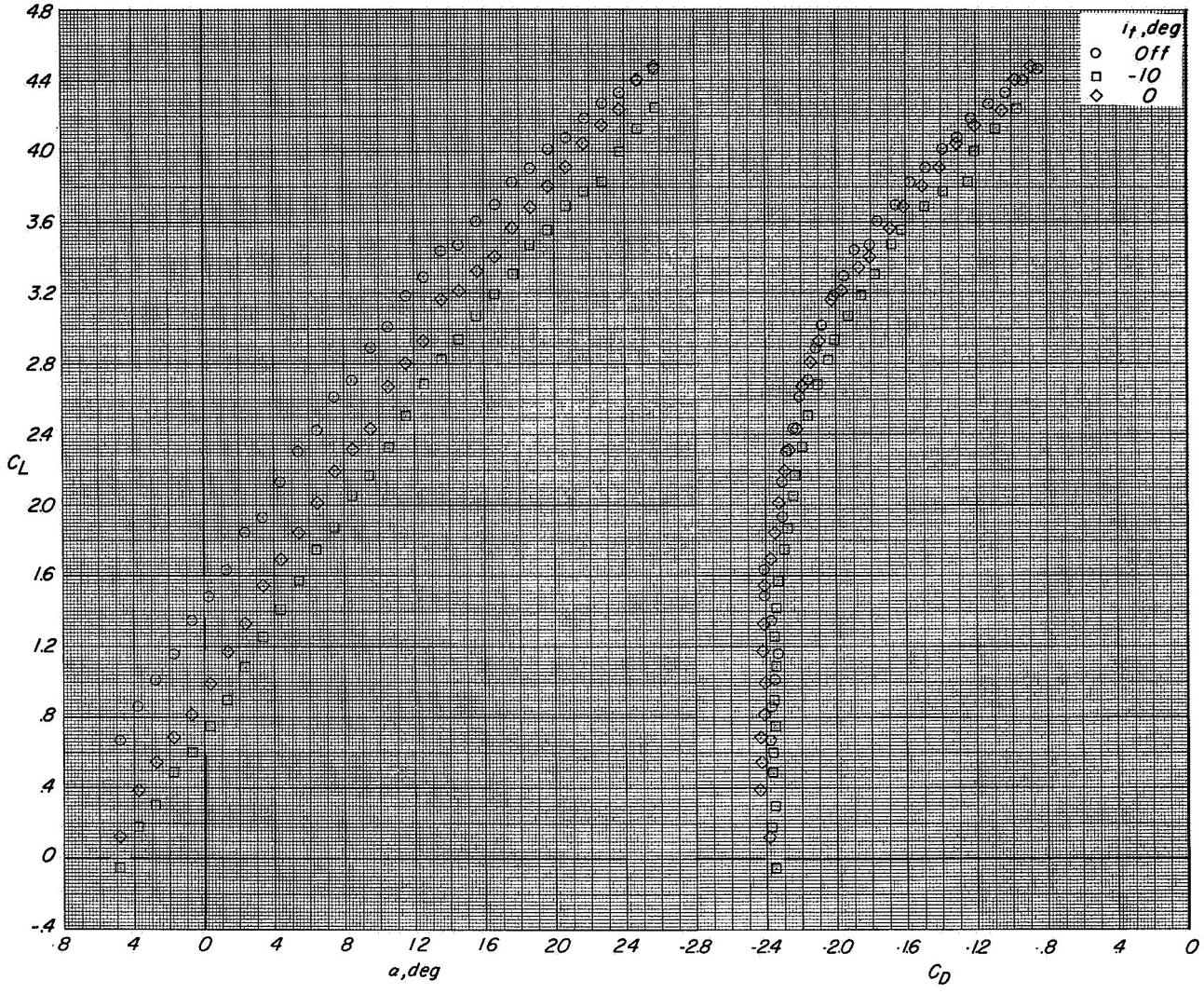

(a) Variation of C_L with α and C_D with C_L.

Figure 41.- Longitudinal aerodynamic characteristics of configuration A with direct-lift engines and lift-cruise engines deflected 0°. $C_T \approx 3.3$.

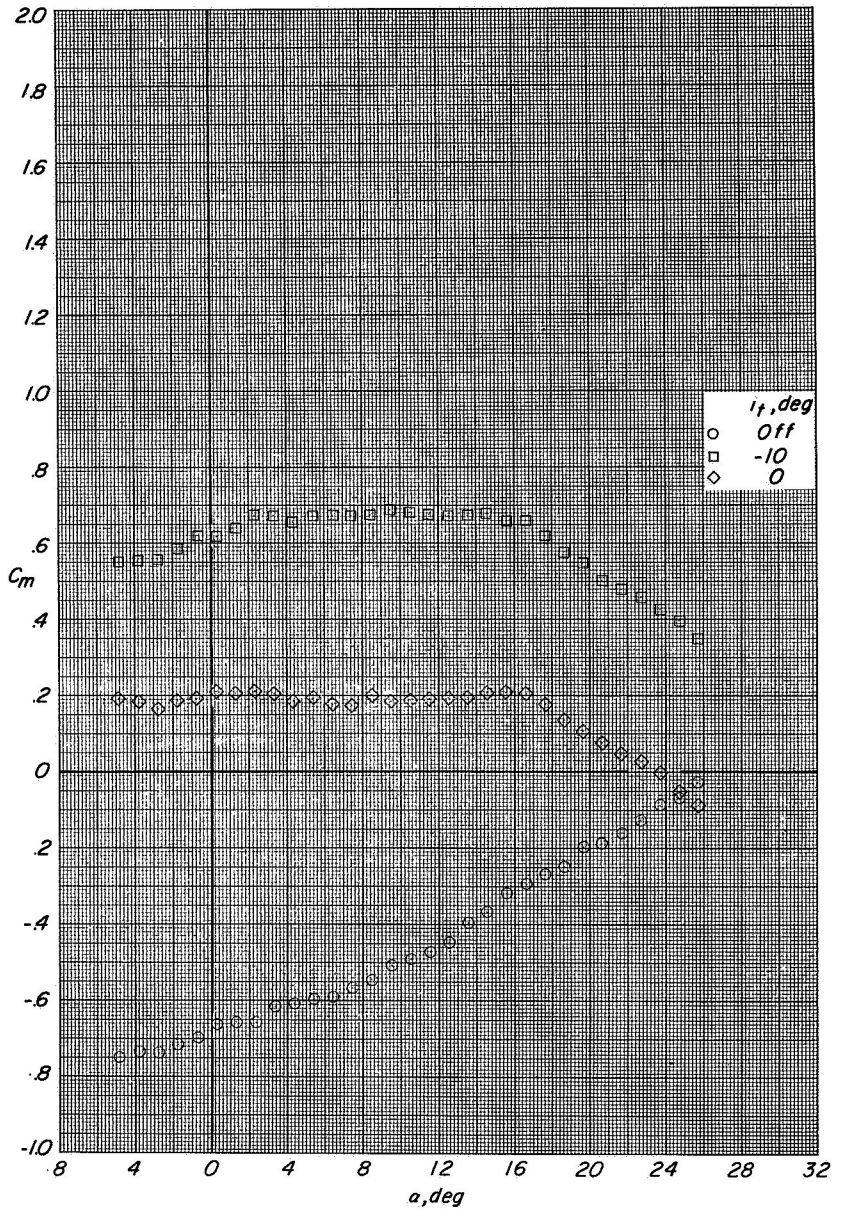

(b) Variation of C_m with α.

Figure 41.- Continued.

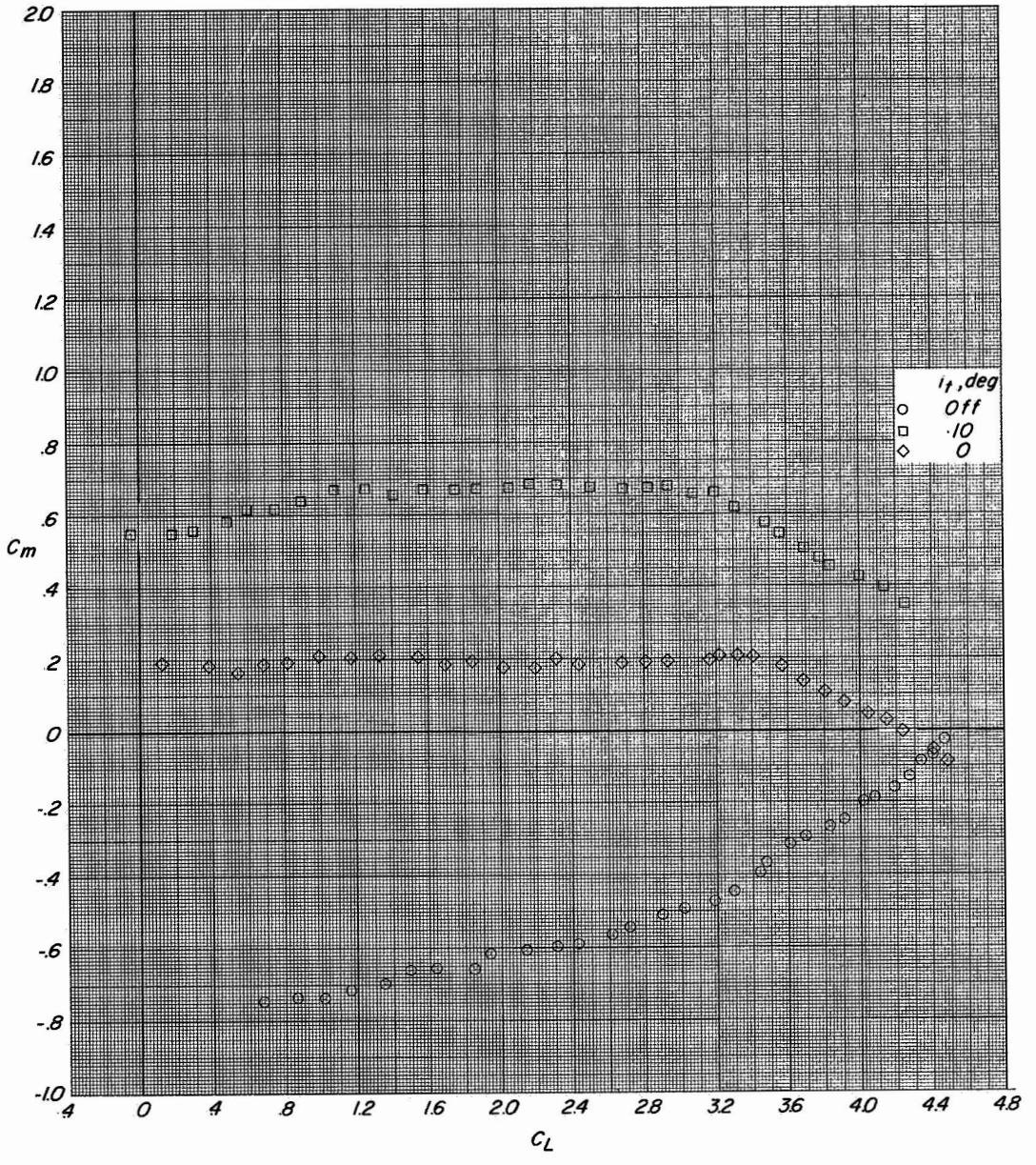

(c) Variation of C_m with C_L.

Figure 41.- Continued.

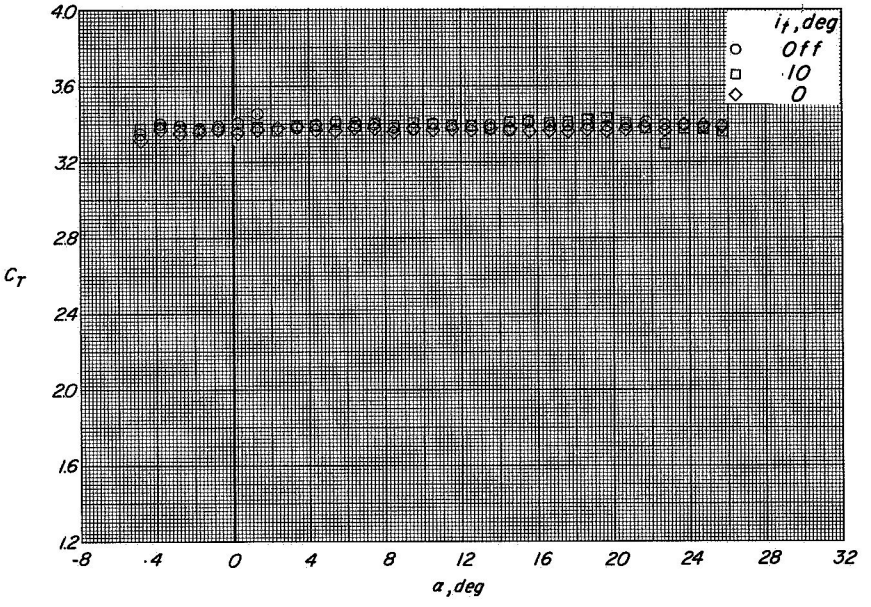

(d) Variation of C_T with α.

Figure 41.- Concluded.

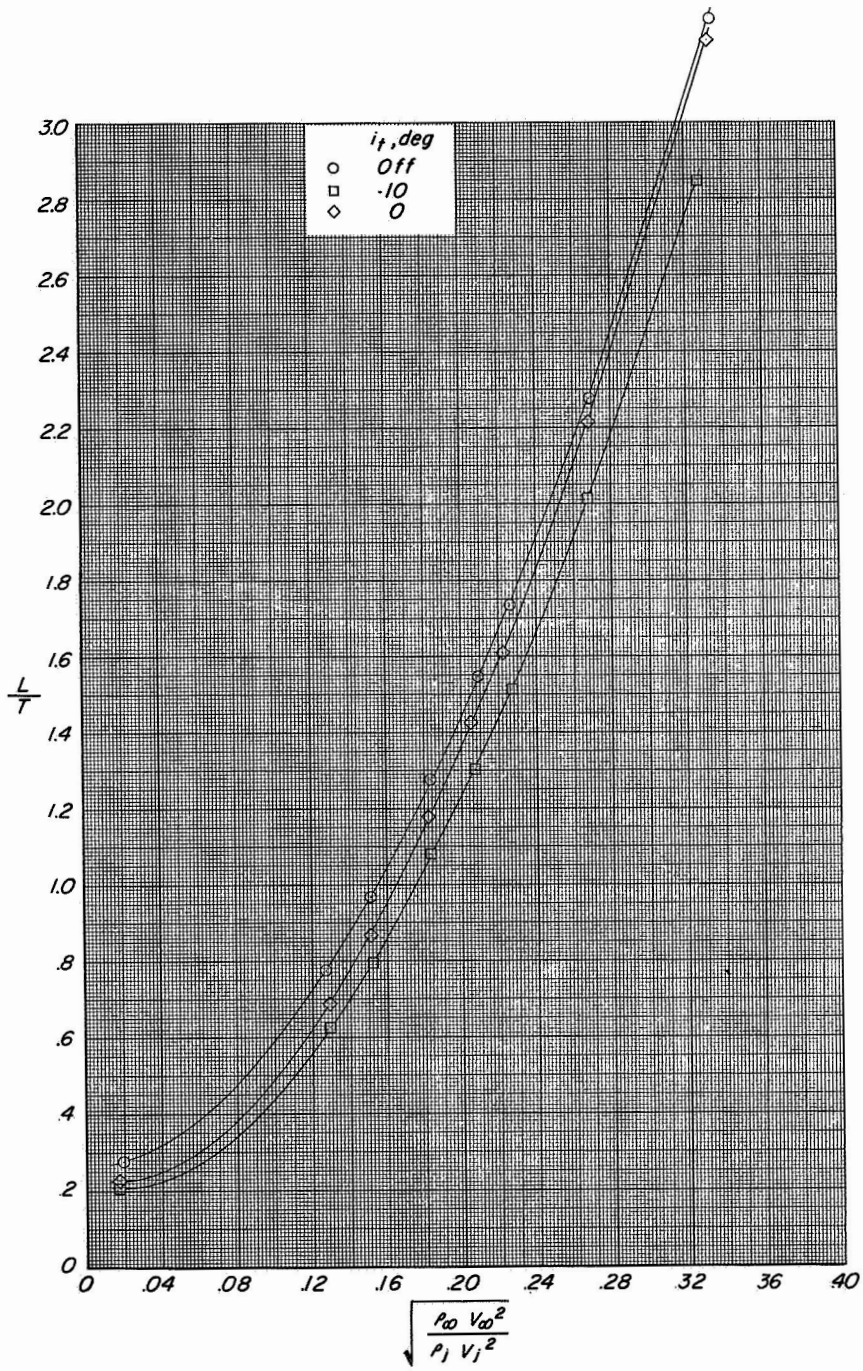

(a) Variation of L/T with effective velocity ratio.

Figure 42.- Longitudinal aerodynamic characteristics of configuration A with direct-lift engines and lift-cruise engines deflected 0°. $\alpha = 12°$.

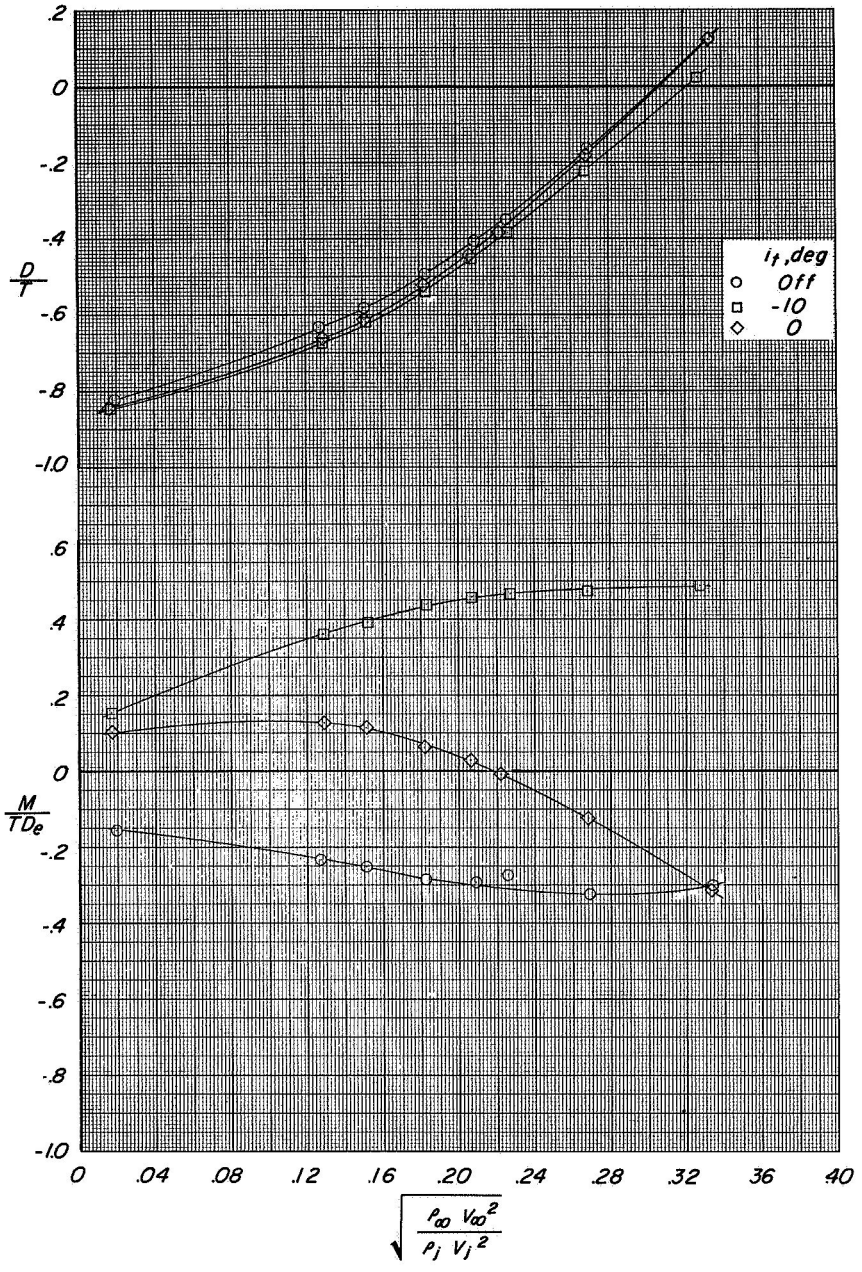

(b) Variation of D/T and M/TD_e with effective velocity ratio.

Figure 42.- Concluded.

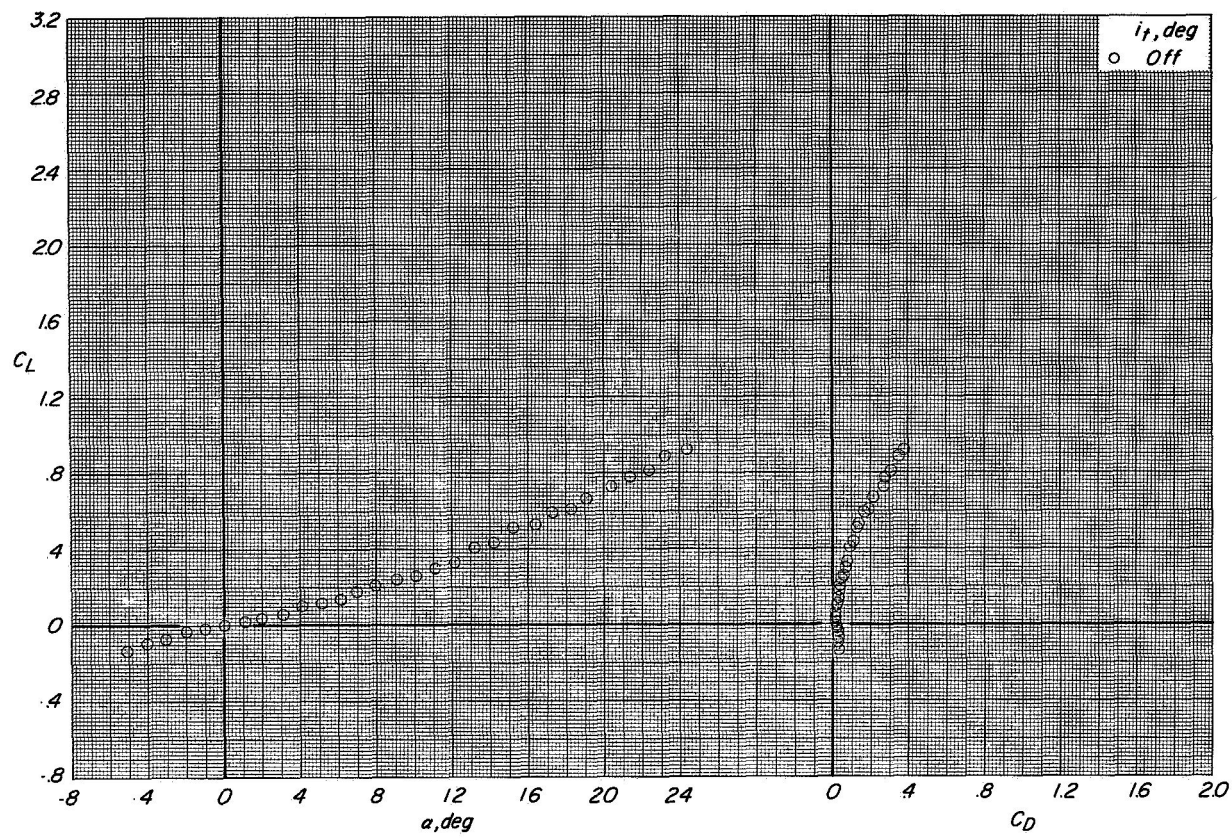

(a) Variation of C_L with α and C_D with C_L.

Figure 43.- Longitudinal aerodynamic characteristics of model with modified wing; fuselage with stub wing. $C_T = 0$.

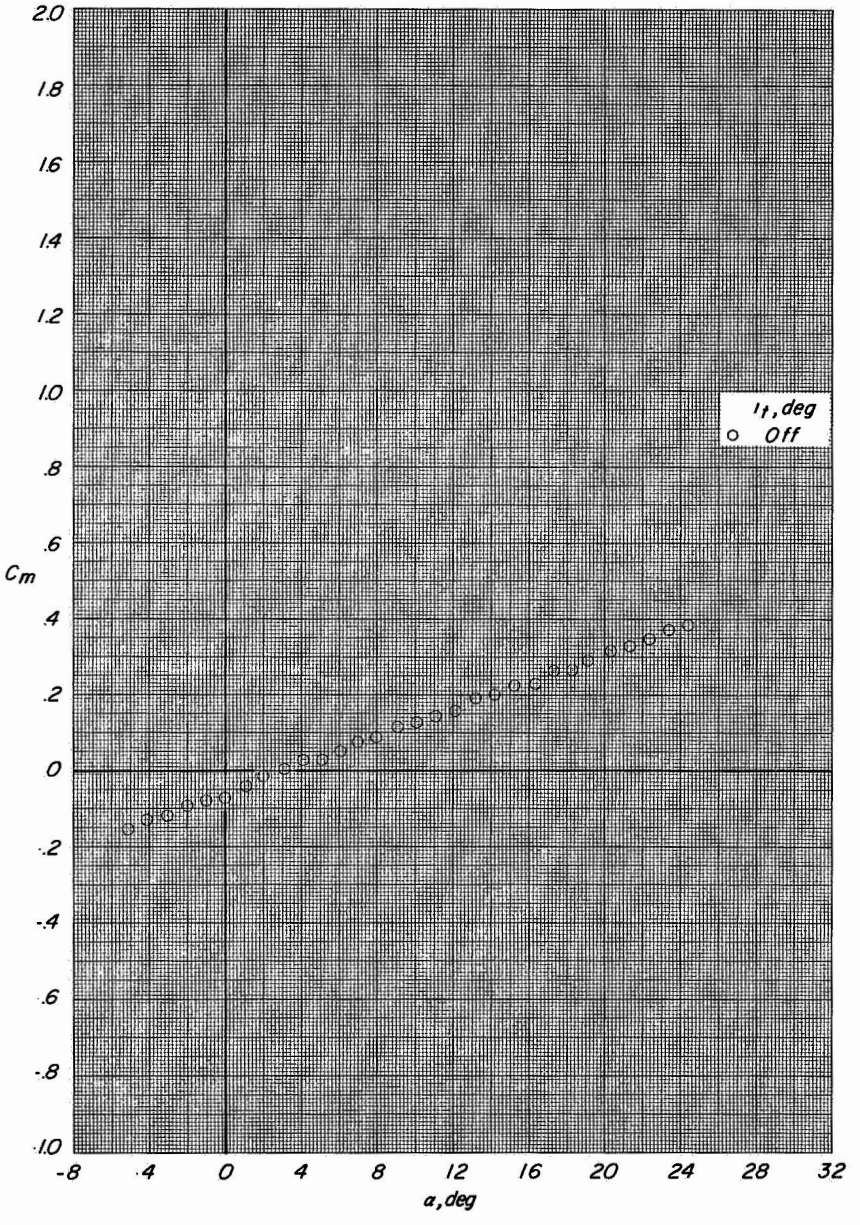

(b) Variation of C_m with α.

Figure 43.- Continued.

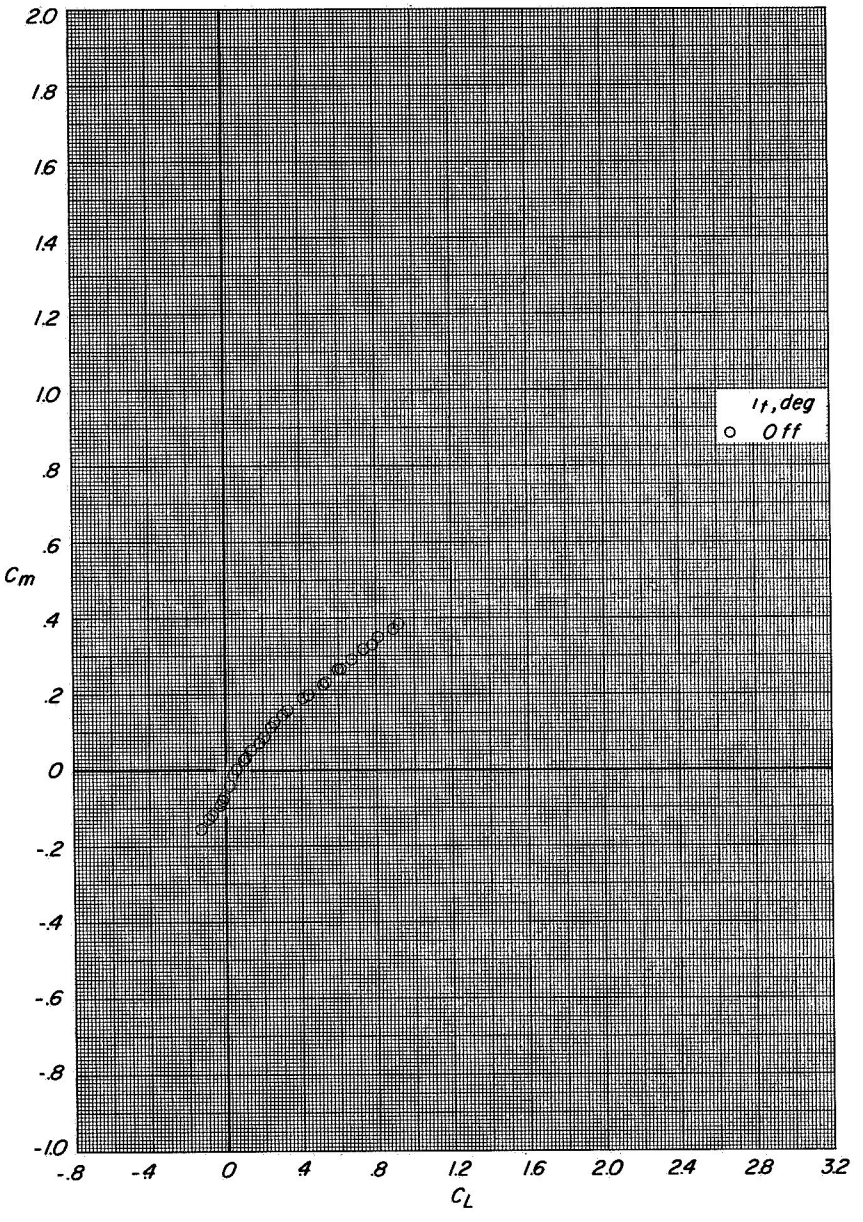

(c) Variation of C_m with C_L.

Figure 43.- Concluded.

CONFIDENTIAL

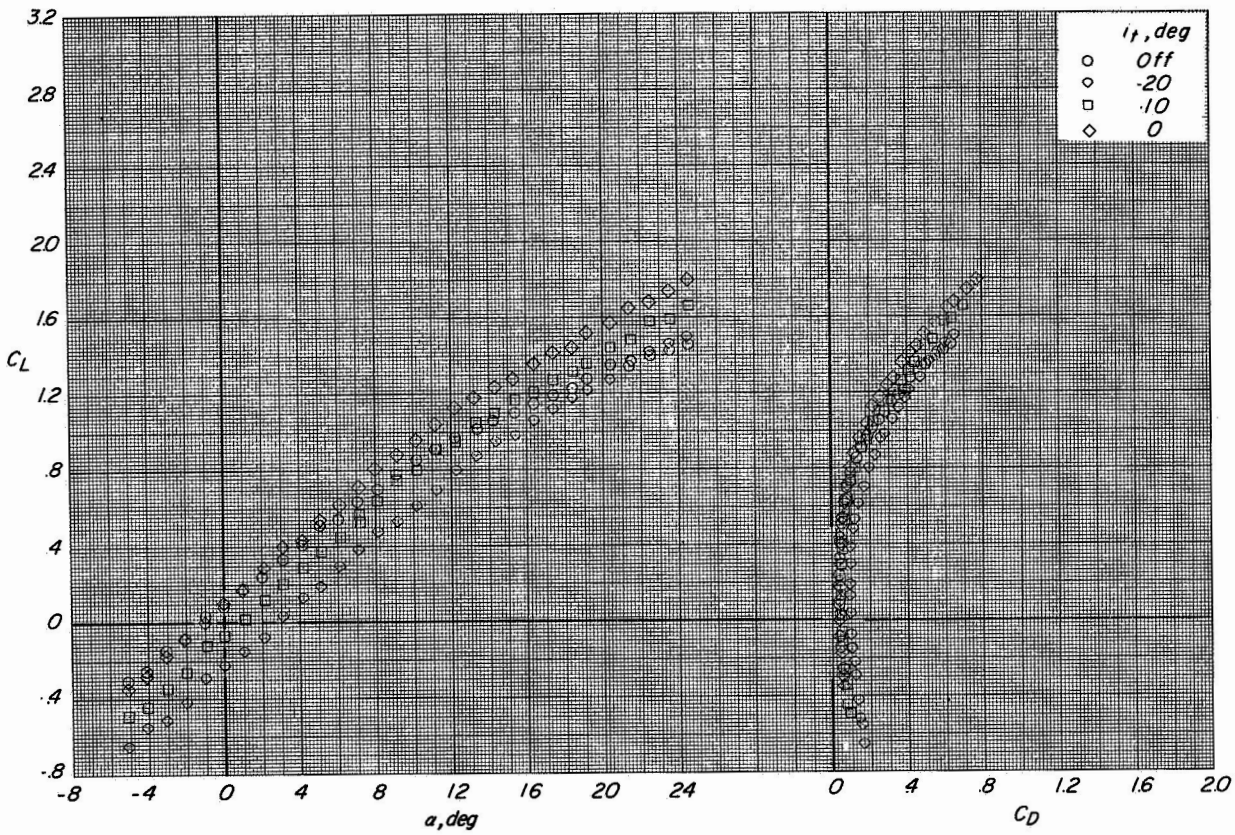

(a) Variation of C_L with α and C_D with C_L.

Figure 44.- Longitudinal aerodynamic characteristics of model with modified wing; fuselage with complete wing; high-lift devices retracted. $C_T = 0$.

CONFIDENTIAL

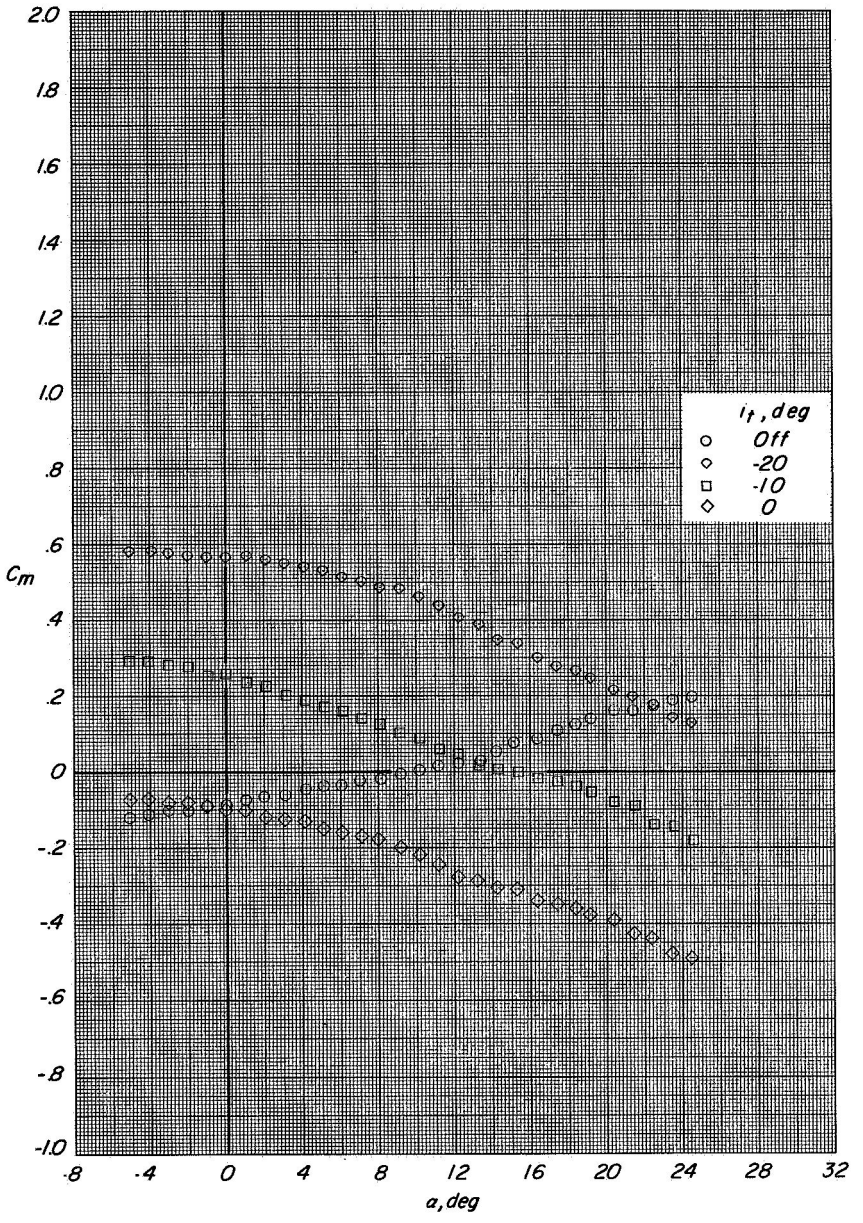

(b) Variation of C_m with α.

Figure 44.- Continued.

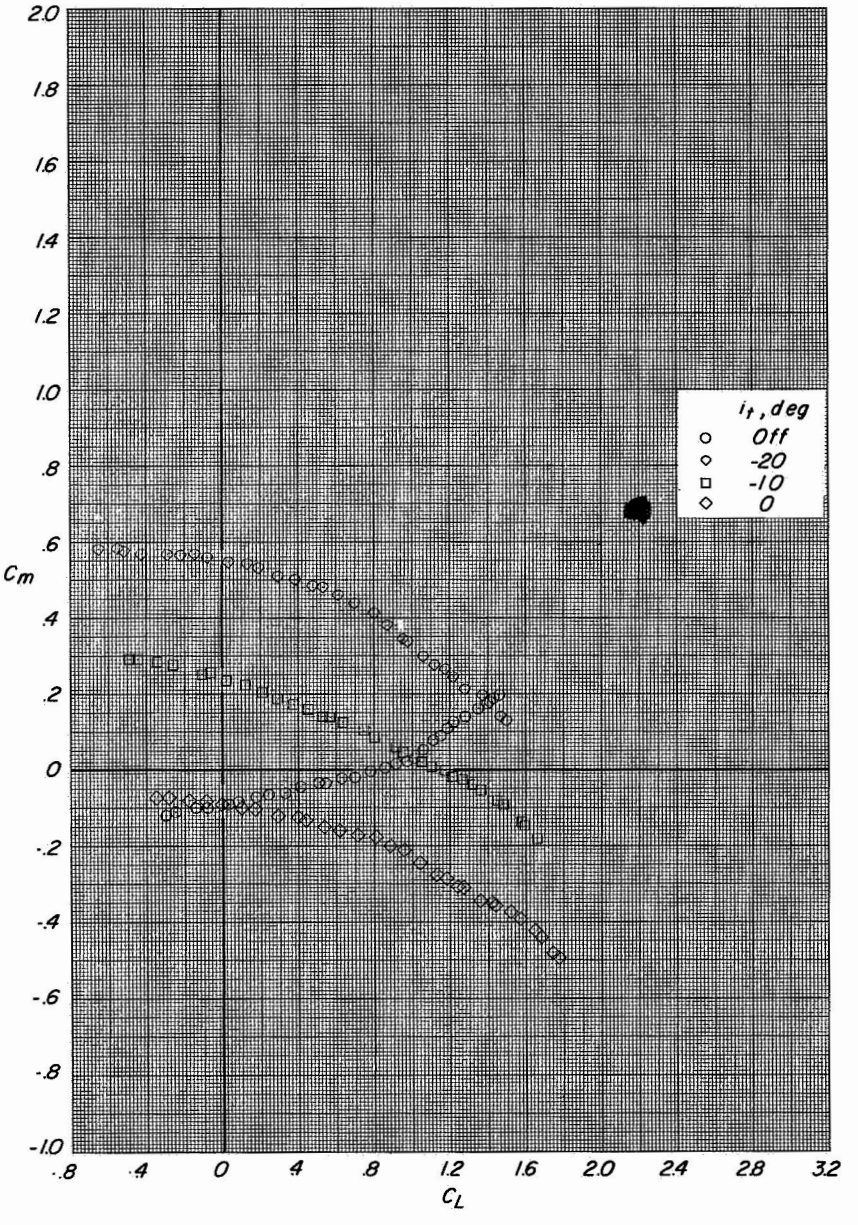

(c) Variation of C_m with C_L.

Figure 44.- Concluded.

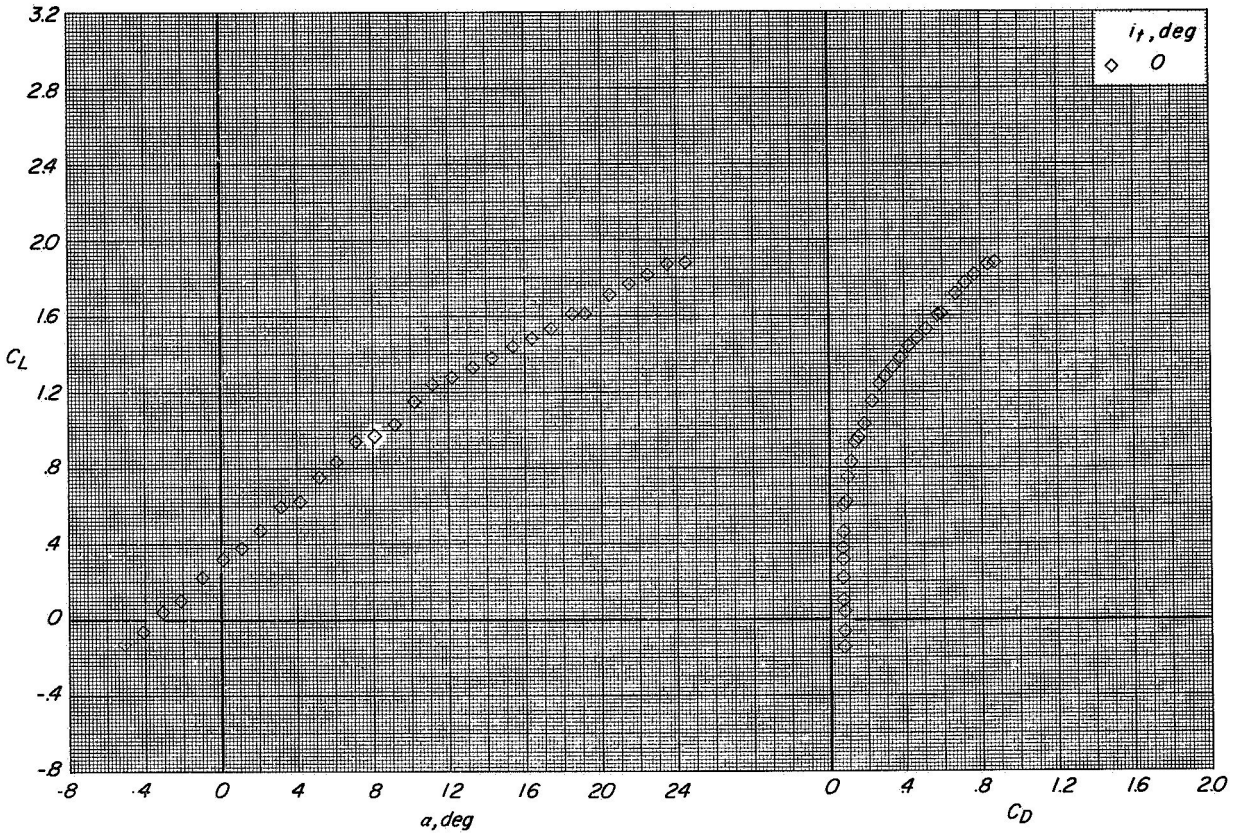

(a) Variation of C_L with α and C_D with C_L.

Figure 45.- Longitudinal aerodynamic characteristics of model with modified wing. $\delta_{LE,OB} = 0^\circ$; $\delta_{LE,IB} = 0^\circ$; $\delta_{TE,W} = 0^\circ$; $\delta_{LE,ST} = 0^\circ$; $\delta_{TE,ST} = 40^\circ$; $C_T = 0$.

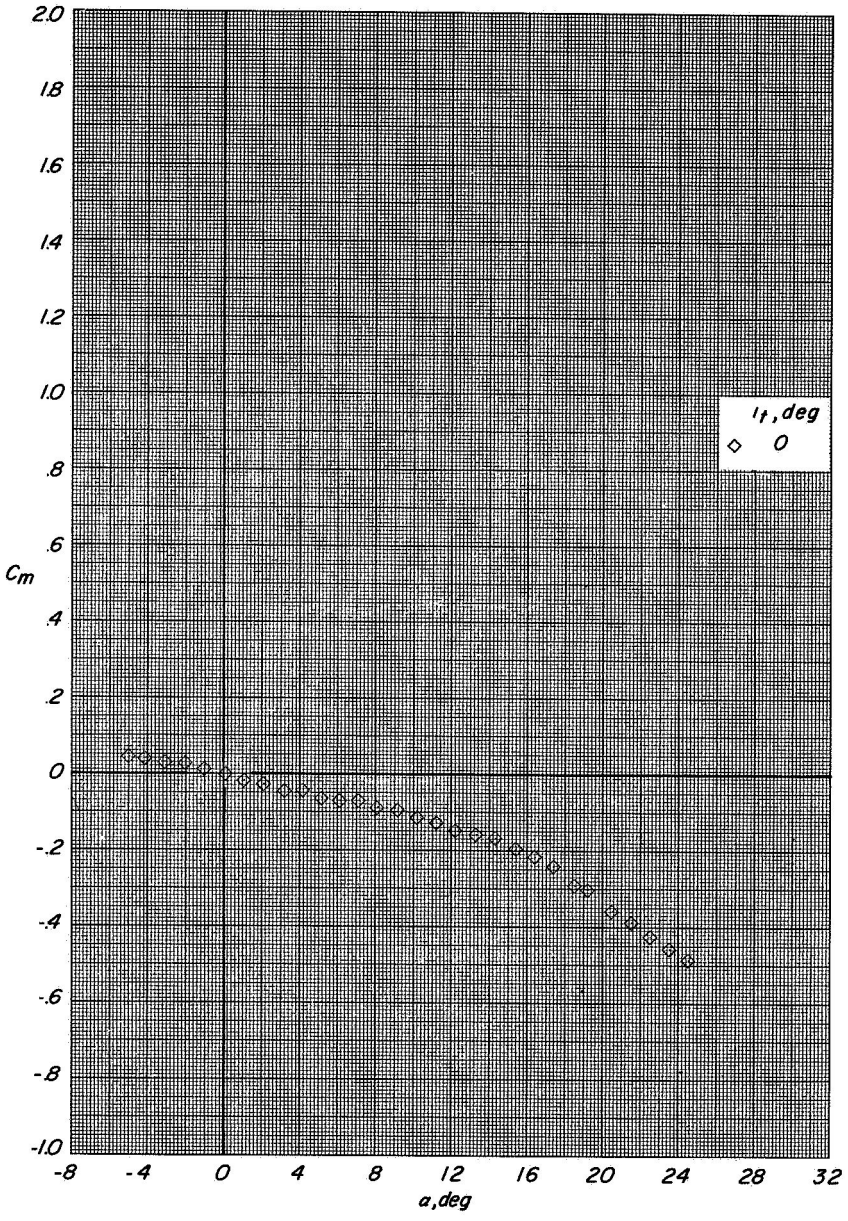

(b) Variation of C_m with α.

Figure 45.- Continued.

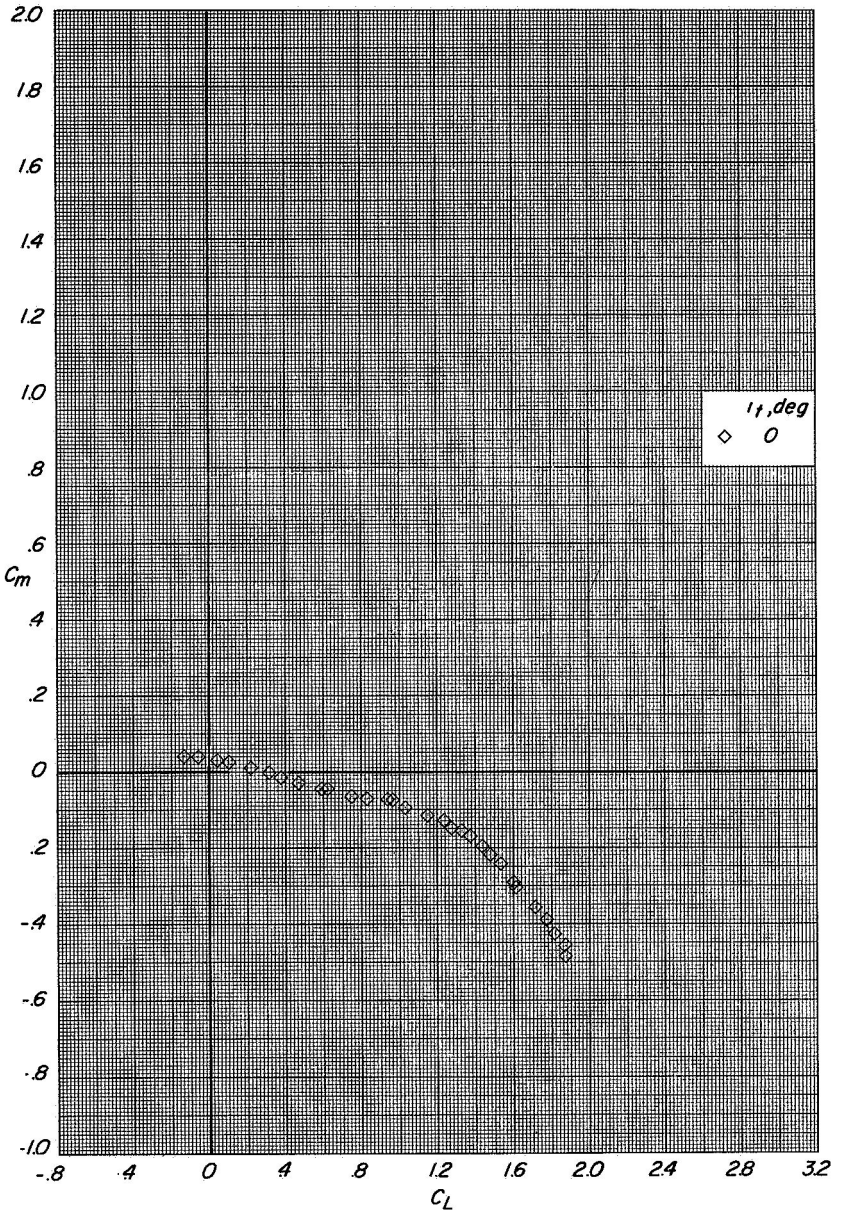

(c) Variation of C_m with C_L.

Figure 45.- Concluded.

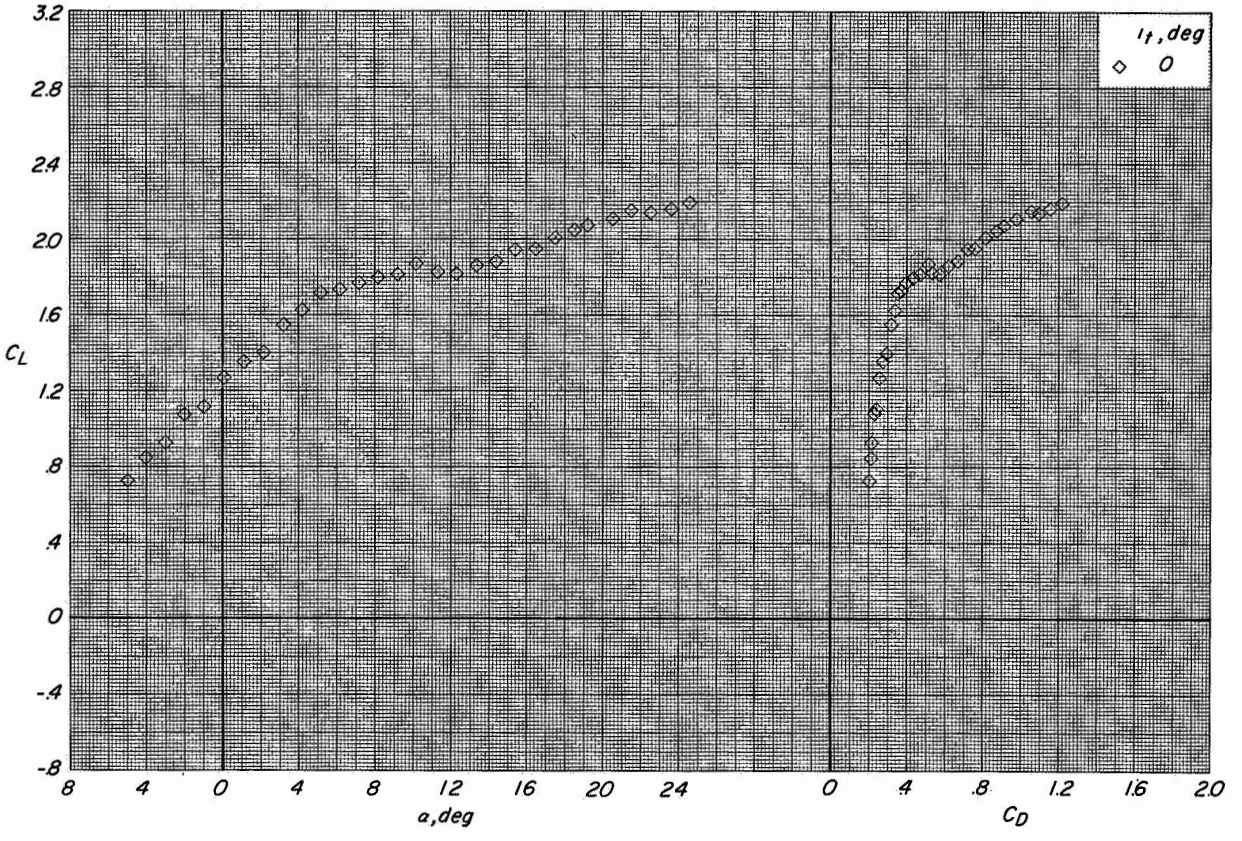

(a) Variation of C_L with α and C_D with C_L.

Figure 46.- Longitudinal aerodynamic characteristics of model with modified wing. $\delta_{LE,OB} = 0^\circ$; $\delta_{LE,IB} = 0^\circ$; $\delta_{TE,W} = 50^\circ$; $\delta_{LE,ST} = 0^\circ$; $\delta_{TE,ST} = 40^\circ$; $C_T = 0$.

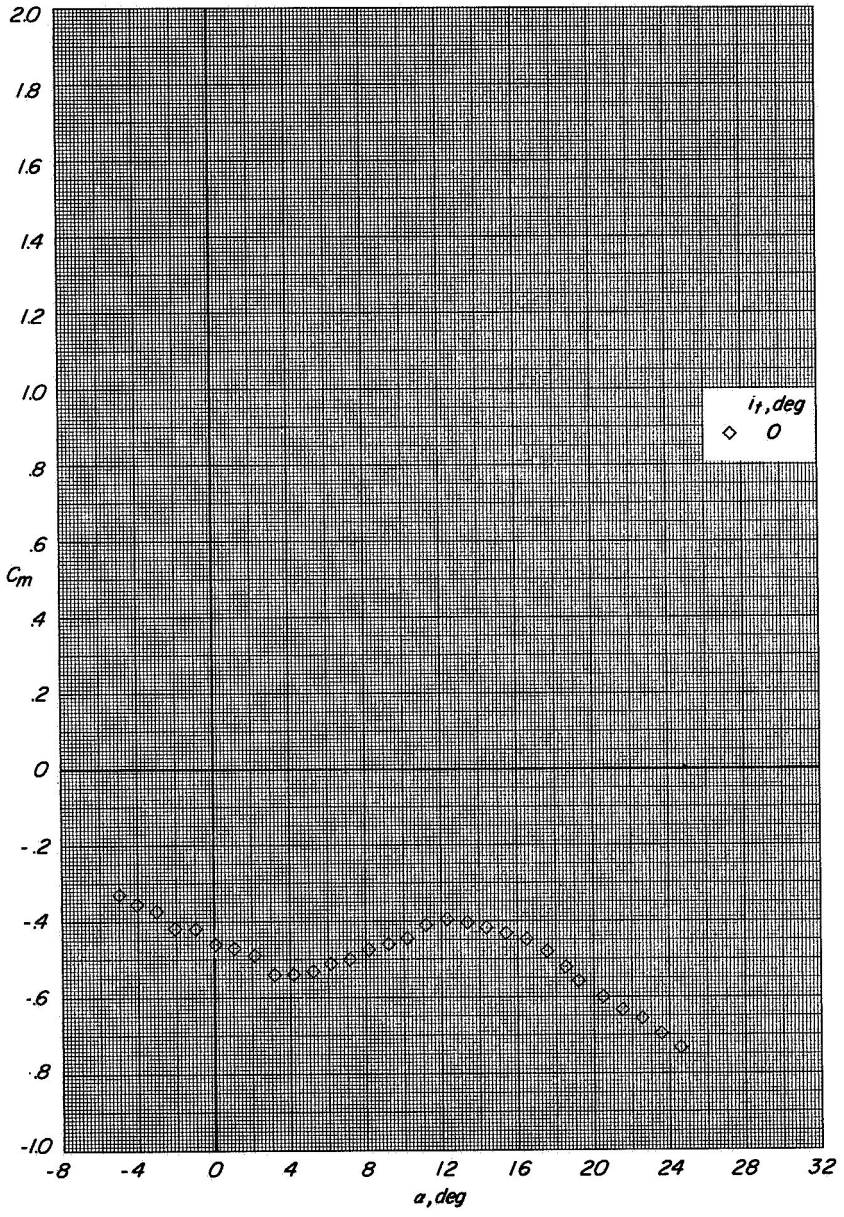

(b) Variation of C_m with α.

Figure 46.- Continued.

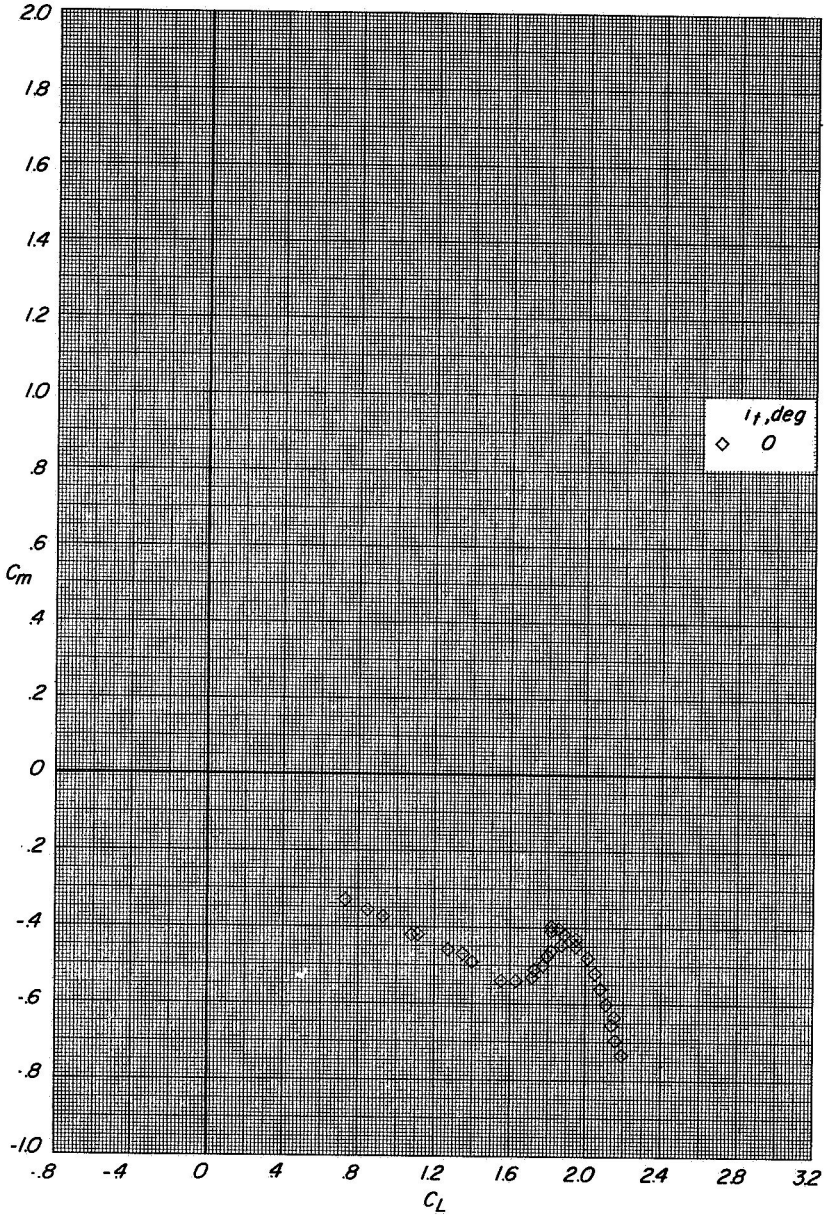

(c) Variation of C_m with C_L.

Figure 46.- Concluded.

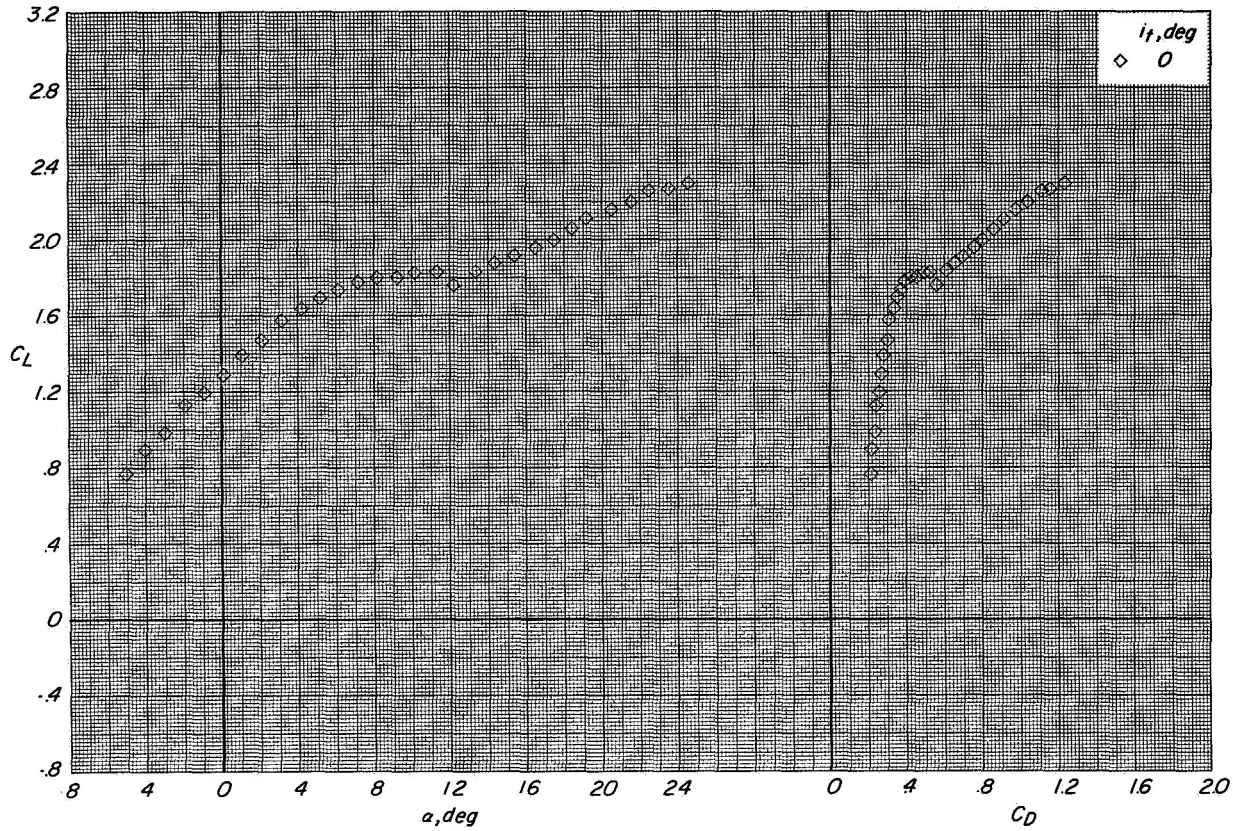

(a) Variation of C_L with α and C_D with C_L.

Figure 47.- Longitudinal aerodynamic characteristics of model with modified wing. $\delta_{LE,OB} = 32^\circ$; $\delta_{LE,IB} = 0^\circ$; $\delta_{TE,W} = 50^\circ$; $\delta_{LE,ST} = 0^\circ$; $\delta_{TE,ST} = 40^\circ$; $C_T = 0$.

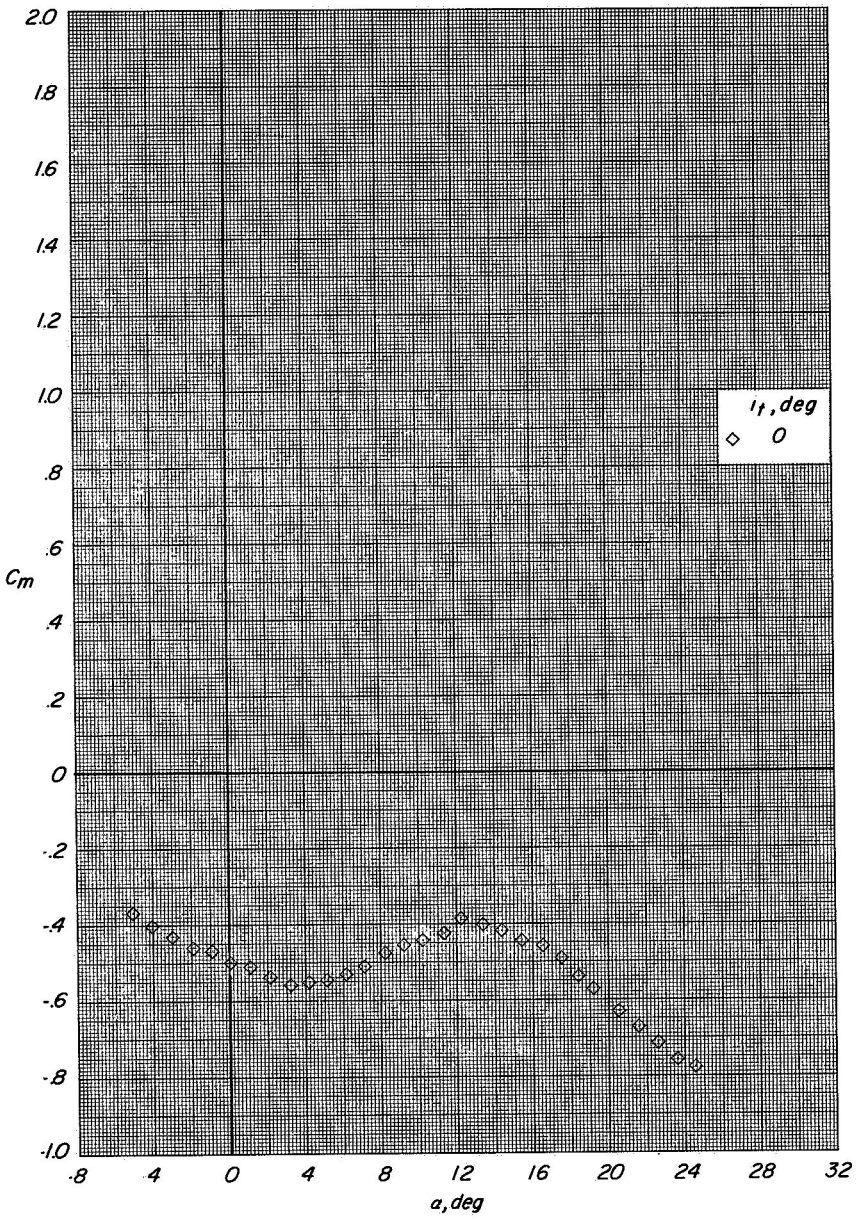

(b) Variation of C_m with α.

Figure 47.- Continued.

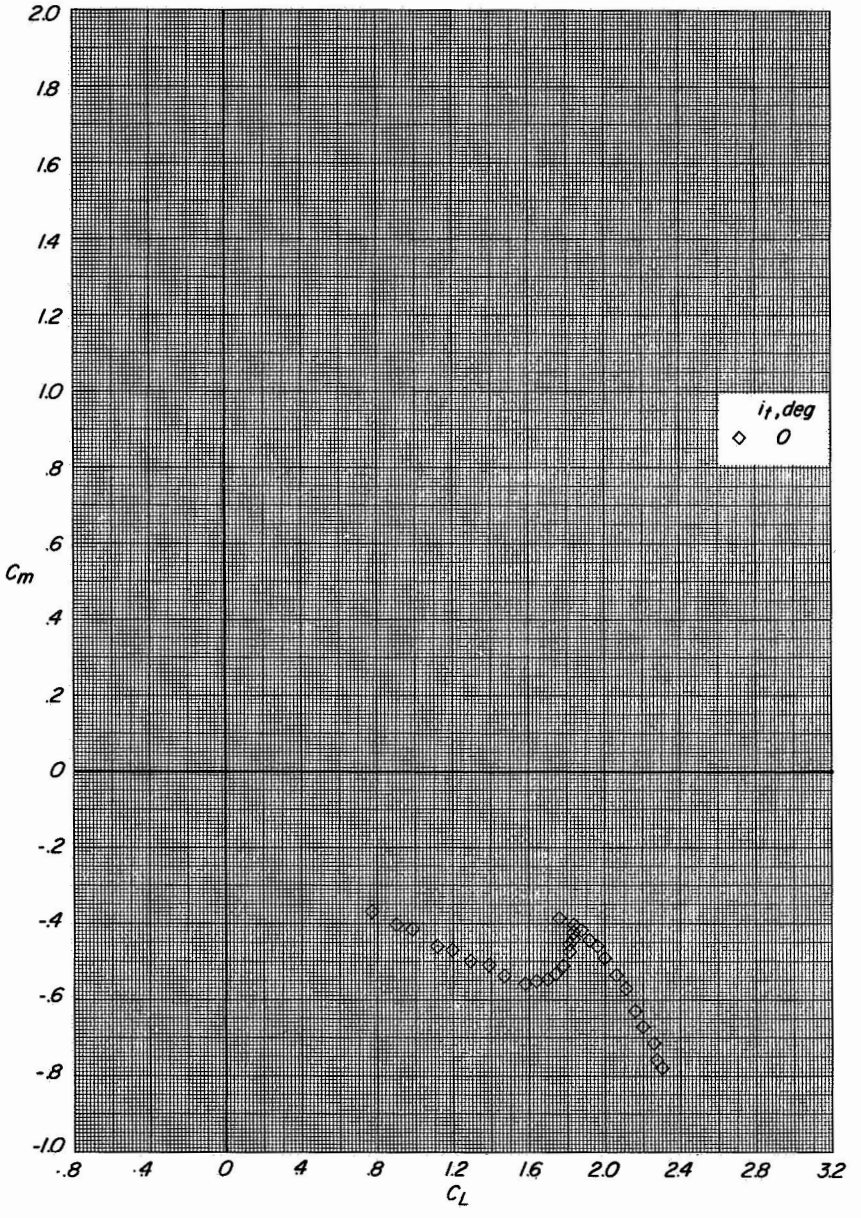

(c) Variation of C_m with C_L.

Figure 47.- Concluded.

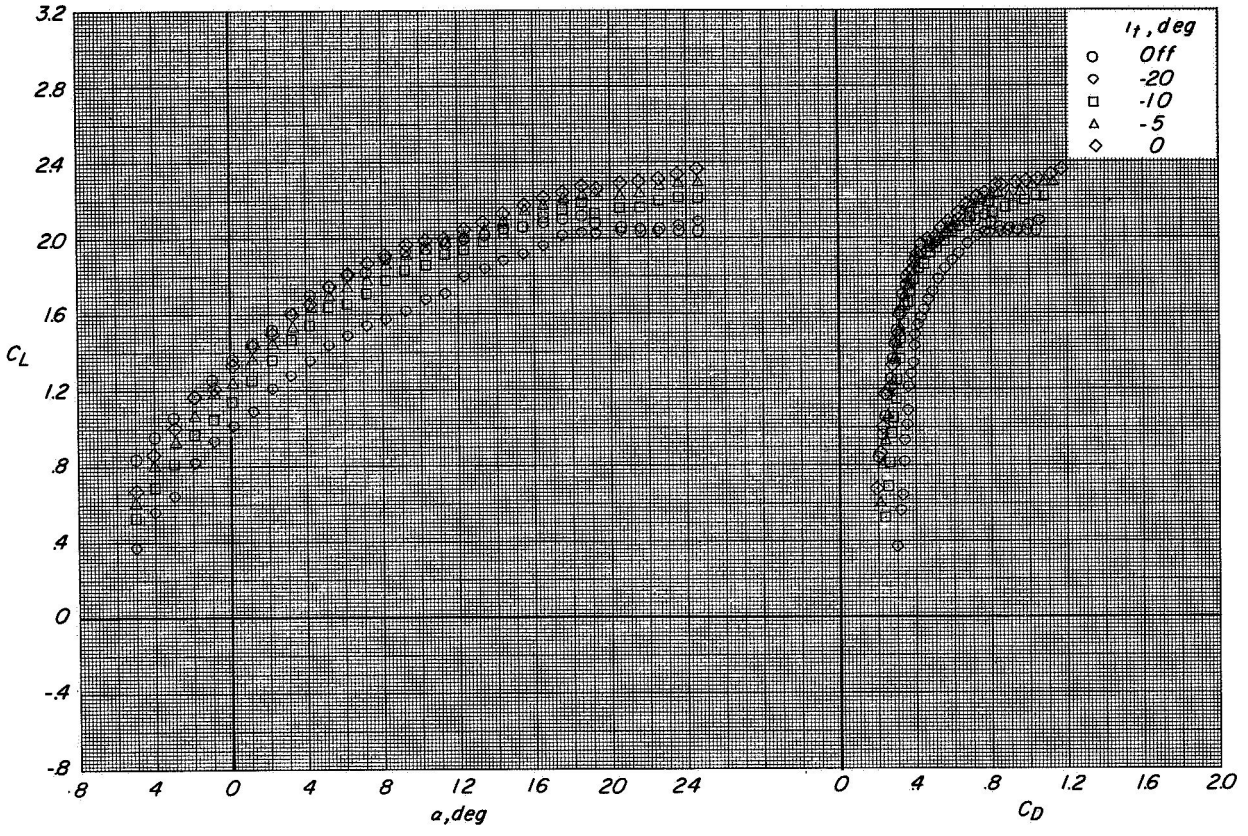

(a) Variation of C_L with α and C_D with C_L.

Figure 48.- Longitudinal aerodynamic characteristics of model with modified wing. $\delta_{LE,OB} = 32^\circ$; $\delta_{LE,IB} = 32^\circ$; $\delta_{TE,W} = 50^\circ$; $\delta_{LE,ST} = 0^\circ$; $\delta_{TE,ST} = 40^\circ$; $C_T = 0$.

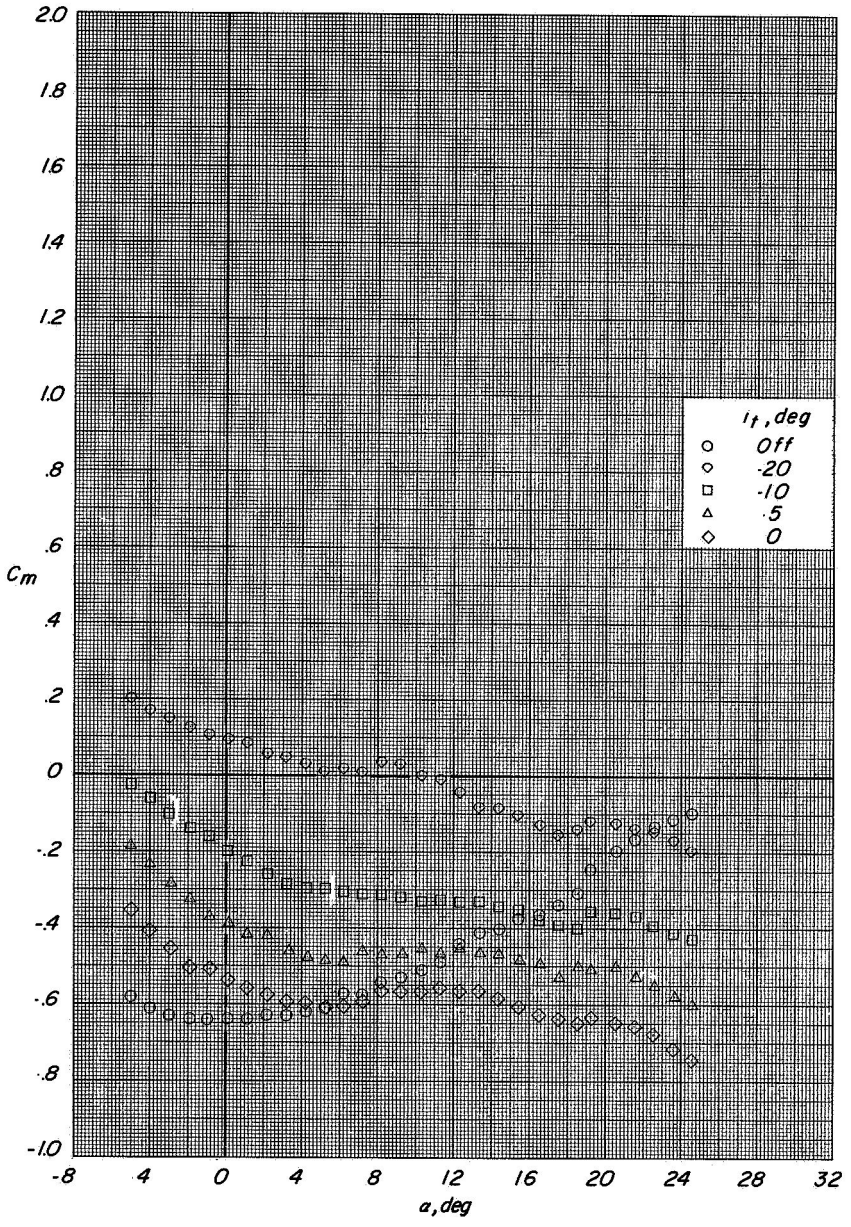

(b) Variation of C_m with α.

Figure 48.- Continued.

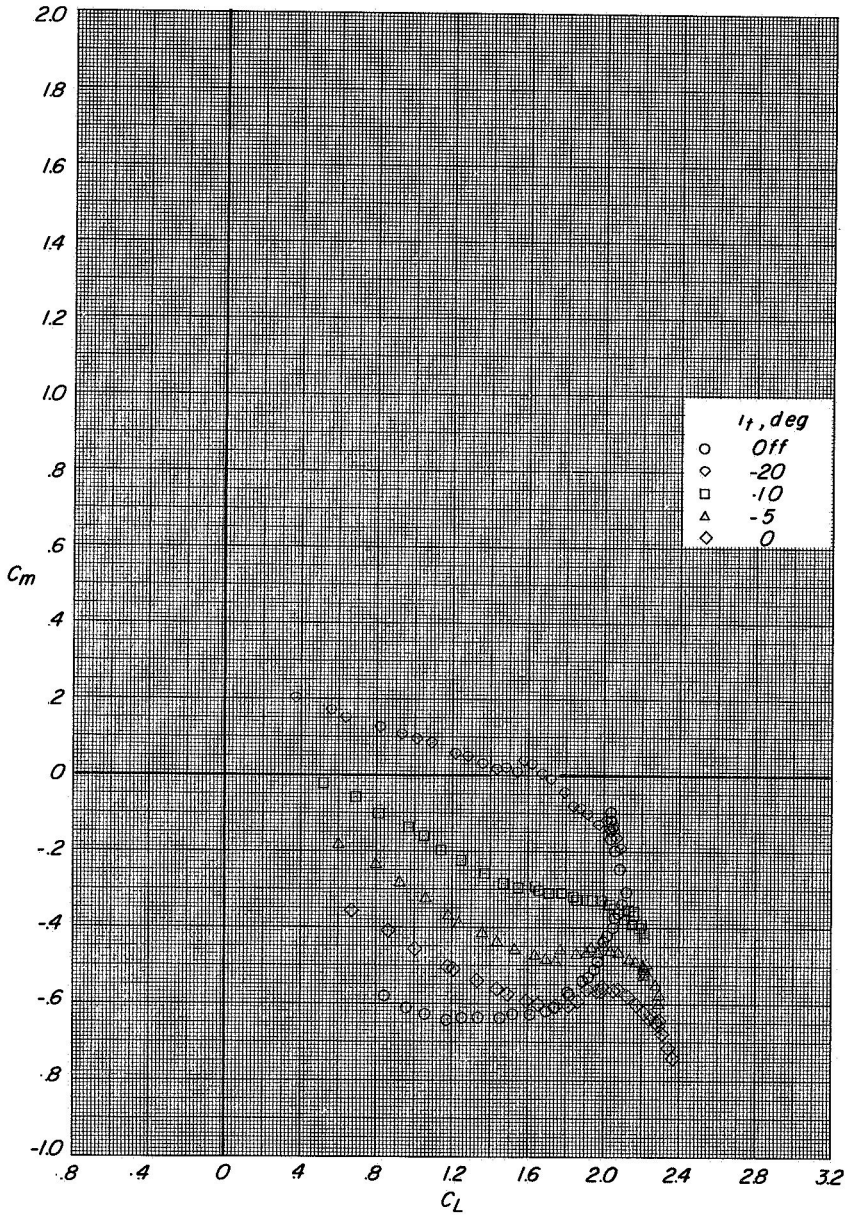

(c) Variation of C_m with C_L.

Figure 48.- Concluded.

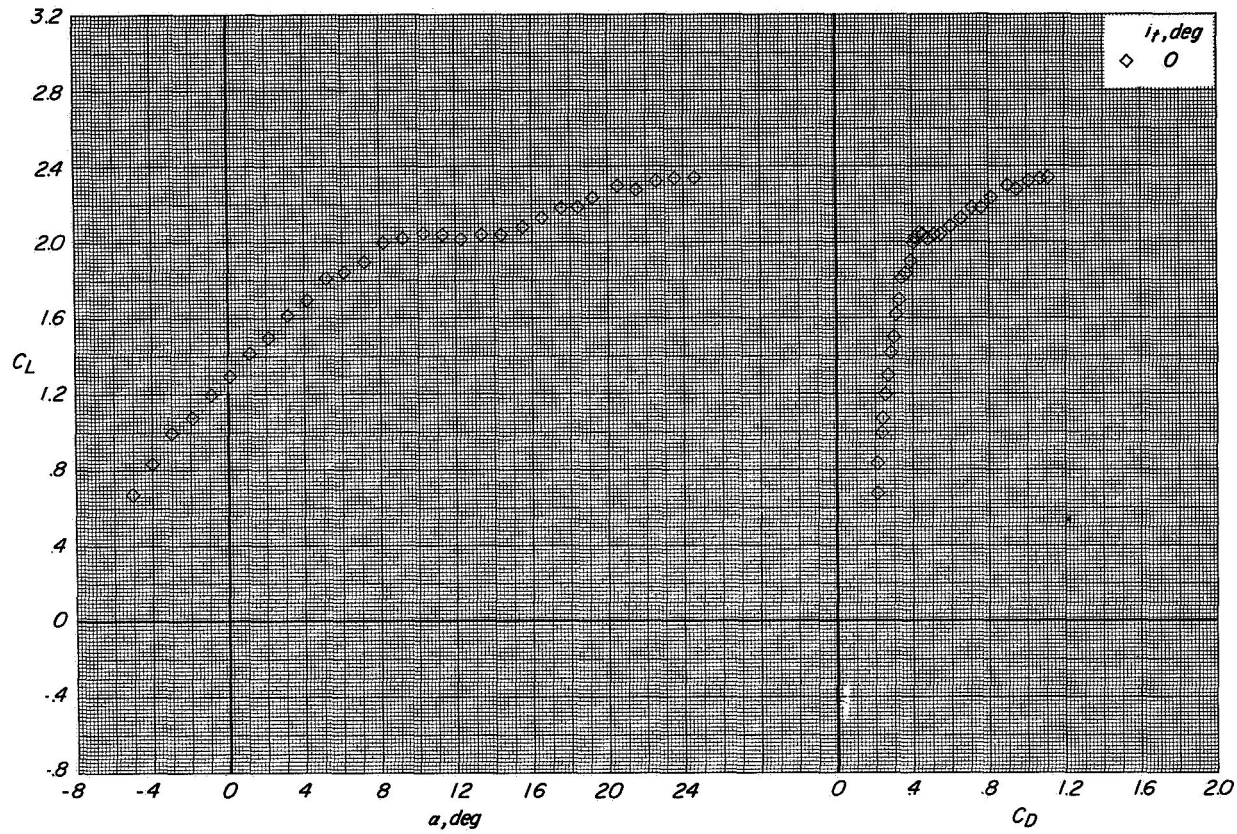

(a) Variation of C_L with α and C_D with C_L.

Figure 49.- Longitudinal aerodynamic characteristics of model with modified wing. $\delta_{LE,OB} = 32^\circ$; $\delta_{LE,IB} = 32^\circ$; $\delta_{TE,W} = 50^\circ$; $\delta_{LE,ST} = 45^\circ$; $\delta_{TE,ST} = 40^\circ$; $C_T = 0$.

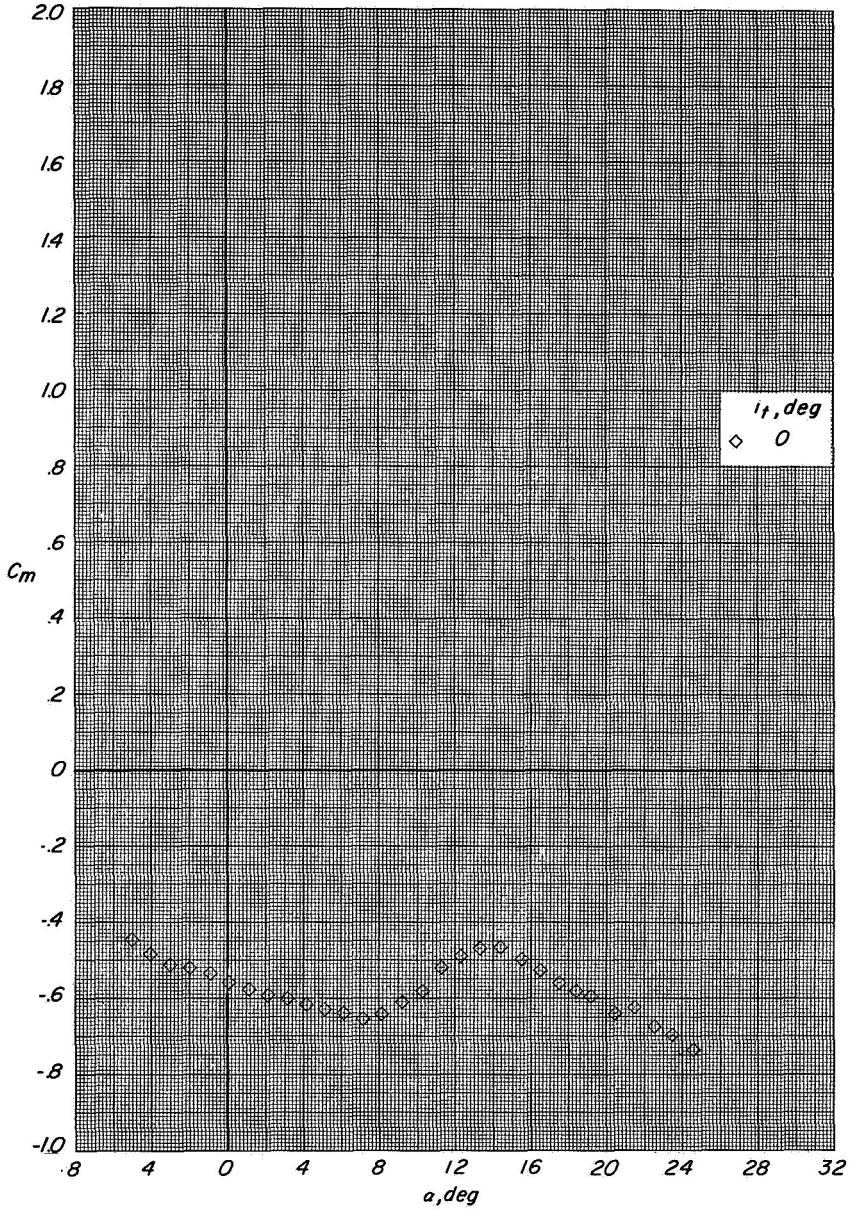

(b) Variation of C_m with α.

Figure 49.- Continued.

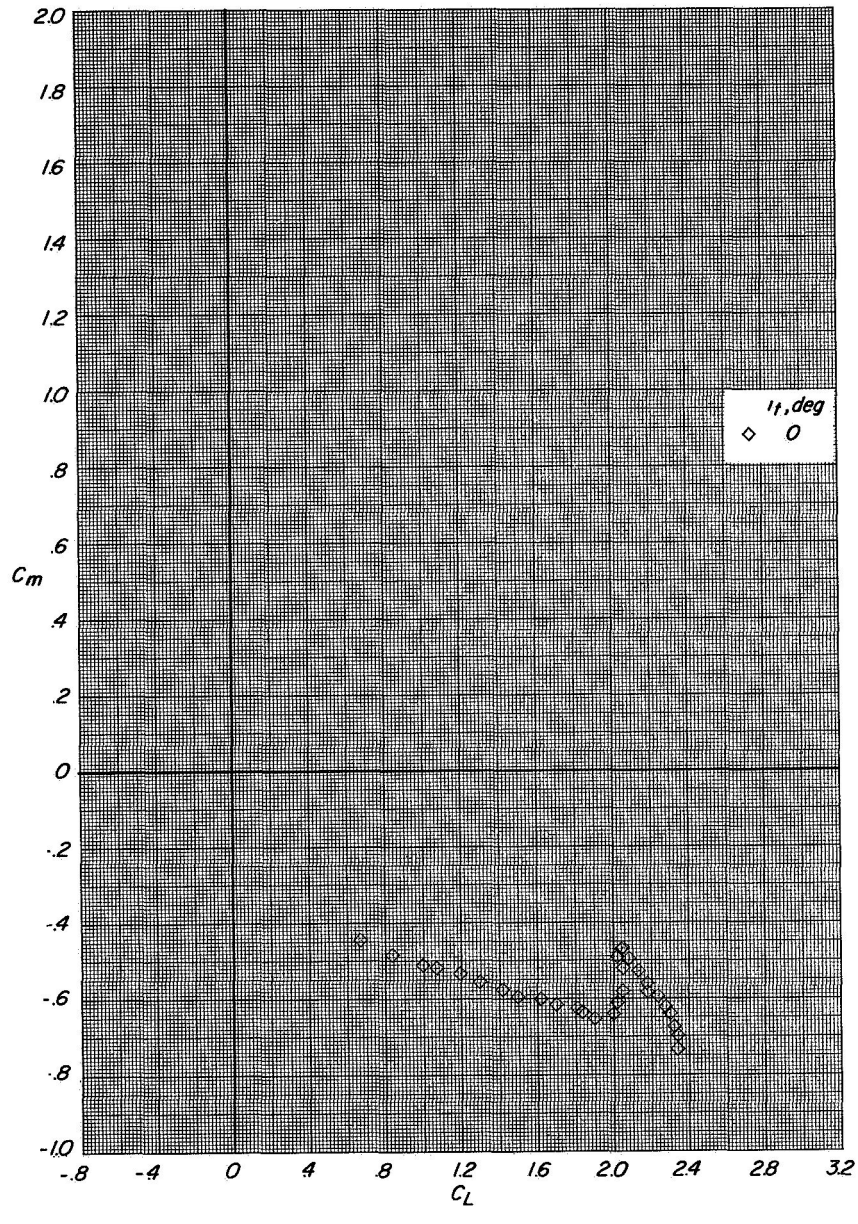

(c) Variation of C_m with C_L.

Figure 49.- Concluded.

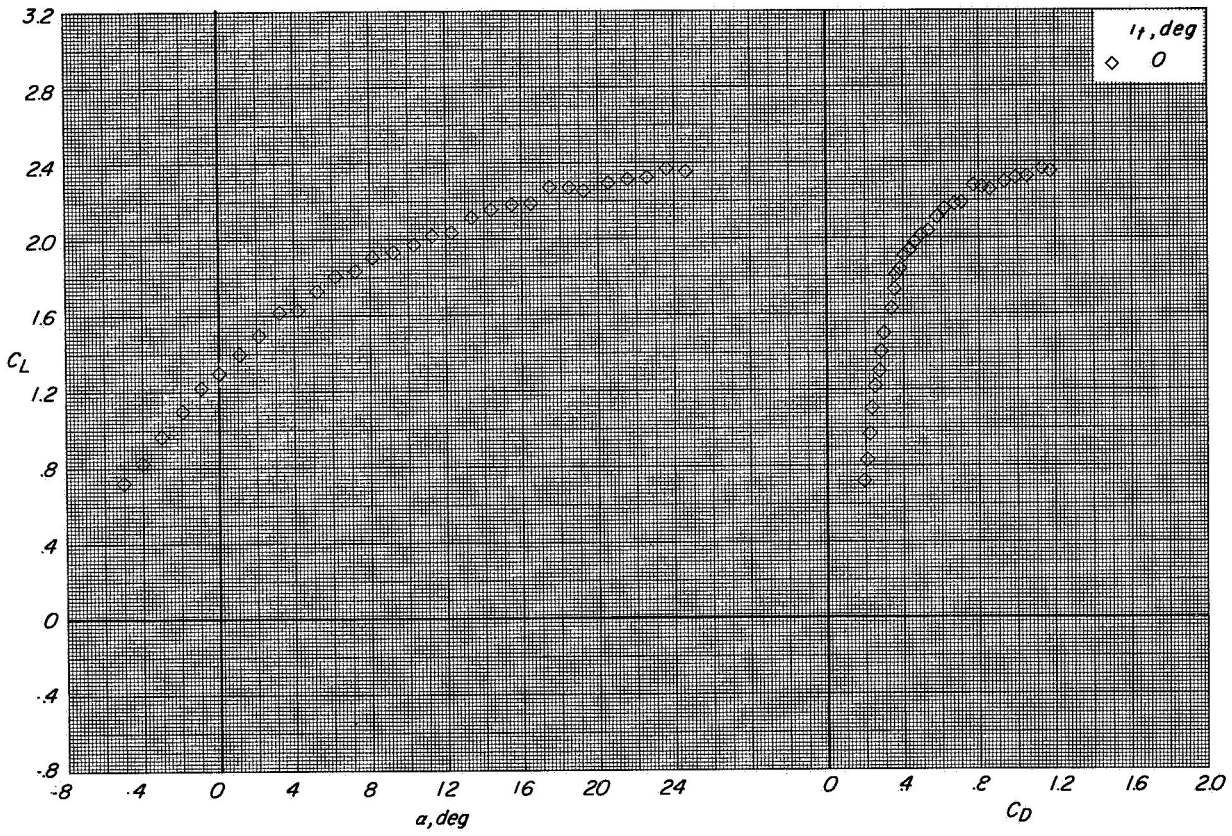

(a) Variation of C_L with α and C_D with C_L.

Figure 50.- Longitudinal aerodynamic characteristics of model with modified wing. $\delta_{LE,OB} = 36.5^\circ$; $\delta_{LE,IB} = 32^\circ$; $\delta_{TE,W} = 50^\circ$; $\delta_{LE,ST} = 0^\circ$; $\delta_{TE,ST} = 40^\circ$; $C_T = 0$.

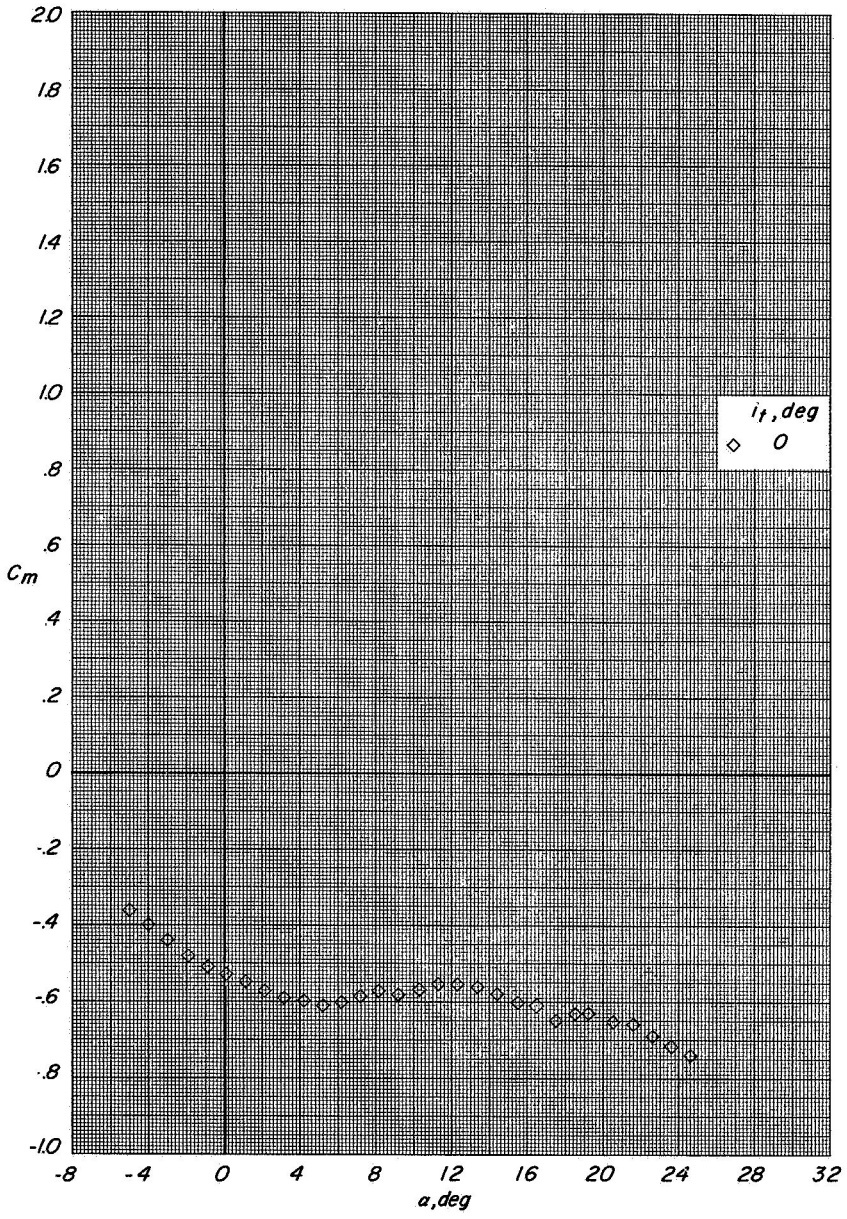

(b) Variation of C_m with α.

Figure 50.- Continued.

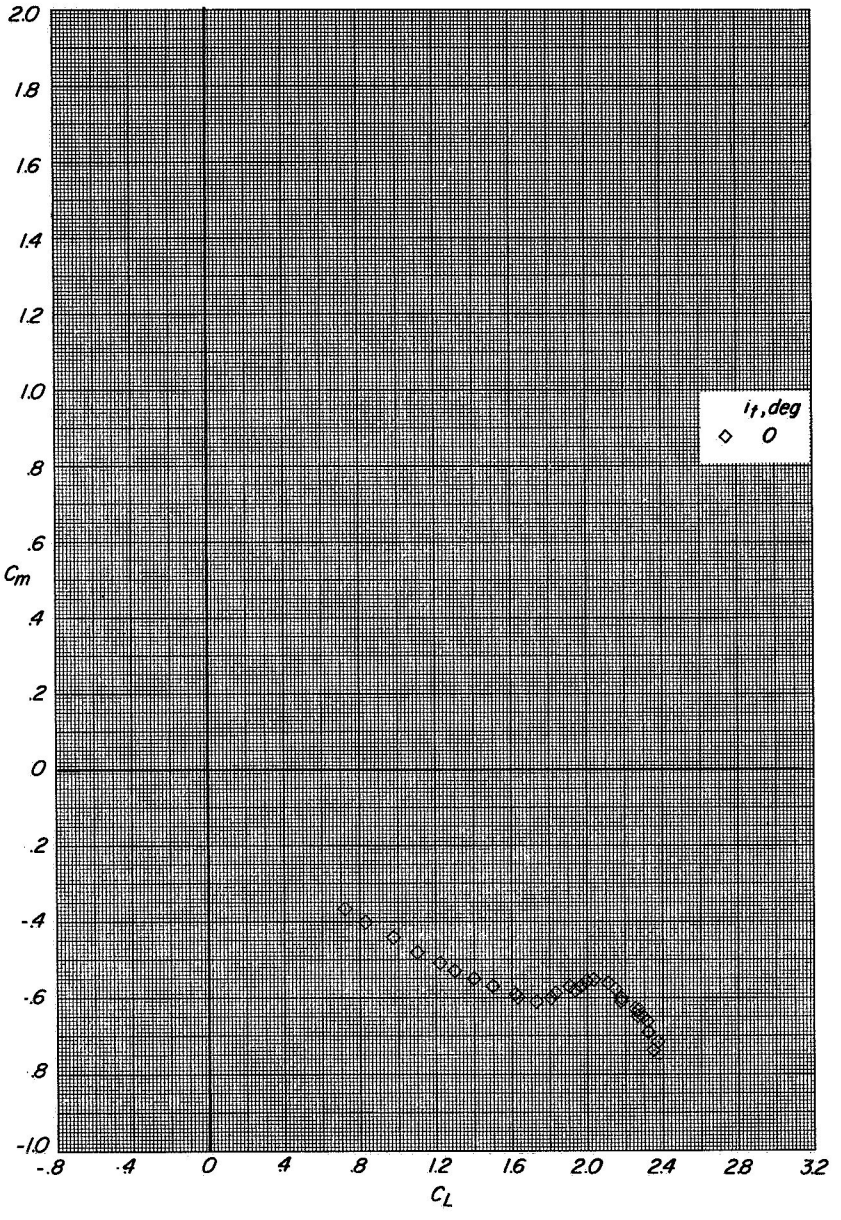

(c) Variation of C_m with C_L.

Figure 50.- Concluded.

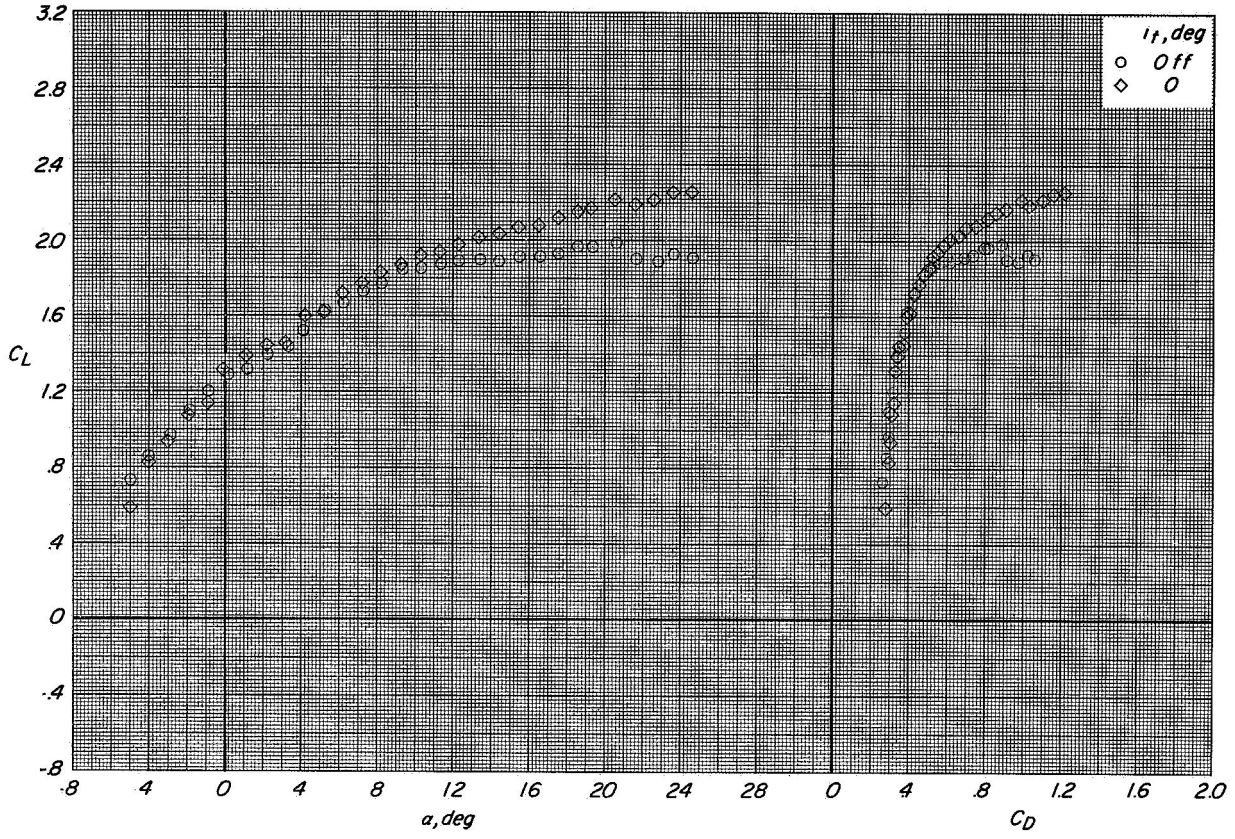

(a) Variation of C_L with α and C_D with C_L.

Figure 51.- Longitudinal aerodynamic characteristics of configuration C with direct-lift engines and lift-cruise engines deflected 90°. $C_T = 0$.

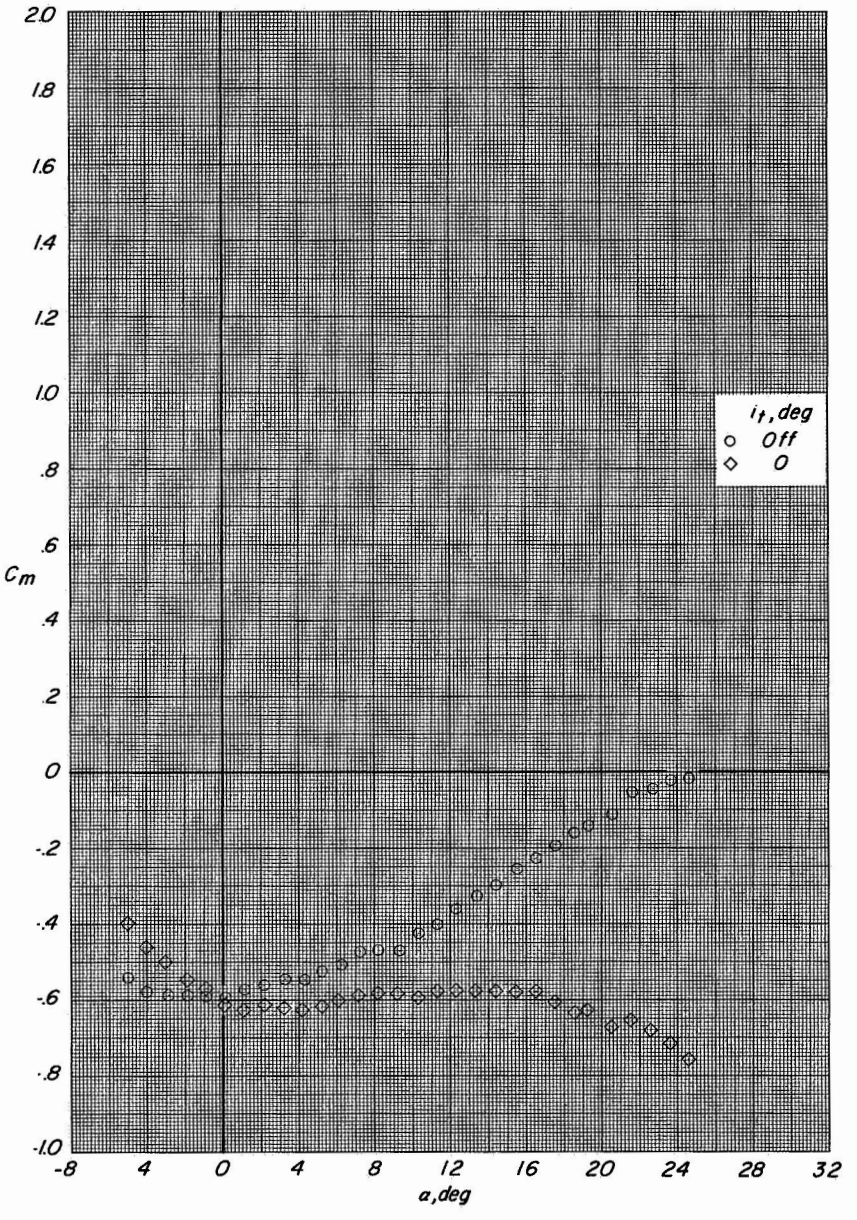

(b) Variation of C_m with α.

Figure 51.- Continued.

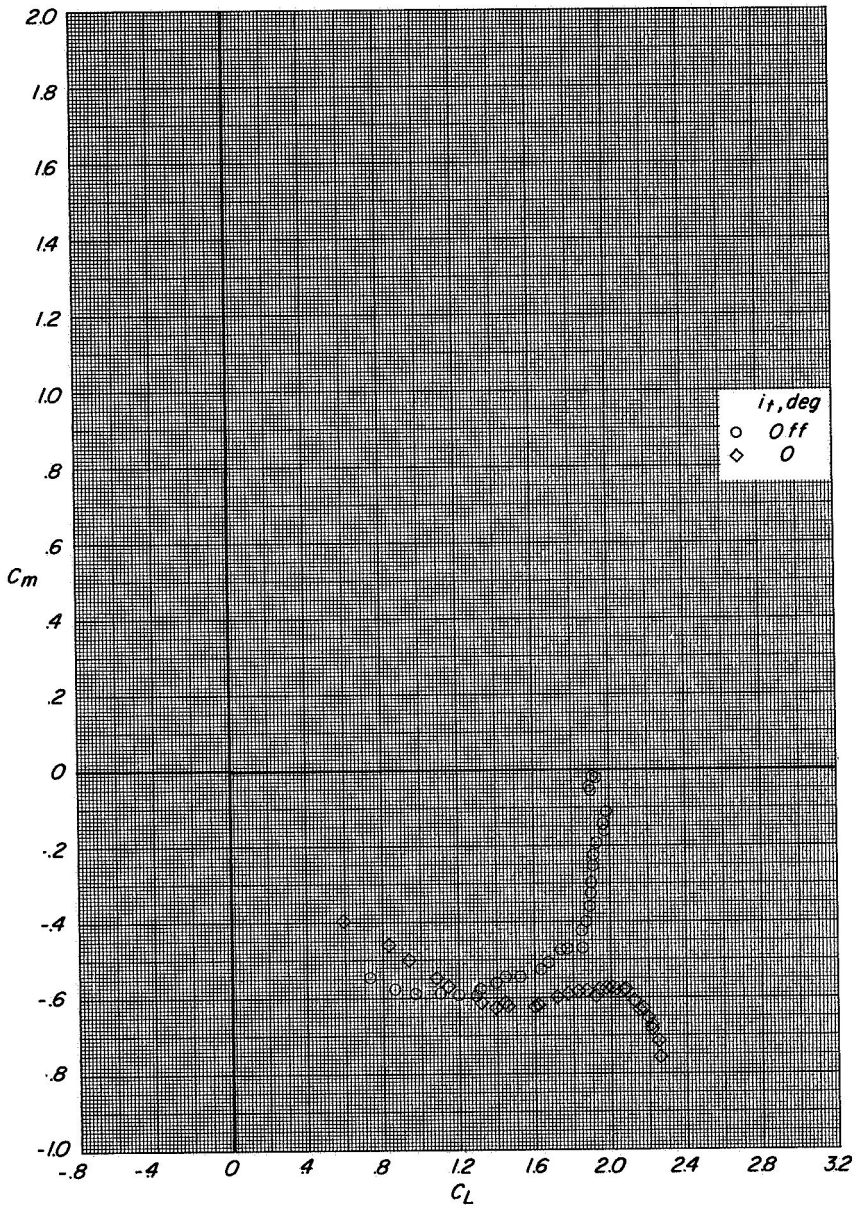

(c) Variation of C_m with C_L.

Figure 51.- Concluded.

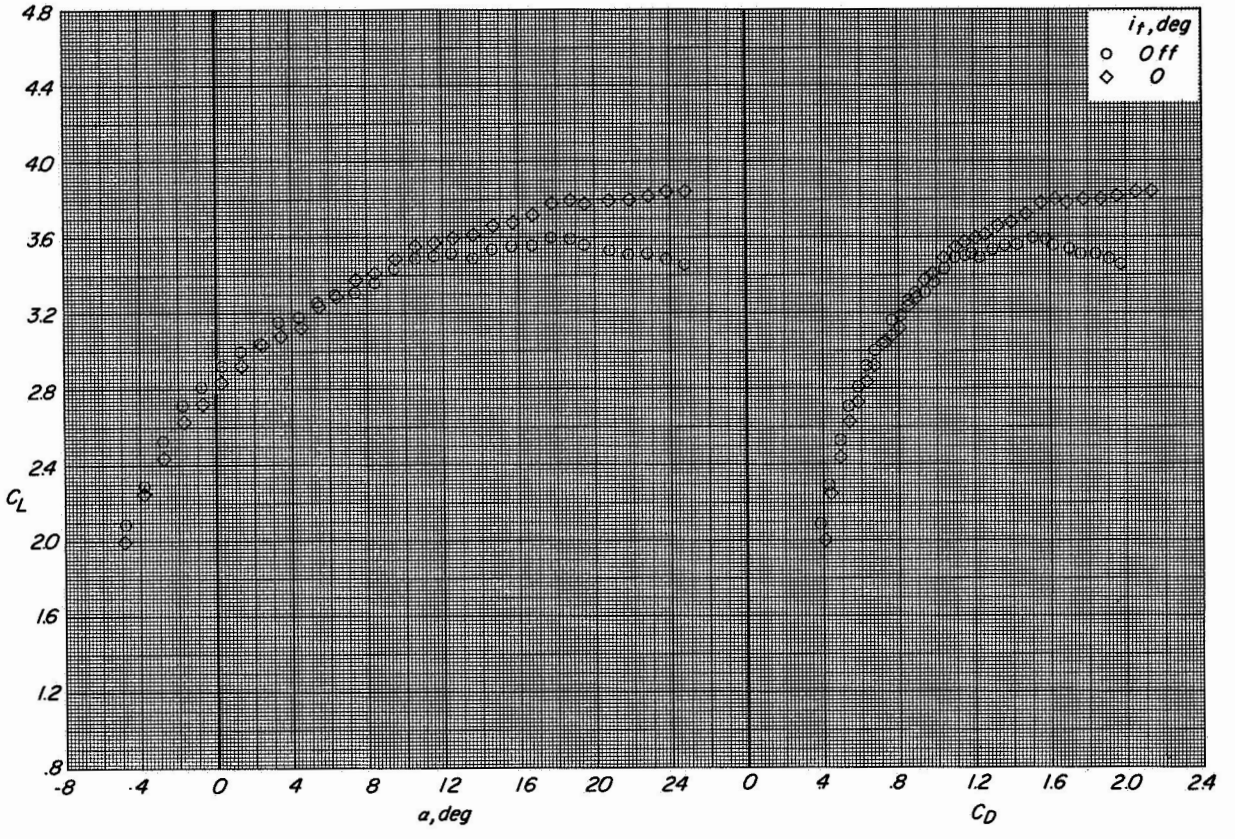

(a) Variation of C_L with α and C_D with C_L.

Figure 52.- Longitudinal aerodynamic characteristics of configuration C with direct-lift engines and lift-cruise engines deflected 90°. $C_T \approx 1.45$.

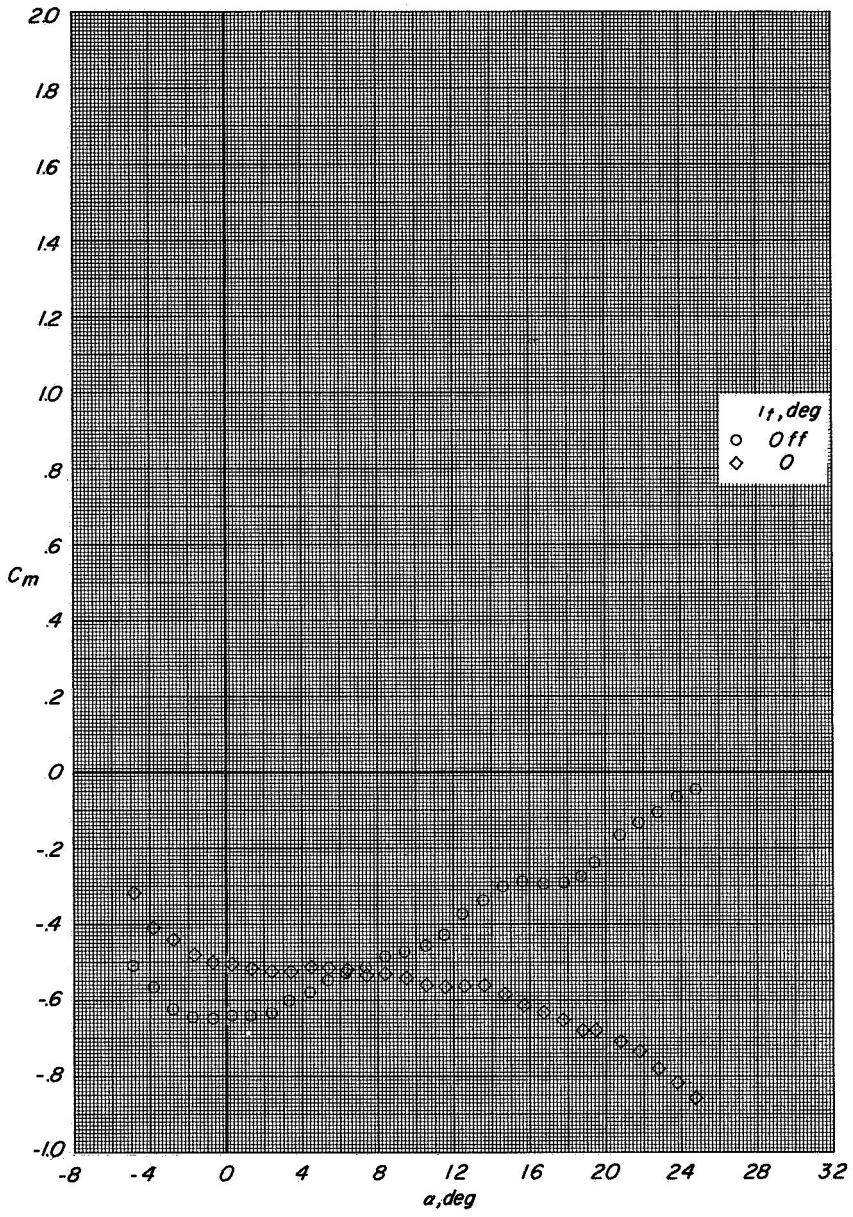

(b) Variation of C_m with α.

Figure 52.- Continued.

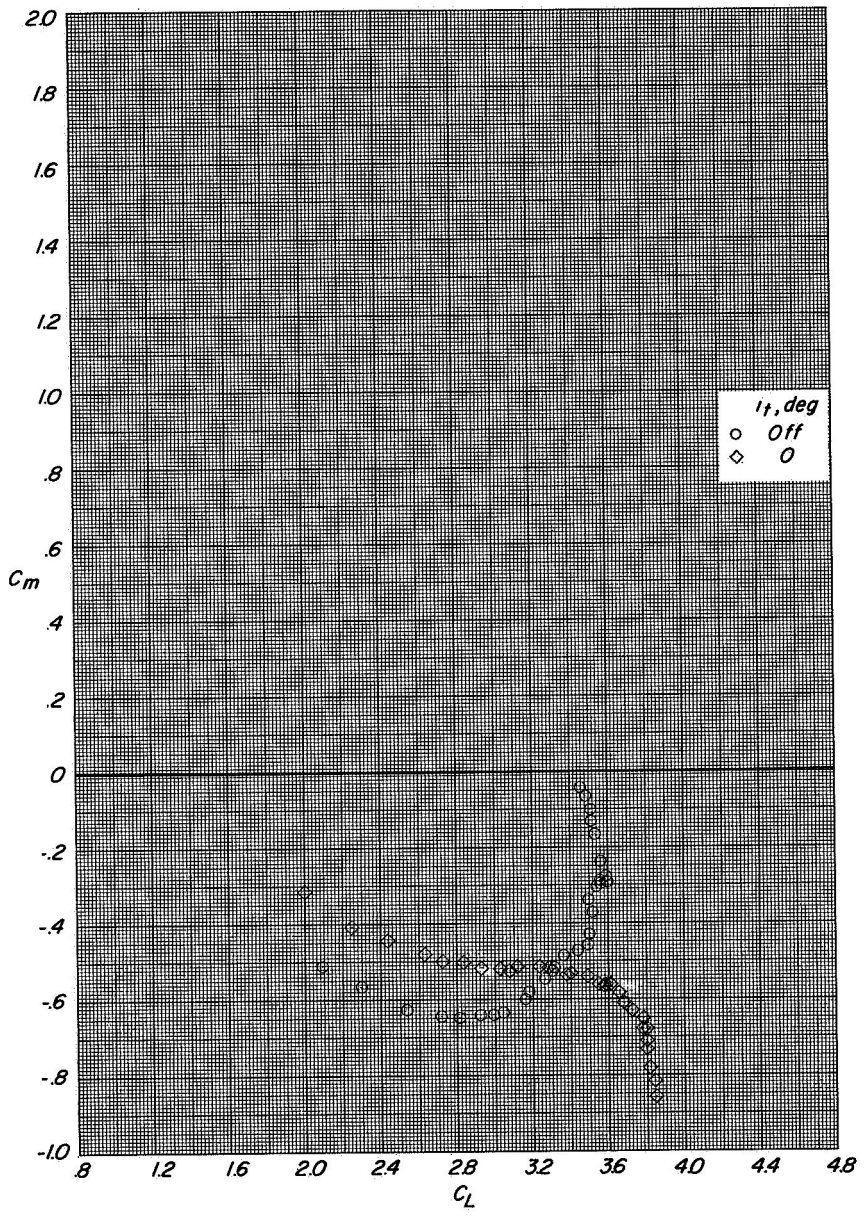

(c) Variation of C_m with C_L.

Figure 52.- Continued.

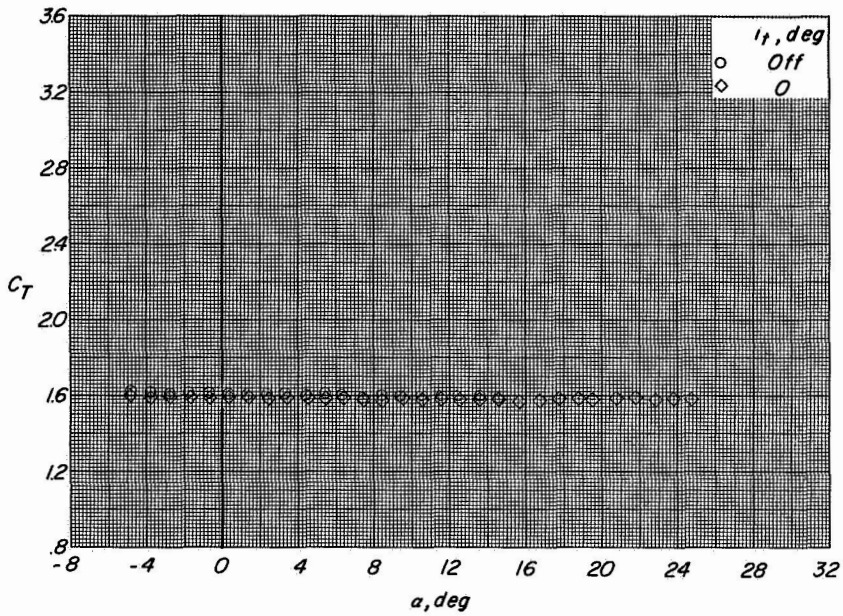

(d) Variation of C_T with α.

Figure 52.- Concluded.

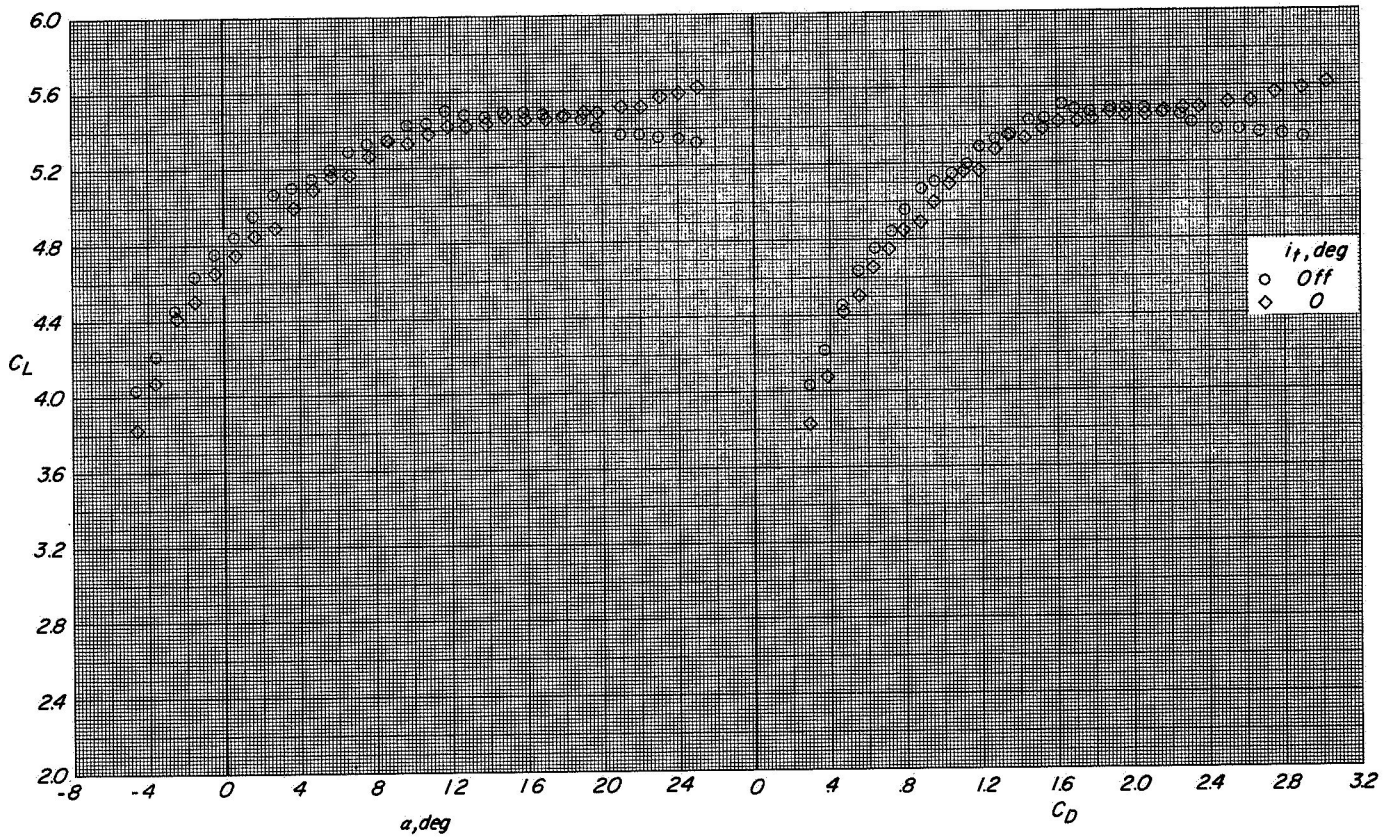

(a) Variation of C_L with α and C_D with C_L.

Figure 53.- Longitudinal aerodynamic characteristics of configuration C with direct-lift engines and lift-cruise engines deflected 90°. $C_T \approx 3.3$.

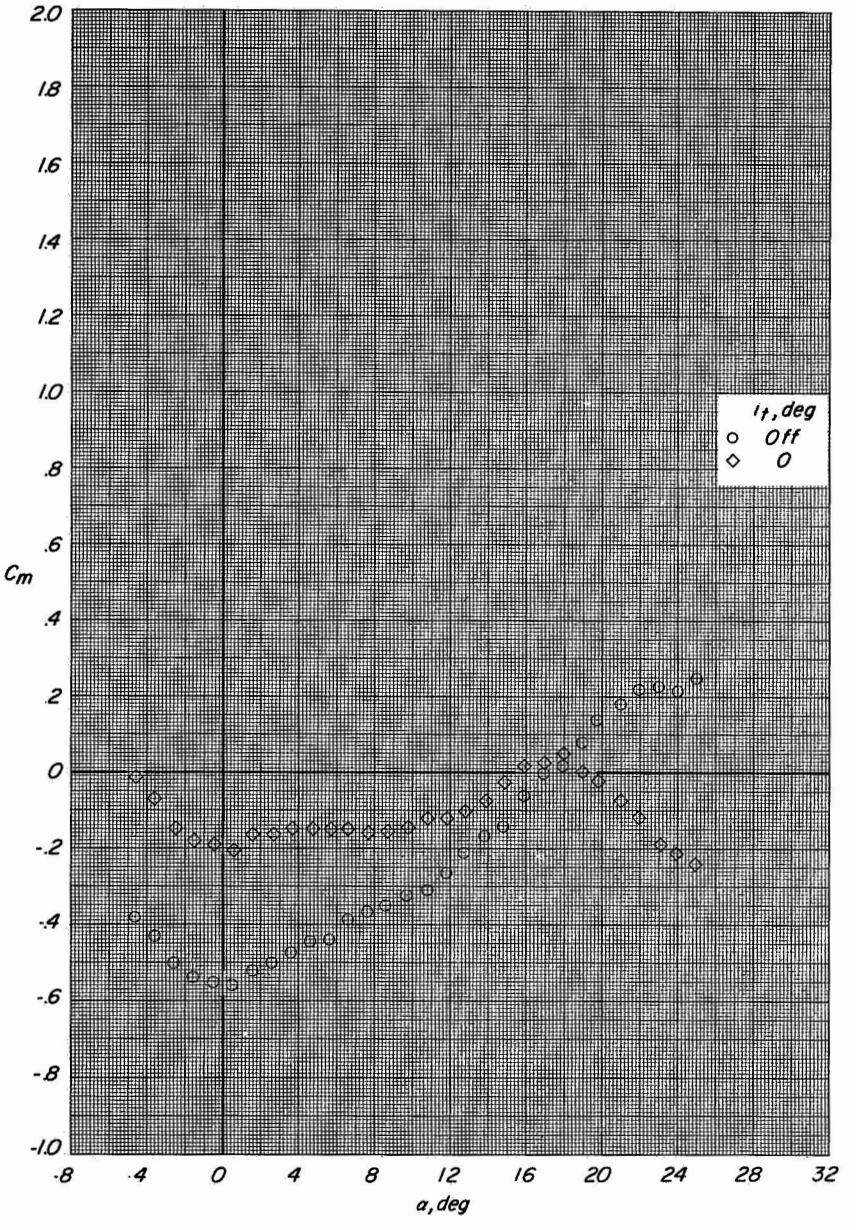

(b) Variation of C_m with α.

Figure 53.- Continued.

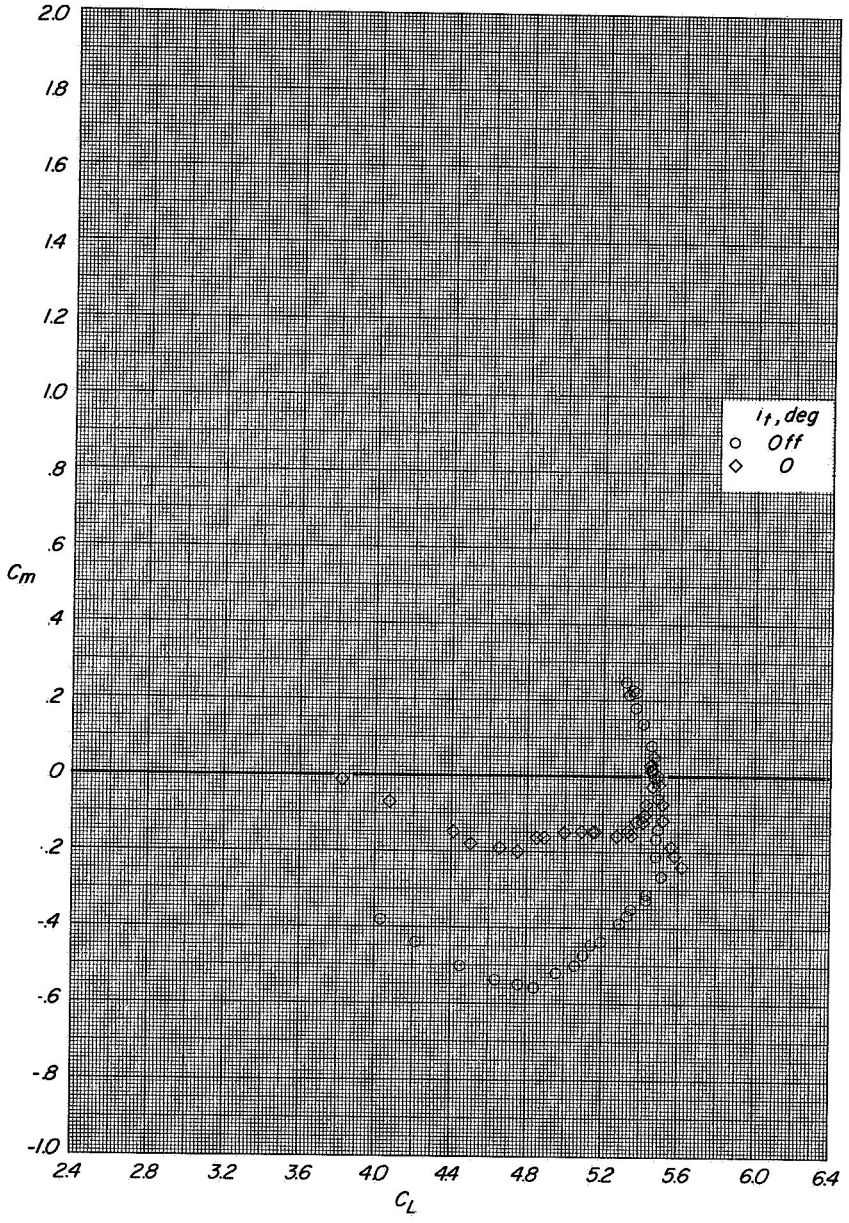

(c) Variation of C_m with C_L.

Figure 53.- Continued.

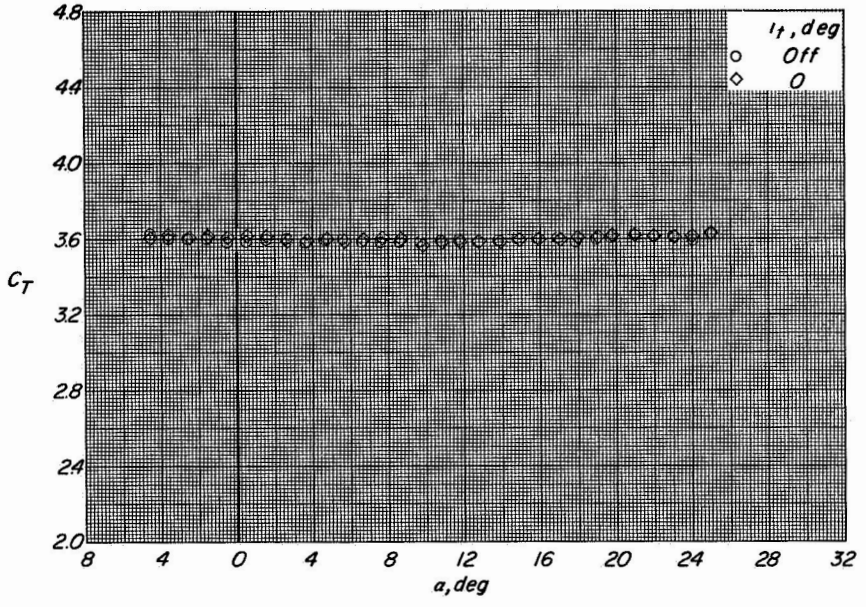

(d) Variation of C_T with α.

Figure 53.- Concluded.

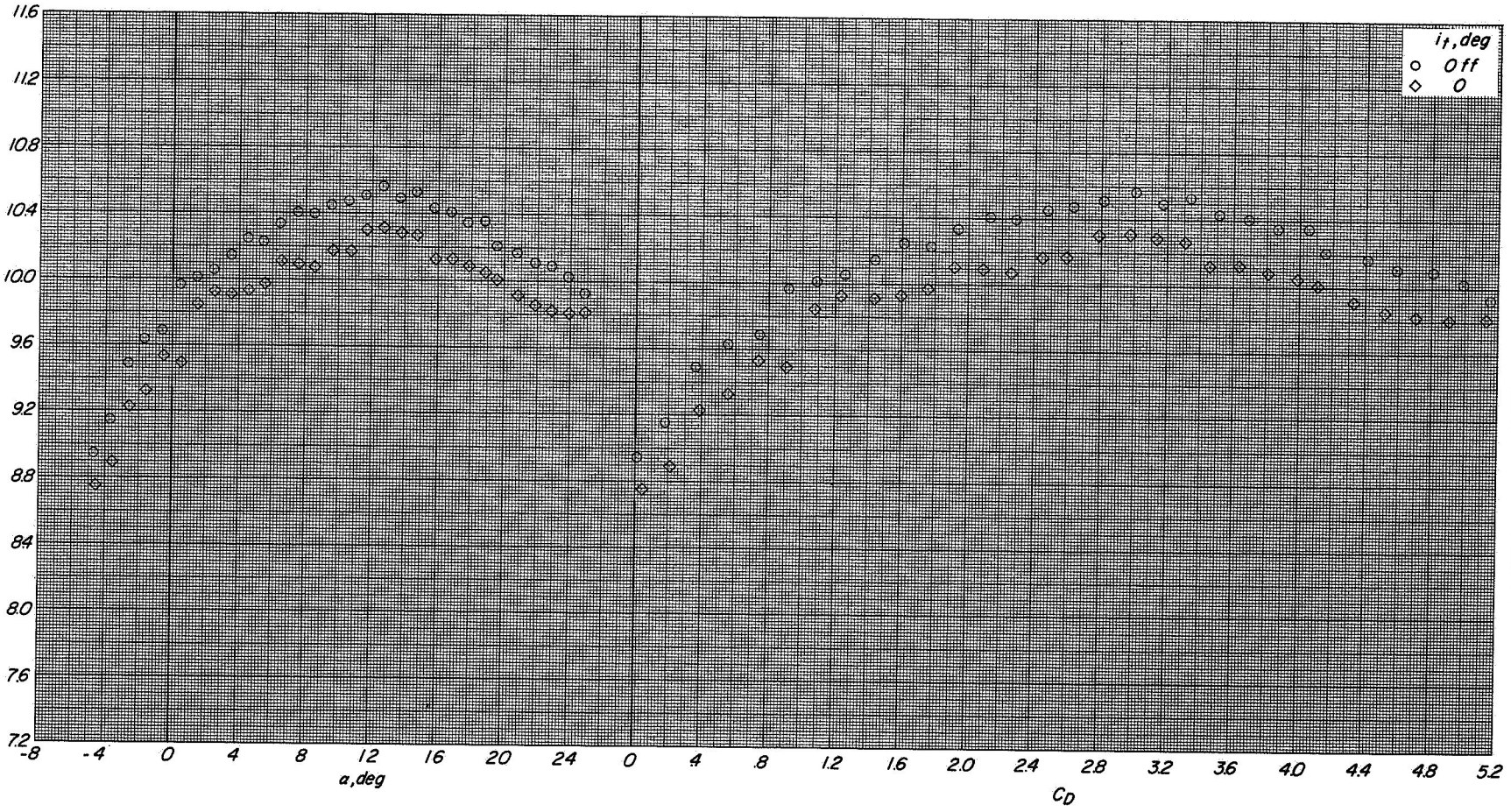

(a) Variation of C_L with α and C_D with C_L.

Figure 54.- Longitudinal aerodynamic characteristics of configuration C with direct-lift engines and lift-cruise engines deflected 90°. $C_T \approx 8$.

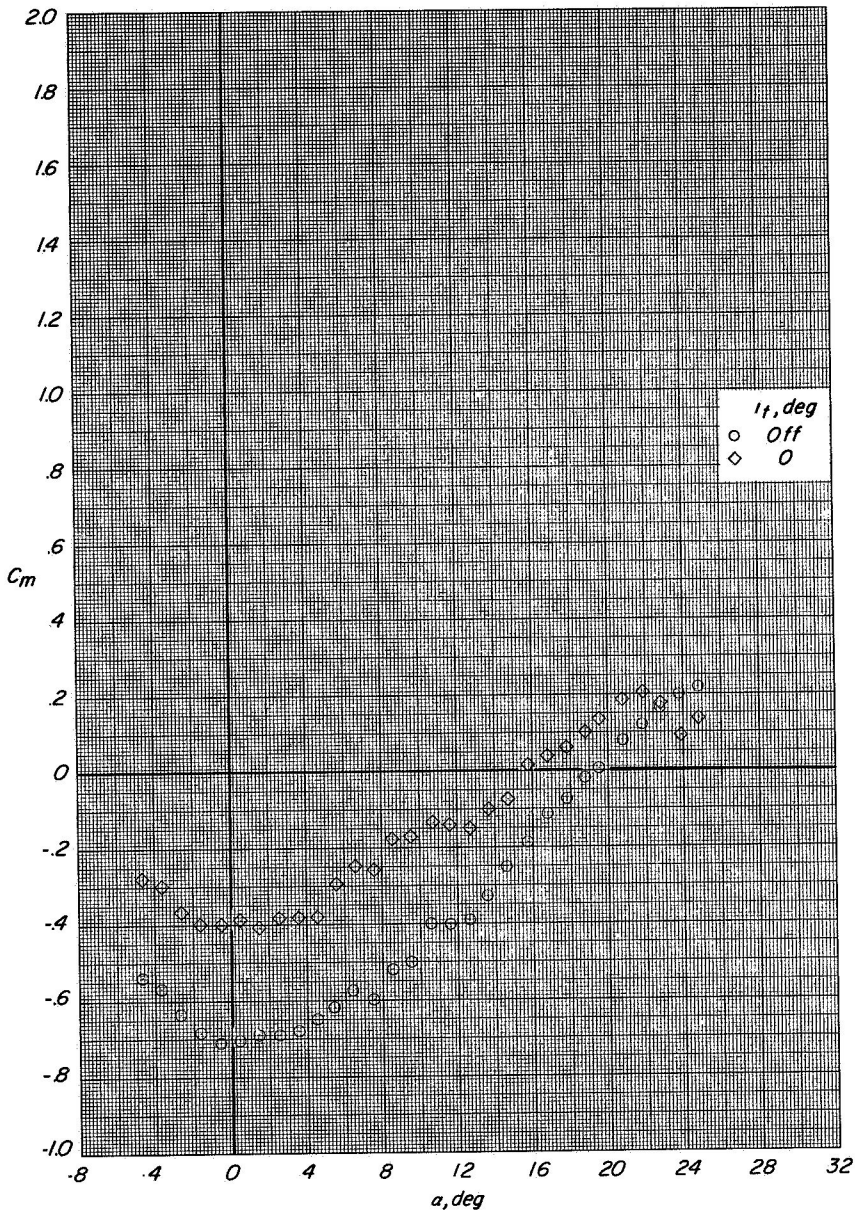

(b) Variation of C_m with α.

Figure 54.- Continued.

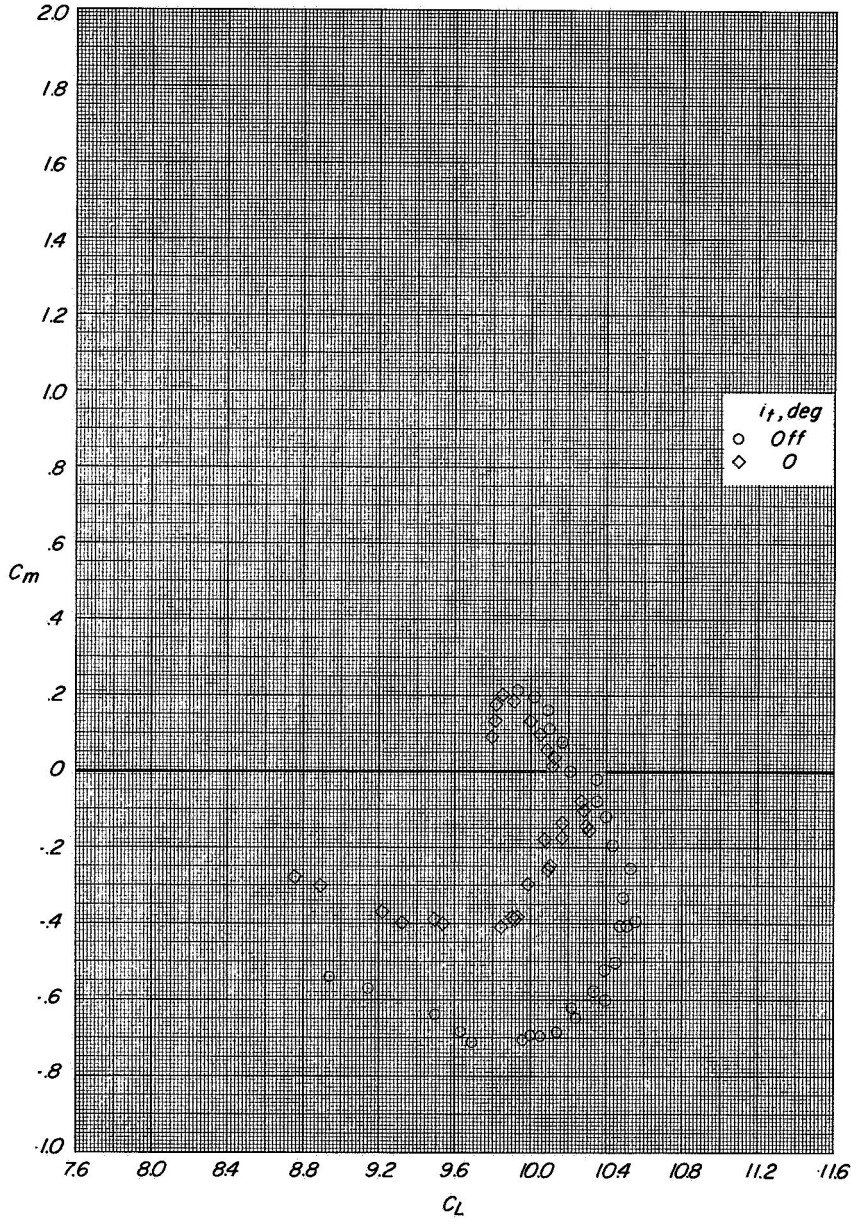

(c) Variation of C_m with C_L.

Figure 54.- Continued.

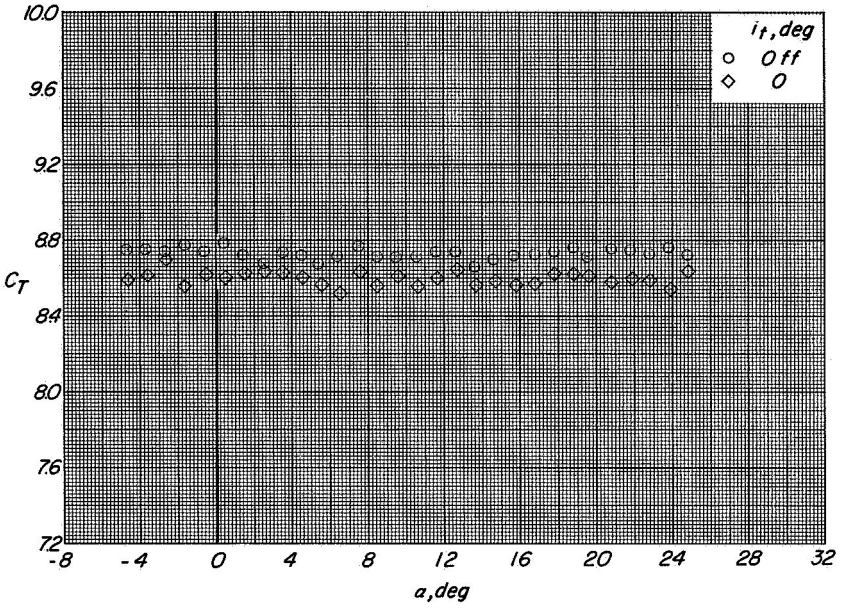

(d) Variation of C_T with α.

Figure 54.- Concluded.

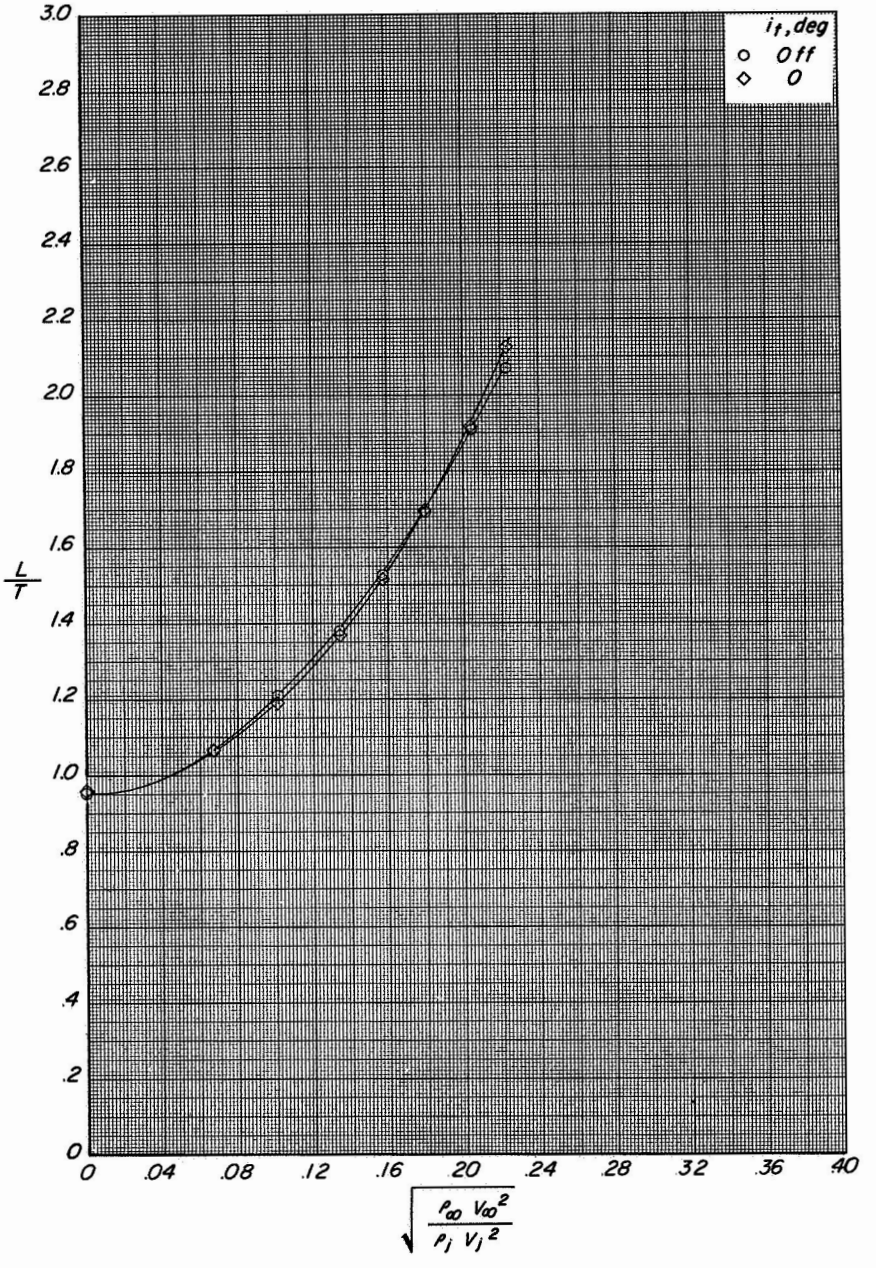

(a) Variation of L/T with effective velocity ratio.

Figure 55.- Longitudinal aerodynamic characteristics of configuration C with direct-lift engines and lift-cruise engines deflected 90°. $\alpha = 12°$.

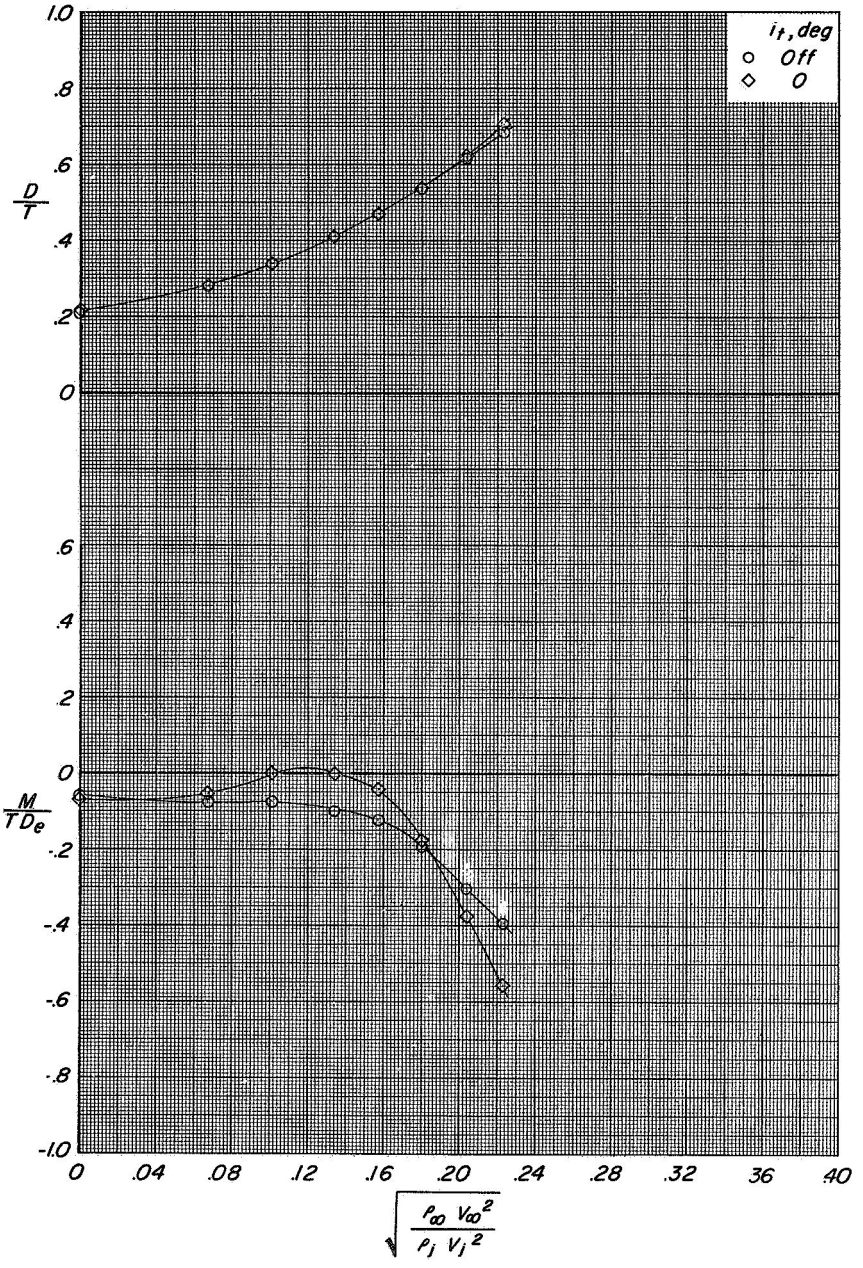

(b) Variation of D/T and M/TD_e with effective velocity ratio.

Figure 55.- Concluded.

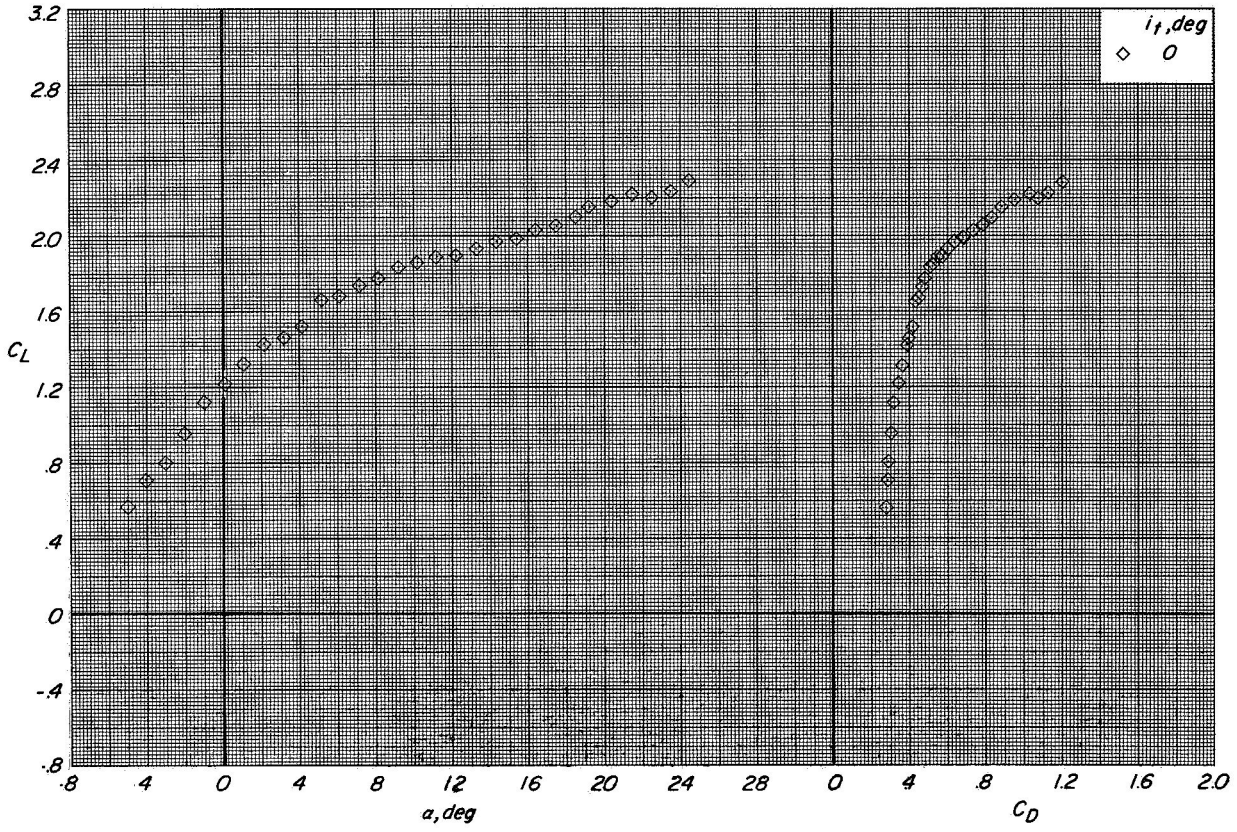

(a) Variation of C_L with α and C_D with C_L.

Figure 56.- Longitudinal aerodynamic characteristics of configuration C with direct-lift engines and lift-cruise engines deflected 25°. C_T = 0.

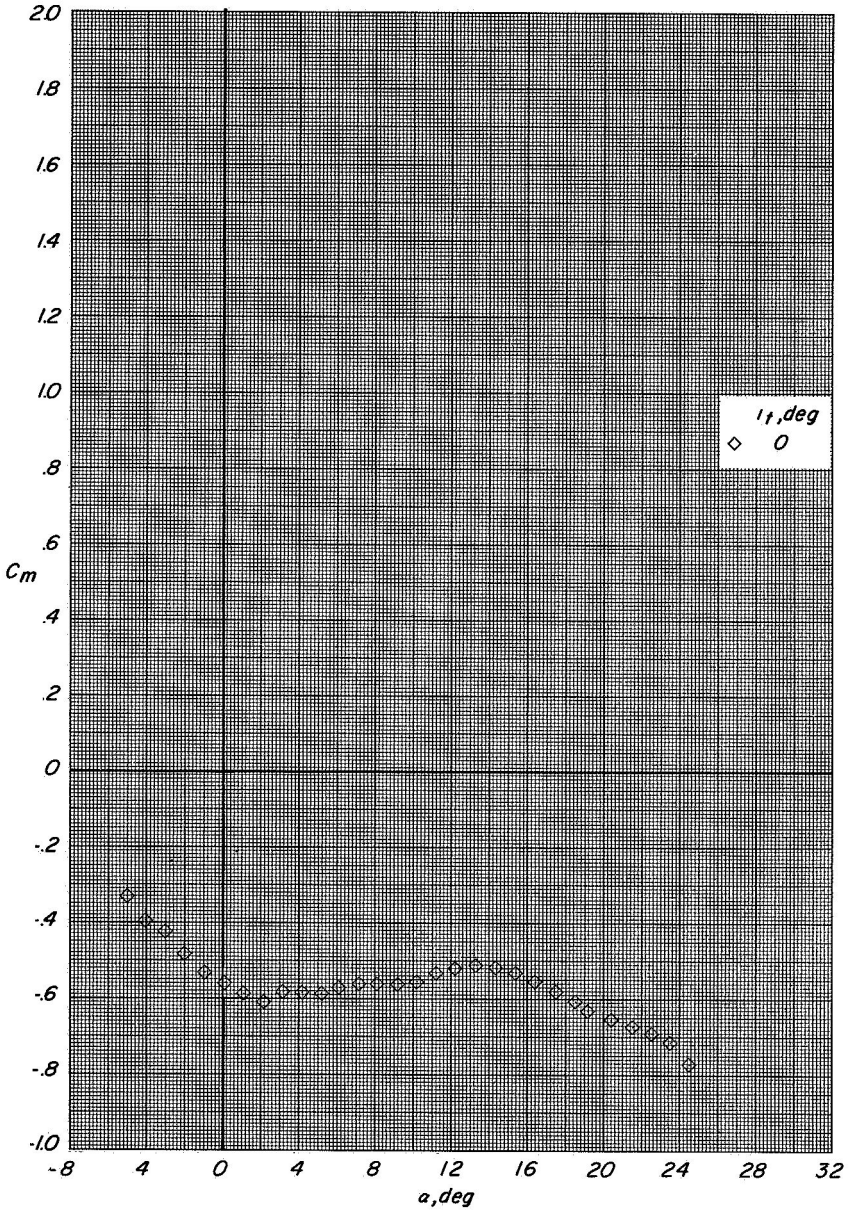

(b) Variation of C_m with α.

Figure 56.- Continued.

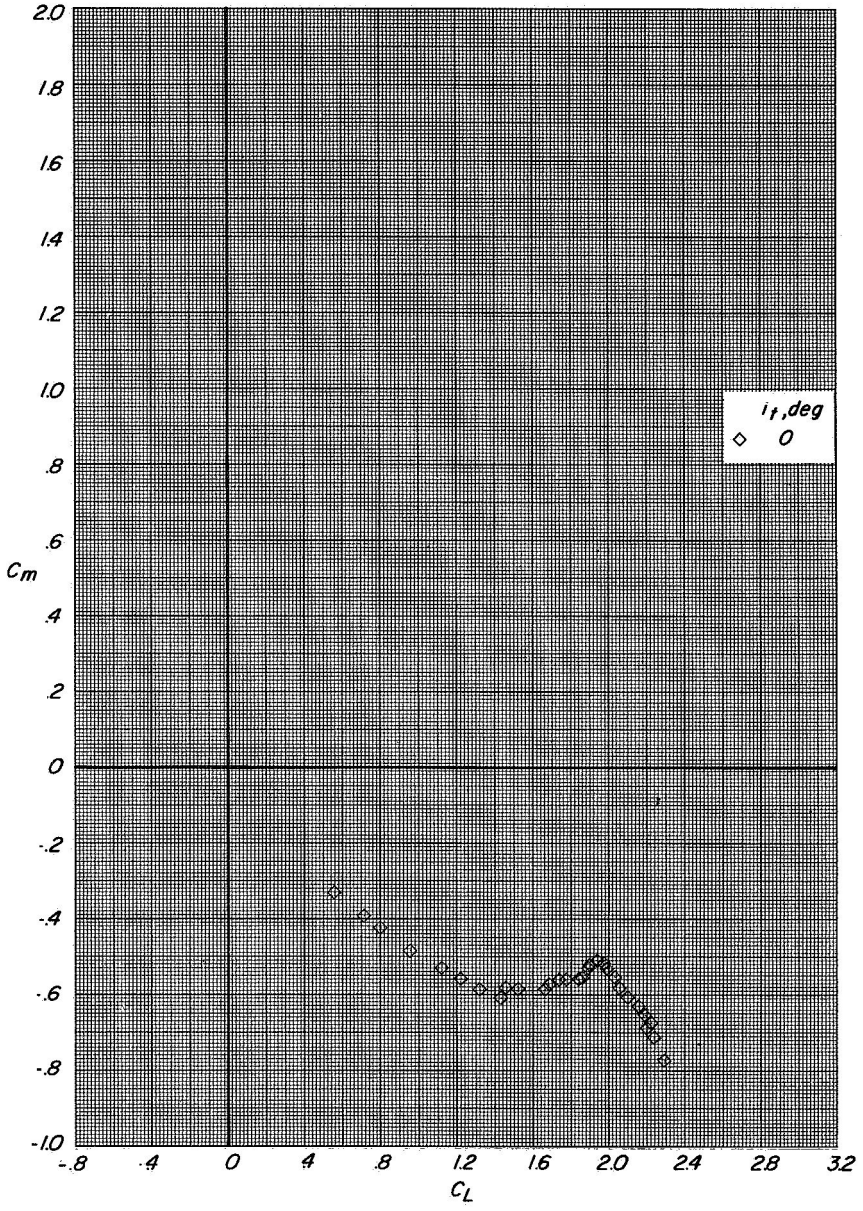

(c) Variation of C_m with C_L.

Figure 56.- Concluded.

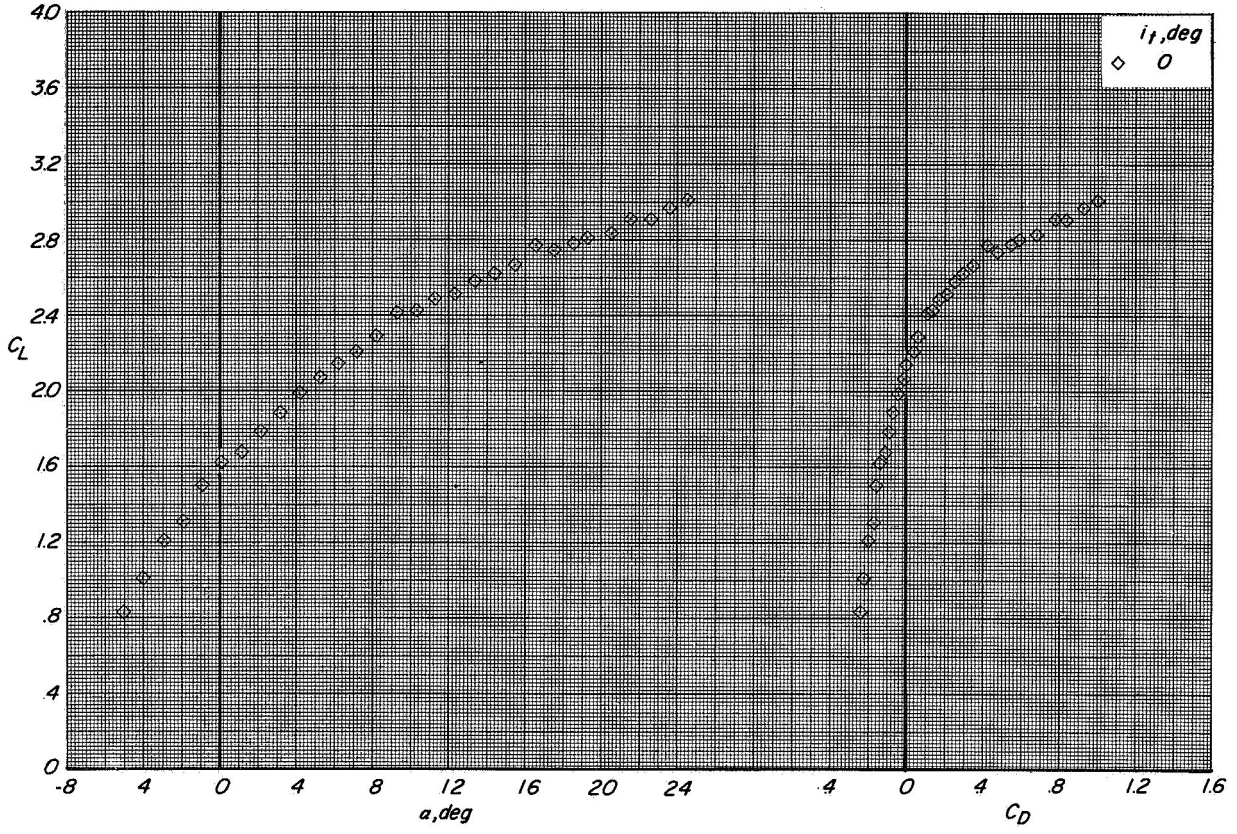

(a) Variation of C_L with α and C_D with C_L.

Figure 57.- Longitudinal aerodynamic characteristics of configuration C with direct-lift engines and lift-cruise engines deflected 25°. $C_T \approx 0.65$

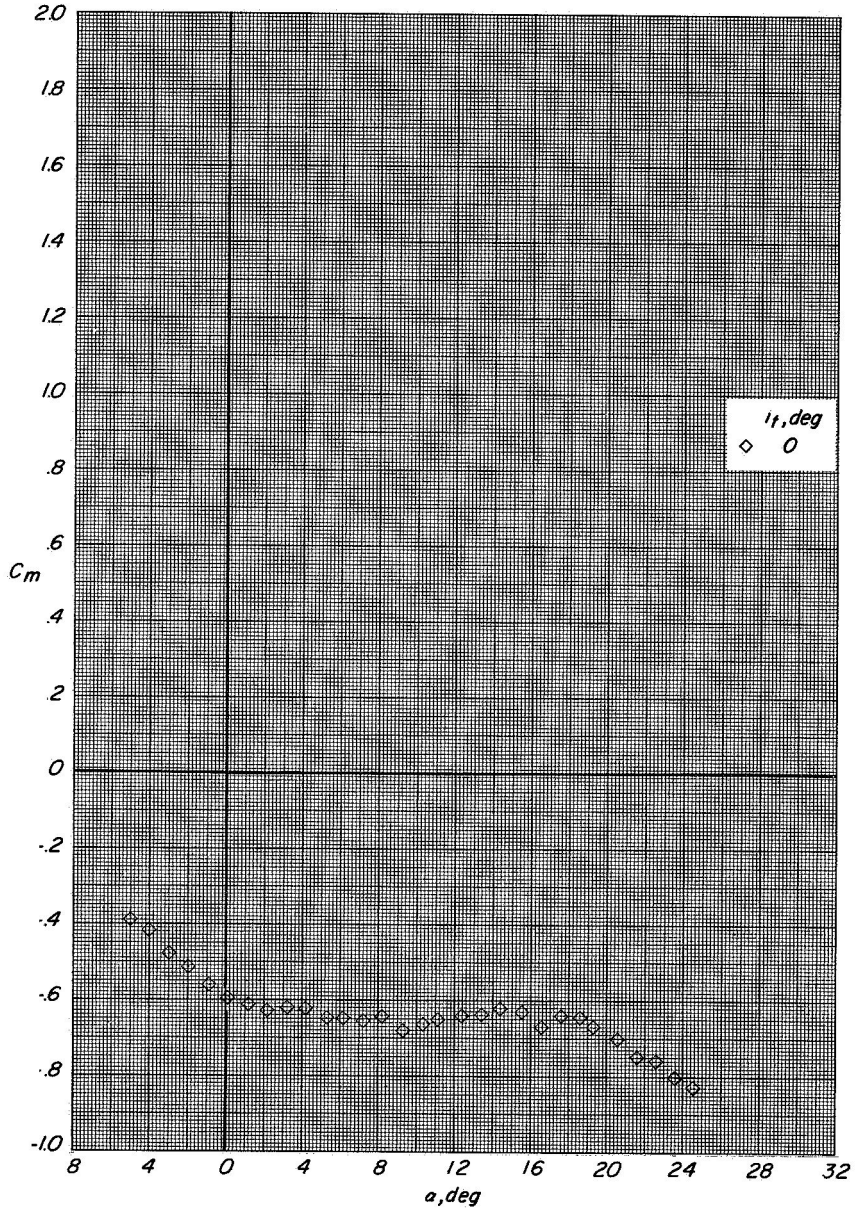

(b) Variation of C_m with α.

Figure 57.- Continued.

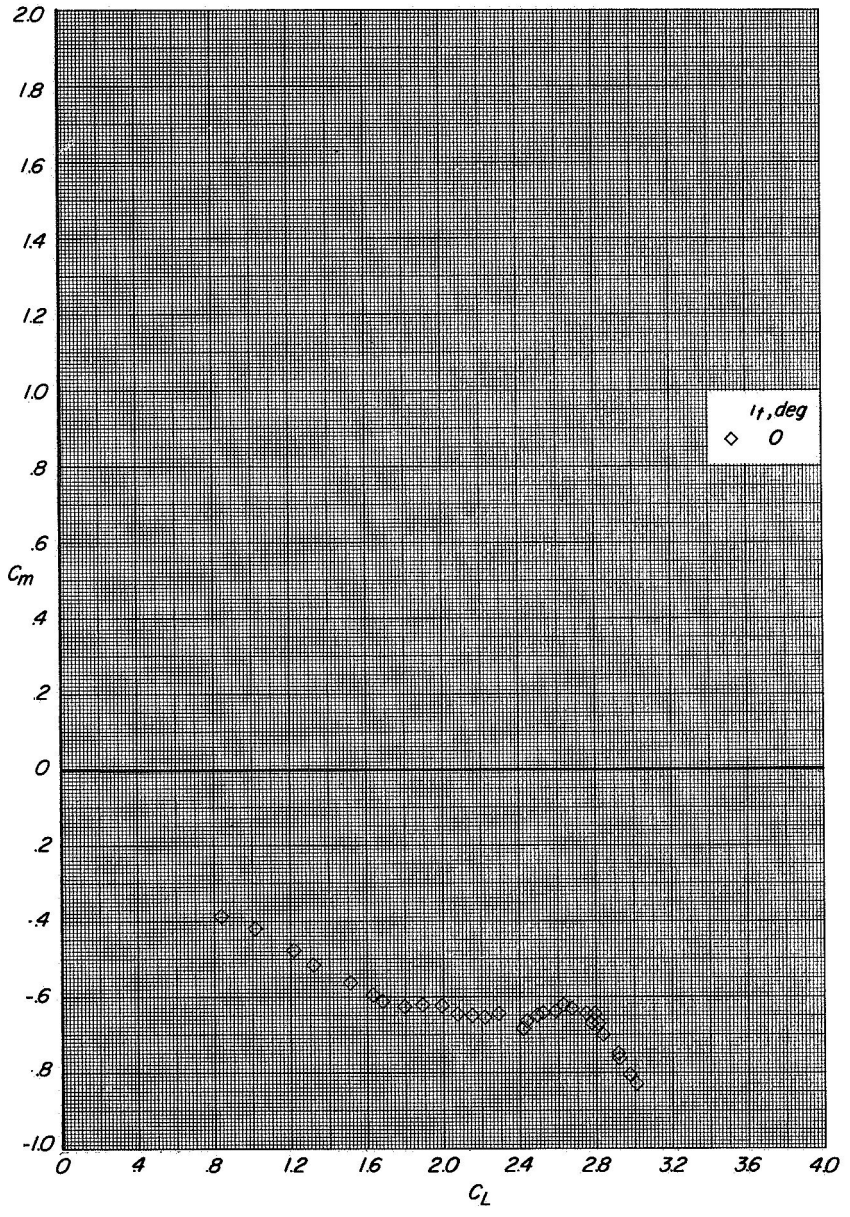

(c) Variation of C_m with C_L.

Figure 57.- Continued.

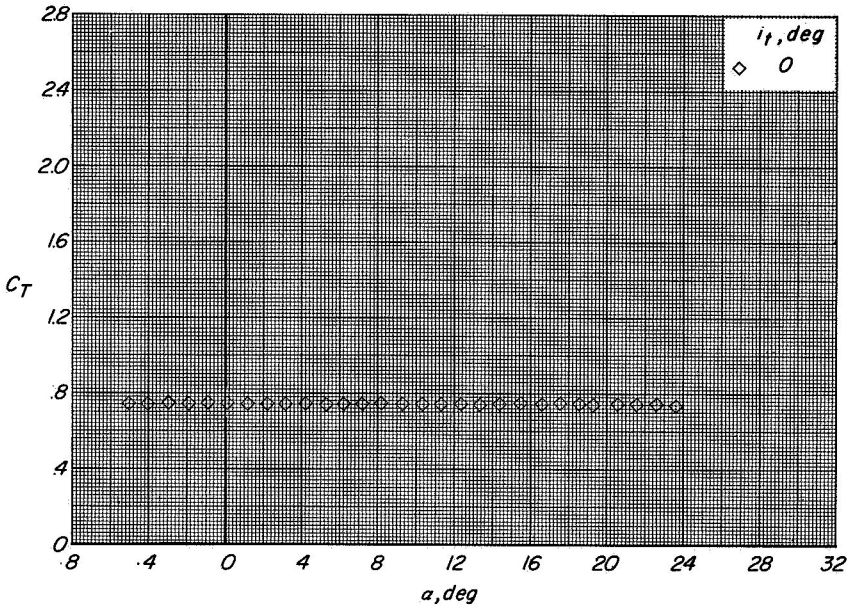

(d) Variation of C_T with α.

Figure 57.- Concluded.

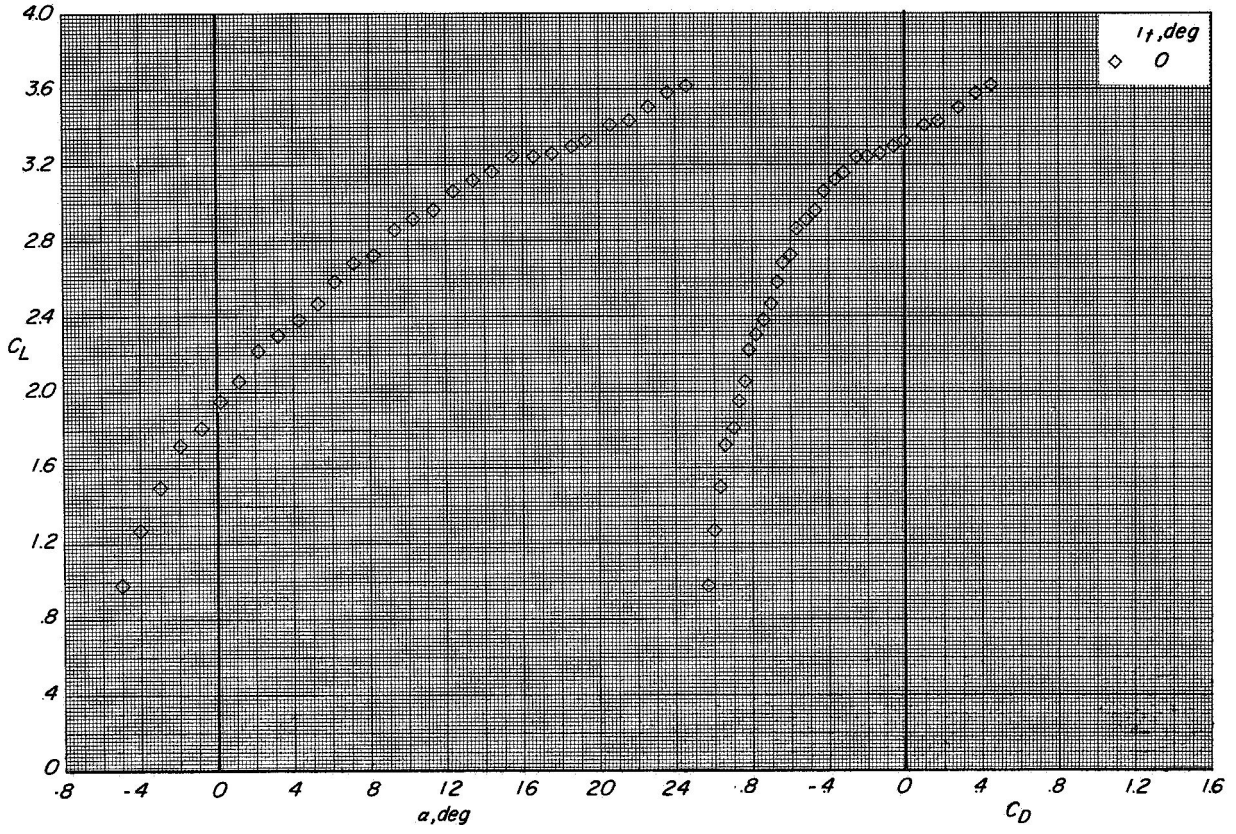

(a) Variation of C_L with α and C_D with C_L.

Figure 58.- Longitudinal aerodynamic characteristics of configuration C with direct-lift engines and lift-cruise engines deflected 25°. $C_T \approx 1.45$

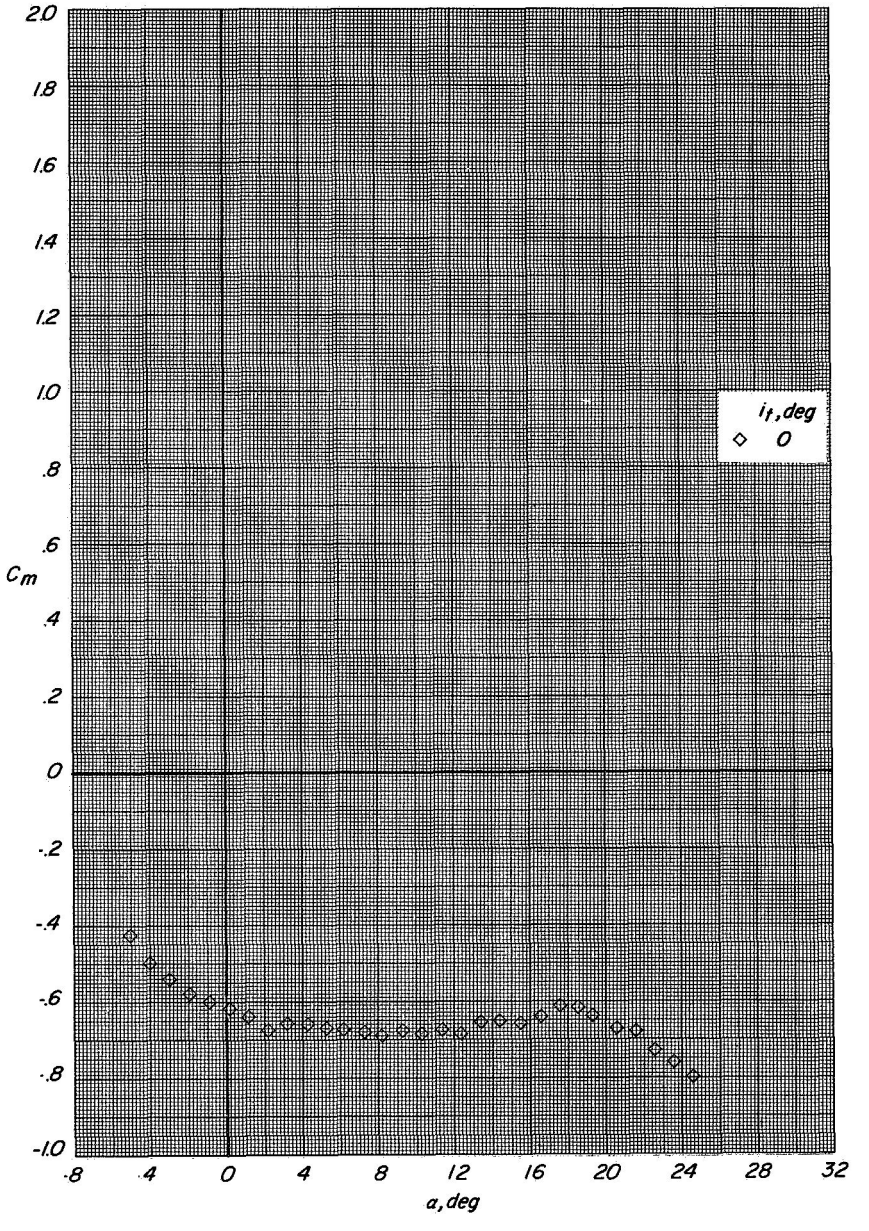

(b) Variation of C_m with α.

Figure 58.- Continued.

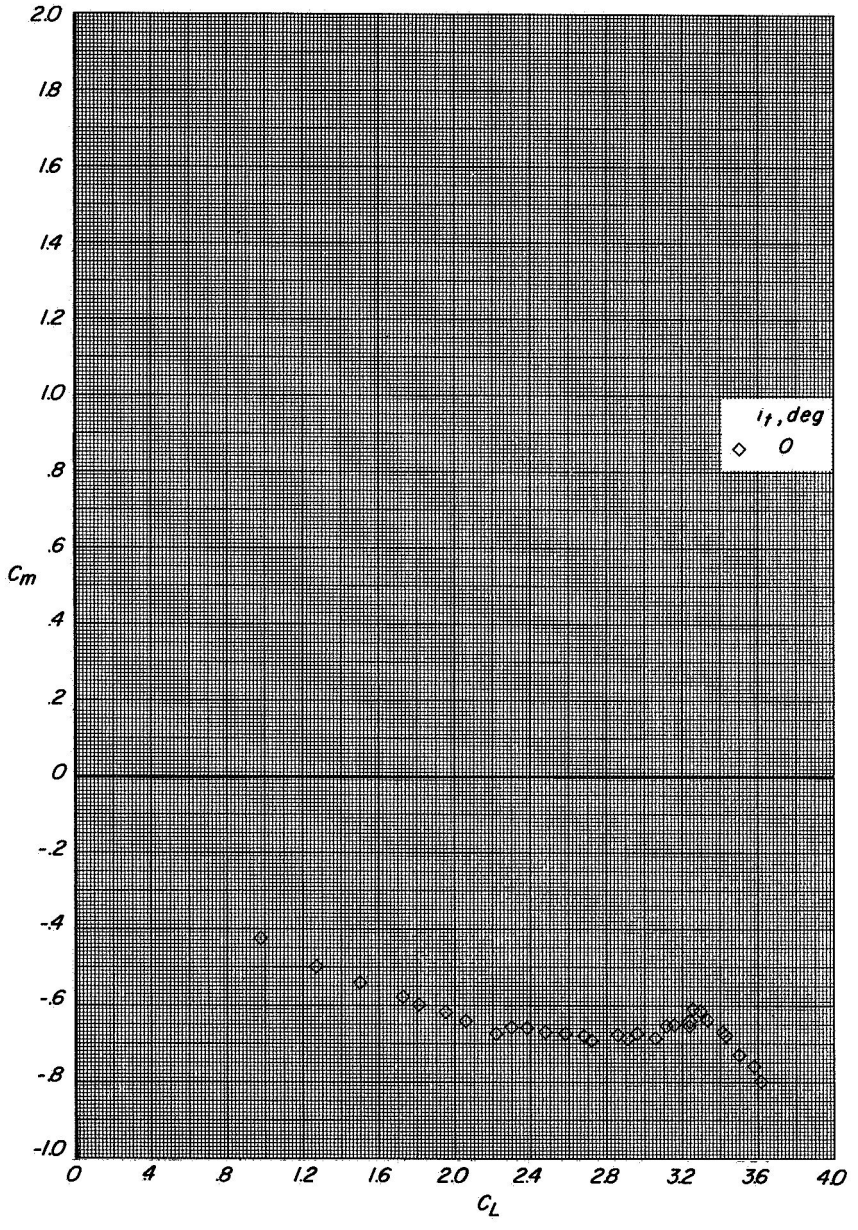

(c) Variation of C_m with C_L.

Figure 58.- Continued.

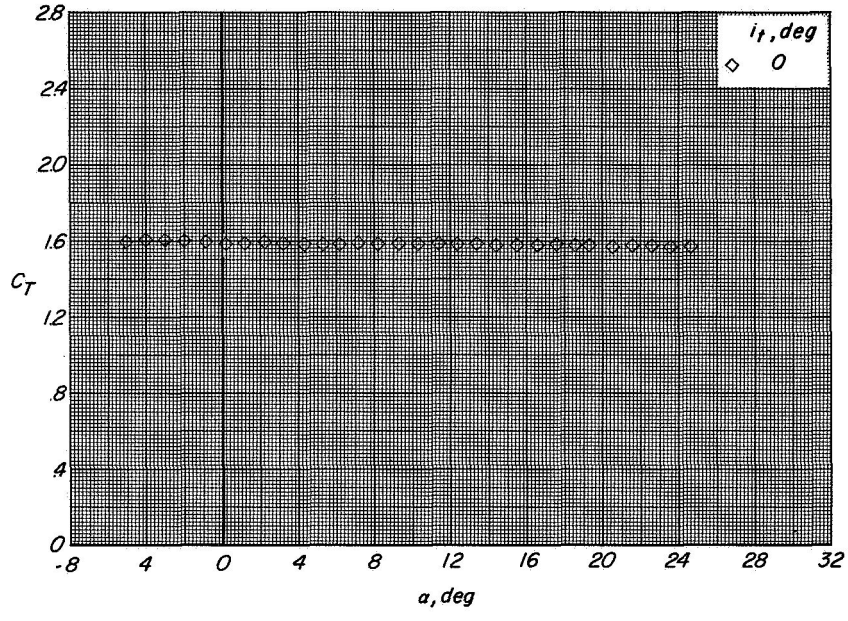

(d) Variation of C_T with α.

Figure 58.- Concluded.

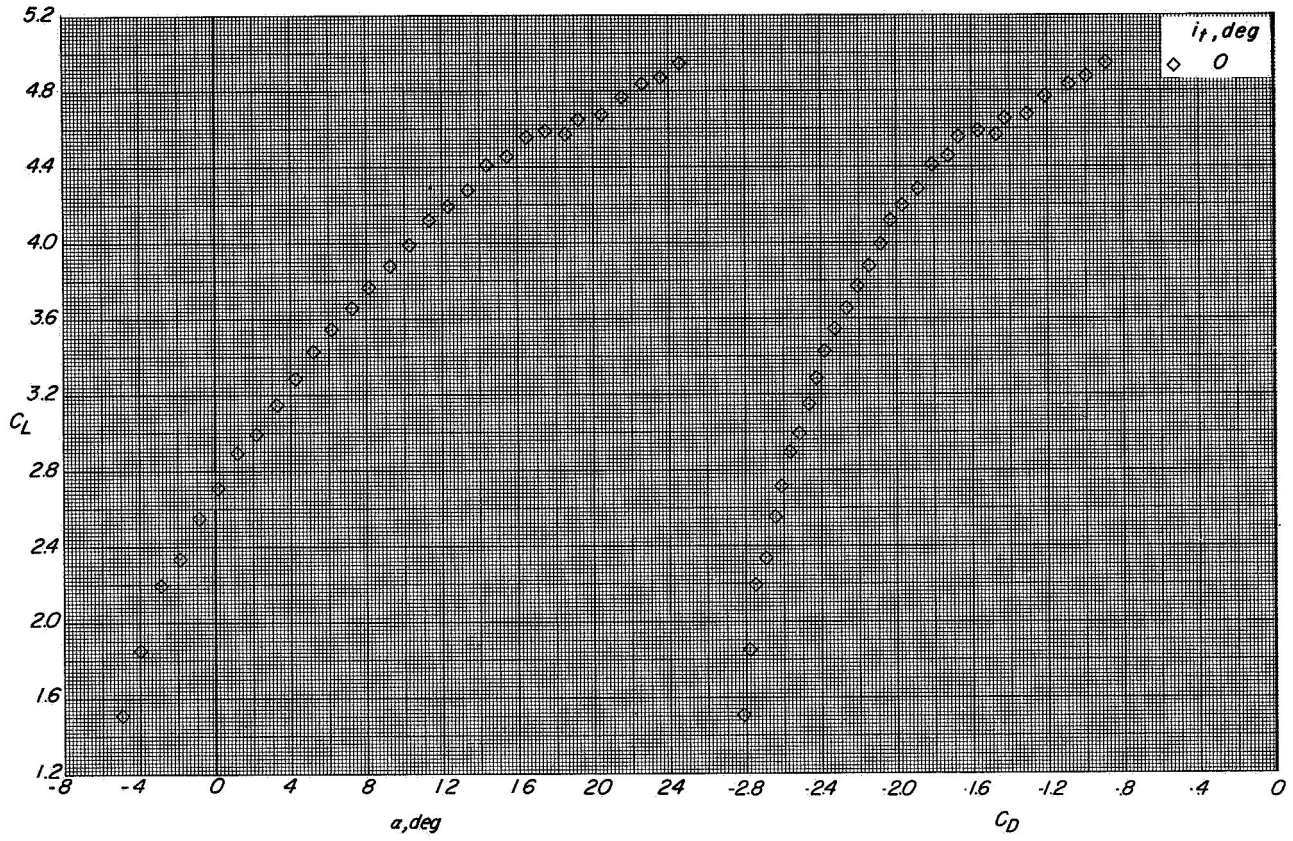

(a) Variation of C_L with α and C_D with C_L.

Figure 59.- Longitudinal aerodynamic characteristics of configuration C with direct-lift engines and lift-cruise engines deflected 25°. $C_T \approx 3.3$.

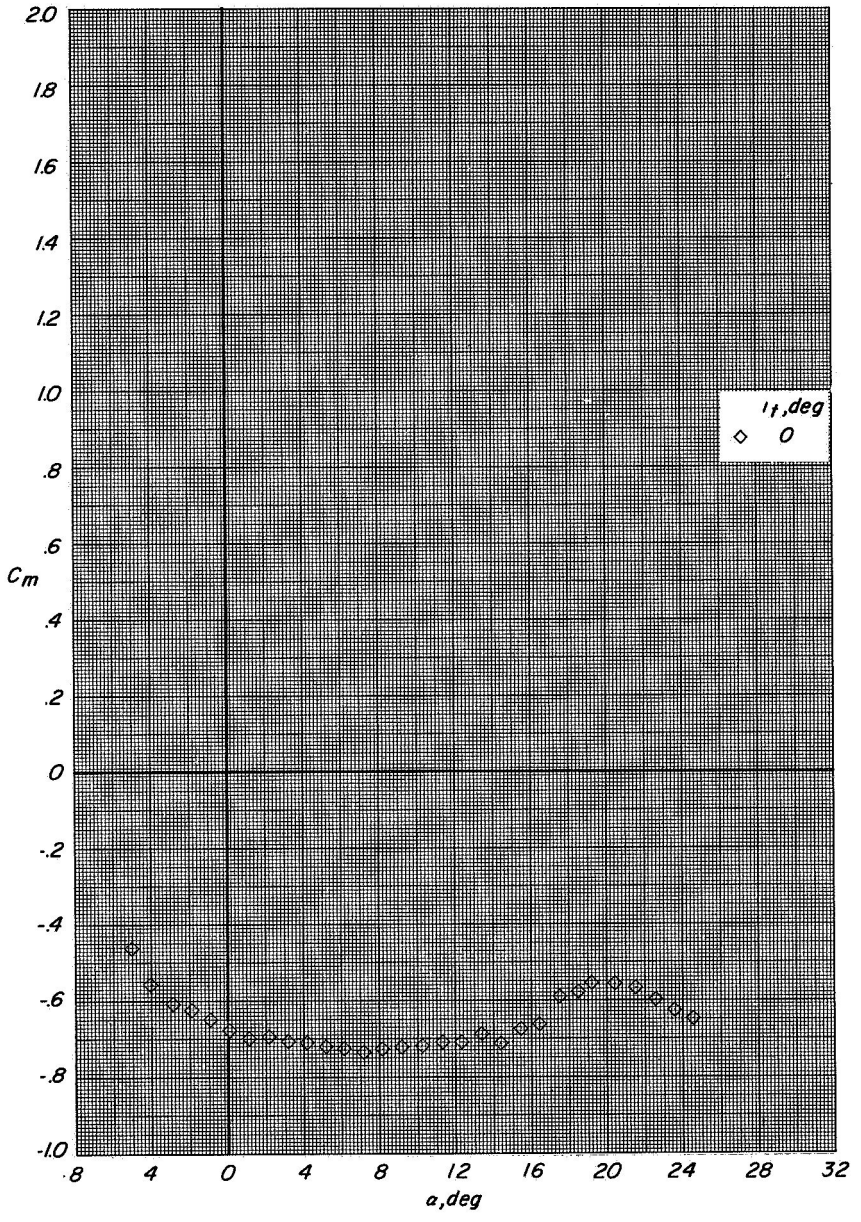

(b) Variation of C_m with α.

Figure 59.- Continued.

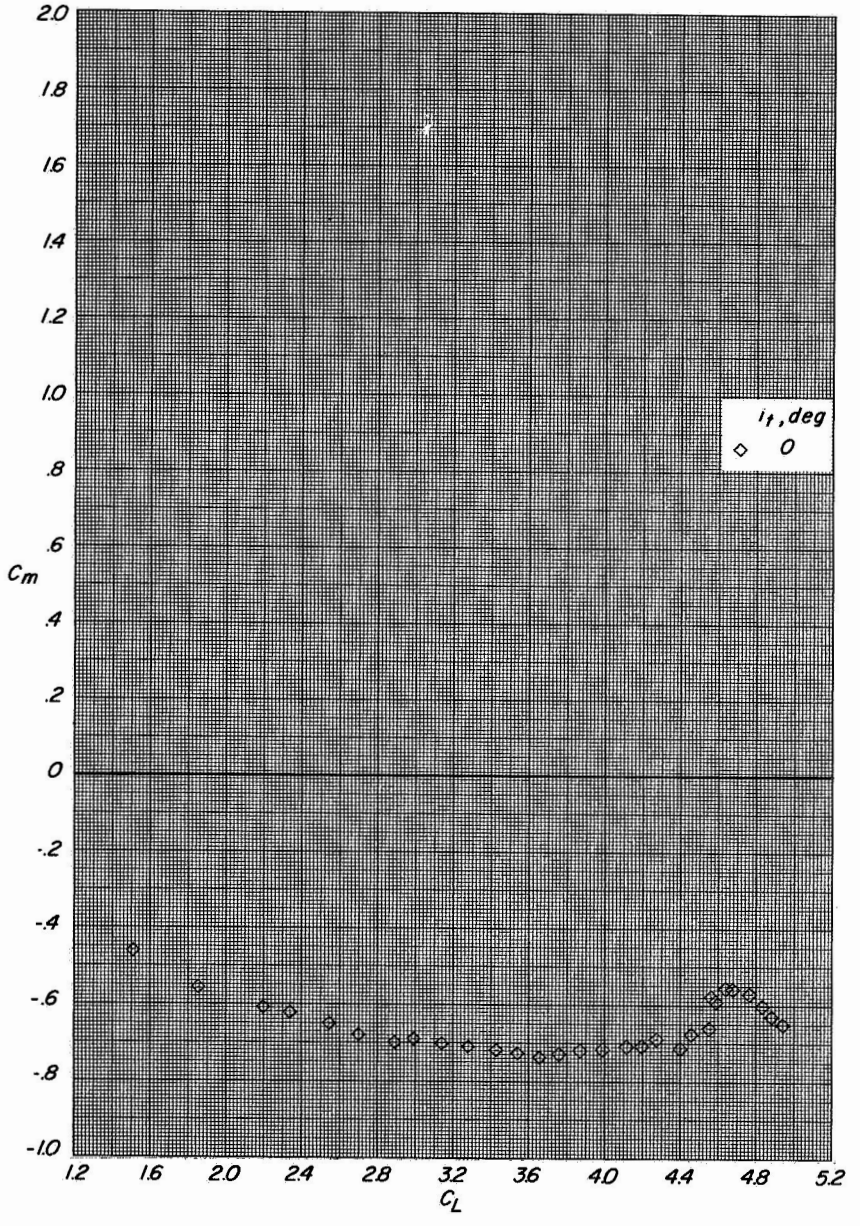

(c) Variation of C_m with C_L.

Figure 59.- Continued.

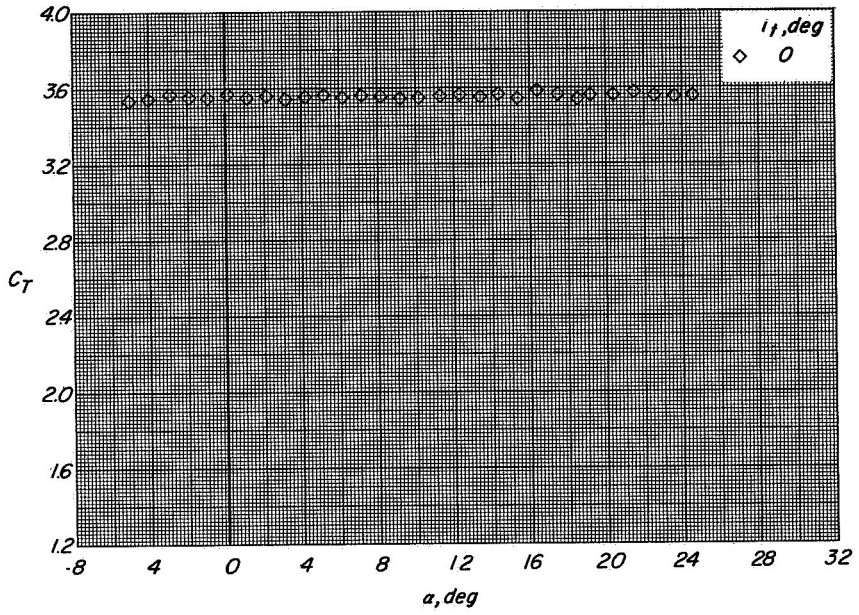

(d) Variation of C_T with α.

Figure 59.- Concluded.

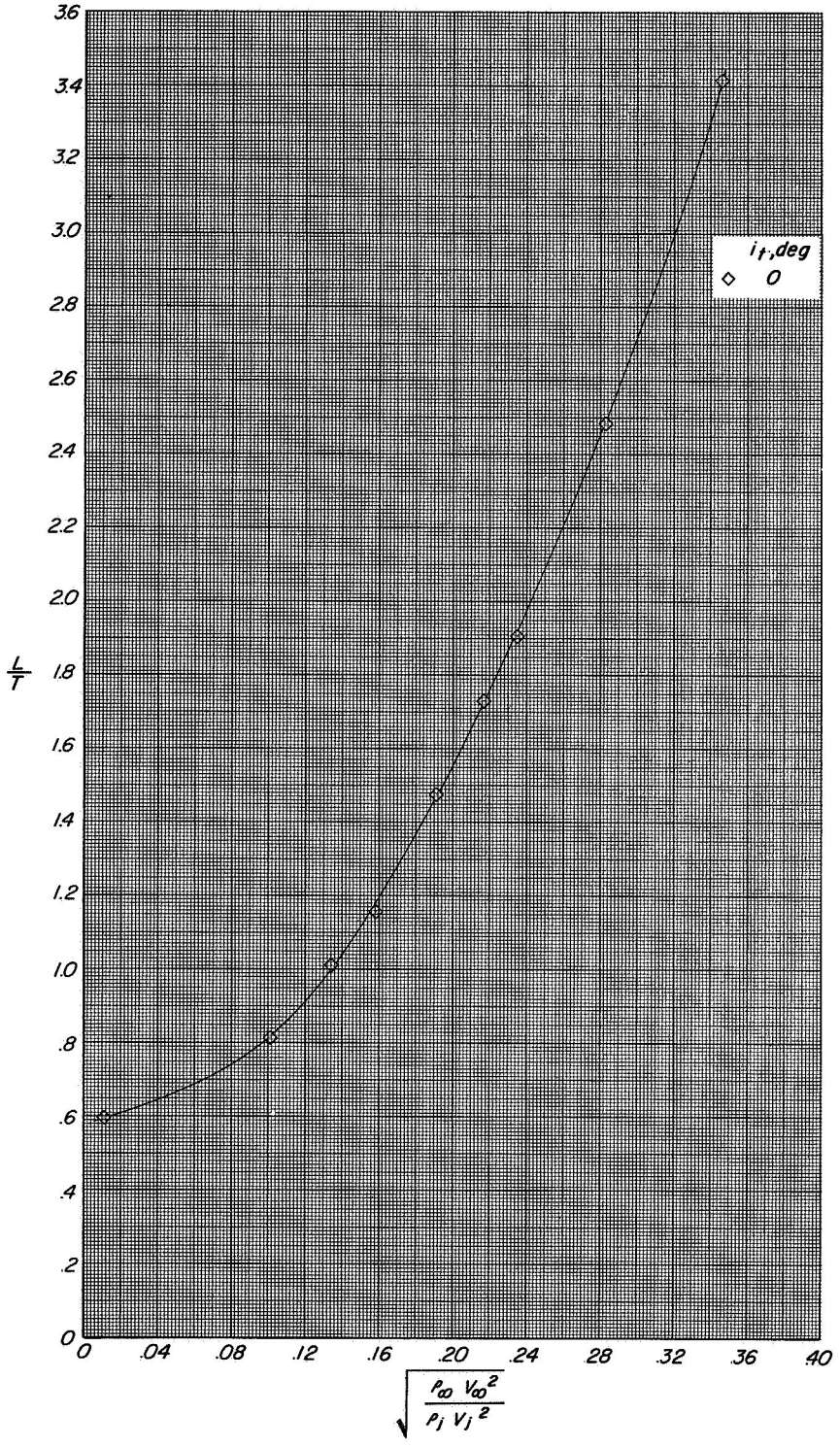

(a) Variation of L/T with effective velocity ratio.

Figure 60.- Longitudinal aerodynamic characteristics of configuration C with direct-lift engines and lift-cruise engines deflected 25°. $\alpha = 12°$.

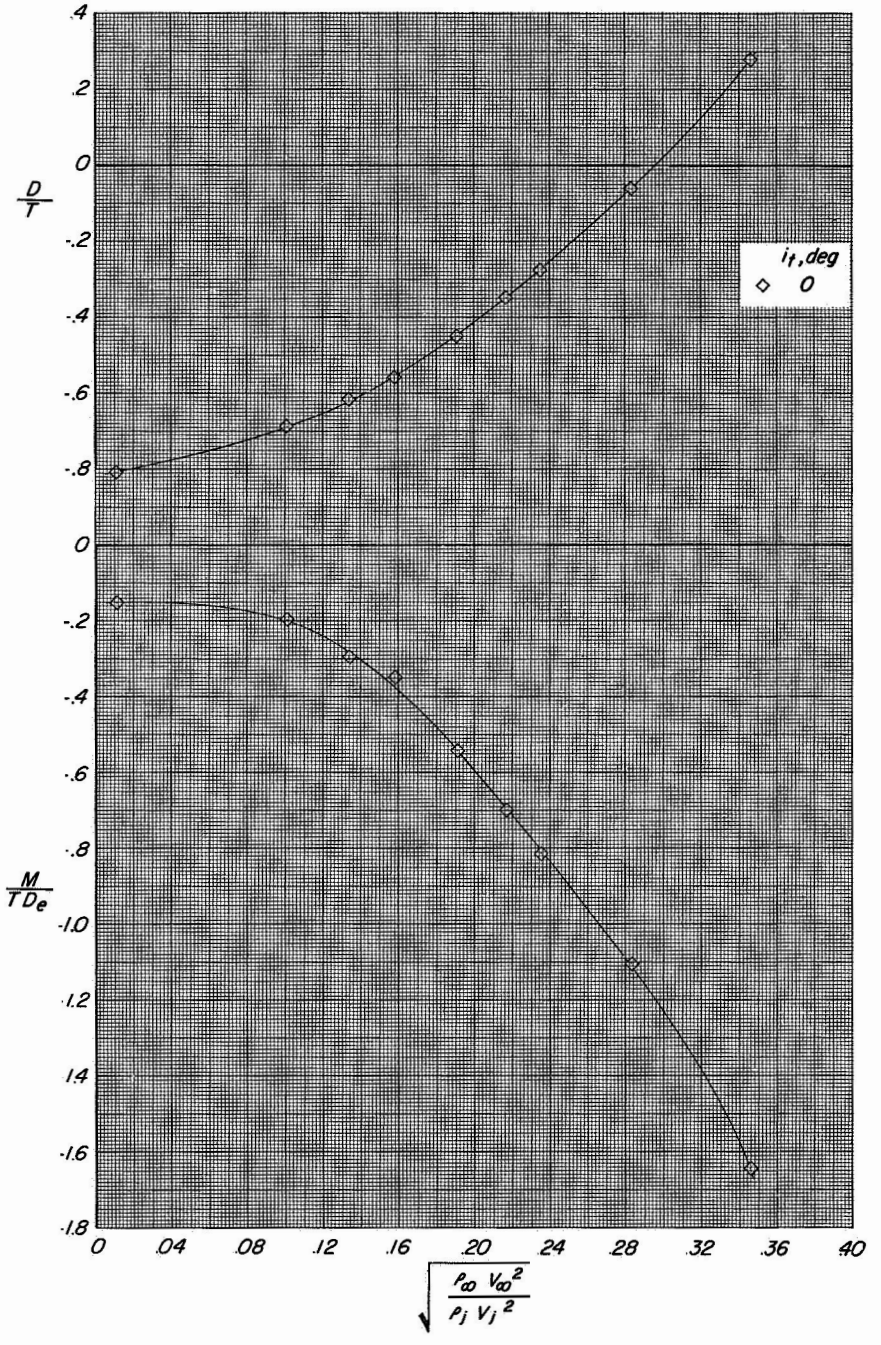

(b) Variation of D/T and M/TD_e with effective velocity ratio.

Figure 60.- Concluded.